MULTIPLE SHEAR KEY CONNECTIONS FOR LOAD-BEARING SHEAR WALL PANELS

by

© REYNAUD L. SERRETTE

A Thesis

Presented to the University of Manitoba

in Partial Fulfillment of the

Requirements for the Degree of

Master of Science in Civil Engineering

Winnipeg, Manitoba

July, 1988

ISBN 0-315-47976-0

MULTIPLE SHEAR KEY CONNECTIONS FOR
LOAD-BEARING SHEAR WALL PANELS

by

Reynaud L. Serrette

A thesis submitted to the Faculty of Graduate Studies of the University of Manitoba in partial fulfillment of the requirements of the degree of

Master of Science

I hereby declare that I am the sole author of this thesis.

I authorize the University of Manitoba to lend and/or reproduce this thesis, in whole or in part, by photocopying or by other means at the request of other institutions or individuals for the purpose of scholarly research.

Reynaud L. Serrette

The University of Manitoba requires that all persons using or photocopying this thesis give their signatures, their addresses, and the date of use.

TO MARIA.

ABSTRACT

Precast load-bearing shear wall panels are used extensively in high-rise construction because of the high quality control of the panels, and the ease and speed of panel assembly at the erection site. The connection between adjacent panels must be designed with adequate strength, ductility and continuity in order to assure the integrity of the structure. Recently, some fabrications have used multiple shear keys at the connection between walls in order to enhance the shear capacity of the connection. This thesis presents the results of a test programme that was undertaken to investigate the behaviour and capacity of multiple shear key connections.

Seven specimens with different connection configurations were tested, including one plain surface connection and two different multiple shear key connections. To simulate the effect of dead load and post-tensioning, two different levels of compressive stress were applied normal to the connections. For two of the connections, bond at the joint surface was destroyed prior to assembly of the specimen in order to determine the effect of cracks at the joint interfaces. The shear load was applied along the centerline of the connection.

Failure of the plain surface connection was characterized by slip along the joint interface. This suggested that the resistance of the connection was provided mainly by shear friction. Cracking in the drypack shear keys controlled the maximum shear capacity of the multiple shear key connections. The ultimate shear capacity of the plain surface connection was also provided by shear friction at the slip surface. In addition to shear friction, the ultimate shear capacity of the multiple

shear key connections was provided by bearing at the slip surface. An examination of the joint interface after testing indicated that there was no bond between the drypack and the wall panel.

A comparison of the behaviour of the different shear key configurations, subjected to similar loading conditions, indicated that the difference in key configuration had no effect on the capacity or behaviour of the multiple shear key connections. An increase in the load level normal to these connections was found to increase the shear capacity, but not in the same proportion. The presence of shear keys in the connection resulted in increases in the maximum and ultimate shear capacities, over the plain surface connection, of up to 60 and 25 percent, respectively.

Rational mathematical models developed to predict the shear capacity of the multiple shear key connection, at various limit states, were in good agreement with the test results.

ACKNOWLEDGEMENTS

This study was carried out under the direct supervision of Dr. S. H. Rizkalla. The author wishes to express his sincere gratitude to Dr. Rizkalla for the idea for this thesis and for his guidance, support and critical commentary at each stage of the study.

The author also wishes to express his gratefulness to Dr. E. Attiogbe for his support throughout the study and for his comments during the writing of this thesis, in the absence of Dr. Rizkalla.

Thanks are extended to Mr. S. Heuvel, P.Eng., Manager of Engineering at Con-Force Structures Limited, Winnipeg, Manitoba, for his advice and for supplying the components and labour for construction of the test specimens.

The author is also appreciative of the help of Instructor Zhi-Cheng Zhao of Hohai University, China.

For their assistance during the testing procedure, the author thanks Messrs. Moray McVey, Ed Lemke, Brian Turnbull, John Clark, Steve Meyerhoff and Martin Green of the Civil Engineering Department. Appreciation is also due to Ms. Jeannie Mak and Ms. Wendy Seversen for typing this manuscript.

Finally, the author wishes to express his heartfelt thanks to his family, who through their positive support and endurance of many seven-day work-weeks made completion of this thesis possible in such a short time.

Thank you all.

TABLE OF CONTENTS

List of Tables

List of Figures

Figure | Page

LIST OF SYMBOLS

A_c	total cross-sectional area of the connection normal to the plane of the specimen
A_{cr}	total cross-sectional area of the diagonal cracks
A_s	cross-sectional area of steel crossing the connection
b	width of the gap between the shear-key lugs
B	shear key area
C_0, C_1, C_2	regression coefficients
d	depth of the shear key
d_h	horizontal component of d_{14}
d_v	vertical component of d_{14}
d_h'	horizontal component of d_{14}'
d_v'	vertical component of d_{14}'
d_h''	horizontal component of d_{14}''
d_v''	vertical component of d_{14}''
d_{ij}	demec gauge length from point i to point j, before the shear load is applied
d_{ij}'	demec gauge length from point i to j, after the shear load is applied
d_{ij}''	demec gauge length from point i to j, after the shear load is applied
D1	direction of the main diagonal
D2	direction of the off-diagonal
f_{cmax}	maximum compressive strength of cracked concrete
f_c'	cylinder compressive strength of the concrete

f_g' equivalent standard cylinder compressive strength of the drypack/infill concrete

f_g'' cube compressive strength of the drypack /infill concrete

f_t tensile strength of the drypack/infill concrete

f_y yield strength of the reinforcement

h maximum height of the shear key

h_1 minimum height of the shear key

h_p maximum height of the shear-key lug

H horizontal direction

$l_{C,D2}$ strain in D2 direction immediately after the preload is applied

n number of shear keys

N gross load normal to the connection

N' net load normal to the connection

P maximum compressive force in the strut

R_i orientation of demec gauge length (i = 1,2,3) before the preload is applied

R_i' orientation of demec gauge lengths (i = 1,2,3) after the preload is applied

R_i'' orientation of demec gauge lengths (i = 1,2,3) after the shear load is applied

t thickness of the connection

V' vertical direction

V shear load

V_a shear capacity immediately after cracking

V_a^f shear friction of the struts

V_a^s	shear resistance of the struts
v_{cr}	cracking shear stress
V_{cr}	cracking shear load
V_{cr}^f	shear friction resistance at cracking
V_{cr}^t	shear resistance due to the drypack tensile strength
V_{max}	maximum shear load
v_{max}	maximum shear stress
$\bar{v}_u$	ultimate shear stress
V_u	ultimate shear load
w	average width of the inclined portion of the strut
α	orientation of diagonal cracks to the horizontal
β	orientation of ϵ_1 from the D1 axis
γ	f_g' coefficient at ultimate load
δ_s	shear slip
δ_w	shear dilation
ϵ_1	principal tensile strain
ϵ_2	principal compressive strain
ϵ_{D1}	strain in the D1 direction
ϵ_{D2}	strain in the D2 direction
ϵ_H	strain in the horizontal direction
ϵ_V	strain in the vertical direction
θ	shear key inclination to the horizontal
μ	friction coefficient
μ_d	friction coefficient along the diagonal cracks
	concrete density factor

σ_n compressive stress normal to the connection

ψ strength reduction factor for cracked drypack

CHAPTER 1

INTRODUCTION

1.1 General

Precast load-bearing shear wall panels are now used extensively in high-rise construction. The attractiveness of precasting is mainly due to such factors as the standardization of the wall panels, the high quality control achieved in the manufacturing plant, and the ease and speed of panel assembly.

Standardization and high quality control are easily achieved because the panels are manufactured in a controlled environment. Ease of assembly requires that two basic conditions be satisfied. These conditions are (1) the use of a minimum number of connections during assembly at the site and (2) the reduction or elimination of problems related to dimensional tolerances. At times, these two conditions may be contradictory and it is left to the engineer to find a satisfactory balance [1]. The speed of assembly is directly related to the first condition and is influenced by the simplicity of the connection and the use of a minimum amount of temporary falsework. In addition, construction in which precast elements are utilized is almost independent of the building season.

Because the required strength and ductility can be easily achieved for the individual wall panels, the most important factor in assuring a safe structure is the detailed design of the connections. A well designed connection should also be economical.

The current trend in the design of wall panel connections utilizes some combination of continuity bars, mechanical shear connectors and/or post-tensioning. The gap between adjacent panels, which is required for alignment, is filled with a drypack concrete. Recently, some fabricators have introduced a system of multiple shear keys at the joint surfaces of the shear wall panels. The behaviour and capacity of this type of connection is not well-defined and as a result, design engineers tend to estimate the capacity of such connections conservatively.

The information in the literature, though useful, is mainly applicable to vertical, non-load-bearing connections in which the joint space is filled with a mortar as opposed to a drypack concrete [2]. Thus, in order to provide some information on the behaviour and capacity of load-bearing multiple shear key wall panel connections, this research programme was undertaken.

1.2 Objective

The primary objective of this research is to investigate the behaviour of multiple shear key connections for precast concrete load-bearing shear wall panels subjected to static shear loading.

An additional objective is to develop rational mathematical models to predict the various limit states of behaviour, including the initiation of cracks, the maximum shear capacity and the ultimate shear capacity.

1.3 Scope

Seven prototype wall panel specimens were tested in this research programme. The seven specimens included three different joint configurations—plain surface and two different multiple shear keys. The multiple shear key connections were tested under two different levels of load normal to the connection. In addition, for two specimens with shear key connections, the bond at the drypack-panel interfaces was eliminated prior to assembly of the specimens in order to simulate the effect of cracks or a lack of bond at these interfaces.

The effects of the difference in shear key configuration, the level of load normal to the connection, the absence of bond at the joint interface and the presence of shear keys at the connection are determined by comparing the load-slip response of the relevant connections. Based on the test results and the observed behaviour of the test specimens, rational mathematical models are developed to predict the capacity of the multiple shear key connections at the limit states of concern. The predictions of the models are compared to the measured test results to determine the reliability of the models.

CHAPTER 2

LITERATURE REVIEW

2.1 Introduction

During the last three decades there has been a tremendous increase in the use of precast concrete elements in structures. Today, in most reinforced concrete structures, precast members are used either in conjunction with cast-in-place members or by themselves.

The use of precast concrete members, such as shear wall panels, offers many advantages. These include the high quality control of the panels which can be achieved in the manufacturing plant, the speed and ease of panel assembly at the construction site, a reduction in construction delays due to the weather, and the ease with which desired architectural finishes may be achieved. Precast construction is especially well suited to apartment buildings where there is a significant amount of repetition between floors.

In comparison to cast-in-place structures, precast concrete structures require the use of a larger number of joints in order to obtain the complete structure. These joints represent regions of high stress concentration. In order to prevent a progressive collapse due to the failure of a single connection, the engineer must ensure that the precast elements are effectively tied together.

A typical connection configuration used in the construction of load-bearing shear walls utilizes some combination of continuity reinforcement, mechanical shear connectors and/or post-tensioning. The gap between adjacent panels, provided for alignment of the wall, is usually filled with a drypack concrete. The connection serves to tie the individual wall panels together in order to achieve strength, continuity and ductility when the shear wall is subjected to bending moments and shear forces, as illustrated in Figure 2.1.

A recent study at the University of Manitoba [3] has shown that the ultimate shear capacity of a plain surface connection may be determined as the sum of the strength contributions from (1) the shear friction resistance, (2) the shear resistance of the continuity reinforcement and (3) the shear resistance of the mechanical connector.

To increase the capacity of the connection, some fabricators cast shear keys into the plain joint surface of the precast wall panels, as shown in Figure 2.2. The behaviour of load-bearing multiple shear key connections is, however, not well defined. As a result, design engineers have a tendency to estimate the capacity of multiple shear key connections conservatively.

In Europe, multiple shear key connections have been used in vertical joints for more than two decades. Consequently, research in Europe is not directly related to load bearing connections. The effectiveness of the presence of shear keys in the connection has, however, been recognized, and this is reflected in the Polish and British National Codes which recommend that for non-load-bearing connections:

shear capacity of the multiple shear key connection	=	6 x	shear capacity of the plain surface connection

In addition, the size of the reinforcement used in Europe is substantially smaller than the continuity reinforcement used in North America, although the total area of reinforcement across the joint may be similar.

In the following section, the present state of knowledge regarding the design of multiple shear key connections is reviewed and summarized.

2.2 Behaviour of Multiple Shear Key Connections

Cholewicki [4] conducted thirty tests on trapezoidal shear key and plain surface connections which were either reinforced or unreinforced. None of these tests considered compressive forces normal to the connection.

Based on his tests, Cholewicki showed that multiple shear key connections have a higher shear capacity than plain surface connections. In addition, two phases of behaviour were identified for the multiple shear key connection:

(1) before and up to the loss of bond at the joint interface

(2) after loss of bond, up to failure of the connection

Figure 2.3 illustrates the two phases described by Cholewicki. The figure indicates that in phase I the presence of bond at the joint interface ensures monolithic behaviour. Phase II could be divided into two stages which describe slip at the joint interface (Figure 2.2 (b)), and diagonal cracking in the infill concrete (Figure 2.2 (c)). Failure of the connection occurred in the second phase, after slipping at the joint interface.

Cholewicki showed that the shear stress distribution along the connection was not uniform. Furthermore, the maximum capacity of the unreinforced multiple shear key connection was dependent on the infill concrete tensile strength, the number of shear keys and the area of the shear keys. For the unreinforced multiple shear key connection, not subjected to compressive normal stresses, the maximum shear capacity, V_{max}, was given by:

$$V_{max} = 0.7\ f_t nht \tag{2.1}$$

where f_t = tensile strength of the infill concrete

n = number of shear keys

h = maximum height of the shear key

t = thickness of the connection

The 0.7 factor was based on the average maximum shear stress, v_{max}, along the connection for different specimens. Cholewicki found that v_{max} may be as low as 0.7 f_t. To use Equation 2.1, the inclined portion of the shear key should be less than 30 degrees to the horizontal. This condition is imposed in order to ensure that slipping at the joint surface does not occur prior to failure.

Hansen, et al. [5] have conducted thirty-six tests on reinforced trapezoidal shear key connections subjected to shear and normal or cyclic loading. The typical shear load-slip behaviour for the multiple shear key connections is illustrated by the solid line in Figure 2.4. In tests where a compressive force was applied normal to the connection, no cracks were formed in the infill concrete nor at the joint interface until the maximum load for the connection was approached. In tests where bond between the panel and the infill concrete was destroyed prior to testing, the maximum load attained and the mode of failure were similar to those specimens with bonded connections, but larger deformations were recorded, as illustrated by the dashed line in Figure 2.4. In the tests involving cyclic loading (up to 20 cycles), the maximum deformations were larger than those for similar specimens under static loading. Failure occurred in the same manner as in the static case, except diagonal cracks in the infill concrete developed in two directions compared to one direction under static loading.

Based on their test results and those of other researchers, Hansen, et al. [5] developed an empirical equation for predicting the maximum shear capacity of a reinforced multiple shear key connection. This equation is expressed as:

$$V_{max} = 0.09nhtf'_g + A_sf_y + \sigma_nA_c \tag{2.2}$$

where f'_g = standard cylinder compressive strength of the infill concrete

A_s = cross-sectional area of steel crossing the connection

f_y = yield strength of the reinforcement

σ_n = compressive stress normal to the connection

A_c = total cross sectional area of the connection

For an unreinforced connection, the A_sf_y term is neglected so that the maximum shear capacity becomes:

$$V_{max} = 0.09nhtf'_g + \sigma_n A_c \tag{2.3}$$

Equations 2.2 and 2.3 are restricted to values of nht/A_c between 0.2 and 0.5. In addition, the ratio between key height (h) and key depth (d), as illustrated in Figure 2.4, should not be more than 8, the depth of the key should not be less than 10 mm and the inclination of the key, θ, to the horizontal should not be greater than 30 degrees.

Chakrabarti, et al. [6] conducted twenty-nine tests on plain surface connections and on reinforced or unreinforced trapezoidal shear key connections for precast wall panels not subjected to normal loads. These investigators observed that, in general, slipping at the joint interface preceded failure of the connection. As in the case of the results obtained by Cholewicki, et al. [4], the capacity of the multiple shear key connections was significantly higher than that of the plain surface connections.

Failure of the multiple shear key connections was characterized by diagonal and vertical cracking in the infill concrete shear keys. In addition, local crushing of the infill concrete was observed. After slip occurred at the joint interface, Chakrabarti, et al. observed that the shear stress distribution along the connection became more uniform. The change from a non-uniform shear stress distribution to a uniform stress distribution was attributed to the loss of rigidity of the connection after slip at the joint interface.

An empirical equation for the maximum shear capacity of the unreinforced shear key connection, using a best-fit straight line, was developed by Chakrabarti, et al. and is given by:

$$V_{max} = 0.093nhtf_g'' \qquad (2.4)$$

where f_g'' = cube compressive strength of the infill concrete.

Neither the Canadian code [7] nor the American code [8] contains any provisions for the design of multiple shear key connections. For their range of applicability, these codes use the shear friction theory. This theory is based on the resistance to shear along a crack which is provided by clamping forces acting normal to the slip surface of the crack. The code equations give the shear capacity as:

$$V_u = \mu\sigma_n A_c \qquad (2.5)$$

where μ = friction coefficient, which depends on surface roughness. Table 2.1 gives the friction coefficients recommended by the codes for various surface conditions. Equation 2.5 implies that the ultimate shear capacity of a given connection is proportional to the load normal to the connection. Neither code accounts for the interlocking effect which is provided by the presence of shear keys, even if cracks exist at the joint interface.

2.3 Significance of the Connection Parameters

Many factors affect the capacity of any unreinforced multiple shear key connection. These include:

(i) Strength of the infill concrete or drypack

(ii) Strength of the wall panel concrete

(iii) Shape, dimensions and number of shear keys

(iv) Adequate packing/filling of the joint space

(v) Uniformity of the infill concrete or drypack

(vi) The presence of cracks in the connection

(vii) The presence of stresses normal to the connection

Foerster [3] showed that for trapezoidal shear key connections in which the panel concrete strength is less than the drypack strength, failure of the connection may result from shearing-off of the panel shear-key lugs, as illustrated in Figure 2.5. On the other hand, if the drypack strength is less than the panel concrete strength, failure occurs as a result of cracking in the drypack shear keys.

Based on data collected from a number of sources, Hansen, et al. [5] have suggested that a relative increase in the shear key area will likely increase the maximum shear load. These researchers also point out that there is a limit to which the relative key area may be increased for failure to be induced by cracking in the drypack. Beyond this limit, failure may occur as a result of cracking in the panel shear-key lugs. Thus, there seemed to be two parameters which control where cracks form in the connection: (1) the relative strengths of the drypack and the panel concrete and (2) the size of the shear keys.

Hansen, et al. also compared the failure load for sinusoidal, triangular and trapezoidal shaped keys. Their findings showed that under similar loading conditions, the use of trapezoidal shear keys resulted in substantially higher failure loads of the connection in comparison to the failure load for the other shear key configurations.

Different limitations have been set forth for the allowable dimensions of trapezoidal shear keys. Cholewicki [4] has defined the important shear key parameters, illustrated in Figure 2.6, to be (1) the key height in the drypack, h, (2) the key height in the panel, h_p, (3) the width of the gap between the shear-key lugs, b, (4) the depth of the key, d, and (5) the inclination of the key to the horizontal, θ. The thickness of the connection is denoted as t in the figure. In Figure 2.7, specific recommendations are given for the dimensions of the shear key based on experimental work carried out by Hansen, et al. [5] and on a report presented to the Prestressed Concrete Institute by Speyer [9]. Hansen, et al. have specified that the inclination of the shear key, θ, should be less than or equal to 30 degrees, the depth of the key, d, should be greater than or equal to 10 mm and the ratio of the maximum key height to the key depth, h/d, should be less than or equal to 8. Speyer has recommended that the inclination of the shear key, θ, should be less than 35 degrees and the ratio of the minimum key height to the key depth, h_1/d, should be less than or equal to 6. Both recommendations assume that the drypack shear key height and the panel shear key height are equal. In addition, the width of the gap between the shear key lugs is not considered.

Adequate packing or filling of the joint space is also of importance since the presence of voids may cause premature and brittle failure of the connection. In addition, non-uniformity of the drypack may result in a highly non-uniform distribution of stresses along the connection.

Cholewicki [4] observed from his tests that the failure load for connections in which bond was artificially destroyed at the joint interface was lower than that for connections in which bond was intact. This result, however, differed from that of Hansen, et al., who found that the destruction of bond may have only a small effect on the shear capacity. In both investigations, however, the unbonded connections exhibited larger deformations than the corresponding bonded connections.

To date, there has been a lack of research on the behaviour and capacity of multiple shear key joints subjected to externally applied normal compressive stress. It is accepted, though, that the presence of compressive stresses normal to the joint can lead to a significant increase in the capacity of the connection.

CHAPTER 3

EXPERIMENTAL PROGRAMME

3.1 Introduction

This experimental programme was designed to investigate the shear behaviour and capacity of load-bearing multiple shear key connections at various limit states. The limit states included (1) serviceability: cracking and excessive deformations during normal use of the structure, (2) strength limit state: related to the maximum shear capacity of the connection, and (3) ultimate shear capacity of the connection. All parameters were held constant, except the joint configuration of the panels and the level of compressive stress applied normal to the connection.

3.2 Description of the Wall Panels

3.2.1 Panel Dimensions

The overall dimensions of all the panels were identical, as shown in Figure 3.1. The panel had a thickness of 200 mm (typical of the elevator shear wall panels in structures), a height of 1660 mm, a width of 1290 mm at the corbel end and an overall width of 930 mm on the opposite end. The depth of the corbel was 540 mm and it framed into the main portion of the panel over a width of 360 mm and a drop of 50 mm.

3.2.2 Joint Configuration

Three different panel joint configurations, as shown in Figures 3.2 to 3.4, were tested. The NK or no-key type configuration, illustrated in Figure 3.2, consisted of a plain joint surface. The LK or large-key type configuration consisted of five shear keys, as shown in Figure 3.3. The key height, h, is 100 mm, the key depth, d, is 35 mm and the inclination of the key is approximately 23 degrees to the horizontal. The same dimensions are used for the shear keys and the shear-key lugs. The SK or small-key type configuration, shown in Figure 3.4, consisted of eight shear keys. Each key had a height of 50 mm, a depth of 25 mm and was inclined at approximately 7 degrees to the horizontal.

3.2.3 Panel Reinforcement

All the test panels were reinforced with the same reinforcement layout and sizes. The only difference was in the length of the reinforcement across the width of the panel which was adjusted depending on the joint configuration. Figures 3.5 to 3.7 show the actual reinforcement scheme for the three types of panels and Figure 3.8 gives the shape and length of the reinforcement used.

The reinforcing bars had a nominal yield strength of 300 MPa. The closed stirrup ties (designated MK2, MK3, MK6 and MK8) used 10M bars and all other reinforcing bars were 20M. A cover of 20 mm was allowed for all the reinforcement. The shear-key lugs were not reinforced, as can be seen in Figures 3.6 and 3.7.

3.3 Specimen Assembly

All the panels used in this test programme were made by Con-Force Structures Limited of Winnipeg, Manitoba and delivered to the Structural Laboratory at the University of Manitoba.

Each specimen consisted of two panels which were assembled in the horizontal position on the floor of the laboratory, as shown in Figure 3.9. A gap of 20 mm was provided between the individual panels. Figure 3.10 shows the two angle irons and the two brackets used to maintain the specimen configuration as the specimen was raised from the horizontal to the vertical position. After all the specimens were in the vertical position, forms were built on the side of the specimen with the angle irons, in order to facilitate drypacking of the joint.

The drypack was compacted into the joint space, as shown in Figure 3.11, by an employee of Con-Force Structures Limited. The drypacked connections were then covered with wet burlap and a polyethylene tarpaulin and allowed to cure for seven days. After curing, the coverings were removed and the specimens were exposed to the laboratory environment until testing.

3.4 Description of the Test Specimens

In this experimental programme, a total of seven specimens with three different joint configurations were tested. Each specimen consisted of two panels connected together by means of a drypack. The three connection configurations used are illustrated in Figures 3.12 to 3.14, for the typical no-key, large-key and small-key specimens, respectively. In all the specimens, the drypack gap width, b, was 20 mm.

Specifically, the following specimens were tested for each connection configuration:

NK series: drypack plain surface connection; specimen 1NK4

LK series: drypack large multiple shear key connection; specimens 1LK2, 2LK2 and 3LK4B

SK series: drypack small multiple shear key connection; specimens 2SK2, 1SK4 and 3SK4B

The number before the series identification refers to the order in which the specimen was tested and the number after the series identification gives the level of compressive stress normal to the connection. The letter "B" used in the specimen name refers to a specimen in which bond at the joint interface was eliminated prior to assembly of the specimen. Appendix A gives a full description of the specimen mark nomenclature used in this programme.

The artificial elimination of bond at the joint interface, in specimens 3LK4B and 3SK4B, was achieved by coating the joint surface with varnish, as shown in Figure 3.15. After the varnish dried and prior to packing the joint with the drypack, the joint surfaces of these specimens were brushed with oil.

3.5 Material Specifications

3.5.1 Concrete

The concrete proportions used by Con-Force Structures Limited, for the panels, were as follows:

Coarse aggregate	884 kg/m^3
Sand	612 kg/m^3
High Early Strength Portland Cement	234 kg/m^3
Flyash	32 kg/m^3

Pozzolith	0.58 kg/m^3
Water	119 kg/m^3

For each panel, six 150 mm x 300 mm standard concrete cylinders were cast according to CSA specifications in order to evaluate the strength of the concrete.

3.5.2 Drypack

The drypack had essentially the same composition as used in the field and the mixing was done by Con-Force personnel. The drypack had a grainy consistency, yet it was able to maintain its shape when compressed in the palm of the hand, as shown in Figure 3.16.

The drypack proportions used were as follows:

	by volume	by weight
Concrete sand	2 parts	2
Normal Portland Cement	1 part	1
Water	approx. 0.5 parts	approx. 0.2

A total of fifteen 75 mm drypack cubes were used to evaluate the strength of the drypack at the time of testing. Six of these cubes were cast in concrete moulds and the remaining nine were cast in wooden moulds.

3.5.3 Concrete Sand

In accordance with the CSA Standard CAN3-A23.1-M77 [10], the concrete sand used in the drypack had the following gradation, as determined by sieve analysis:

Sieve Size	Total Percentage Passing by Mass
10 mm	100
5 mm	97.3
2.5 mm	88.5
1.25 mm	76.1
630 μm	54.6
315 μm	17.2
160 μm	4.0

3.6 Instrumentation

3.6.1 Concrete and Drypack Strain

The concrete and drypack strains were measured using manually operated mechanical strain gauges (demec gauges). Strains were measured at demec stations in the vicinity of the connection, on both sides of the specimen. Figures 3.17 to 3.19 illustrate the position of the demec stations on the two sides, A and B, of the no-key, large-key and small-key connections, respectively.

A 50.8 mm (2 inch) demec gauge length was used on side B of each specimen while a 200 mm (7 7/8 inch) demec gauge length was used on side A. The smaller gauge length used on side B allowed the evaluation of strains at localized regions in the drypack and concrete. The 200 mm demec gauge length measured average strains across the connection. These average strains were used to calculate shear slip and dilation. The accuracy of the 50.8 mm and 200 mm demec gauges were ± 0.0023 mm and ± 0.002 mm, respectively.

At each demec station, strains were measured in three directions, as shown in Figure 3.20. Also shown in this figure are the six demec points which typically make up a demec station. These stainless steel demec points were attached to the concrete and drypack surfaces using a "Five Minute Epoxy Adhesive".

In addition to the calculation of shear slip and dilation, the principal strains and the crack orientation were also calculated from the demec readings.

3.6.2 Stroke Measurements

The stroke applied by the testing machine was measured using a linear variable differential transformer (LVDT). The LVDT was set up as shown in Figure 3.21. The range of the LVDT was ± 12.7 mm and its accuracy was 0.5 percent.

The readings from the LVDT were recorded directly by a Hewlett Packard 34702A multimeter and converted from volts to millimeters by applying a conversion factor to the voltage readings.

3.6.3 Testing Machine

A Baldwin 2670 kN Universal Testing Machine equipped with an MTS 2310 signal amplifier, a 464 MTS data display, a Hewlett Packard 7044A

X-Y plotter and a Hewlett Packard 34702A multimeter were used for testing.

3.7 Testing Procedure

3.7.1 Test Setup

After the drypack was cured, the centerline of the connection was marked on each specimen and the demec points were attached at predetermined stations along the length of the connection, as described previously.

Supported by two cranes, the specimen was then installed in the testing machine with the connection oriented in the vertical position. The centerline of the connection was aligned with the centerline of the top and bottom platforms of the testing machine. After alignment, the bottom platform of the test machine was brought into contact with the specimen. Between the bottom platform of the test machine and the specimen, a steel bearing pad and quick-set plaster-of-paris was used. The plaster-of-paris was used to achieve uniform contact between the specimen and the bearing pad. At this stage, the vertical alignment of the specimen was rechecked and adjusted using a plumb bob and a mason's level. Following this, the top steel bearing pad was placed on top of the specimen. Quick set plaster-of-paris was also used at the top support to ensure uniform contact between the bearing pad and the specimen. The top platform of the testing machine was then brought into contact with the top bearing pad. Installation of the specimen was now complete, as shown in Figure 3.22.

Each bearing pad, at the top and bottom supports, consisted of two steel plates separated by two 3.2 mm thick sheets of teflon, as illustrated in Figure 3.23. The teflon plates allowed the specimen to dilate freely without any resistance to sliding at the top and bottom supports.

After hardening of the plaster-of-paris, a post-tensioning system was used to apply compressive stresses along the ends of the specimen, as shown in Figure 3.24, in order to prevent premature failure in the individual panels. Each pair of post-tensioning bars was tensioned for a total load of 200 kN ± 10 percent. The prestressing forces were monitored during the post-tensioning operation by an indicator connected to strain gauges on the bars. Figure 2.25 shows the hydraulic jacking scheme used to apply the 200 kN load.

Next, the preload apparatus was attached to the specimen, as shown in Figure 3.26. To achieve the desired level of preload a set of four hydraulic jacks and eight Dywidag bars were used to apply a compressive stress normal to the connection. Figure 3.27 shows the hydraulic jacking system and Figure 3.28 shows the reaction end of the preload system. At the reaction end, a system of rollers against a steel plate was used in order to avoid any shearing distortions in the Dywidag bars which may have added to the strength of the connection.

The post-tensioning bars were calibrated individually using the Baldwin Testing Machine and a strain indicator while the four hydraulic jacks, for the preload system, were calibrated as a unit using the Baldwin Testing Machine and an Enerpac hydraulic pump equipped with a pressure gauge.

The complete test setup is shown in Figure 3.29.

3.7.2 Testing Sequence

Initial demec readings at each demec station and the stroke displacement were taken and recorded at the beginning of the test, prior to application of the preload. After the desired level of preload (2 MPa or 4 MPa) was applied, all the instrumentation was read and the readings were recorded. The preload was kept constant throughout the test by means of a regulator valve on the oil pump.

The test proceeded by increasing the vertical shear load along the centerline of the connection, in a stepwise manner, in increments of 100 kN with a time interval of approximately ten minutes between increments. The complete loading system is shown in Figure 3.30. After each increment of load, the instrumentation was read and recorded, and cracks that appeared in the connection were marked with a black felt pen.

Subsequent to achieving the maximum shear load, the test was continued using stroke control. Each test was terminated after the connection had undergone extensive deformation and crushing, and the shear capacity of the connection was approximately constant.

During each test, the load-stroke behaviour of the particular connection was plotted with the X-Y plotter. Photographs of the connection were taken at the maximum load and at the end of the test.

The duration of each test was approximately three hours.

CHAPTER 4

TEST DATA

4.1 Introduction

In this chapter, the experimental data for the seven specimens tested in this research programme are presented in tabular and/or graphical form.

The data include the specimen material properties, the shear capacity of the connections, the mechanical demec gauge readings and the stroke measurements.

4.1 Material Properties

4.2.1 Panel Concrete

The average compressive strength and average tensile splitting strength of the panel concrete at the time of testing are given in Table 4.1. The standard error in the estimated average strengths are also given in the same table.

4.2.2 Drypack Grout

Table 4.2 gives the average compressive strength of the drypack, as determined from the 75 mm cubes.

The average compressive strength that was measured using the cubes from the concrete moulds was higher than similar cubes made in the wooden moulds.

During the cube making process, it was observed that the wooden mould absorbed water from the drypack as the drypack was being compacted. This absorption of water was not evident in the concrete moulds. As a result, it was thought that the cubes from the wooden moulds had a lower degree of hydration than the cubes from the concrete moulds. This lower degree of hydration would explain the lower compressive strength attained by the cubes made in the wooden moulds.

Since the strength of the cubes from the concrete mould is likely to be more representative of the strength of the drypack in the connection, the average compressive strength of the drypack is taken as the average strength of the cubes from the concrete moulds.

Table 4.2 also gives the equivalent standard cylinder compressive strength of the cubes. The equivalent strength was estimated as 0.73 times the cube compressive strength [11].

4.3 Test Results

4.3.1 Shear Load

The load at which cracking was first observed, the maximum shear load and the ultimate shear load for each connection are summarized in Table 4.3 and illustrated in Figures 4.1 to 4.2, respectively, for all the test specimens. Furthermore, the tables show that the cracking and maximum load are coincident.

4.3.2 Mechanical Demec Gauge Readings

The measured demec gauge readings for all the specimens are given in Tables 4.4 to 4.10. The demec stations labelled with an "A" correspond to readings taken on side A of the specimen. Similarly, the demec stations labelled with a "B" correspond to demec gauge readings taken on side B.

Each demec gauge division on side A represents 8.0 microstrain whereas each division on side B represents 24.8 microstrain.

4.3.3 Stroke Measurements

Tables 4.11 to 4.17 give the stroke readings (as recorded from the voltmeter) and the equivalent stroke displacements for all the specimens.

The relationships between the applied shear load and the stroke displacement are presented in Figures 4.4 to 4.10 for all the specimens.

CHAPTER 5

ANALYSIS AND EVALUATION OF TEST RESULTS

5.1 Introduction

In this chapter, the experimental data presented in chapter four are used to compute the concrete and drypack strains and the shear displacements (slip and dilation).

The crack patterns at the maximum and ultimate shear loads are also presented.

5.2 Concrete and Drypack Strains

The concrete and drypack strains were calculated using the demec readings given in Tables 4.4 to 4.10 and are presented in Tables 5.1 to 5.7 for all the test specimens. The strains were calculated after each load increment by subtracting the specific demec reading from the demec reading corresponding to the stage immediately after the preload was applied. The difference in demec readings was then multiplied by the appropriate conversion factor to determine the strains. The conversion factors used for the 50.8 mm and 200 mm demec gauge were 24.8 and 8.0 microstrain per division, respectively.

The principal strains and their orientation were calculated from the diagonal strains, ϵ_{D1} and ϵ_{D2}, and the horizontal strain, ϵ_H, measured for the concrete and drypack, as follows:

$$\epsilon_1, \epsilon_2 = \left(\frac{\epsilon_{D1} + \epsilon_{D2}}{2} \right) \pm \left(\frac{\epsilon_{D1} - \epsilon_{D2}}{2} \right)^2 + \left[\epsilon_H - \left(\frac{\epsilon_{D1} + \epsilon_{D2}}{2} \right) \right]^2 \qquad (5.1)$$

$$\beta = \frac{1}{2} \tan^{-1} \left(\frac{\epsilon_{D1} + \epsilon_{D2} - 2\epsilon_H}{\epsilon_{D1} - \epsilon_{D2}} \right) \tag{5.2}$$

where ϵ_1 = principal tensile strain

ϵ_2 = principal compressive strain

β = direction of the principal tensile strain from the D1 axis.

The magnitude of the principal strains are given in Tables 5.8 to 5.14, for all the specimens. The angles given in these tables define the orientation of the diagonal crack with respect to the horizontal axis of the specimens.

The relationships between the applied shear load and the principal tensile strain, for each specimen tested, are given in Figures 5.1 through 5.28. The strains do not correspond to the complete loading history of the connection since the mechanical demec gauge ranges were exceeded shortly after the maximum load was reached.

Figures 5.1 to 5.7 represent the shear load-average principal tensile strain history of the connections with respect to the demec stations on side A of the specimens. In Figures 5.8 to 5.14, respectively, the initial part of the curves in Figures 5.1 to 5.7 are magnified to allow a closer examination of the response of the connection. These figures indicate that the average strains measured at the ends and mid-height of the connections were approximately the same. This suggests that the stress distribution along the connection may be uniform.

The principal tensile strains for the demec stations on side B of the test specimens are shown in Figures 5.15 to 5.21. In each figure, a single representative demec station is shown for the load-principal tensile strain behaviour of the concrete shear-key lugs. In Figures 5.22 to 5.28, respectively, the initial part of the curves in Figures 5.15 to 5.21 are magnified to allow a closer examination of the localized response of the concrete and drypack to the applied shear load. These figures show that under initial loading, the connection behaved monolithically. However, just prior to reaching the maximum load, a large increase in strain is observed in the drypack only. This indicates that close to the maximum load deformation of the connection is primarily confined to the drypack.

5.3 Shear Slip and Dilation

The slip and dilation for a particular connection were calculated based on the demec gauge readings in the D1, D2 and H directions at the demec stations on side A of the specimen (see Figure 3.20). The strain measurements on side A were used since these measurements were based on the average conditions at the connection, in contrast to the localized measurements at the demec stations on side B.

The shear slip and dilation of the connection at a particular load level may be calculated using the gauge lengths between diametrically located demec points and the corresponding measured strains. The relevant derivations are presented in Appendix B. Based on the expressions derived, the joint deformations are calculated as follows:

slip,

$$\delta_s = d'_{14} \cos R2' - d''_{14} \cos R2'' \qquad (5.3)$$

and dilation,

$$\delta_w = d''_{14} \sin R2'' - d'_{14} \sin R2' \tag{5.4}$$

where $d'_{14} = 200\ (1 + L_{c,D2})$ (5.5)

$$d''_{14} = 200\ (1 + L_{c,D2} + \epsilon_{D2}) \tag{5.6}$$

$$R2' = \cos^{-1}\left[\frac{(d'_{14}/2)^2 + (d_{46})^2 - (d'_{36}/2)^2}{(d'_{14})(d_{46})}\right] \tag{5.7}$$

$$R2'' = \cos^{-1}\left[\frac{(d''_{14}/2)^2 + (d_{46})^2 - (d'_{36}/2)^2}{(d''_{14})(d_{46})}\right] \tag{5.8}$$

$L_{c,D2} = 8 \times 10^{-6}$ x (demec reading in the D2 direction after the preload is applied—demec reading for the 200 mm demec gauge calibration bar)

ϵ_{D2} = increase in strain in the D2 direction after the preload is applied

The average shear slip and dilation for the test specimens are contained in Tables 5.15 to 5.21. In Figures 5.29 to 5.35 and 5.36 to 5.42, the shear load-slip and shear load-dilation curves, respectively, are given for all the specimens.

The complete shear load-slip and shear load-dilation relationships could not be achieved using the demec gauge since the range of the gauge was exceeded shortly after the connection had attained its maximum shear capacity. The complete shear load-slip history of the connections, shown in Figures 5.29 to 5.35, were, however, achieved by combining the shear load-net stroke measurements, for the particular connection, with the shear load-slip curve for that connection. The curves were extended at the point where the demec gauge was no longer functional. Combination with the stroke measurements was possible since after the maximum tion with the stroke measurements was possible since after the maximum load is reached, the net increase in slip is approximately equal to the net increase in stroke [3].

In Figures 5.43 to 5.49, the dilation-slip behaviour of all the connections tested in this programme is given. Negative dilations correspond to a decrease in the width of the connection. The figures show that as the load normal to the connection increases, the dilation decreases, as expected.

5.4 Cracking Patterns

In this section, the observed crack patterns for each of the specimens are given.

For all the connections tested, except specimen 1NK4, the crack patterns corresponding to the initiation of cracking are shown in Figures 5.51 to 5.55. In each case, diagonal cracks were initiated in the drypack shear keys.

The crack patterns observed at the end of each test, for all the connections, are shown in Figures 5.56 to 5.62. The drypack shear keys were subjected to crushing and cracks were continuous along the connection. Figures 5.63 to 5.69 show close-ups of the top and bottom of the connections, at the end of testing.

In contrast to the multiple shear key connections, the crack pattern of the no-key specimen (specimen 1NK4) was characterized by slip at the drypack-panel interface and the formation of a few cracks in the drypack, parallel to the applied preload.

Figures 5.70 to 5.76 show the crack pattern at the end of each test with the individual panels of the specimen taken apart. The notable features from these figures are (1) the lack of bond at the drypack-panel interfaces and (2) the roughness of the slip surface for the multiple shear key connections.

CHAPTER 6

DISCUSSION OF TEST RESULTS

6.1 Introduction

In this chapter, the behaviour of each specimen tested in this study is discussed.

On the basis of the test results presented in Chapter 5, the effects of the various structural parameters, including the presence and configuration of the shear keys, the load normal to the connection and the interface bond strength are determined. Consistent with the observed cracking behaviour, the mechanisms of shear transfer before and after cracking are then presented. Rational mathematical models are developed to predict the cracking, maximum and ultimate shear strengths of the shear key connections. The predicted shear capacities are compared to the test results in order to determine the reliability of the proposed models.

6.2 Specimen Behaviour

6.2.1 General

The measured loads and the observed behaviour of the multiple shear key connections tested in this programme suggest that for the large-key specimens, 1LK2 and 2LK4, and the small-key specimens, 2SK2 and 1SK4, the initiation of diagonal cracks in the drypack controlled the maximum shear capacity of the connection. For specimens 3LK4B and 3SK4B, the initiation of diagonal cracks did not coincide with the maximum shear capacity. However, the extension of initial cracks and the formation of new cracks in the drypack shear keys determined the maximum shear capacity.

The capacity of the plain surface connection, specimen 1NK4, was dependent mainly on the friction resistance along the slip surface of the connection. The ultimate shear capacity for the specimens in this experimental programme is defined as the shear load at 5 mm of slip between the individual panels. This 5 mm of slip was chosen to define the ultimate capacity because all the connections were tested to at least this value and the shear loads attained at this value were approximately constant.

In the following sections, a detailed description of the observed behaviour for each specimen is given.

6.2.2 Specimen 1NK4

Specimen 1NK4 comprised a plain surface drypack connection subjected to a preload of 4 MPa normal to the connection.

The relationship between the applied shear load and the slip in the direction of the load is shown in Figure 5.29. The curve indicates that there is no significant change in the stiffness of the connection up to a shear load level of 400 kN, after which the stiffness of the connection gradually decreased.

At the maximum load of 540 kN, and a few cracks, parallel to the applied preload, appeared in the drypack. At this stage, the shear capacity suddenly dropped by 7 percent and remained constant. The behaviour at ultimate, for this connection, was characterized by a considerable increase in the slip at constant load, as shown in Figure

5.29.

The crack pattern for specimen 1NK4 at ultimate load is shown in Figure 5.56. After the specimen was removed from the testing machine, the individual panels were taken apart in order to examine the condition of the interfaces. Based on the examination of these surfaces, shown in Figure 5.70, the following observations were made:

i. the surface cracks did not extend through the thickness of the connection;

ii. the slip surfaces were smooth;

iii. there were voids in the drypack;

iv. the slip surface area was less than the cross-sectional area of the connection.

The load-slip history of the connection and the observed slip surface suggest that no bond existed at the drypack-panel interface. Therefore, the resistance to the applied load is mainly due to shear friction along the drypack-panel interface.

6.2.2 Specimen 1LK2

Specimen 1LK2 comprised a large drypack multiple shear key connection subjected to a preload of 2 MPa normal to the connection.

Figure 5.30 shows that the initial stiffness of the connection is approximately constant up to an applied shear load of 500 kN. The corresponding slip in this range was very small. As the shear load was increased further, the stiffness of the connection decreased and diagonal cracks were initiated in the drypack keys, as shown in Figure 5.50. Initiation of these cracks corresponds to the maximum shear capacity of 569 kN for this connection.

After the maximum load was reached, an increase in slip resulted in a relatively gradual decrease in shear capacity, as shown in Figure 5.30. At ultimate load, deformation of the connection was characterized by crushing of the drypack, slip along the diagonal cracks, slip along the interfaces between the drypack keys and the initiation of surface cracks in the panels, as shown in Figure 5.57.

Similar to specimen 1NK4, the panels of specimen 1LK2 were taken apart after testing to examine the crack surface at ultimate. Figure 5.71 suggests that the resistance to the shear load at ultimate was provided by a mechanism of bearing and friction along a rough surface. Furthermore, there was no evidence of bond at the drypack-panel interface.

6.2.3 Specimen 2LK4

Specimen 2LK4 was identical in configuration to specimen 1LK2. However, it was subjected to a preload of 4 MPa normal to the connection.

In general, the behaviour of specimen 2LK4 was similar to that of specimen 1LK2. The initiation of diagonal cracks in the drypack keys coincided with the maximum shear load capacity of the connection. The shear resistance of the connection decreased after the maximum load was reached. As the slip increased further, the connection exhibited a relatively constant shear load resistance. The ultimate capacity of this connection was also characterized by crushing of the drypack and slip along the diagonal cracks and the vertical drypack-panel interface.

The relationship between the applied shear load and shear slip is shown in Figure 5.31. The increased confinement provided by the 4 MPa preload, normal to the connection, enhanced the tensile strength of the drypack and increased the shear friction resistance of the connection. As a result, both the maximum and ultimate shear capacities were higher than the capacities obtained for specimen 1LK2.

Figures 5.58 and 5.72, respectively, show the crack pattern at ultimate and after the specimen was taken apart. As for the previous connection, there was no evidence of bond at the drypack-panel interface.

6.2.4 Specimen 3LK4B

Specimen 3LK4B was similar to specimen 2LK4, except the panel joint surfaces were coated with a bond breaking agent in order to simulate the effect of shrinkage cracks at the drypack-panel interface or a lack of bond which is likely to occur when a drypack is used.

The initiation of cracks for this specimen began at a shear load of 500 kN. The cracks extended horizontally across the narrow section of the drypack shear keys. The formation of these cracks did not have any significant effect on the overall stiffness of the connection, as shown in Figure 5.32.

At a shear load of approximately 1000 kN, the first diagonal cracks appeared in the drypack shear keys. The measured maximum shear capacity of 1058 kN was characterized by extensions of the initial diagonal cracks and the formation of new diagonal cracks in some of the drypack shear keys, as shown in Figure 5.52.

Subsequent increase in stroke beyond the maximum load resulted in crushing of the drypack shear keys and the formation of cracks in the panels. The loss in load carrying capacity after reaching the maximum load was quite significant, as shown in Figure 5.32.

The crack patterns at ultimate and after the specimen was taken apart, are shown in Figures 5.59 and 5.73, respectively. As in the previous specimens, the crack pattern at ultimate revealed a similar mechanism of shear transfer which involved a combination of bearing and shear friction along a rough surface.

6.2.5 Specimen 2SK2

Specimen 2SK2 comprised a small drypack multiple shear key connection subjected to a preload of 2 MPa normal to the connection.

The observed behaviour of this specimen was similar to that of specimen 1LK2. The initiation of diagonal cracking in the drypack shear keys controlled the maximum shear capacity of the connection. After the maximum load, the shear capacity decreased then became approximately constant at large displacement, as shown in Figure 5.33.

The only significant difference in behaviour between the previous multiple shear key specimens and specimen 2SK2 was the intensity of cracking in the panels of specimen 2SK2, as shown in Figure 5.53. Spalling of the surface of the shear-key lugs was also observed at the mid-height region of the connection. At ultimate, the same mode of shear transfer described for the previous specimens was observed, as shown in Figure 5.74. In addition, there was no evidence of the presence of bond at the drypack-panel interface.

6.2.6 Specimen 1SK4

Specimen 1SK4 was similar to specimen 2SK2, except this specimen was subjected to a preload of 4 MPa normal to the connection. It should be noted that before testing, one end of the connection, approximately 156 mm x 20 mm x 100 mm, was repaired with epoxy because of the presence of large holes in the drypack.

The behaviour of specimen 1SK4 was very similar to the behaviour of specimen 2SK2. However, in comparison to specimen 2SK2, the 4 MPa preload level for specimen 1SK4 enhanced the tensile strength of the drypack and the shear friction along the slip surfaces. As a result, the load carrying capacity of specimen 1SK4 was higher than that of specimen 2SK2.

In Figure 5.34, the load-slip history indicates that after the maximum shear load was attained, there was a decrease in the shear load resistance with increasing slip displacement. However, the shear capacity was approximately constant beyond a slip displacement of 5 mm, as observed for the previous specimens.

The crack patterns at ultimate and after the panels were taken apart, are shown in Figures 5.61 and 5.75, respectively. There was no evidence of bond at the drypack-panel interface.

6.2.7 Specimen 3SK4B

Specimen 3SK4B was identical to specimen 1SK4, except, the panel joint surfaces were coated with a bond breaking agent.

The initiation of diagonal cracks in the drypack shear keys occurred at approximately 600 kN. These cracks did not extend completely across the drypack key area. Furthermore, the initiation of cracking did not have any significant effect on the stiffness of the connection, as shown in Figure 5.35.

As the applied shear load was increased, some of the existing diagonal cracks were extended and new diagonal cracks formed in the drypack, as shown in Figure 5.55. The formation of these new cracks controlled the maximum shear capacity of the connection.

Figure 5.33 shows that there was a significant loss of load carrying capacity as the stroke was increased beyond the maximum load. At large values of slip, the shear resistance was approximately constant.

The crack patterns at ultimate and after the panels were taken apart, are given in Figures 5.62 and 5.76. As in the case of specimen 1SK4, cracking in the panel, spalling of the surface of the shear-key lugs and crushing of the drypack were observed at ultimate load. In addition, there was cracking in the drypack between the shear-key lugs and there was no evidence of bond at the drypack-panel interface.

6.3 Effect of Shear Key Configuration

6.2.1 Preload of 2MPa

The shear load-slip response of the large and small multiple shear key connections tested at a preload of 2 MPa normal to the connection are shown in Figure 6.1.

The behaviour of specimen 1LK2 is virtually identical to the behaviour of specimen 2SK2. This result suggests that the differences in the shear key configuration, in this study, had no effect on the behaviour or the capacity of the connections at the 2 MPa preload level.

6.3.2 Preload of 4MPa

The shear load-slip response of the large and small multiple shear key connections tested at a preload of 4 MPa normal to the connection are given in Figure 6.2.

The resistance of specimen 2LK4 is practically identical to that of specimen 1SK4, up to the maximum load. At ultimate, the shear capacity of the large-key (LK) specimen was approximately 10 percent higher than that of the small-key (SK) specimen.

Since cracking decreases the strength of concrete, the lower ultimate shear capacity of specimen 1SK4 in comparison to specimen 2LK4 is probably due to the fact that at ultimate, more cracking occurred in the small-key connection than in the large-key connection.

The behaviour of the unbonded specimens (specimens 3LK4B and 3SK4B) tested at a preload of 4 MPa is compared in Figure 6.3. The initial stiffness of the two connections are essentially the same and the difference in ultimate capacities is comparable to the difference observed between specimens 2LK4 and 1SK4. The maximum shear capacities of specimens 3LK4B and 3SK4B are, however, quite different. On the basis of the test results, no explanation for this difference was possible, and additional tests are recommended to investigate this behaviour.

6.4 Effect of the Preload Normal to the Connection

The effect of the level of preload normal to the connection is shown in Figures 6.4 and 6.5 for the small and large multiple shear key connections, respectively. In each figure the connection behaviour is compared at the 2 MPa and 4 MPa preload levels.

It is clear from both figures that an increase in the level of preload from 2 MPa to 4 MPa substantially increases both the maximum and ultimate shear capacities. Specifically, the maximum shear capacities of specimens 2LK4 and 1SK4 were approximately 60 percent higher than those of specimens 1LK2 and 2SK2. This increase in maximum shear capacity is attributed to the enhancement of the tensile strength of the drypack and the increase in the shear friction at the drypack-panel interface as a result of an increase in confinement provided by the higher level of preload.

At ultimate, the small-key connection exhibited a 50 percent increase in shear capacity as the preload was changed from 2 MPa to 4 MPa. For the same change in preload, the large-key connection exhibited an increase of 80 percent in the ultimate load. These increases in ultimate load are attributed to the enhancement in the bearing and shear friction resistance which resulted from an increase in the confinement stresses.

From the above discussion, it is clear that the percentage increase in shear capacity is less than the percentage increase in the preload normal to the connection. Therefore, the simple shear friction theory of the ACI and CSA codes [8,7] seems inappropriate for predicting the ultimate shear capacity of multiple shear key connections.

6.5 Effect of Bond

The effect of bond may be determined by comparing the shear load-slip relationships for the bonded and unbonded specimens with similar key configurations at the 4 MPa preload level, as shown in Figures 6.6 and 6.7 for the small-key and large-key specimens, respectively.

The similarity in the curves shown in Figure 6.6 for specimens 3SK4B and 1SK4 suggests that either there was no significant bond at the drypack-panel interface of specimen 1SK4 or bond at the interface did not have any significant effect on the connection behaviour. An examination of the joint surfaces of specimen 1SK4 after testing supported the former conclusion: there was no evidence of bond at the drypack-panel interface. This lack of bond is not surprising since a dry mix was used to connect the two panel surfaces.

The curves shown in Figure 6.7 for the large-key connections indicate a behaviour that is similar to that of the small-key connection, but under initial loading and at ultimate only. The large difference in the maximum capacities of specimens 3LK4B and 2LK4 could be explained by the existence of significant bond strength at the joint interface of specimen 3LK4B. This, however, was not possible since the possibility of bond at the joint interface was eliminated prior to assembly of the specimen. Moreover, after testing, when the individual panels of specimens 3LK4B and 2LK4 were taken apart, there was no evidence of bond at the joint interface of either specimen. Therefore, the difference in maximum shear capacities cannot be explained on the basis of these test results. The test results therefore indicate that there was no evidence of bond between the drypack and the panels in any of the specimens tested. As a result, the effect of bond cannot be determined from the results of the study.

6.6 Effect of the Presence of Shear Keys

The influence of the presence of shear keys at the connection is determined by comparing the load-slip responses of specimens 1SK4 and 2LK4 with specimen 1NK4, as shown in Figures 6.8 and 6.9, respectively. In general, both figures show that the presence of shear keys at the connection can greatly enhance the shear capacity of the connection.

The maximum shear capacity may be increased by as much as 60 percent. This increase is due to the fact that, in addition to enhancement in shear friction resistance, the keyed joints are capable of resisting the applied shear by an interlocking mechanism between the adjacent panels. This interlocking mechanism is not present in the plain surface connections.

At ultimate, the capacities of specimens 1SK4 and 2LK4 were 18 and 25 percent, respectively, greater than those of specimen 1NK4. These increases in ultimate capacity are attributed to the highly roughened slip surface which resulted from diagonal cracking in the drypack shear keys. Thus, instead of only shear friction along a flat slip surface, as in the case of specimen 1NK4, the shear resistance at ultimate for the keyed specimens is provided by a combination of bearing and shear friction along a rough slip surface.

6.7 Mechanism of Shear Transfer

6.7.1 General

Based on the test results, the behaviour and shear capacity of the connections may be dependent on the following six parameters.

(1) the presence of shear keys in the joint

(2) the dimensions of the shear keys

(3) the drypack strength

(4) the concrete strength

(5) the magnitude of the preload normal to the connection

(6) the bond strength at the drypack-panel interface

For the specimens tested in this programme, there was no evidence of bond at any of the drypack-panel interfaces, as discussed in Section 6.5. Based on this observation, the mechanisms of shear transfer for the plain surface and multiple shear key connections are summarized in the following sections.

6.7.2 Plain Surface Connection

(i) Initially, the applied shear load was resisted by the friction along the drypack-panel interfaces.

(ii) The maximum load, which is required to overcome the frictional resistance, was accompanied by a relatively small amount of slip.

(iii) The ultimate shear capacity, characterized by an increase in slip under constant load, was provided by the shear friction resistance along the slip plane, as illustrated in Figure 6.10.

Based on the above mechanism of shear transfer, the ultimate shear capacity of the plain surface connection may be determined using the simple shear friction theory which is expressed as:

$$V_u = \mu \sigma_n A_c \qquad (6.1)$$

where μ = friction coefficient at the drypack-panel interface

σ_n = applied compressive stress normal to the connection

A_c = gross cross-sectional area of the connection normal to the plane of the specimen

The friction coefficient, μ, may be estimated by dividing the applied shear load at ultimate by the total load applied normal to the connection. For specimen 1NK4, the value of μ is 0.62.

In a previous study [3], which included nine plain surface connections, the friction coefficient for slip at the drypack-panel interface was calculated to be 0.7 ± 0.1. Thus, $\mu = 0.62$ for this study agrees well with the results from the previous study.

6.7.3 <u>Multiple Shear Key Connections</u>

(i) <u>Cracking</u>

Initially, the applied load is carried by friction along the drypack-panel interface and the resistance to deformation provided by the drypack shear keys. There are two possible shear friction paths, as illustrated in Figures 6.11 and 6.12. Figure 6.11 (a) suggests that shear slip may occur at the drypack-panel interface between the shear keys, at the vertical interface within the drypack keys and along the bearing inclined surface of the drypack keys. The mechanism of shear friction resistance related to the slip surface shown in Figure 6.11 (a) is illustrated in Figure 6.11 (b).

If, however, the shear keys are rectangular or very close to being rectangular, the friction path could be different as described in Figure 6.12. This friction path neglects shear friction at the interfaces around the drypack key because the shear keys are assumed not to be deformable.

Due to the difference in material properties between the drypack and the concrete, in addition to the sharp changes in geometry at the corners of the shear keys, high tensile stresses are induced at the outer corners of the drypack key, as shown in Figure 6.13 (a). This behaviour has been confirmed by finite element analyses performed recently by Zhao, et al. [12]. When the tensile stress reaches the tensile strength of the drypack, diagonal cracks are initiated in the drypack, as illustrated in Figure 6.13 (b). The presence of load normal to the connection enhances the tensile strength of the drypack and delays the onset of diagonal cracking. Thus, prior to cracking, the applied shear load is mainly resisted by the shear friction as described in Figures 6.11. or 6.12 and the tensile strength of the drypack.

On the basis of this discussion, the mechanism of shear resistance before cracking in the drypack may be described by two possible models as follows:

MODEL I

This model is based on the shear friction mechanism provided by slipping along the vertical and inclined drypack-panel bearing surfaces, in addition to the load required to initiate diagonal cracks in the drypack keys, as illustrated in Figure 6.14. Therefore, the cracking shear capacity of the connection, V_{cr}, may be estimated as:

$$V_{cr} = V^f_{cr} + V^t_{cr} \tag{6.2}$$

where V^f_{cr} = shear friction contribution

V^t_{cr} = drypack tensile strength contribution, which controls the maximum bearing stresses along the sloped edge of the drypack shear key

The shear friction contribution, V^f_{cr}, may be calculated as:

$$V^f_{cr} = \mu\sigma_n(A_c - ndt\times\tan\theta) \tag{6.3}$$

where n = number of shear keys

d = depth of the shear key

t = thickness of the connection

θ = inclination of the key

These parameters are defined in Figure 2.5.

The drypack tensile strength contribution, V^t_{cr}, may be calculated as:

$$V^t_{cr} = v_{cr}\times A_{cr} \tag{6.4}$$

where v_{cr} = cracking shear strength of the drypack

A_{cr} = total cross-sectional area of the diagonal cracks

The cracking shear strength, v_{cr}, may be evaluated by using a Mohr's circle representation for the state of stress given in Figure 6.13, as:

$$v_{cr} = \sqrt{f_t(\sigma_n + f_t)} \tag{6.5}$$

where f_t = tensile strength of the drypack

The tensile strength of the drypack could be estimated as [13]:

$$f_t = 0.6\sqrt{f'_g} \tag{6.6}$$

where f'_g = equivalent standard cylinder compressive strength of the drypack

The total cross-sectional area of the diagonal cracks can be computed as:

$$A_{cr} = nt\sqrt{h^2 + b^2} \tag{6.7}$$

where h = maximum height of the shear key

b = width of the drypack between shear-key lugs

These parameters are also defined in Figure 2.5.

Accordingly, the shear resistance based on Model I may be estimated as follows:

$$V_{cr} = \mu\sigma_n(A_c - \text{ndtxtan}\ \theta) + \sqrt{f_t(\sigma_n + f_t)}\ A_{cr} \tag{6.8}$$

MODEL II

Model II is essentially the same as Model I, except, no slip is assumed to occur at the interfaces around the drypack shear key, as shown in Figure 6.16. This assumption is admissible since striations--an indicator of scraping action--were observed only at the drypack-panel interfaces between the shear keys. As a result, the shear strength of the connection, based on Model II, may be estimated as:

$$V_{cr} = \mu\sigma_n(A_c - nht) + \sqrt{f_t(\sigma_n + f_t)}\, A_{cr} \qquad (6.9)$$

Based on the material properties and the shear key configuration of the connections tested in this study and using a friction coefficient of $\mu = 0.6$, the shear capacity of the small and large multiple shear key connections, at cracking, were determined using the proposed models. The results are compared to the test results in Table 6.1 and Figure 6.17.

From Figure 6.17, it can be seen that Model I provides more accurate predictions of the cracking shear load, however, the capacities of three of the six connections tested are overestimated. Model II, on the other hand, provides more conservative predictions of the cracking load for design purposes. This figure also indicates that a higher levels of preload, Model II becomes more conservative.

Appendix C provides sample calculations based on Models I and II for specimen 2SK2. Calculation of the shear capacity of the other connections may be done in a similar manner using the material strength data given in Table 4.2 and the connection configuration data given in Figures 3.3 and 3.4.

(ii) Immediately after Cracking

After cracking, the ability of the drypack to carry tensile stresses is significantly reduced. As a result, the applied shear load is mainly resisted by a system of struts between the diagonal cracks and shear friction along the slipped surfaces, as shown in Figure 6.18.

The shear resistance contribution provided by the strut mechanism depends mainly on the compressive resistance of the cracked drypack and the size of the strut. Thus, for a high strength drypack, the multiple shear key connection may be capable of resisting a higher shear load than the load required to initiate diagonal cracks. This behaviour was observed for the pilot multiple shear key connection tested by Foerster [3], as shown in Figure 6.19. On the other hand, a connection with a relatively low drypack strength may not have sufficient capacity to accommodate a full redistribution of the cracking shear load. In this instance, the cracking load would represent the maximum shear capacity of the connection, as was observed in the present study.

Based on the preceding discussion, the shear capacity, V_a, immediately after cracking in the multiple shear key connections may be calculated as:

$$V_a = V_a^s + V_a^f \tag{6.10}$$

where V_a^s = shear resistance of the strut mechanism

V_a^f = shear friction resistance along the slip surface

These two components of shear resistance will be discussed individually as follows:

(a) Shear Resistance of the Strut Mechanism (V_a^s)

The panels may be assumed to act as rigid planes connected by n-1 struts, as shown in Figure 6.20 (a), where n represents the number of shear keys in the connection. The vertical portion of the strut is under high confinement stresses from the load normal to the connection whereas the inclined portions are bounded on one side by a crack. Since cracked concrete is weaker than uncracked concrete [14,15], the compressive axial capacity of the inclined portion of the strut will control the capacity of the strut.

The compressive strength, P, of the strut may be estimated as:

$$P = \psi f_g' t(w) \tag{6.11}$$

where ψ = compressive strength reduction factor

w = average width of the inclined portion of the strut

The reduction factor ψ, accounts for the decrease in compressive strength of the drypack as a result of diagonal cracking.

The average width of the inclined portion of the strut may be estimated as:

$$w = \frac{1}{2} \frac{(b + d)}{\cos \theta} \tag{6.12}$$

where $b/\cos\theta$ and $d/\cos\theta$ are as defined in Figure 6.18.

From statics, as shown in Figures 6.20 (b) and 6.21, the shear resistance of the strut mechanism, V_a^s, can be predicted by the vertical component of the compressive force in the strut as:

$$V_a^s = (n-1)P\sin\alpha \tag{6.13}$$

where α = inclination of the diagonal crack

$$= \tan^{-1}(h/b) \tag{6.14}$$

(b) <u>Shear Friction Resistance (V_a^f)</u>

The resistance provided by shear friction consisted of two parts: (1) shear friction along the vertical slip surfaces between the drypack shear keys and (2) shear friction along the diagonal cracks. Figure 6.21 indicates that the horizontal component of the strut forces reduces the compressive load normal to the connection from N to N'. Thus, based on the net normal compressive load, the shear friction resistance may be evaluated as:

$$V_a^f = \mu(\sigma_n - \frac{(n-1)P\cos\alpha)}{A_c}(A_c - nht)$$
$$+ \mu_d(\sigma_n - \frac{(n-1)P\cos\alpha)}{A_c}(nht) \tag{6.15}$$

where μ_d = coefficient of friction along the drypack diagonal cracks. The first term of Equation 6.15 represents the shear friction along the vertical slip surfaces while the second term represents the shear friction along the diagonal crack. Conservatively, μ_d may be assumed equal to μ and equation 6.15 may be simplified as follows:

$$V_a^f = \mu(\sigma_n - \frac{(n-1)P\cos\alpha}{A_c})A_c \tag{6.16}$$

Thus, the shear resistance, V_a, of the connection immediately after cracking may be estimated as:

$$V_a = (n-1)P\sin\alpha + \mu(\sigma_n - \frac{(n-1)P\cos\alpha}{A_c})A_c \tag{6.17}$$

For each connection tested, the compressive strength reduction factor, ψ, was calculated by equating V_a to V_{max}, the maximum shear load. Rearranging, the terms of equation 6.17 and setting $V_a = V_{max}$ gives:

$$\psi = \frac{V_{max} - \mu\sigma_n A_c}{(\sin\alpha - \mu\cos\alpha)(n-1)f_g'tw} \tag{6.18}$$

Table 6.2 shows the calculated values of ψ for each connection tested using Equation 6.18. The difference in the ψ values between the connections suggests that the large drypack shear keys have a higher after-cracking compressive strength than the small drypack shear keys and an increase in the level of load normal to the connection also increases the compressive strength of the cracked drypack. Collins and Mitchel [15,16] suggested that the maximum compressive strength of cracked concrete, f_{cmax}, may be taken as:

$$f_{cmax} = \frac{f'_c}{0.8 + 170\epsilon_1} \leq f'_c \tag{6.19}$$

where ϵ_1 = average principal tensile strain in the cracked concrete

f'_c= cylinder compressive strength of the concrete.

In terms of the compressive strength reduction factor, Equation 6.19 becomes:

$$\psi = \frac{1}{0.8 + 170\epsilon_1} \leq 1.0 \tag{6.20}$$

Equation 6.20 is assumed to be applicable to the cracked drypack shear keys. In applying this equation, f'_c is taken as the equivalent standard cylinder compressive strength of the drypack, f'_g as given in Table 4.2.

From Tables 5.8 to 5.14, it is evident that ϵ_1 depends on the level of load normal to the connection. Table 6.2 gives the calculated values of ψ based on Equation 6.20. From this table, it can be seen that the calculated values of ψ, based on the model (Equation 6.18), are in good agreement with the ψ factors predicted by Equation 6.20.

In general, for the multiple shear key connections tested in this study, the average principal tensile strain at cracking, ϵ_1, ranged between 0.0026 and 0.004 strain. Therefore, based on these limited test results, the average strain for all the multiple shear key connections tested in this study may be conservatively estimated as 0.005 strain.

The corresponding value of ψ, using Equation 6.20, is 0.60. As more data become available, a more accurate procedure could be developed to estimate ψ based on the level of preload and size of the shear keys.

The predicted shear capacities of the multiple shear key connections after cracking are compared to the measured maximum shear capacities in Table 6.3 and Figure 6.22.

Since the maximum shear load also defines the cracking load in this study, the proximity of the data points to the line of equality between the predicted load after cracking and the measured maximum load, shown in Figure 6.22, suggests that mechanism of shear resistance immediately after cracking is capable of transferring the same shear load as that required to cause cracking. This observation is corroborated by the shear load-slip relationships shown in Figures 5.30 to 5.35. In these figures, there is no sudden loss in load-carrying capacity after the maximum shear load is reached.

Appendix C provides a sample calculation for this model, using specimen 2SK2. Calculations for the other multiple shear key connections may be done in a similar manner using the material strength data given in Table 4.2 and the connection configuration data given in Figures 3.3 and 3.4.

(iii) <u>Ultimate</u>

The behaviour of the multiple shear key connections, at ultimate, was characterized by a significant increase in slip at an approximately constant load. As a result, the ultimate shear capacity was dependent on a combination of the shear friction and bearing resistance along the slip surface, as indicated in Figures 5.70 to 5.76.

A linear multiple regression analysis was used to develop a mathematical model to predict the ultimate shear capacity of the connections. A linear regression model was chosen based on the work of Hansen, et al. [5], Cholewicki [4] and Chakrabarti [6]. These researchers have suggested that linear modelling is appropriate due to the wide scatter of data.

The basis of the multiple regression model is to relate the dependent parameter, in this instance the ultimate shear load, to a set of independent parameters. The two independent parameters considered to be important in the model for determining the ultimate shear capacity of the multiple shear key connections are, in normalized form, B/A_c which represents the ratio of the shear key area to the cross-sectional area of the connection ($B = nht$) and σ_n/f'_g which represents the ratio of the stress applied normal to the connection to the equivalent standard cylinder compressive strength of the drypack. The dependent parameter is also used in the normalized form as $\bar{v}_u/f'_g$ which represents the ratio of the average ultimate stress to the equivalent standard cylinder compressive strength of the drypack ($\bar{v}_u = V_u/A_c$).

The required form of the regression model is:

$$\frac{\bar{v}_u}{f'_g} = C_0 + C_1 \frac{B}{A_c} + C_2 \frac{\sigma_n}{f'_g} \tag{6.21}$$

where C_0, C_1 and C_2 are coefficients to be determined from the analysis. These coefficients were determined using the data given in Table 6.4 and the "Number Cruncher Statistical System" software package for the PC.

The ultimate shear capacity of the tested multiple shear key connections was subsequently estimated as:

$$\frac{\bar{v}_u}{f'_g} = 0.024 + .025 \frac{B}{A_c} + 0.556 \frac{\sigma_n}{f'_g} \tag{6.22}$$

Further investigation of the model given by Equation 6.22 revealed that the standard error in the $\frac{B}{A_c}$ and $\frac{\sigma_n}{f'_g}$ coefficients were 0.045 and .062, respectively. The standard error in the $\frac{B}{A_c}$ coefficient is quite significant. As a result, the $\frac{B}{A_c}$ parameter was considered not to be relevant for the present study and it was consequently neglected in the analysis. This is consistent with the behaviour discussed in Section 6.3, which indicated that the difference in shear key configuration had no significant effect on the shear capacity of the connection.

Using a simple linear regression analysis model of the form:

$$\frac{\bar{v}_u}{f'_g} = C_0 + C_1 \frac{\sigma_n}{f'_g} \tag{6.23}$$

and the data given in Table 6.4, the ultimate shear capacity of the multiple shear key connections may be estimated as:

$$\frac{\bar{v}_u}{f'_g} = 0.035 + 0.556 \frac{\sigma_n}{f'_g} \tag{6.24}$$

The standard error in the $\frac{\sigma_n}{f'_g}$ coefficient is 0.0049. Equation 6.24 may be re-written to give the ultimate shear load directly as:

$$V_u = 0.035\ f_g' A_c + 0.556\ \sigma_n A_c \tag{6.25}$$

Equation 6.25 could be further simplified as follows:

$$V_u = 0.2\ \sqrt{f_g'} A_c + \frac{\sigma_n A_c}{2} \tag{6.26}$$

The first term of Equation 6.26 was calculated by taking two extreme values of the drypack compressive strength (20 MPa and 40 MPa) and equating $.035f_g'$ to $\gamma\sqrt{f_g'}$. The average value of γ for f_g' of 20 MPa and 40 MPa, 0.2, was then used for γ in the equation. The first term of Equations 6.25 and 6.26 represent the bearing resistance to the applied shear load. In the second term, instead of using 0.556, the coefficient may be conservatively estimated as 0.5. This term represents the shear friction resistance of the connection at ultimate.

The predicted ultimate shear capacity of the tested connections, based on Equations 6.25 and 6.26, are compared to the test results in Table 6.5 and Figure 6.23. From Figure 6.23, it is evident that the simplified equation agrees well with the model developed directly from the statistical analysis. The predicted ultimate loads are also in good agreement with the measured loads.

Appendix C provides sample calculations of the predicted ultimate shear capacity based on the models given by Equations 6.25 and 6.26, for specimen 2SK2. Similar calculations can be done for the other multiple shear key specimens using the data given in Table 4.2 and Figures 3.3 and 3.4.

Summarizing, equations were derived to predict the shear capacity of multiple shear key connections at various limits states including:

i. <u>Cracking</u>

MODEL I : $V_{cr} = \mu\sigma_n(A_c - ndt\times\tan\theta) + \sqrt{f_t(\sigma_n + f_t)}\, A_{cr}$

MODEL II : $V_{cr} = \mu\sigma_n(A_c - nht) + \sqrt{f_t(\sigma_n + f_t)}\, A_{cr}$

ii. <u>Immediately After Cracking</u>

$$V_a = (n-1)P\sin\alpha + \mu\left[\sigma_n - \frac{(n-1)P\cos\alpha}{A_c}\right]A_c$$

iii. <u>Ultimate</u>

$$V_u = 0.2\sqrt{f_g'}\,A_c + \frac{\sigma_n A_c}{2}$$

CHAPTER 7

SUMMARY AND CONCLUSIONS

7.1 Summary

The main objective of this research programme was to investigate the behaviour of multiple shear key connections for precast concrete load-bearing shear wall panels under static shear loading, at various limit states. These limit states are: the initiation of cracks, the maximum shear capacity and the ultimate shear capacity.

Seven prototype specimens were tested in the experimental programme. The specimens consisted of three different joint configurations. The three types of joint configuration used were:

NK series : drypack plain surface connection

LK series : large drypack multiple shear key connection

SK series : small drypack multiple shear key connection

To investigate the effects of dead load and post-tensioning, the multiple shear key connections were subjected to two different levels of load normal to the connection. The effect of cracks or the absence of bond at the joint interface was also studied by the eliminating bond at the joint interface in two multiple shear key connections.

7.2 CONCLUSIONS

Based on the test results of the seven specimens tested in this study and one specimen tested in a previous study [3], the following conclusions can be drawn:

1. The use of a high strength drypack may change the mode of failure

of multiple shear key connections from cracking in the drypack shear keys to cracking in the shear-key lugs of the panels.

2. The difference in the shear key configurations had no significant effect on the behaviour or capacity of the connection.
3. An increase in the level of compressive preload normal to the connection increases the shear capacity of the connection. However, the percentage increase in shear capacity is less than the percentage increase in the preload.
4. The presence of shear keys in the connection increases the shear capacity of the connection in comparison to a plain surface connection.
5. The cracking load of the multiple shear key connection may be safely estimated using design Model II. The resistance to cracking is provided by shear friction at the slip surfaces and the tensile strength of the drypack. Under moderate levels of load normal to the connection, the drypack tensile strength contributes more to the resistance of the connection.
6. The mathematical model developed to predict the shear capacity of the multiple shear key connection, immediately after cracking, is in good agreement with the test results. The resistance to shear is provided by shear friction along the slip surface and the compressive strength of the struts which form as a result of diagonal cracking in the drypack shear keys. The more significant resistance contribution is provided by the compressive strength of the strut.
7. The predicted ultimate shear capacity of the multiple shear key

connections are in good agreement with the test results. The ultimate shear resistance is dependent on the shear friction along the slip surface and bearing resistance due to the roughness of the slip surface. Under moderate levels of load normal to the connection, the shear friction component provides the higher resistance of the two components.

7.3 Recommendations for Future Research

1. Multiple shear key connections with significantly different key dimensions and areas should be tested in order to fully understand the effect of the key dimensions.
2. Tests should be conducted to investigate the capacity of reinforced multiple shear key connections.
3. Research is needed to investigate the combined effect of flexural, shear and axial loading on multiple shear key connections.
4. The behaviour of multiple shear key connections under repeated loading should also be studied.

REFERENCES

1. Council on Tall Buildings and Urban Habitat, Structural Design of Tall Concrete and Masonry Buildings, American Society of Civil Engineers, Vol. CB, 1978.

2. Fintel, M., ed., Handbook of Concrete Engineering, Van Nostrand Reinhold Company, New York, New York, 1985.

3. Foerster, H.R., "Behaviour of the Connections Typically Used in Precast Concrete Load-Bearing Shear Wall Panels", a thesis presented to the University of Manitoba in partial fulfillment of the requirements for the degree of Master of Science in Structural Engineering, June, 1987.

4. Cholewicki, A., "Loadbearing Capacity and Deformability of Vertical Joints in Structural Walls of Large Panel Buildings", Building Science, Vol. 6, No. 1, May, 1971, pp. 163-184.

5. Hansen, K., et al., "Keyed Shear Joints", SBI-Rapport 97, Danish Building Research Institute, Statens Byggeforskningsinstitut, 1976, 33pp.

6. Chakrabarti, et al., "Shear Characteristics of Cast-in-Place Vertical Joints in Storey-High Precast Wall Assembly", ACI Structural Journal, Vol. 85, No. 1, January-February, 1988.

7. Canadian Standards Association (CSA), "Design of Concrete Structures for Buildings (CAN3-A23.3-M84)", Rexdale, Ontario, 1984.

8. American Concrete Institute, "Building Code Requirements for Reinforced Concrete (ACI 318M-83)", Detroit, Michigan, 1984.

9. Speyer, I.J., "Considerations for the Design of Precast Concrete Bearing Wall Buildings to Withstand Abnormal Loads", PCI Journal, Vol. 21, NO. 2, March-April, 1976, pp. 18-51.

10. Canadian Standards Association (CSA), "Concrete Materials and Methods of Concrete Construction (CAN3-A23.1-M77)", Rexdale, Ontario, 1977.

11. Soroka, I., Portland Cement Paste and Concrete, Chemical Publishing Co., Inc., New York, New York, 1979.

12. Zhao, Z.C., et al., "Analysis and Optimum Design of the Multiple Shear Key Connections Used for Precast Wall Panels", abstract submitted to the International Conference on Computing in Civil Engineering, Vancouver, British Colombia, 1988.

13. Park, R. and Pauley, T., Reinforced Concrete Structures, John Wiley and Sons, New York, New York, 1975.

14. Hsu, T.T.C., et al., "Theory of Shear Transfer Strength of Reinforced Concrete", ACI Structural Journal, Vol. 84, No. 2, March-April, 1987.

15. Collins, M.P., Personal Correspondence, 26 May, 1988.

16. Collins, M.P. and Mitchell, D., Prestressed Concrete Basics, Ottawa, Ontario, 1987.

Table 2.1 Friction Coefficients

Type of Surface	Friction Coefficient**	
	ACI	CSA
Cracked monolithic concrete	1.4 λ	1.25 λ
Intentionally roughened surface*	1.0 λ	0.9 λ
Non-intentionally roughened surface	0.6 λ	0.5 λ

* surface intentionally roughened to a maximum amplitude of 5 mm.

** λ = 1.0 for normal density concrete

λ = .85 for semi-low density concrete

λ = .75 for low density concrete

Table 4.1 PANEL CONCRETE STRENGTH

Specimen	Compressive Strength at the Time of Testing (MPa)	Tensile Splitting Strength at the Time of Testing (MPa)
1NK4	49.1 ± 0.9	12.9 ± 1.3
1LK2	42.6 ± 0.2	13.4 ± 1.6
2LK4	30.4 ± 0.4	11.1 ± 0.1
3LK4B	46.5 ± 2.6	15.0 ± 1.8
2SK2	44.0 ± 0.2	13.4 ± 1.6
1SK4	29.3 ± 1.0	11.0 ± 0.5
3SK4B	49.5 ± 0.5	13.2 ± 2.2

Table 4.2 DRYPACK STRENGTH

Date of Packing	Average Compressive Strength at the Time of Testing (MPa)	
	Cube Strength, f'_g	Equivalent Cylinder Strength, f'_g
87 07 13 (BM)*	36.46 ± 2.85	26.62 ± 2.08
87 07 13 (WM)**	25.07 ± 2.40	18.30 ± 1.75
87 07 14 (WM)**	23.45 ± 2.04	17.12 ± 1.49

* concrete mould

** wooden mould

- specimens 1NK4, 2SK2 and 1SK4 were drypacked on 87 07 13
- specimens 1LK2, 2LK4, 3LK4B and 3SK4B were drypacked on 87 07 14

Table 4.3 SUMMARY OF EXPERIMENTAL SHEAR STRENGTHS

Joint Configuration	Specimen	Diagonal Cracking Load (kN)	Maximum Load (kN)	Ultimate Load (kN)*
LK	1LK2	569	569	418
	2LK4	867	867	688
	3LK4B	1000	1058	624
SK	2SK2	559	559	419
	1SK4	884	884	622
	3SK4B	893**	893	648
NK	1NK4	540	540	507

* defined at 5.0 mm of slip

** appearance of diagonal cracks at 600 kN, but no loss of stiffness

Table 4.4 Demec Readings for Specimen 1NK4

DEMEC POINT	L O A D	V (kN)	0	0	100	200	300	400	500	516	532	540	515	518	511
		M (MPa)	0	4	4	4	4	4	4	4	4	4	4	4	4
	DIRECTION		DEMEC READINGS												
	D1		865	832	825	817	804	782	698	638	564	505	285		
1A	D2		940	898	901	905	910	925	1010	1070	1145	1209	1451	2143	
	H		893	835	836	835	832	830	831	833	837	844	862	941	1048
	D1		846	816	811	807	798	781	696	637	565	506	284		
2A	D2		931	889	891	896	901	914	993	1057	1130	1194	1429	2102	
	H		886	830	830	833	831	829	828	832	835	840	851	903	978
	D1		827	794	786	778	765	745	661	599	528	466	240		
3A	D2		937	895	897	901	911	922	1000	1060	1133	1194	1423	2079	
	H		896	840	836	835	836	831	828	831	835	836	839	869	820
	D1		915	916	916	916	915	915	908	912	913	910	911	911	910
1B	D2		906	904	905	906	907	907	905	908	908	909	908	909	907
	V		920	922	922	922	922	923	919	921	922	919	918	916	913
	D1		988	901	903	909	913	927	997	1055	1129	1187	1421	2073	
2B	D2		889	811	808	801	788	762	630	535	420	325			
	H		913	793	793	789	784	776	735	711	679	657	579	346	105
	D1		969	968	968	966	966	967	965	969	967	968	968	974	969
3B-L	D2		886	882	882	885	880	882	882	882	881	881	880	886	882
	H		930	924	924	924	924	924	926	926	926	925	927	932	926
	D1		974	890	892	896	900	913	979	1030	1102	1159	1380	2000	
3B-M	D2		856	785	783	777	765	739	608	511	396	298			
	H		906	786	788	786	782	773	730	702	672	644	558	206	42
	D1		922	918	920	921	919	923	922	922	923	920	921	925	923
3B-R	D2		919	917	917	916	915	915	916	916	916	915	914	917	916
	H		919	911	914	913	913	913	915	915	915	914	915	919	917
	D1		956	862	863	869	875	889	957	1013	1080	1142	1359	1978	
4B	D2		824	738	731	723	706	675	540	438	320	220			
	H		908	770	770	768	768	753	708	681	650	624	532	273	
	D1		910	912	912	913	910	907	907	905	904	903	902	904	903
5B	D2		920	921	921	921	922	922	923	923	923	921	923	922	920
	H		916	916	916	916	915	916	914	912	913	910	911	912	911

Table 4.5 Demec Readings for Specimen 1LK2

DEMEC POINT	LOAD														
	V (kN)	0	0	100	200	300	400	500	521	491	455	423	407	367	361
	M (MPa)	0	2	2	2	2	2	2	2	2	2	2	2	2	2
	DIRECTION	DEMEC READINGS													
	D1	707	748	738	725	713	695	671	420	247	3				
1A	D2	185	162	166	179	191	212	240	666	870	1146	1630	2135		
	H	940	878	878	879	881	882	889	1019	1051	1077	1111	1142	1247	1302
	D1	882	828	821	814	804	789	766	542	376	129				
2A	D2	926	915	917	925	934	952	981	1402	1614	1896	1894			
	H	902	849	852	853	856	859	867	996	1029	1055	1087	1115	1200	1246
	D1	856	822	813	799	788	769	740	485	313	70				
3A	D2	911	915	917	928	937	956	988	1399	1613	1889	1879			
	H	890	856	856	857	862	866	867	987	1022	1049	1090	1124	1219	1281
	D1	911	914	915	911	911	908	905	905	906	906	907	907	909	
1B	D2	921	926	928	925	925	925	926	925	926	928	928	927	926	
	V	908	908	909	907	906	904	902	902	903	904	904	905	905	
	D1	915	912	914	913	914	913	916	915	914	914	915	914	915	915
2B-L	D2	921	920	922	921	920	918	918	915	916	916	918	917	918	919
	H	914	911	914	913	914	914	914	912	913	913	913	912	913	914
	D1	920	919	920	920	920	919	920	920	918	920	917	918	918	918
2B-R	D2	913	912	912	911	910	909	907	902	902	905	905	907	910	911
	H	912	909	909	909	910	910	911	911	910	910	909	909	910	911
	D1	1255	1256	1258	1259	1260	1262	1266	1618	1719	1839				
2B-M	D2	891	890	890	890	889	886	873	731	666	604				
	H	1123	1129	1130	1129	1130	1132	1131	1272	1286	1336				
	D1	891	891	894	893	894	895	896	1097	1168	1262				
3B-M	D2	544	545	549	548	546	547	540	473	439	427				
	H	1354	1354	1357	1357	1359	1359	1363	1512	1557	1632				
	D1	909	908	908	908	908	908	909	909	894	910	909	912	909	908
3B-L	D2	900	907	905	905	904	903	901	895	908	895	896	898	900	902
	H	1012	910	910	910	911	910	910	908	917	907	907	908	909	909
	D1	915	911	912	913	914	915	915	914	907	914	913	914	914	913
3B-R	D2	909	911	910	910	908	907	905	906	908	907	908	909	911	911
	H	910	908	908	908	908	908	908	906	908	908	909	910	910	911
	D1	911	913	911	910	908	906	904	903	904	905	905	905	904	
4B	D2	908	912	913	914	913	914	913	913	915	915	914	914	915	
	V	915	916	917	916	915	914	911	912	913	912	913	913	913	

Table 4.6 Demec Readings for Specimen 2LK4

DEMEC POINT	L O A D	V (kN)	0	0	100	200	300	400	500	600	700	800	839	749	715	716
		M (MPa)	0	4	4	4	4	4	4	4	4	4	4	4	4	4
	DIRECTION								DEMEC READINGS							
1A	D1			780	773	766	757	745	737	720	706	676	480	162		
	D2			923	918	923	931	937	941	954	973	1002	1258	1594	2010	
	H			792	792	793	793	791	792	794	796	800	837	860	871	
2A	D1			766	761	755	751	740	734	722	707	680	490	181		
	D2			866	868	871	877	880	886	897	912	943	1206	1551	1970	
	H			811	810	811	813	814	816	819	824	831	883	909	917	
3A	D1			775	767	757	750	738	729	710	691	655	444	131		
	D2			794	895	903	910	912	920	932	955	995	1266	1608	2024	
	H			796	799	799	800	801	801	800	802	814	860	883	891	
1B	D1		914	912	909	902	901	897	896	894	887	888	887	886	883	886
	D2		913	914	914	911	912	913	914	915	913	916	915	915	913	914
	V		911	912	913	910	920	910	911	908	907	904	905	906	906	906
2B-L	D1		919	912	910	914	915	914	912	918	918	920	918	918	916	918
	D2		915	911	910	911	910	908	908	909	906	904	903	905	907	908
	H		879	874	870	873	871	871	873	874	872	872	873	874	876	877
2B-R	D1		918	915	913	916	913	913	914	914	915	913	915	915	915	916
	D2		914	913	912	914	912	911	911	911	911	908	906	907	908	910
	H		911	906	902	905	904	903	905	906	907	905	907	907	905	907
2B-M	D1		950	951	947	949	949	950	952	953	954	966	1202	1267		
	D2		946	948	945	946	947	946	947	945	940	932	960	1014		
	H		945	948	944	946	945	944	946	945	947	953	1135	1213		
3B-M	D1		544	544	540	541	540	541	544	543	545	548	649	799		
	D2		916	818	815	816	815	816	816	814	811	805	812	816		
	H		935	937	935	935	935	934	937	937	937	938	1023	1165		
3B-L	D1		916	912	907	910	910	909	910	912	912	912	915	913	909	
	D2		914	911	908	909	909	908	908	907	905	902	898	901	900	
	H		920	907	904	904	905	906	908	908	908	910	910	906	900	
3B-R	D1		915	912	910	911	912	914	915	914	914	916	917	918	916	
	D2		914	912	908	908	907	907	907	905	902	901	901	888	885	
	H		917	907	905	905	906	907	908	909	907	908	907	900	897	
4B	D1		917	917	914	916	915	914	908	905	903	897	900	900	899	899
	D2		921	921	920	920	921	922	923	921	921	922	923	922	921	924
	V		906	906	905	905	905	905	904	900	897	893	893	893	893	894

Table 4.7 Demec Readings for Specimen 3LK4B

DEMEC POINT	LOAD														
	V (kN)	0	0	100	200	300	400	500	600	700	800	900	1000	1058	800
	M (MPa)	0	4	4	4	4	4	4	4	4	4	4	4	4	4
	DIRECTION	DEMEC READINGS													
	D1	855	810	805	797	788	778	767	754	736	717	694	645	454	
1A	D2	954	886	892	895	900	910	919	929	942	967	1000	1084	1385	2001
	H	892	802	806	801	806	807	806	805	810	812	820	847	920	946
	D1	854	814	810	804	798	789	781	771	757	740	721	685	497	
2A	D2	932	870	875	876	882	888	895	905	919	940	969	1052	1347	1956
	H	894	815	815	814	817	820	820	823	825	829	839	871	949	984
	D1	841	808	798	791	783	772	761	748	731	712	692	640	405	
3A	D2	937	891	889	896	901	910	920	929	945	970	1006	1091	1399	2013
	H	897	826	827	825	826	828	827	830	833	835	839	865	922	945
	D1	926	998	992	982	978	974	970	968	965	961	958	957	957	957
1B	D2	925	994	994	994	994	994	996	996	996	997	997	998	998	997
	V	907	965	964	964	962	962	961	961	958	956	953	952	952	955
	D1	925	984	984	984	984	982	983	985	987	987	987	987	989	989
2B-L	D2	923	990	991	991	989	989	987	987	985	982	980	979	968	962
	H	912	973	973	973	973	973	973	974	975	976	977	977	973	970
	D1	915	977	977	978	978	978	978	978	979	979	980	981	983	982
2B-R	D2	921	991	991	989	989	987	988	986	987	985	980	975	971	977
	H	914	974	974	975	975	976	976	977	978	978	980	980	982	981
	D1	919	983	984	983	984	985	985	984	985	987	989	1049	1384	
2B-M	D2	915	982	981	981	981	981	982	982	980	976	971	958	792	
	H	897	961	962	961	961	962	962	962	962	963	964	1000	1068	
	D1	932	994	994	994	995	995	995	996	997	999	1000	1001	1249	1700
3B-M	D2	914	983	983	982	982	981	982	980	979	974	967	958	923	961
	H	960	1026	1025	1025	1025	1025	1025	1025	1026	1026	1026	1030	1149	1228
	D1	926	985	984	984	985	985	985	985	985	986	986	988	990	987
3B-L	D2	931	994	993	995	994	994	994	993	992	990	988	981	973	980
	H	915	968	968	968	968	969	969	970	971	972	973	973	973	973
	D1	915	973	971	972	973	973	974	974	976	978	979	980	979	978
3B-R	D2	922	985	983	983	982	980	981	979	975	973	970	965	955	898
	H	922	978	977	977	978	978	979	979	980	981	983	984	979	979
	D1	918	977	975	975	974	973	973	972	969	967	964	962	962	965
4B	D2	919	987	987	987	986	986	988	988	988	989	988	988	988	988
	V	912	981	981	981	982	981	981	980	978	975	973	970	970	975

Table 4.8 Demec Readings for Specimen 2SK2

DEMEC POINT	LOAD											
	V (kN)	0	0	100	200	300	400	500	559	509	456	418
	N (MPa)	0	2	2	2	2	2	2	2	2	2	2
	DIRECTION	DEMEC READINGS										
1A	D1	857	841	832	819	801	779	742	657	487	193	
	D2	924	890	896	902	915	940	990	1162	1463	1906	
	H	898	863	863	861	863	865	876	941	1035	1144	
2A	D1	717	705	699	690	680	665	647	578	404	100	
	D2	924	895	896	904	917	938	979	1139	1436	1869	
	H	892	860	860	861	862	865	887	955	1044	1135	
3A	D1	855	844	833	819	798	779	742	645	462	138	
	D2	927	898	906	914	929	952	995	1148	1435	1850	
	H	885	857	856	855	856	859	864	910	985	1057	
1B	D1	925	925	923	919	919	919	918	913	916	913	916
	D2	921	919	924	924	922	921	923	922	922	923	922
	V	913	914	913	914	911	917	907	904	915	905	906
2B-L	D1	920	919	919	916	920	918	921	920	925	919	920
	D2	916	914	914	914	913	912	910	909	913	911	914
	H	909	904	906	905	904	906	904	905	908	909	907
2B-R	D1	916	914	919	914	918	912	915	916	919	915	911
	D2	911	914	915	913	913	911	912	903	899	907	910
	H	916	917	916	914	915	916	917	914	914	918	916
2B-M	D1	923	926	926	926	926	924	924	917	1057	1451	
	D2	923	925	926	925	926	926	928	936	927	939	
	H	902	905	905	907	906	905	906	912	1094	1369	
3B-M	D1	915	925	927	925	922	925	943	1042	1134	1326	
	D2	964	964	964	962	959	958	955	948	967	969	
	H	952	954	955	955	954	955	965	1030	1083	1235	
3B-L	D1	929	926	923	924	928	926	924	931	913		
	D2	937	934	932	931	929	925	919	910	806		
	H	882	872	872	873	872	873	874	877	863		
3B-R	D1	927	923	923	925	924	922	925	928	923	909	
	D2	913	908	907	908	907	905	904	897	874	810	
	H	906	897	898	899	898	895	897	894	872	773	
4B	D1	926	922	921	918	914	911	907	913	909	906	903
	D2	910	912	911	912	915	914	914	904	917	915	912
	V	910	911	909	906	903	898	898	897	898	898	898

Table 4.9 Demec Readings for Specimen 1SK4

DEMEC POINT	LOAD															
	V (kN)	0	0	100	200	300	400	500	600	700	800	884	840	724	672	621
	M (MPa)	0	4	4	4	4	4	4	4	4	4	4	4	4	4	4
	DIRECTION	DEMEC READINGS														
	D1	718	673	663	648	628	605	580	553	520	474	300	280			
1A	D2	925	862	867	865	881	890	905	932	950	1003	1176	1194	1507	1862	33
	H	890	804	804	803	799	797	794	793	793	797	802	805	802	802	828
	D1	853	818	813	804	791	777	760	743	725	699	569	554	240		
2A	D2	907	850	854	859	867	878	893	909	930	974	1175	1185	1524	1885	39
	H	870	797	799	799	798	799	799	804	808	821	867	870	881	889	957
	D1	855	825	817	808	793	775	756	737	713	682	538	516	201		
3A	D2	910	869	875	878	886	901	915	932	953	998	1201	1221	1568	1947	39
	H	889	833	833	833	832	832	834	832	835	847	892	892	913	938	1055
	D1	909	909	911	914	912	909	906	903	901	900	899	900	900	901	904
1B	D2	928	930	930	934	934	934	933	933	934	935	935	935	934	934	936
	V	912	913	913	914	919	917	915	909	905	908	904	898	902	909	912
	D1	914	908	909	910	910	910	910	908	910	919	923	925	936	892	
2B-L	D2	909	905	906	907	906	904	905	899	896	886	864	863	908	752	
	H	917	900	902	902	903	901	902	900	900	900	897	896	930	679	
	D1	903	899	905	901	902	902	902	901	900	900	904	906	900		
2B-R	D2	916	911	912	912	911	910	907	906	906	905	891	890	868		
	H	909	889	891	892	891	891	891	890	890	891	888	887	848		
	D1	924	920	924	930	924	924	927	921	922	920	930	932	935	939	
2B-M	D2	917	919	921	924	923	923	924	923	926	925	896	888	806	772	
	H	912	917	918	922	922	920	919	916	919	918	924	926	930	928	
	D1	905	905	908	911	910	909	909	907	908	934	1071	1085	1438		
3B-M	D2	912	914	917	919	919	918	918	917	918	919	868	858	911		
	H	911	913	916	918	917	916	916	916	916	933	1006	1010			
	D1	914	910	913	916	915	914	915	914	915	917	922	922	926	922	
3B-L	D2	945	940	942	944	943	942	941	940	938	935	917	912	906	904	
	H	922	909	910	914	914	914	914	914	915	917	919	919	915	900	
	D1	914	906	909	913	912	913	913	913	916	916	919	918	911	904	898
3B-R	D2	917	919	915	917	915	915	913	912	911	910	909	909	908	904	907
	H	912	895	898	900	900	900	901	902	903	905	910	911	897	883	846
	D1	909	912	915	917	915	916	912	912	911	910	908	908	909	912	912
4B	D2	914	913	915	917	916	917	918	916	917	918	917	918	918	918	920
	V	948	947	948	949	947	944	938	915	912	910	908	907	910	911	914

Table 4.10 Demec Readings for Specimen 3SK4B

DEMEC POINT	LOAD	V (kN)	0	0	100	200	300	400	500	600	700	800	893	710	658
		M (MPa)	0	4	4	4	4	4	4	4	4	4	4	4	4
	DIRECTION		DEMEC READINGS												
1A	D1		864	833	824	814	804	791	775	758	730	678	386		
	D2		897	857	858	867	871	878	892	907	936	1000	1371	1777	
	H		878	823	820	821	820	820	822	822	827	840	904	923	
2A	D1		861	835	828	824	815	808	801	788	770	739	502	121	
	D2		896	853	855	860	864	871	881	891	915	976	1350	1768	
	H		871	817	817	818	818	820	822	824	831	851	951	973	
3A	D1		863	839	831	821	810	798	785	767	741	692	404	23	
	D2		891	862	859	866	871	880	889	906	931	996	1368	1778	
	H		871	826	826	825	825	825	824	825	828	840	904	926	
1B	D1		981	980	980	979	979	979	977	977	974	973	974	974	975
	D2		997	997	997	998	997	997	997	997	997	997	997	997	986
	V		961	961	960	960	960	959	957	957	956	954	954	955	956
2B-M	D1		981	979	980	980	980	982	982	983	986	1030	1257		
	D2		986	987	986	984	982	982	980	978	974	960	858		
	H		971	974	974	973	975	974	975	975	977	1002	1077		
2B-L	D1		929	929	929	928	928	928	928	928	930	930	944	1014	
	D2		964	963	962	962	962	961	959	958	956	955	908	921	
	H		989	984	984	984	984	984	985	984	984	984	977	1027	
2B-R	D1		1050	1049	1049	1050	1050	1050	1050	1050	1051	1052	1056	1052	
	D2		994	992	992	991	991	991	990	989	988	985	976	980	
	H		980	977	976	976	977	977	977	977	978	978	975	974	
3B-M	D1		992	991	991	991	991	991	991	991	989	989	974	949	
	D2		925	924	922	922	922	922	923	922	922	919	919	925	
	H		982	980	979	979	981	981	981	981	981	980	988	986	
3B-L	D1		1020	1017	1017	1017	1017	1017	1017	1018	1017	1018	1020	1017	
	D2		999	986	985	986	984	984	984	983	981	978	969	975	
	H		1002	997	997	997	997	997	997	997	997	998	998	994	
3B-R	D1		948	946	947	947	948	948	948	948	949	952	966	965	
	D2		935	933	932	932	932	932	930	929	928	923	915	919	
	H		975	970	970	970	970	971	971	970	970	971	973	973	
4B	D1		981	982	980	979	976	975	971	969	968	964	964	966	966
	D2		999	989	988	989	988	988	988	988	989	988	988	988	988
	V		984	986	985	984	984	982	982	981	979	979	978	979	980

Table 4.11 Measured Stroke for Specimen 1NK4

LOAD, kN	0	0	100	200	300	400	500	516	532	540	515
STROKE, volts	0.0000	0.0000	0.2171	0.3038	0.4085	0.6436	0.9869	1.1285	1.2315	1.3008	1.4312
STROKE, mm	0.0000	0.0000	1.1608	1.6244	2.1842	3.4413	5.2769	6.0340	6.5847	6.9552	7.6525

	518	511	513	513	510	508	507
(continued)	1.7427	2.0428	2.0821	2.1276	2.1777	2.2290	2.2751
	9.3180	10.9226	11.1328	11.3761	11.6439	11.9182	12.1647

Table 4.12 Measured Stroke for Specimen 1LK2

LOAD, kN	0	0	100	200	300	400	500	521	491	455	423
STROKE, volts	0.0000	0.0450	0.1530	0.2037	0.2480	0.2957	0.3543	0.5160	0.6024	0.7072	0.8945
STROKE, mm	0.0000	0.2478	0.8426	1.1218	1.3657	1.6284	1.9511	2.8416	3.3174	3.8945	4.9259

	407	367	361
(continued)	1.0896	1.7847	2.1047
	6.0003	9.8281	11.5904

Table 4.13 Measured Stroke for Specimen 2LK4

LOAD, kN	0	0	100	200	300	400	500	600	700	800	839
STROKE, volts	0.0000	0.0000	0.6360	0.7495	1.0865	1.4994	1.7399	1.9189	2.0769	2.2305	2.4153
STROKE, mm	0.0000	0.0000	0.7910	1.4318	3.3346	5.6659	7.0238	8.0345	8.9266	9.7938	10.8372
	749	715	716	706	699	688					
(continued)	2.6000	2.8000	2.9000	3.0000	3.1000	3.2000					
	11.8801	13.0093	13.5740	14.1386	14.7032	15.2678					

Table 4.14 Measured Stroke for Specimen 3LK4B

LOAD, kN	0	0	100	200	300	400	500	600	700	800	900
STROKE, volts	0.0000	0.0000	0.1842	0.2759	0.3632	0.4741	0.6179	0.7807	0.9370	1.0639	1.1658
STROKE, mm	0.0000	0.0000	0.9849	1.4752	1.9420	2.5350	3.3039	4.1744	5.0101	5.6886	6.2335
	1000	1058	800	729	743	710	692	675	651	645	
(continued)	1.2734	1.4152	1.6781	1.9073	1.9567	2.0452	2.1343	2.2589	2.3914	2.4501	
	6.8088	7.5670	8.9727	10.1983	10.4624	10.9356	11.4120	12.0782	12.7867	13.1006	

Table 4.15 Measured Stroke for Specimen 2SK2

LOAD, kN	0	0	100	200	300	400	500	559	509	456	418
STROKE, volts	0.0000	0.0000	0.1194	0.1982	0.2793	0.4071	0.6065	0.7063	0.9630	1.1586	1.5000
STROKE, mm	0.0000	0.0000	0.6742	1.1191	1.5770	2.2986	3.4244	3.9879	5.4373	6.5417	8.4693
	428	421	420	421	423	421	419				
(continued)	1.5326	1.6117	1.6987	1.7921	1.8576	1.9690	2.0261				
	8.6534	9.1000	9.5912	10.1185	10.4884	11.1174	11.4397				

Table 4.16 Measured Stroke for Specimen 1SK4

LOAD, kN	0	0	100	200	300	400	500	600	700	800	884
STROKE, volts	0.0000	0.1368	0.2940	0.3646	0.4196	0.4764	0.5347	0.5968	0.6723	0.7684	0.9056
STROKE, mm	0.0000	0.7315	1.5720	1.9495	2.2436	2.5473	2.8590	3.1911	3.5948	4.1086	4.8422
	840	724	672	621	624	621	616				
(continued)	0.9800	1.1069	1.2527	1.5610	1.7000	1.9000	2.0000				
	5.2400	5.9186	6.6981	8.3466	9.0898	10.1592	10.6939				

Table 4.17 Measured Stroke for Specimen 3SK4B

LOAD, kN	0	0	100	200	300	400	500	600	700	800	893
STROKE, volts	0.0000	0.0000	0.1697	0.2460	0.3241	0.4208	0.5275	0.6632	0.7905	0.9137	1.0790
STROKE, mm	0.0000	0.0000	0.9074	1.3154	1.7329	2.2500	2.8205	3.5461	4.2268	4.8855	5.7694

	710	658	654	637	628	620	614	606
(continued)	1.2960	1.4968	1.6031	1.6796	1.7652	1.8562	1.9395	2.0147
	6.9297	8.0033	8.5717	8.9808	9.4385	9.9250	10.3704	10.7725

Table 5.1 Concrete and Drypack Strains for Specimen 1NK4

DEMEC POINT	LOAD													
	V (kN)	0	0	100	200	300	400	500	516	532	540	515	518	511
	M (MPa)	0	4	4	4	4	4	4	4	4	4	4	4	4
	DIRECTION	MEASURED STRAIN (uE)												
	ED1	---	0	-56	-120	-224	-400	-1072	-1552	-2144	-2616	-4376	---	---
1A	ED2	---	0	24	56	96	216	896	1376	1976	2488	4424	9960	---
	EH	---	0	8	0	-24	-40	-32	-16	16	72	216	848	1704
	ED1	---	0	-40	-72	-144	-280	-960	-1432	-2008	-2480	-4256	---	---
2A	ED2	---	0	16	56	96	200	832	1344	1928	2440	4320	9704	---
	EH	---	0	0	24	8	-8	-16	16	40	80	168	584	1184
	ED1	---	0	-64	-128	-232	-392	-1064	-1560	-2128	-2624	-4432	---	---
3A	ED2	---	0	16	48	128	216	840	1320	1904	2392	4224	9472	---
	EH	---	0	-32	-40	-32	-72	-96	-72	-40	-32	-8	232	-160
	ED1	---	0	0	0	-25	-25	-198	-99	-74	-149	-124	-124	-149
1B	ED2	---	0	25	50	74	74	25	99	99	124	99	124	74
	EV	---	0	0	0	0	25	-74	-25	0	-74	-99	-149	-223
	ED1	---	0	50	198	298	645	2381	3819	5654	7093	12896	29066	---
2B	ED2	---	0	-74	-248	-570	-1215	-4489	-6845	-9697	-12053	---	---	---
	EH	---	0	0	-99	-223	-422	-1438	-2034	-2827	-3373	-5307	-11086	-17062
	ED1	---	0	0	-50	-50	-25	-74	25	-25	0	0	149	25
3B-L	ED2	---	0	0	74	-50	0	0	0	-25	-25	-50	99	0
	EH	---	0	0	0	0	0	50	50	50	25	74	198	50
	ED1	---	0	50	149	248	570	2207	3472	5258	6671	12152	27528	---
3B-M	ED2	---	0	-50	-198	-496	-1141	-4390	-6795	-9647	-12078	---	---	---
	EH	---	0	50	0	-99	-322	-1389	-2083	-2827	-3522	-5654	-14384	-18451
	ED1	---	0	50	74	25	124	99	99	124	50	74	174	124
3B-R	ED2	---	0	0	-25	-50	-50	-25	-25	-25	-50	-74	0	-25
	EH	---	0	74	50	50	50	99	99	99	74	99	198	149
	ED1	---	0	25	174	322	670	2356	3745	5406	6944	12326	27677	---
4B	ED2	---	0	-174	-372	-794	-1562	-4910	-7440	-10366	-12846	---	---	---
	EH	---	0	0	-50	-50	-422	-1538	-2207	-2976	-3621	-5902	-12326	---
	ED1	---	0	0	25	-50	-124	-124	-174	-198	-223	-248	-198	-223
5B	ED2	---	0	0	0	25	25	50	50	50	0	50	25	-25
	EH	---	0	0	0	-25	0	-50	-99	-74	-149	-124	-99	-124

Table 5.2 Concrete and Drypack Strains for Specimen 1LK2

DEMEC POINT	LOAD														
	V (kN)	0	0	100	200	300	400	500	521	491	455	423	407	367	361
	M (MPa)	0	2	2	2	2	2	2	2	2	2	2	2	2	2
	DIRECTION	MEASURED STRAIN (uE)													
1A	ED1	---	0	-80	-184	-280	-424	-616	-2624	-4008	-5960	---	---	---	---
	ED2	---	0	32	136	232	400	624	4032	5664	7872	11744	15784	---	---
	EH	---	0	0	8	24	32	88	1128	1384	1592	1864	2112	2952	3392
2A	ED1	---	0	-56	-112	-192	-312	-496	-2288	-3616	-5592	---	---	---	---
	ED2	---	0	16	80	152	296	528	3896	5592	7848	7832	---	---	---
	EH	---	0	24	32	56	80	144	1176	1440	1648	1904	2128	2808	3176
3A	ED1	---	0	-72	-184	-272	-424	-656	-2696	-4072	-6016	---	---	---	---
	ED2	---	0	16	104	176	328	584	3872	5584	7792	7712	---	---	---
	EH	---	0	0	8	48	80	88	1048	1328	1544	1872	2144	2904	3400
1B	ED1	---	0	25	-74	-74	-149	-223	-223	-198	-198	-174	-174	-124	---
	ED2	---	0	50	-25	-25	-25	0	-25	0	50	50	25	0	---
	EV	---	0	25	-25	-50	-99	-149	-149	-124	-99	-99	-74	-74	---
2B-L	ED1	---	0	50	25	50	25	99	74	50	50	74	50	74	74
	ED2	---	0	50	25	0	-50	-50	-124	-99	-99	-50	-74	-50	-25
	EH	---	0	74	50	74	74	74	25	50	50	50	25	50	74
2B-R	ED1	---	0	25	25	25	0	25	25	-25	25	-50	-25	-25	-25
	ED2	---	0	0	-25	-50	-74	-124	-248	-248	-174	-174	-124	-50	-25
	EH	---	0	0	0	25	25	50	50	25	25	0	0	25	50
2B-M	ED1	---	0	50	74	99	149	248	8978	11482	14458	---	---	---	---
	ED2	---	0	0	0	-25	-99	-422	-3943	-5555	-7093	---	---	---	---
	EH	---	0	25	0	25	74	50	3546	3894	5134	---	---	---	---
3B-M	ED1	---	0	74	50	74	99	124	5109	6870	9201	---	---	---	---
	ED2	---	0	99	74	25	50	-124	-1786	-2629	-2926	---	---	---	---
	EH	---	0	74	74	124	124	223	3918	5034	6894	---	---	---	---
3B-L	ED1	---	0	0	0	0	0	25	25	-347	50	25	99	25	0
	ED2	---	0	-50	-50	-74	-99	-149	-298	25	-298	-273	-223	-174	-124
	EH	---	0	0	0	25	0	0	-50	174	-74	-74	-50	-25	-25
3B-R	ED1	---	0	25	50	74	99	99	74	-99	74	50	74	74	50
	ED2	---	0	-25	-25	-74	-99	-149	-124	-74	-99	-74	-50	0	0
	EH	---	0	0	0	0	0	0	-50	0	0	25	50	50	74
4B	ED1	---	0	-50	-74	-124	-174	-223	-248	-223	-198	-198	-198	-223	---
	ED2	---	0	25	50	25	50	25	25	74	74	50	50	74	---
	EV	---	0	25	0	-25	-50	-124	-99	-74	-99	-74	-74	-74	---

Table 5.3 Concrete and Drypack Strains for Specimen 2LK4

DEMEC POINT	LOAD													
	V (kN)	0	0	100	200	300	400	500	600	700	800	839	749	715	716
	M (MPa)	0	4	4	4	4	4	4	4	4	4	4	4	4	4
	DIRECTION	MEASURED STRAIN (uE)													
1A	ED1	---	0	-56	-112	-184	-280	-344	-480	-592	-832	-2400	-4944	---	---
	ED2	---	0	-40	0	64	112	144	248	400	632	2680	5368	8696	---
	EH	---	0	0	8	8	-8	0	16	32	64	360	544	632	---
2A	ED1	---	0	-40	-88	-120	-208	-256	-352	-472	-688	-2208	-4680	---	---
	ED2	---	0	16	40	88	112	160	248	368	616	2720	5480	8832	---
	EH	---	0	-8	0	16	24	40	64	104	160	576	784	848	---
3A	ED1	---	0	-64	-144	-200	-296	-368	-520	-672	-960	-2648	-5152	---	---
	ED2	---	0	808	872	928	944	1008	1104	1288	1608	3776	6512	9840	---
	EH	---	0	24	24	32	40	40	32	48	144	512	696	760	---
1B	ED1	---	0	-74	-248	-273	-372	-397	-446	-620	-595	-620	-645	-719	-645
	ED2	---	0	0	-74	-50	-25	0	25	-25	50	25	25	-25	0
	EV	---	0	25	-50	198	-50	-25	-99	-124	-198	-174	-149	-149	-149
2B-L	ED1	---	0	-50	50	74	50	0	149	149	198	149	149	99	149
	ED2	---	0	-25	0	-25	-74	-74	-50	-124	-174	-198	-149	-99	-74
	EH	---	0	-99	-25	-74	-74	-25	0	-50	-50	-25	0	50	74
2B-R	ED1	---	0	-50	25	-50	-50	-25	-25	0	-50	0	0	0	25
	ED2	---	0	-25	25	-25	-50	-50	-50	-50	-124	-174	-149	-124	-74
	EH	---	0	-99	-25	-50	-74	-25	0	25	-25	25	25	-25	25
2B-M	ED1	---	0	-99	-50	-50	-25	25	50	74	372	6225	7837	---	---
	ED2	---	0	-74	-50	-25	-50	-25	-74	-198	-397	298	1637	---	---
	EH	---	0	-99	-50	-74	-99	-50	-74	-25	124	4638	6572	---	---
3B-M	ED1	---	0	-99	-74	-99	-74	0	-25	25	99	2604	6324	---	---
	ED2	---	0	-74	-50	-74	-50	-50	-99	-174	-322	-149	-50	---	---
	EH	---	0	-50	-50	-50	-74	0	0	0	25	2133	5654	---	---
3B-L	ED1	---	0	-124	-50	-50	-74	-50	0	0	0	74	25	-74	---
	ED2	---	0	-74	-50	-50	-74	-74	-99	-149	-223	-322	-248	-273	---
	EH	---	0	-74	-74	-50	-25	25	25	25	74	74	-25	-174	---
3B-R	ED1	---	0	-50	-25	0	50	74	50	50	99	124	149	99	---
	ED2	---	0	-99	-99	-124	-124	-124	-174	-248	-273	-273	-595	-670	---
	EH	---	0	-50	-50	-25	0	25	50	0	25	0	-174	-248	---
4B	ED1	---	0	-74	-25	-50	-74	-223	-298	-347	-496	-422	-422	-446	-446
	ED2	---	0	-25	-25	0	25	50	0	0	25	50	25	0	74
	EV	---	0	-25	-25	-25	-25	-50	-149	-223	-322	-322	-322	-322	-298

Table 5.4 Concrete and Drypack Strains for Specimen 3LK4B

DEMEC POINT	LOAD														
	V (kN)	0	0	100	200	300	400	500	600	700	800	900	1000	1058	800
	M (MPa)	0	4	4	4	4	4	4	4	4	4	4	4	4	4
	DIRECTION	MEASURED STRAIN (uE)													
1A	ED1	---	0	-40	-104	-176	-256	-344	-448	-592	-744	-928	-1320	-2848	---
	ED2	---	0	48	72	112	192	264	344	448	648	912	1584	3992	8920
	EH	---	0	32	-8	32	40	32	24	64	80	144	360	944	1152
2A	ED1	---	0	-32	-80	-128	-200	-264	-344	-456	-592	-744	-1032	-2536	---
	ED2	---	0	40	48	96	144	200	280	392	560	792	1456	3816	8688
	EH	---	0	0	-8	16	40	40	64	80	112	192	448	1072	1352
3A	ED1	---	0	-80	-136	-200	-288	-376	-480	-616	-768	-928	-1344	-3224	---
	ED2	---	0	-16	40	80	152	232	304	432	632	920	1600	4064	8976
	EH	---	0	8	-8	0	16	8	32	56	72	104	312	768	952
1B	ED1	---	0	-149	-397	-496	-595	-694	-744	-818	-918	-992	-1017	-1017	-1017
	ED2	---	0	0	0	0	0	50	50	50	74	74	99	99	74
	EV	---	0	-25	-25	-74	-74	-99	-99	-174	-223	-298	-322	-322	-248
2B-M	ED1	---	0	0	0	0	-50	-25	25	74	74	74	74	124	124
	ED2	---	0	25	25	-25	-25	-74	-74	-124	-198	-248	-273	-546	-694
	EH	---	0	0	0	0	0	0	25	50	74	99	99	0	-74
2B-L	ED1	---	0	0	25	25	25	25	25	50	50	74	99	149	124
	ED2	---	0	0	-50	-50	-99	-74	-124	-99	-149	-273	-397	-496	-347
	EH	---	0	0	25	25	50	50	74	99	99	149	149	198	174
2B-R	ED1	---	0	25	0	25	50	50	25	50	99	149	1637	9945	---
	ED2	---	0	-25	-25	-25	-25	0	0	-50	-149	-273	-595	-4712	---
	EH	---	0	25	0	0	25	25	25	25	50	74	967	2654	---
3B-M	ED1	---	0	0	0	25	25	25	50	74	124	149	174	6324	17509
	ED2	---	0	0	-25	-25	-50	-25	-74	-99	-223	-397	-620	-1488	-546
	EH	---	0	-25	-25	-25	-25	-25	-25	0	0	0	99	3050	5010
3B-L	ED1	---	0	-25	-25	0	0	0	0	0	25	25	74	124	50
	ED2	---	0	-25	25	0	0	0	-25	-50	-99	-149	-322	-521	-347
	EH	---	0	0	0	0	25	25	50	74	99	124	124	124	124
3B-R	ED1	---	0	-50	-25	0	0	25	25	74	124	149	174	149	124
	ED2	---	0	-50	-50	-74	-124	-99	-149	-248	-298	-372	-496	-744	-2158
	EH	---	0	-25	-25	0	0	25	25	50	74	124	149	25	25
4B	ED1	---	0	-50	-50	-74	-99	-99	-124	-198	-248	-322	-372	-372	-298
	ED2	---	0	0	0	-25	-25	25	25	25	50	25	25	25	25
	EV	---	0	0	0	25	0	0	-25	-74	-149	-198	-273	-273	-149

Table 5.5 Concrete and Drypack Strains for Specimen 2SK2

DEMEC POINT	LOAD V (kN)	0	0	100	200	300	400	500	559	509	456	418
	LOAD M (MPa)	0	2	2	2	2	2	2	2	2	2	2
	DIRECTION	MEASURED STRAIN (uE)										
1A	ED1	---	0	-200	-304	-448	-624	-920	-1600	-2960	-5312	---
	ED2	---	0	-224	-176	-72	128	528	1904	4312	7856	---
	EH	---	0	-280	-296	-280	-264	-176	344	1096	1968	---
2A	ED1	---	0	-144	-216	-296	-416	-560	-1112	-2504	-4936	---
	ED2	---	0	-224	-160	-56	112	440	1720	4096	7560	---
	EH	---	0	-256	-248	-240	-216	-40	504	1216	1944	---
3A	ED1	---	0	-176	-288	-456	-608	-904	-1680	-3144	-5736	---
	ED2	---	0	-168	-104	16	200	544	1768	4064	7384	---
	EH	---	0	-232	-240	-232	-208	-168	200	800	1376	---
1B	ED1	---	0	-50	-25	-149	-149	-174	-298	-223	-298	-223
	ED2	---	0	124	-124	74	50	99	74	74	99	74
	EV	---	0	-25	50	-74	74	-174	-248	25	-223	-198
2B-L	ED1	---	0	0	-74	25	-25	50	25	149	0	25
	ED2	---	0	0	0	-25	-50	-99	-124	-25	-74	0
	EH	---	0	50	25	0	50	0	25	99	124	74
2B-R	ED1	---	0	124	0	99	-50	25	50	124	25	-74
	ED2	---	0	25	-25	-25	-74	-50	-273	-372	-174	-99
	EH	---	0	-25	-74	-50	-25	0	-74	-74	25	-25
2B-M	ED1	---	0	0	0	0	-50	-50	-223	3249	13020	---
	ED2	---	0	25	0	25	25	74	273	50	347	---
	EH	---	0	0	50	25	0	25	174	4687	11507	---
3B-M	ED1	---	0	50	0	-74	0	446	2902	5183	9945	---
	ED2	---	0	0	-50	-124	-149	-223	-397	74	124	---
	EH	---	0	25	25	0	25	273	1885	3199	6969	---
3B-L	ED1	---	0	-74	-50	50	0	-50	124	-322	---	---
	ED2	---	0	-50	-74	-124	-223	-372	-595	-3174	---	---
	EH	---	0	0	25	0	25	50	124	-223	---	---
3B-R	ED1	---	0	0	50	25	-25	50	124	0	-347	---
	ED2	---	0	-25	0	-25	-74	-99	-273	-843	-2430	---
	EH	---	0	25	50	25	-50	0	-74	-620	-3075	---
4B	ED1	---	0	-25	-99	-198	-273	-372	-223	-322	-397	-471
	ED2	---	0	-25	0	74	50	50	-198	124	74	0
	EV	---	0	-50	-124	-198	-322	-322	-347	-322	-322	-322

Table 5.6 Concrete and Drypack Strains for Specimen 1SK4

DEMEC POINT	LOAD															
	V (kN)	0	0	100	200	300	400	500	600	700	800	884	840	724	672	621
	M (MPa)	0	4	4	4	4	4	4	4	4	4	4	4	4	4	4
	DIRECTION	MEASURED STRAIN (uE)														
1A	ED1	---	0	-80	-200	-360	-544	-744	-960	-1224	-1592	-2984	-3144	---	---	---
	ED2	---	0	40	24	152	224	344	560	704	1128	2512	2656	5160	8000	-6632
	EH	---	0	0	-8	-40	-56	-80	-88	-88	-56	-16	8	-16	-16	192
2A	ED1	---	0	-40	-112	-216	-328	-464	-600	-744	-952	-1992	-2112	-4624	---	---
	ED2	---	0	32	72	136	224	344	472	640	992	2600	2680	5392	8280	-6488
	EH	---	0	16	16	8	16	16	56	88	192	560	584	672	736	1280
3A	ED1	---	0	-64	-136	-256	-400	-552	-704	-896	-1144	-2296	-2472	-4992	---	---
	ED2	---	0	48	72	136	256	368	504	672	1032	2656	2816	5592	8624	-6640
	EH	---	0	0	0	-8	-8	8	-8	16	112	472	472	640	840	1776
1B	ED1	---	0	50	124	74	0	-74	-149	-198	-223	-248	-223	-223	-198	-124
	ED2	---	0	0	99	99	99	74	74	99	124	124	124	99	99	149
	EV	---	0	0	25	149	99	50	-99	-198	-124	-223	-372	-273	-99	-25
2B-L	ED1	---	0	25	50	50	50	50	0	50	273	372	422	694	-397	---
	ED2	---	0	25	50	25	-25	0	-149	-223	-471	-1017	-1042	74	-3794	---
	EH	---	0	50	50	74	25	50	0	0	0	-74	-99	744	-5481	---
2B-R	ED1	---	0	149	50	74	74	74	50	25	25	124	174	25	---	---
	ED2	---	0	25	25	0	-25	-99	-124	-124	-149	-496	-521	-1066	---	---
	EH	---	0	50	74	50	50	50	25	25	50	-25	-50	-1017	---	---
2B-M	ED1	---	0	99	248	99	99	174	25	50	0	248	298	372	471	---
	ED2	---	0	50	124	99	99	124	99	174	149	-570	-769	-2802	-3646	---
	EH	---	0	25	124	124	74	50	-25	50	25	174	223	322	273	---
3B-M	ED1	---	0	74	149	124	99	99	50	74	719	4117	4464	13218	---	---
	ED2	---	0	74	124	124	99	99	74	99	124	-1141	-1389	-74	---	---
	EH	---	0	74	124	99	74	74	74	74	496	2306	2406	---	---	---
3B-L	ED1	---	0	74	149	124	99	124	99	124	174	298	298	397	298	---
	ED2	---	0	50	99	74	50	25	0	-50	-124	-570	-694	-843	-893	---
	EH	---	0	25	124	124	124	124	124	149	198	248	248	149	-223	---
3B-R	ED1	---	0	74	174	149	174	174	174	248	248	322	298	124	-50	-198
	ED2	---	0	-99	-50	-99	-99	-149	-174	-198	-223	-248	-248	-273	-372	-298
	EH	---	0	74	124	124	124	149	174	198	248	372	397	50	-298	-1215
4B	ED1	---	0	74	124	74	99	0	0	-25	-50	-99	-99	-74	0	0
	ED2	---	0	50	99	74	99	124	74	99	124	99	124	124	124	174
	EV	---	0	25	50	0	-74	-223	-794	-868	-918	-967	-992	-918	-893	-818

Table 5.7 Concrete and Drypack Strains for Specimen 3SK4B

DEMEC POINT	LOAD													
	V (kN)	0	0	100	200	300	400	500	600	700	800	893	710	658
	M (MPa)	0	4	4	4	4	4	4	4	4	4	4	4	4
DIRECTION		MEASURED STRAIN (uE)												
	ED1	---	0	-72	-152	-232	-336	-464	-600	-824	-1240	-3576	---	---
1A	ED2	---	0	8	80	112	168	280	400	632	1144	4112	7360	---
	EH	---	0	-24	-16	-24	-24	-8	-8	32	136	648	800	---
	ED1	---	0	-56	-88	-160	-216	-272	-376	-520	-768	-2664	-5712	---
2A	ED2	---	0	16	56	88	144	224	304	496	984	3976	7320	---
	EH	---	0	0	8	8	24	40	56	112	272	1072	1248	---
	ED1	---	0	-64	-144	-232	-328	-432	-576	-784	-1176	-3480	-6528	---
3A	ED2	---	0	-24	32	72	144	216	352	552	1072	4048	7328	---
	EH	---	0	0	-8	-8	-8	-16	-8	16	112	624	800	---
	ED1	---	0	0	-25	-25	-25	-74	-74	-149	-174	-149	-149	-124
1B	ED2	---	0	0	25	0	0	0	0	0	0	0	0	-273
	EV	---	0	-25	-25	-25	-50	-99	-99	-124	-174	-174	-149	-124
	ED1	---	0	25	25	25	74	74	99	174	1265	6894	---	---
2B-M	ED2	---	0	-25	-74	-124	-124	-174	-223	-322	-670	-3199	---	---
	EH	---	0	0	-25	25	0	25	25	74	694	2554	---	---
	ED1	---	0	0	-25	-25	-25	-25	-25	25	25	372	2108	---
2B-L	ED2	---	0	-25	-25	-25	-50	-99	-124	-174	-198	-1364	-1042	---
	EH	---	0	0	0	0	0	25	0	0	0	-174	1066	---
	ED1	---	0	0	25	25	25	25	25	50	74	174	74	---
2B-R	ED2	---	0	0	-25	-25	-25	-50	-74	-99	-174	-397	-298	---
	EH	---	0	-25	-25	0	0	0	0	25	25	-50	-74	---
	ED1	---	0	0	0	0	0	0	0	-50	-50	-422	-1042	---
3B-M	ED2	---	0	-50	-50	-50	-50	-25	-50	-50	-124	-124	25	---
	EH	---	0	-25	-25	25	25	25	25	25	0	198	149	---
	ED1	---	0	0	0	0	0	0	25	0	25	74	0	---
3B-L	ED2	---	0	-25	0	-50	-50	-50	-74	-124	-198	-422	-273	---
	EH	---	0	0	0	0	0	0	0	0	25	25	-74	---
	ED1	---	0	25	25	50	50	50	50	74	149	496	471	---
3B-R	ED2	---	0	-25	-25	-25	-25	-74	-99	-124	-248	-446	-347	---
	EH	---	0	0	0	0	25	25	0	0	25	74	74	---
	ED1	---	0	-50	-74	-149	-174	-273	-322	-347	-446	-446	-397	-397
4B	ED2	---	0	-25	0	-25	-25	-25	-25	0	-25	-25	-25	-25
	EV	---	0	-25	-50	-50	-99	-99	-124	-174	-174	-198	-174	-149

Table 5.8 Principal Strains and Crack Orientation for Specimen 1NK4

DEMEC POINT	LOAD													
	V (kN)	0	0	100	200	300	400	500	516	532	540	515	518	511
	M (MPa)	0	4	4	4	4	4	4	4	4	4	4	4	4
	DIRECTION						PRINCIPAL CONCRETE STRAINS (uE)							
	E1	---	0	31	62	101	220	898	1378	1978	2492	4428	---	---
1A	E2	---	0	-63	-126	-229	-404	-1074	-1554	-2146	-2620	-4380	---	---
	ANGLE	---	---	60	55	52	50	47	46	46	47	46	---	---
	E1	---	0	18	64	100	202	833	1345	1930	2442	4322	---	---
2A	E2	---	0	-42	-80	-148	-282	-961	-1433	-2010	-2482	-4258	---	---
	ANGLE	---	---	57	58	52	49	47	46	46	46	46	---	---
	E1	---	0	17	48	129	216	840	1321	1905	2393	4225	---	---
3A	E2	---	0	-65	-128	-233	-392	-1064	-1561	-2129	-2625	-4433	---	---
	ANGLE	---	---	39	45	48	47	45	46	46	46	46	---	---
	E1	---	0	30	60	80	74	25	102	100	137	129	194	180
1B	E2	---	0	-5	-10	-31	-25	-199	-102	-75	-162	-154	-194	-254
	ANGLE	---	---	23	23	32	45	48	38	41	33	26	20	15
	E1	---	0	51	210	306	655	2402	3845	5697	7134	---	---	---
2B	E2	---	0	-76	-260	-579	-1225	-4510	-6870	-9739	-12094	---	---	---
	ANGLE	---	---	129	144	141	139	138	138	138	138	---	---	---
	E1	---	0	0	76	0	5	57	52	50	27	77	202	52
3B-L	E2	---	0	0	-51	-99	-30	-132	-27	-99	-52	-127	46	-27
	ANGLE	---	---	---	39	---	67	78	99	---	99	97	99	99
	E1	---	0	70	151	249	571	2221	3489	5284	6707	---	---	---
3B-M	E2	---	0	-70	-200	-497	-1142	-4403	-6812	-9674	-12113	---	---	---
	ANGLE	---	---	113	131	133	136	138	137	137	137	---	---	---
	E1	---	0	80	80	60	125	125	125	139	89	124	228	174
3B-R	E2	---	0	-31	-31	-85	-50	-50	-50	-40	-89	-124	-55	-74
	ANGLE	---	---	103	122	105	131	113	113	118	107	108	109	108
	E1	---	0	50	178	353	670	2365	3756	5422	6967	---	---	---
4B	E2	---	0	-198	-376	-824	-1563	-4920	-7452	-10382	-12869	---	---	---
	ANGLE	---	---	117	130	126	134	137	137	137	137	---	---	---
	E1	---	0	0	30	27	40	50	56	50	6	52	25	-25
5B	E2	---	0	0	-5	-52	-139	-125	-180	-198	-229	-250	-199	-223
	ANGLE	---	---	---	157	36	62	41	36	45	36	40	42	45

Table 5.9 Principal Strains and Crack Orientation for Specimen 1LK2

DEMEC POINT	LOAD														
	V (kN)	0	0	100	200	300	400	500	521	491	455	423	407	367	361
	M (MPa)	0	2	2	2	2	2	2	2	2	2	2	2	2	2
	DIRECTION	PRINCIPAL CONCRETE STRAINS (uE)													
1A	E1	---	0	37	139	236	402	630	4059	5696	7901	---	---	---	---
	E2	---	0	-85	-187	-284	-426	-622	-2651	-4040	-5989	---	---	---	---
	ANGLE	---	---	57	51	50	48	49	49	48	48	---	---	---	---
2A	E1	---	0	37	91	168	308	544	3918	5614	7868	---	---	---	---
	E2	---	0	-77	-123	-208	-324	-512	-2310	-3638	-5612	---	---	---	---
	ANGLE	---	---	70	58	57	53	52	48	48	47	---	---	---	---
3A	E1	---	0	24	112	196	349	596	3904	5618	7823	---	---	---	---
	E2	---	0	-80	-192	-292	-445	-668	-2728	-4106	-6047	---	---	---	---
	ANGLE	---	---	61	54	57	54	51	49	48	48	---	---	---	---
1B	E1	---	0	55	-15	-25	-24	6	-22	3	52	56	25	1	---
	E2	---	0	20	-85	-74	-150	-229	-226	-201	-201	-180	-174	-125	---
	ANGLE	---	---	23	67	45	39	36	38	38	39	36	45	39	---
2B-L	E1	---	0	74	50	80	82	114	86	80	80	85	60	85	95
	E2	---	0	25	0	-31	-107	-65	-136	-130	-130	-60	-85	-60	-45
	ANGLE	---	---	---	---	103	102	118	122	113	113	120	120	120	113
2B-R	E1	---	0	30	25	40	35	74	100	60	66	16	15	26	50
	E2	---	0	-5	-25	-65	-110	-174	-323	-332	-215	-239	-164	-100	-99
	ANGLE	---	---	157	135	113	105	108	110	107	113	105	107	96	---
2B-M	E1	---	0	50	90	100	158	275	9059	11533	14556	---	---	---	---
	E2	---	0	0	-15	-26	-109	-448	-4025	-5606	-7190	---	---	---	---
	ANGLE	---	---	135	157	141	124	124	130	132	131	---	---	---	---
3B-M	E1	---	0	104	80	128	130	255	5782	7692	10270	---	---	---	---
	E2	---	0	69	44	-29	19	-255	-2459	-3452	-3996	---	---	---	---
	ANGLE	---	---	23	67	99	103	105	118	119	119	---	---	---	---
3B-L	E1	---	0	10	10	35	21	45	47	222	57	33	100	37	10
	E2	---	0	-60	-60	-110	-120	-169	-319	-544	-305	-281	-224	-185	-134
	ANGLE	---	---	113	113	105	113	117	121	75	127	126	133	122	120
3B-R	E1	---	0	25	52	74	99	102	77	1	75	60	85	76	80
	E2	---	0	-25	-27	-74	-99	-151	-127	-174	-100	-85	-60	-2	-31
	ANGLE	---	---	135	144	135	135	129	142	86	131	120	120	126	103
4B	E1	---	0	40	51	29	50	27	25	74	79	50	50	74	---
	E2	---	0	-65	-76	-128	-174	-226	-249	-223	-203	-198	-198	-223	---
	ANGLE	---	---	67	51	54	48	39	48	45	37	45	45	45	---

Table 5.10 Principal Strains and Crack Orientation for Specimen 2LK4

DEMEC POINT	LOAD														
	V (kN)	0	0	100	200	300	400	500	600	700	800	839	749	715	716
	M (MPa)	0	4	4	4	4	4	4	4	4	4	4	4	4	4
	DIRECTION						PRINCIPAL CONCRETE STRAINS (uE)								
	E1	---	0	1	29	81	126	164	271	416	650	2690	5379	---	---
1A	E2	---	0	-97	-141	-201	-294	-364	-503	-608	-850	-2410	-4955	---	---
	ANGLE	---	---	85	69	59	56	56	55	52	51	47	47	---	---
	E1	---	0	16	44	93	127	178	270	396	645	2741	5494	---	---
2A	E2	---	0	-40	-92	-125	-223	-274	-374	-500	-717	-2229	-4694	---	---
	ANGLE	---	---	49	55	54	57	56	56	55	53	49	47	---	---
	E1	---	0	930	975	1018	1006	1063	1145	1322	1621	3776	6512	---	---
3A	E2	---	0	-186	-247	-290	-358	-423	-561	-706	-973	-2648	-5152	---	---
	ANGLE	---	---	26	28	30	33	34	36	38	41	45	45	---	---
	E1	---	0	35	-20	215	30	65	50	35	58	48	62	41	44
1B	E2	---	0	-110	-303	-538	-427	-462	-471	-680	-604	-643	-682	-785	-689
	ANGLE	---	---	75	71	81	65	66	58	62	51	56	58	61	59
	E1	---	0	26	80	136	75	2	161	162	208	149	149	111	155
2B-L	E2	---	0	-100	-31	-86	-100	-76	-61	-137	-184	-198	-149	-111	-80
	ANGLE	---	---	6	167	167	157	126	148	147	144	135	135	122	126
	E1	---	0	26	74	-20	-25	-20	2	31	-14	55	50	10	45
2B-R	E2	---	0	-100	-25	-55	-74	-55	-76	-80	-159	-228	-198	-134	-95
	ANGLE	---	---	6	---	23	---	113	99	103	105	109	108	120	113
	E1	---	0	-69	-50	2	26	55	75	79	395	6529	8339	---	---
2B-M	E2	---	0	-104	-50	-76	-100	-55	-100	-203	-420	-6	1134	---	---
	ANGLE	---	---	23	---	9	174	167	157	127	125	123	120	---	---
	E1	---	0	-48	-44	-48	-44	10	10	50	139	2875	7198	---	---
3B-M	E2	---	0	-126	-80	-126	-80	-60	-134	-198	-363	-420	-924	---	---
	ANGLE	---	---	81	67	81	23	113	105	117	119	118	116	---	---
	E1	---	0	-64	-25	-50	-25	26	40	50	105	157	50	-74	---
3B-L	E2	---	0	-134	-74	-50	-124	-150	-139	-198	-329	-405	-273	-273	---
	ANGLE	---	---	67	---	---	---	94	107	108	105	113	119	135	---
	E1	---	0	-39	-23	10	57	86	96	80	130	137	152	101	---
3B-R	E2	---	0	-109	-101	-134	-132	-136	-220	-278	-304	-286	-598	-671	---
	ANGLE	---	---	113	126	120	123	122	113	118	120	125	131	132	---
	E1	---	0	-15	-25	0	25	55	0	7	39	86	57	21	97
4B	E2	---	0	-85	-25	-50	-74	-228	-298	-354	-510	-458	-454	-467	-469
	ANGLE	---	---	67	---	45	45	53	45	37	36	30	30	33	33

Table 5.11 Principal Strains and Crack Orientation for Specimen 3LK4B

DEMEC POINT	LOAD														
	V (kN)	0	0	100	200	300	400	500	600	700	800	900	1000	1058	800
	M (MPa)	0	4	4	4	4	4	4	4	4	4	4	4	4	4
	DIRECTION	PRINCIPAL CONCRETE STRAINS (uE)													
	E1	---	0	56	72	126	203	272	351	465	660	924	1602	4012	---
1A	E2	---	0	-48	-104	-190	-267	-352	-455	-609	-756	-940	-1338	-2868	---
	ANGLE	---	---	61	48	57	54	52	50	52	50	50	49	48	---
	E1	---	0	40	48	100	157	211	294	407	574	810	1478	3845	---
2A	E2	---	0	-32	-80	-132	-213	-275	-358	-471	-606	-762	-1054	-2565	---
	ANGLE	---	---	42	49	53	56	54	54	52	51	51	50	49	---
	E1	---	0	16	49	92	167	242	322	452	646	926	1611	4081	---
3A	E2	---	0	-112	-145	-212	-303	-386	-498	-636	-782	-934	-1355	-3241	---
	ANGLE	---	---	75	57	57	55	52	54	53	51	48	49	48	---
	E1	---	0	15	65	55	74	111	121	98	113	98	116	116	118
1B	E2	---	0	-164	-462	-551	-670	-756	-815	-867	-956	-1016	-1033	-1033	-1061
	ANGLE	---	---	62	66	62	63	60	61	58	56	53	52	52	56
	E1	---	0	30	30	5	2	6	45	99	131	159	164	185	175
2B-M	E2	---	0	-5	-5	-30	-76	-105	-95	-149	-255	-333	-363	-606	-746
	ANGLE	---	---	23	23	113	81	103	113	117	113	110	111	119	121
	E1	---	0	0	40	40	69	65	95	120	129	204	239	319	258
2B-L	E2	---	0	0	-65	-65	-144	-114	-194	-169	-228	-402	-536	-666	-482
	ANGLE	---	---	---	113	113	108	107	105	105	107	107	110	110	110
	E1	---	0	35	5	25	52	50	30	55	120	189	1723	9945	---
2B-R	E2	---	0	-35	-30	-25	-27	0	-5	-55	-169	-313	-681	-4712	---
	ANGLE	---	---	113	113	135	126	135	113	122	120	119	124	135	---
	E1	---	0	25	5	35	27	35	51	75	131	176	288	6375	18153
3B-M	E2	---	0	-25	-30	-35	-52	-35	-76	-100	-230	-424	-734	-1539	-1190
	ANGLE	---	---	---	157	157	144	157	141	131	127	123	115	130	146
	E1	---	0	0	25	0	25	25	51	77	113	143	194	258	189
3B-L	E2	---	0	-50	-25	0	-25	-25	-76	-127	-187	-267	-442	-654	-486
	ANGLE	---	---	---	45	---	---	---	96	97	102	103	109	113	108
	E1	---	0	-25	-20	15	26	50	61	124	179	240	295	253	528
3B-R	E2	---	0	-74	-55	-90	-150	-125	-185	-298	-352	-463	-617	-848	-2562
	ANGLE	---	---	---	113	113	113	113	113	115	116	114	114	117	114
	E1	---	0	10	10	29	10	35	29	25	58	32	48	48	25
4B	E2	---	0	-60	-60	-128	-134	-110	-128	-199	-256	-329	-395	-395	-298
	ANGLE	---	---	67	67	81	75	60	54	48	36	37	32	32	43

Table 5.12 Principal Strains and Crack Orientation for Specimen 2SK2

DEMEC POINT	LOAD											
	V (kN)	0	0	100	200	300	400	500	559	509	456	418
	M (MPa)	0	2	2	2	2	2	2	2	2	2	2
	DIRECTION						PRINCIPAL CONCRETE STRAINS (uE)					
	E1	---	0	-143	-155	-71	128	528	1914	4336	7893	---
1A	E2	---	0	-281	-325	-449	-624	-920	-1610	-2984	-5349	---
	ANGLE	---	---	175	24	42	44	46	48	48	48	---
	E1	---	0	-102	-122	-40	120	440	1734	4123	7592	---
2A	E2	---	0	-266	-254	-312	-424	-560	-1126	-2531	-4968	---
	ANGLE	---	---	165	13	31	38	46	49	49	48	---
	E1	---	0	-112	-94	16	200	544	1775	4080	7407	---
3A	E2	---	0	-232	-298	-456	-608	-904	-1687	-3160	-5759	---
	ANGLE	---	---	2	32	44	45	45	48	48	47	---
	E1	---	0	144	59	80	109	156	119	104	135	119
1B	E2	---	0	-69	-208	-155	-208	-230	-342	-253	-333	-268
	ANGLE	---	---	27	101	36	71	23	27	62	29	25
	E1	---	0	50	35	25	50	54	56	156	128	76
2B-L	E2	---	0	-50	-110	-25	-125	-103	-155	-32	-203	-51
	ANGLE	---	---	---	75	135	94	126	113	123	96	96
	E1	---	0	185	51	144	-23	27	54	129	66	-24
2B-R	E2	---	0	-37	-76	-69	-101	-52	-277	-377	-215	-150
	ANGLE	---	---	167	174	162	99	126	129	129	113	96
	E1	---	0	30	50	30	27	76	314	5083	14647	---
2B-M	E2	---	0	-5	-50	-5	-52	-51	-264	-1784	-1280	---
	ANGLE	---	---	23	---	67	54	51	60	104	116	---
	E1	---	0	50	31	3	50	483	3019	5246	10312	---
3B-M	E2	---	0	0	-80	-201	-198	-260	-514	11	-243	---
	ANGLE	---	---	135	103	97	108	122	125	129	124	---
	E1	---	0	1	26	57	65	95	273	340	---	---
3B-L	E2	---	0	-125	-150	-132	-288	-517	-744	-3836	---	---
	ANGLE	---	---	84	94	123	110	106	113	112	---	---
	E1	---	0	27	60	35	-25	54	124	44	593	---
3B-R	E2	---	0	-52	-10	-35	-74	-103	-273	-888	-3371	---
	ANGLE	---	---	99	113	113	135	126	135	148	164	---
	E1	---	0	0	40	131	154	104	-74	216	124	15
4B	E2	---	0	-50	-139	-255	-377	-427	-348	-415	-447	-487
	ANGLE	---	---	---	17	23	19	26	3	23	28	35

Table 5.13 Principal Strains and Crack Orientation for Specimen 1SK4

DEMEC POINT	LOAD															
	V (kN)	0	0	100	200	300	400	500	600	700	800	884	840	724	672	621
	M (MPa)	0	4	4	4	4	4	4	4	4	4	4	4	4	4	4
	DIRECTION	PRINCIPAL CONCRETE STRAINS (uE)														
	E1	---	0	43	50	160	238	357	568	719	1139	2521	2667	---	---	---
1A	E2	---	0	-83	-226	-368	-558	-757	-968	-1239	-1603	-2993	-3155	---	---	---
	ANGLE	---	---	54	63	52	53	51	49	50	49	47	47	---	---	---
	E1	---	0	37	79	142	232	351	485	654	1007	2614	2699	5400	---	---
2A	E2	---	0	-45	-119	-222	-336	-471	-613	-758	-967	-2006	-2131	-4632	---	---
	ANGLE	---	---	60	56	53	52	50	51	51	50	48	49	47	---	---
	E1	---	0	49	77	143	262	379	511	682	1045	2673	2833	5603	---	---
3A	E2	---	0	-65	-141	-263	-406	-563	-711	-906	-1157	-2313	-2489	-5003	---	---
	ANGLE	---	---	49	54	52	51	51	49	50	49	48	48	47	---	---
	E1	---	0	60	199	150	120	89	90	161	139	184	317	203	107	154
1B	E2	---	0	-10	24	24	-21	-89	-165	-260	-238	-308	-416	-327	-206	-129
	ANGLE	---	---	157	176	84	67	62	30	23	33	25	14	19	36	37
	E1	---	0	50	50	76	52	60	31	75	286	415	451	859	1692	---
2B-L	E2	---	0	0	50	-2	-27	-10	-180	-248	-484	-1060	-1071	-90	-5883	---
	ANGLE	---	---	---	---	99	126	113	113	119	128	125	127	110	167	---
	E1	---	0	159	76	76	80	94	69	56	79	163	195	217	---	---
2B-R	E2	---	0	14	-2	-2	-31	-119	-144	-155	-203	-535	-542	-1258	---	---
	ANGLE	---	---	150	99	126	122	117	117	113	109	121	125	156	---	---
	E1	---	0	130	274	124	124	251	156	199	164	368	468	995	1187	---
2B-M	E2	---	0	19	98	74	74	47	-32	24	-15	-690	-939	-3425	-4361	---
	ANGLE	---	---	167	157	---	---	173	12	23	28	115	115	113	114	---
	E1	---	0	74	154	149	124	124	80	104	728	4241	4590	---	---	---
3B-M	E2	---	0	74	119	99	74	74	44	69	115	-1265	-1515	---	---	---
	ANGLE	---	---	---	157	---	---	---	67	23	128	126	127	---	---	---
	E1	---	0	101	149	134	130	145	139	179	253	443	469	500	302	---
3B-L	E2	---	0	23	99	64	19	4	-40	-104	-204	-716	-866	-946	-897	---
	ANGLE	---	---	171	135	113	103	113	107	109	110	114	114	120	131	---
	E1	---	0	110	190	184	199	224	246	308	346	477	486	160	-28	720
3B-R	E2	---	0	-135	-66	-134	-124	-199	-246	-258	-321	-403	-437	-308	-394	-1216
	ANGLE	---	---	113	120	116	119	115	113	116	113	110	108	119	149	179
	E1	---	0	101	175	149	273	354	869	945	996	972	1023	972	1019	996
4B	E2	---	0	23	48	0	-74	-230	-794	-870	-922	-972	-998	-923	-895	-823
	ANGLE	---	---	171	174	---	---	6	1	2	3	3	3	3	2	3

Table 5.14 Principal Strains and Crack Orientation for Specimen 3SK4B

DEMEC POINT	LOAD													
	V (kN)	0	0	100	200	300	400	500	600	700	800	893	710	658
	M (MPa)	0	4	4	4	4	4	4	4	4	4	4	4	4
	DIRECTION	PRINCIPAL CONCRETE STRAINS (uE)												
	E1	---	0	9	82	116	175	289	408	643	1158	4131	---	---
1A	E2	---	0	-73	-154	-236	-343	-473	-608	-835	-1254	-3595	---	---
	ANGLE	---	---	51	50	51	52	51	50	50	49	48	---	---
	E1	---	0	21	60	96	154	232	316	511	999	4002	7335	---
2A	E2	---	0	-61	-92	-168	-226	-280	-388	-535	-783	-2690	-5727	---
	ANGLE	---	---	60	54	55	54	52	53	52	50	49	47	---
	E1	---	0	4	44	88	159	229	364	565	1084	4063	7340	---
3A	E2	---	0	-92	-156	-248	-343	-445	-588	-797	-1188	-3495	-6540	---
	ANGLE	---	---	78	59	58	55	53	51	51	49	48	47	---
	E1	---	0	25	35	5	27	35	35	15	36	50	31	-93
1B	E2	---	0	-25	-35	-30	-52	-110	-110	-164	-210	-198	-180	-304
	ANGLE	---	---	---	23	23	9	15	15	28	23	18	23	113
	E1	---	0	25	25	56	77	95	121	215	1343	6944	---	---
2B-M	E2	---	0	-25	-74	-155	-127	-194	-245	-364	-748	-3248	---	---
	ANGLE	---	---	135	135	113	128	120	121	120	124	131	---	---
	E1	---	0	5	0	0	2	32	15	50	55	430	2196	---
2B-L	E2	---	0	-30	-50	-50	-76	-156	-164	-198	-228	-1422	-1129	---
	ANGLE	---	---	113	---	---	99	102	107	117	116	125	126	---
	E1	---	0	25	35	25	25	27	31	65	95	180	78	---
2B-R	E2	---	0	-25	-35	-25	-25	-52	-80	-114	-194	-403	-301	---
	ANGLE	---	---	---	157	135	135	126	122	118	120	129	129	---
	E1	---	0	0	0	31	31	27	31	25	8	221	338	---
3B-M	E2	---	0	-50	-50	-80	-80	-52	-80	-124	-181	-767	-1355	---
	ANGLE	---	---	135	135	103	103	99	103	---	102	81	70	---
	E1	---	0	5	0	10	10	10	31	26	71	144	13	---
3B-L	E2	---	0	-30	0	-60	-60	-60	-80	-150	-245	-491	-286	---
	ANGLE	---	---	113	---	113	113	113	122	113	113	116	123	---
	E1	---	0	25	25	52	52	60	54	77	162	499	471	---
3B-R	E2	---	0	-25	-25	-27	-27	-85	-103	-127	-261	-449	-347	---
	ANGLE	---	---	135	135	144	126	120	126	128	125	132	134	---
	E1	---	0	-20	2	-14	-25	-15	-17	0	-16	-22	-21	-15
4B	E2	---	0	-55	-76	-159	-174	-282	-330	-347	-455	-450	-400	-407
	ANGLE	---	---	67	36	60	45	56	54	45	53	50	51	54

Table 5.15 Average Shear Slip and Dilation for Specimen 1NK4

LOAD, kN	0	100	200	300	400	500	516	532	540	515	515
AVG. SLIP, mm	0.0000	0.0072	0.0181	0.0324	0.0662	0.2515	0.3915	0.5576	0.6996	0.6996	1.2275
STA. 1A-DILATION, mm	0.0000	-0.0023	-0.0045	-0.0091	-0.0130	-0.0127	-0.0129	-0.0126	-0.0102	0.0003	---
STA. 2A-DILATION, mm	0.0000	-0.0017	-0.0011	-0.0034	-0.0057	-0.0092	-0.0066	-0.0064	-0.0039	0.0016	---
STA. 3A-DILATION, mm	0.0000	-0.0017	-0.0011	-0.0034	-0.0057	-0.0092	-0.0066	-0.0064	-0.0039	0.0016	---

	518	511	513	513	510	508	507
	2.8931	4.4977	4.7079	4.9512	5.2190	5.4933	5.7398
(continued)	---	---	---	---	---	---	---
	---	---	---	---	---	---	---
	---	---	---	---	---	---	---

Table 5.16 Average Shear Slip and Dilation for Specimen 1LK2

LOAD, kN	0	100	200	300	400	500	521	491	455	423	407
AVG. SLIP, mm	0.0000	0.0091	0.0305	0.0536	0.0948	0.1567	1.0058	1.4563	2.0706	2.3904	3.4648
STA. 1A-DILATION, mm	0.0000	-0.0034	-0.0033	-0.0032	-0.0014	0.0009	0.1002	0.1170	0.1330	0.4026	0.6846
STA. 2A-DILATION, mm	0.0000	-0.0028	-0.0023	-0.0028	-0.0012	0.0022	0.1120	0.1363	0.1525	0.0785	---
STA. 3A-DILATION, mm	0.0000	-0.0028	-0.0023	-0.0028	-0.0012	0.0022	0.1120	0.1363	0.1525	0.0785	---

	367	361
	7.2926	9.0548
(continued)	---	---
	---	---
	---	---

Table 5.17 Average Shear Slip and Dilation for Specimen 2LK4

LOAD, kN	0	100	200	300	400	500	600	700	800	839	749
AVG. SLIP, mm	0.0000	0.0215	0.0313	0.0458	0.0590	0.0718	0.0994	0.1354	0.2027	0.7537	1.5106
STA. 1A-DILATION, mm	0.0000	-0.0634	-0.0645	-0.0651	-0.0685	-0.0708	-0.0731	-0.0703	-0.0709	-0.0381	-0.0312
STA. 2A-DILATION, mm	0.0000	-0.0017	-0.0034	-0.0023	-0.0068	-0.0068	-0.0074	-0.0074	-0.0052	0.0351	0.0523
STA. 3A-DILATION, mm	0.0000	-0.0017	-0.0034	-0.0023	-0.0068	-0.0068	-0.0074	-0.0074	-0.0052	0.0351	0.0523

(continued)

LOAD, kN	715	716	706	699	688
AVG. SLIP, mm	2.6398	3.2044	3.7690	4.3337	4.8983
STA. 1A-DILATION, mm	---	---	---	---	---
STA. 2A-DILATION, mm	---	---	---	---	---
STA. 3A-DILATION, mm	---	---	---	---	---

Table 5.18 Average Shear Slip and Dilation for Specimen 3LK4B

LOAD, kN	0	100	200	300	400	500	600	700	800	900	1000
AVG. SLIP, mm	0.0000	0.0115	0.0181	0.0317	0.0494	0.0675	0.0907	0.1226	0.1705	0.2334	0.3977
STA. 1A-DILATION, mm	0.0000	0.0006	-0.0023	-0.0045	-0.0046	-0.0057	-0.0074	-0.0103	-0.0069	-0.0013	0.0182
STA. 2A-DILATION, mm	0.0000	0.0006	-0.0023	-0.0023	-0.0040	-0.0045	-0.0046	-0.0046	-0.0023	0.0033	0.0297
STA. 3A-DILATION, mm	0.0000	0.0006	-0.0023	-0.0023	-0.0040	-0.0045	-0.0046	-0.0046	-0.0023	0.0033	0.0297

(continued)

LOAD, kN	1058	800	729	743	710	692	675	651	645
AVG. SLIP, mm	1.0086	2.4143	3.6399	3.9040	4.3772	4.8536	5.5198	6.2283	6.5422
STA. 1A-DILATION, mm	0.0789	---	---	---	---	---	---	---	---
STA. 2A-DILATION, mm	0.0889	---	---	---	---	---	---	---	---
STA. 3A-DILATION, mm	0.0889	---	---	---	---	---	---	---	---

Table 5.19 Average Shear Slip and Dilation for Specimen 2SK2

LOAD, kN	0	100	200	300	400	500	559	509	456	418	428
AVG. SLIP, mm	0.0000	-0.0168	0.0015	0.0307	0.0784	0.1669	0.4872	1.0912	2.0018	3.9294	4.1134
STA. 1A-DILATION, mm	0.0000	-0.0108	-0.0147	-0.0176	-0.0159	-0.0086	0.0402	0.1127	0.1925	---	---
STA. 2A-DILATION, mm	0.0000	-0.0260	-0.0266	-0.0249	-0.0216	-0.0086	0.0424	0.1103	0.1786	---	---
STA. 3A-DILATION, mm	0.0000	-0.0260	-0.0266	-0.0249	-0.0216	-0.0086	0.0424	0.1103	0.1786	---	---

	421	420	421	423	421	419
	4.5601	5.0513	5.5786	5.9485	6.5774	6.8998
(continued)	---	---	---	---	---	---
	---	---	---	---	---	---
	---	---	---	---	---	---

Table 5.20 Average Shear Slip and Dilation for Specimen 1SK4

LOAD, kN	0	100	200	300	400	500	600	700	800	884	840
AVG. SLIP, mm	0.0000	0.0111	0.0219	0.0486	0.0758	0.1124	0.1573	0.2042	0.3025	0.7096	0.7405
STA. 1A-DILATION, mm	0.0000	-0.0028	-0.0125	-0.0148	-0.0227	-0.0284	-0.0285	-0.0371	-0.0334	-0.0350	-0.0363
STA. 2A-DILATION, mm	0.0000	-0.0006	-0.0028	-0.0057	-0.0074	-0.0085	-0.0091	-0.0074	0.0027	0.0422	0.0393
STA. 3A-DILATION, mm	0.0000	-0.0006	-0.0028	-0.0057	-0.0074	-0.0085	-0.0091	-0.0074	0.0027	0.0422	0.0393

	724	672	621	624	621	616
	1.4708	2.2504	3.8988	4.6421	5.7115	6.2462
(continued)	---	---	---	---	---	---
	0.0506	---	---	---	---	---
	0.0506	---	---	---	---	---

Table 5.21 Average Shear Slip and Dilation for Specimen 2SK4B

LOAD, kN	0	100	200	300	400	500	600	700	800	893	710
AVG. SLIP, mm	0.0000	0.0072	0.0213	0.0334	0.0503	0.0752	0.1031	0.1588	0.2855	1.0629	1.9567
STA. 1A-DILATION, mm	0.0000	-0.0045	-0.0051	-0.0085	-0.0119	-0.0130	-0.0142	-0.0137	-0.0070	0.0357	---
STA. 2A-DILATION, mm	0.0000	-0.0028	-0.0023	-0.0051	-0.0051	-0.0034	-0.0051	-0.0017	0.0151	0.0911	0.1076
STA. 3A-DILATION, mm	0.0000	-0.0028	-0.0023	-0.0051	-0.0051	-0.0034	-0.0051	-0.0017	0.0151	0.0911	0.1076

(continued)

658	654	637	628	620	614
3.0304	3.5988	4.0078	4.4655	4.9521	5.3975
---	---	---	---	---	---
---	---	---	---	---	---
---	---	---	---	---	---

Table 6.1 Predicted Cracking Shear Load

Specimen	Cracking shear load, kN		
	Model I	Model II	Test
1LK2	632	530	569
2LK4	931	727	867
3LK4B	931	727	1000
2SK2	580	490	559
1SK4	882	701	884
3SK4B	882	701	893
SP25*	1101	1059	1300

* specimen from a previous study [3]

Table 6.2 Drypack Compressive Strength Reduction Factors

Specimen	Reduction Factor, ψ	
	Equation (6.18)	Equation (6.20)
1LK2	0.7064	0.6787
2LK4	0.8200	0.7565
3LK4B	1.7718	0.9382
2SK2	0.6257	0.6620
1SK4	0.7800	0.8048
3SK4B	1.0155	1.000

Table 6.3 Predicted Shear Capacity Immediately After Cracking

	Shear capacity immediately after cracking, kN	
Specimen	Model	Test*
1LK2	569	569
2LK4	813	867
3LK4B	813	1058
2SK2	598	559
1SK4	843	884
3SK4B	843	893
SP25**	1018	1527

* maximum load

** specimen from previous study [3]

Table 6.4 Parameters for Regression Analysis

Specimen	PARAMETER		
	$\bar{v}_u/f'_g$	B/A_c	σ_n/f'_g
1LK2	0.0770	0.4902	0.0752
2LK4	0.1268	0.4902	0.1504
3LK4B	0.1150	0.4902	0.1504
2SK2	0.0772	0.3922	0.0752
1SK4	0.1146	0.3922	0.1504
3SK4B	0.1194	0.3922	0.1504

Table 6.5 Predicted Ultimate Shear Load

Specimen	Ultimate shear load, kN		
	Regression Model	Simplified Model	Test
1LK2	417	414	418
2LK4	644	618	688
3LK4B	644	618	624
2SK2	417	414	419
1SK4	644	618	622
3SK4B	644	618	648
SP25*	764	677	988

* specimen from previous study [3]

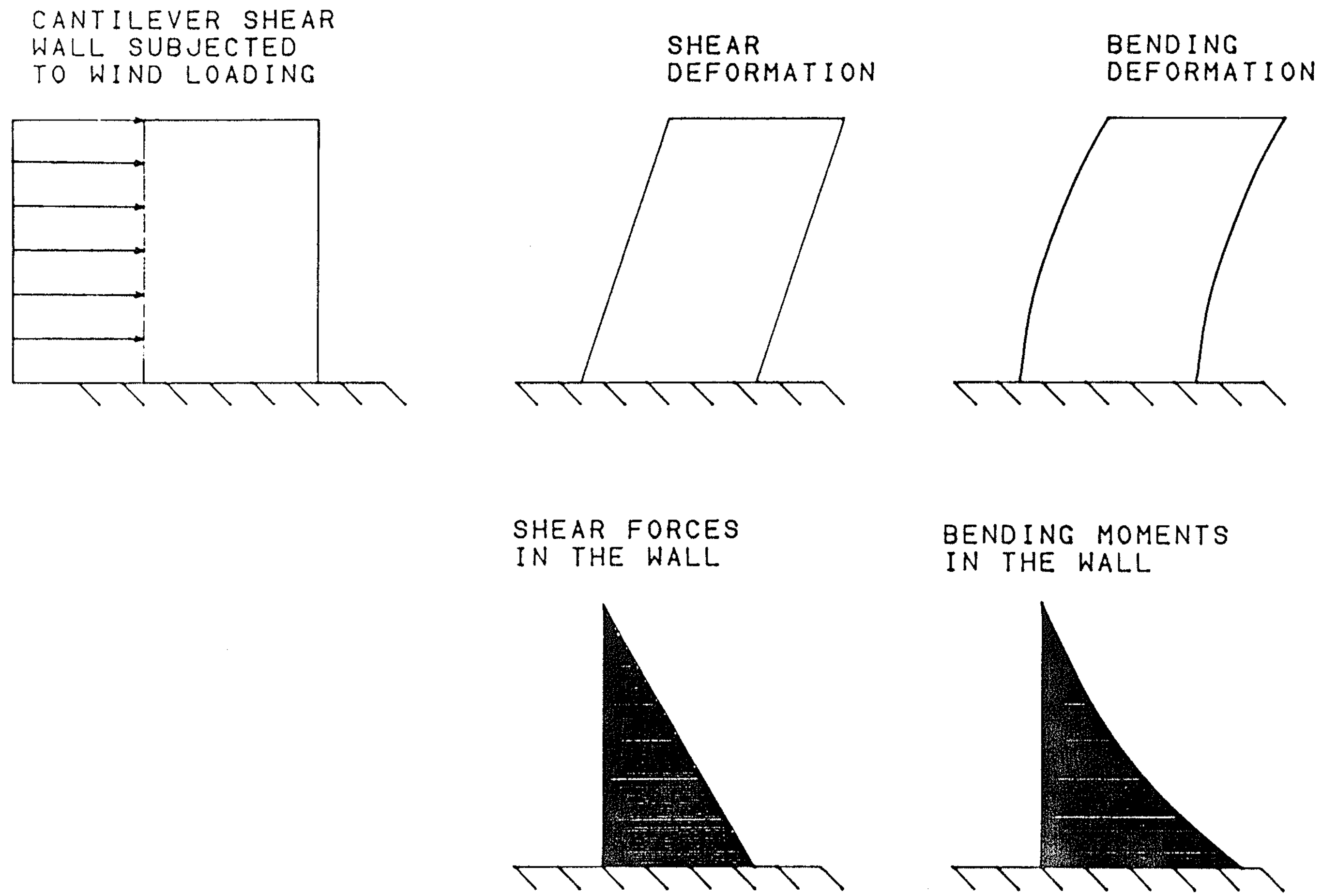

Figure 2.1 Cantilever Shear Wall Subjected to Lateral Load

Figure 2.2 Elevator Shaft Shear Wall with Multiple Shear Key Connection

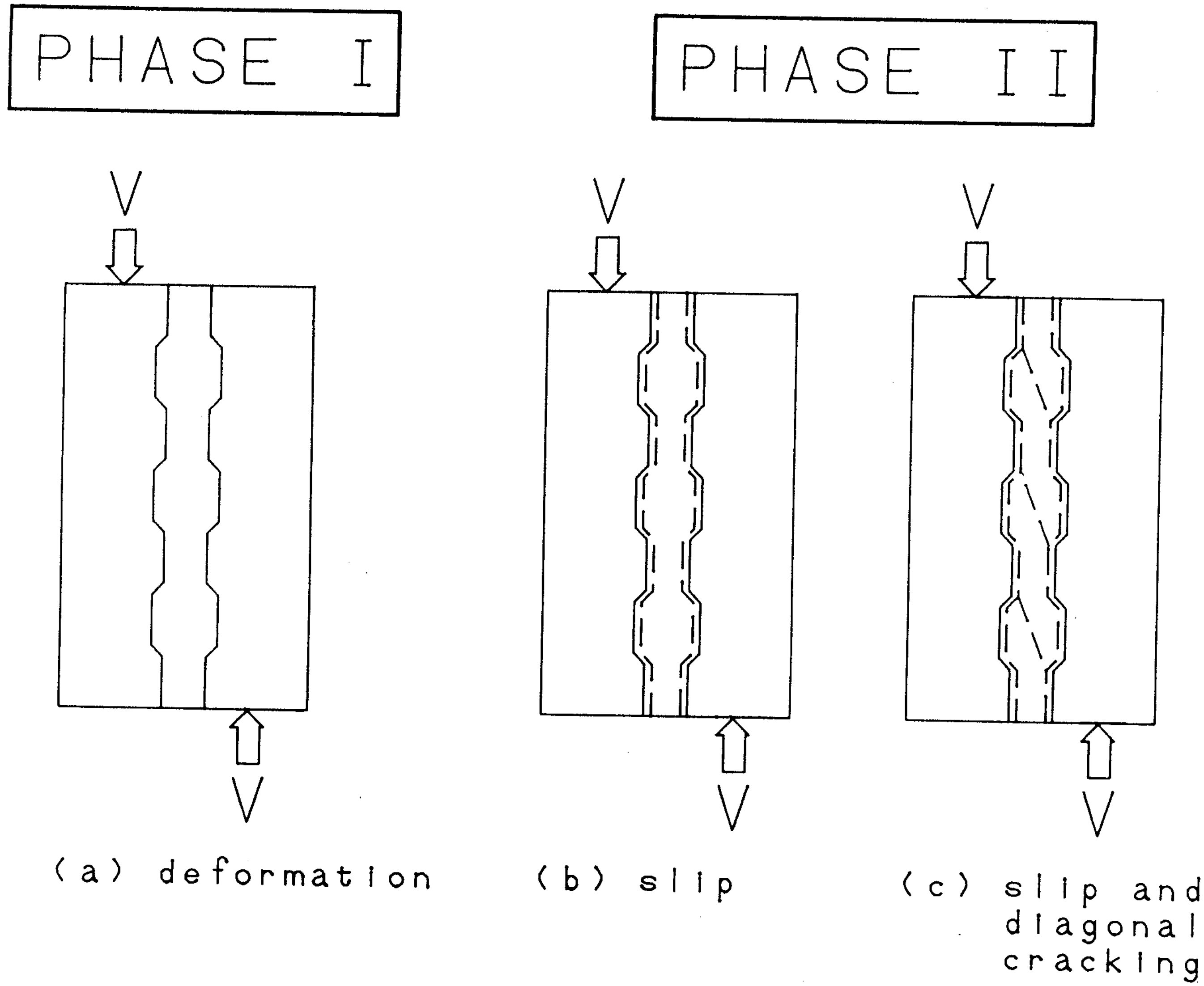

Figure 2.3 Cracking Behaviour of Multiple Shear Key Connections

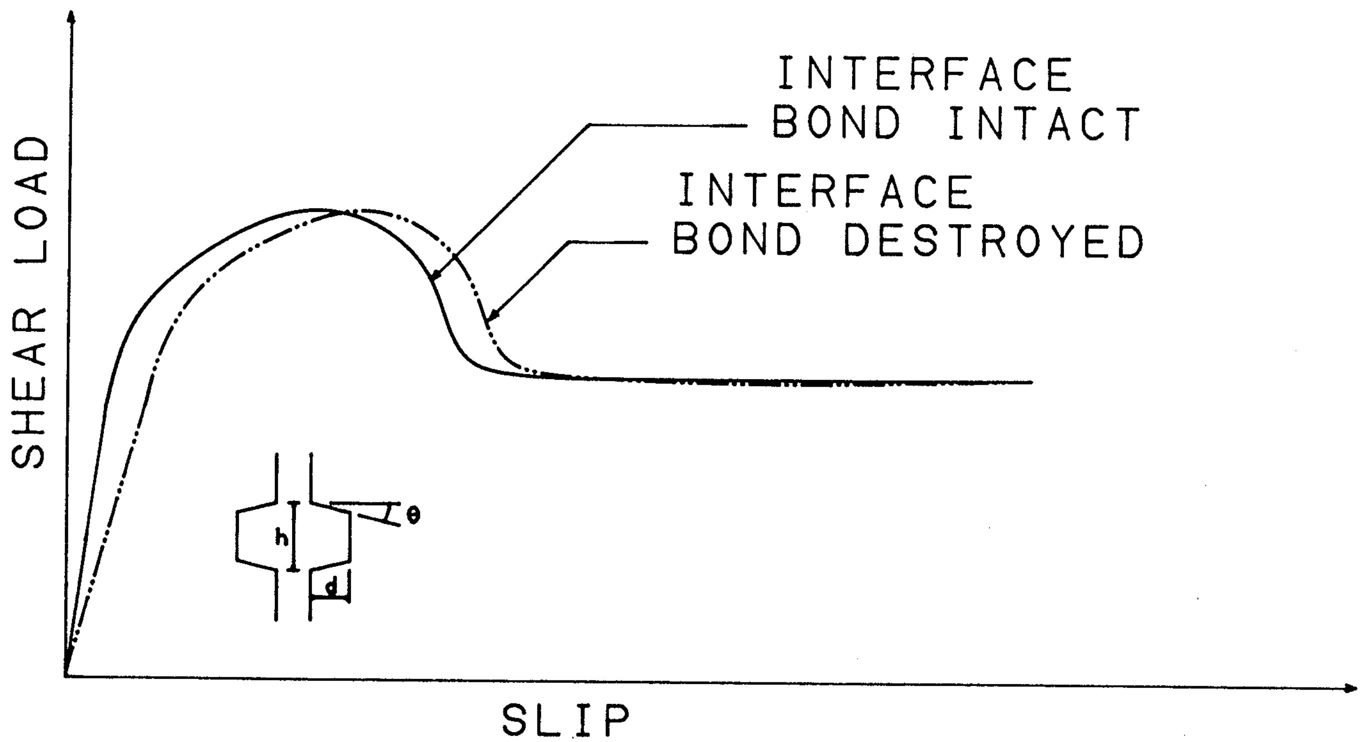

Figure 2.4 Typical Shear Load-Slip Relationship for Multiple Shear Key Connections

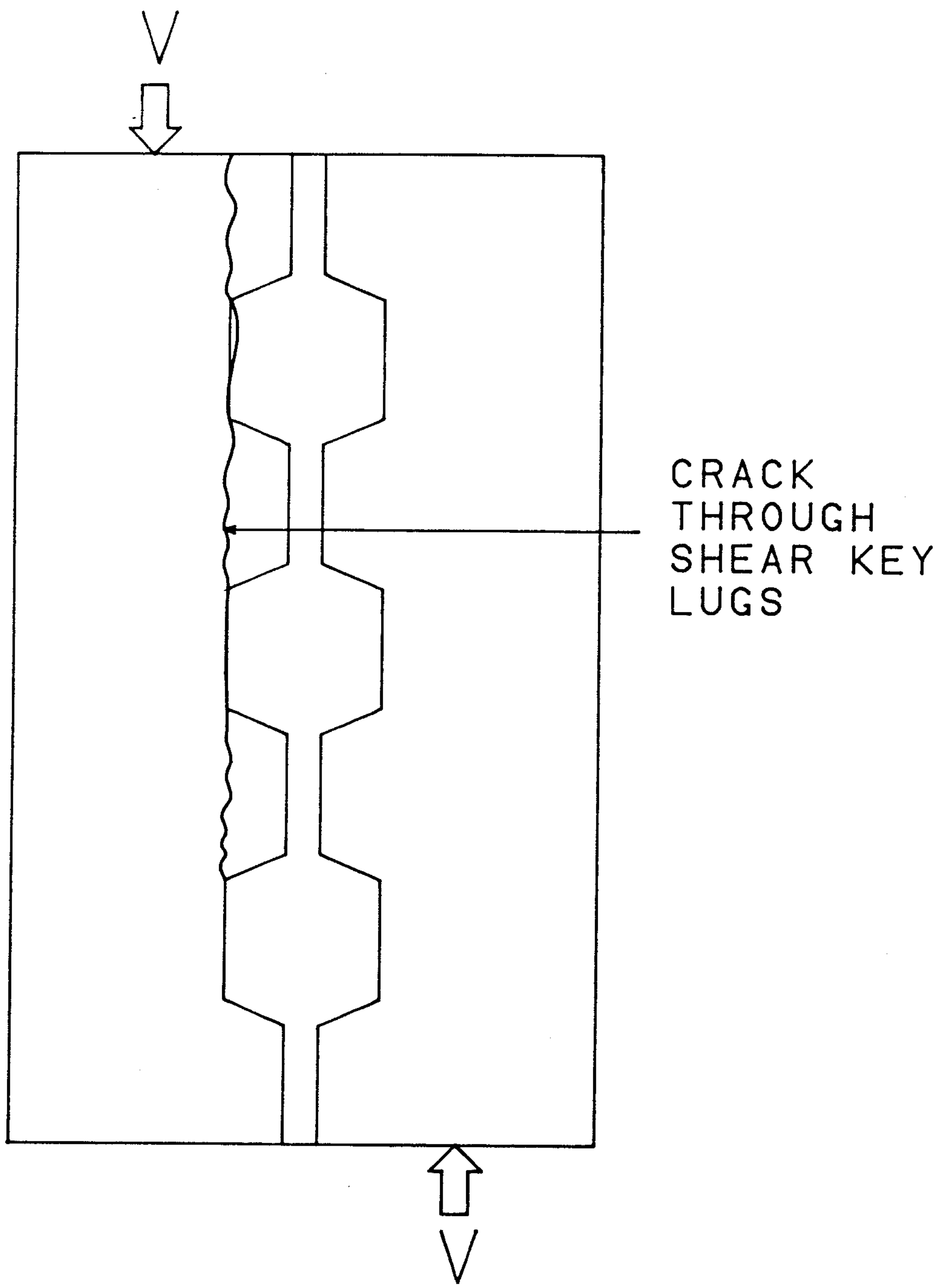

Figure 2.5 Failure Mode for High Strength Drypack

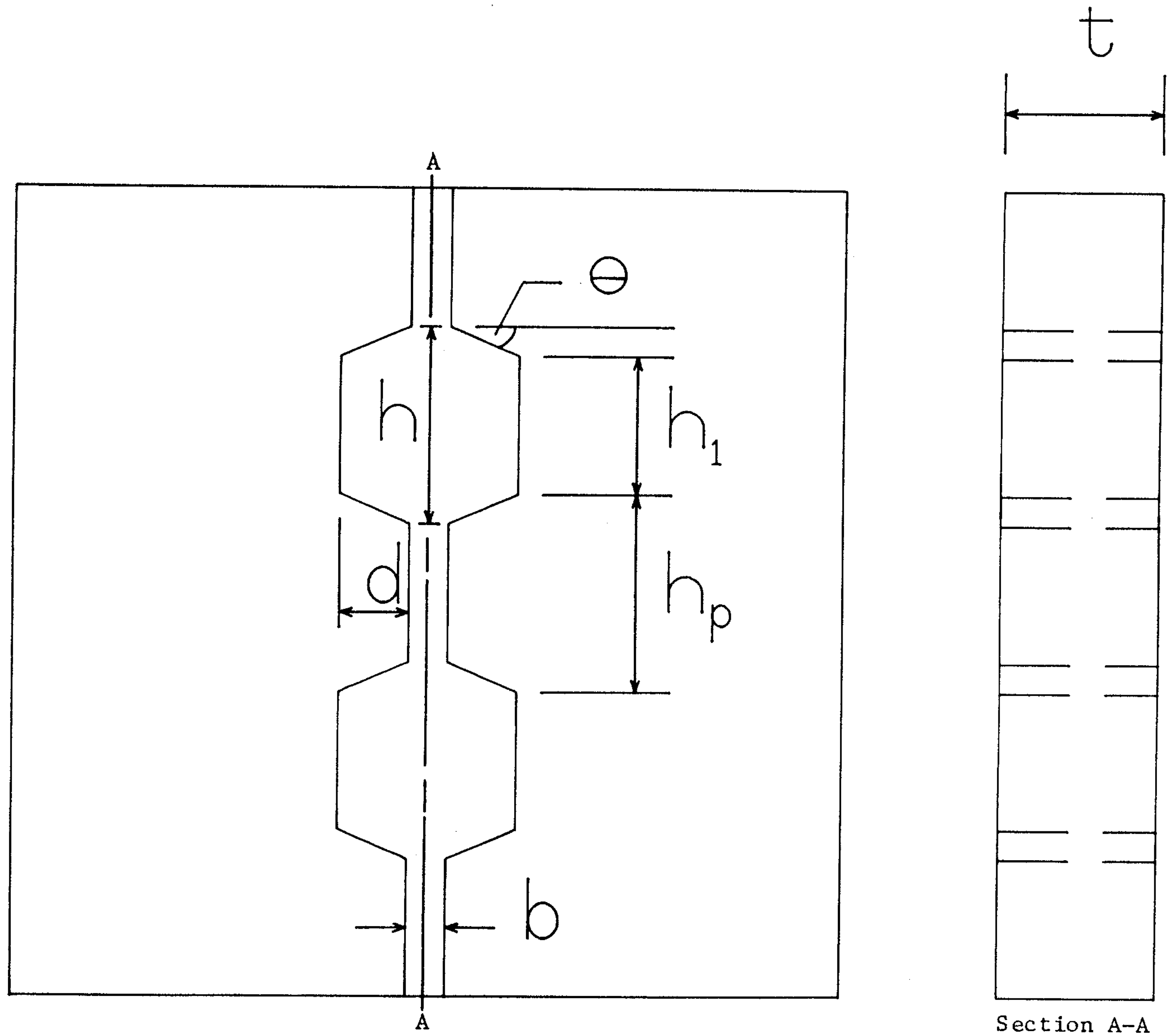

Figure 2.6 Shear Key Dimensions

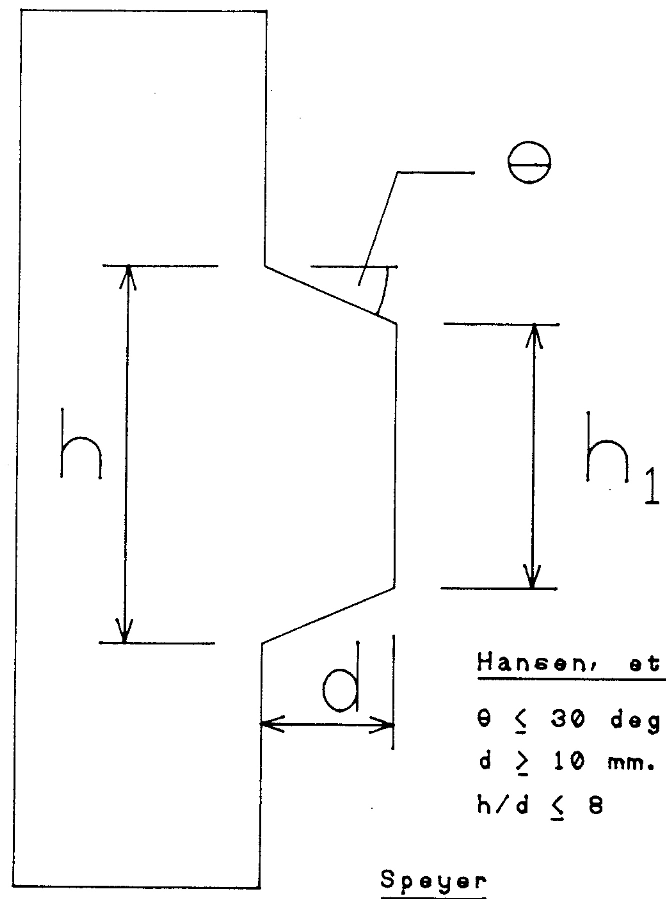

<u>Hansen, et al.</u>

$\theta \leq 30$ degrees

$d \geq 10$ mm.

$h/d \leq 8$

<u>Speyer</u>

$\theta \leq 30$ to 35 degrees

$h_1/d \leq 6$

$h_p = h$

Figure 2.7 Recommended Shear Key Dimensions

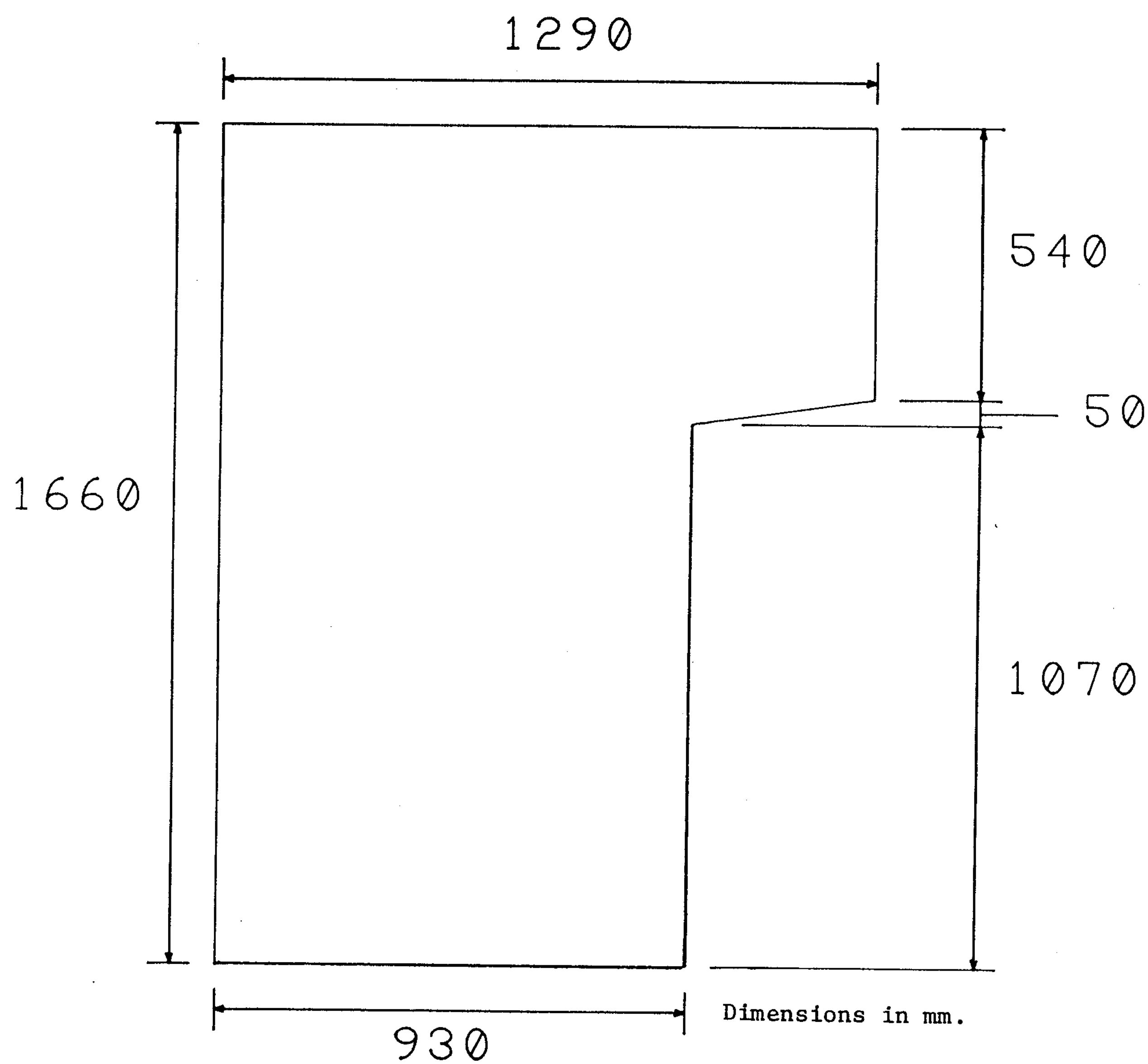

Figure 3.1 Overall Panel Dimensions

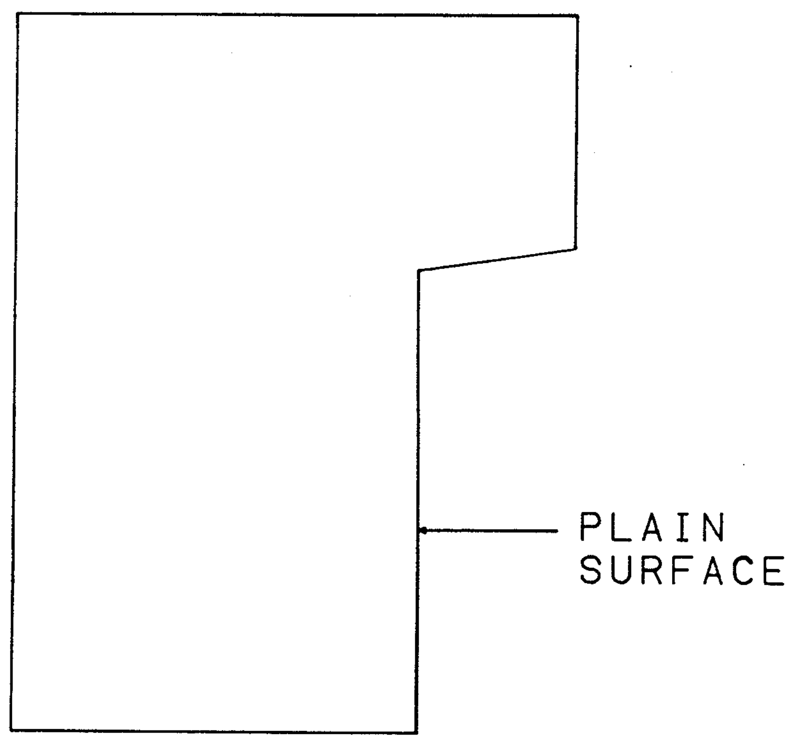

Figure 3.2 NK or No-Key Panel Configuration

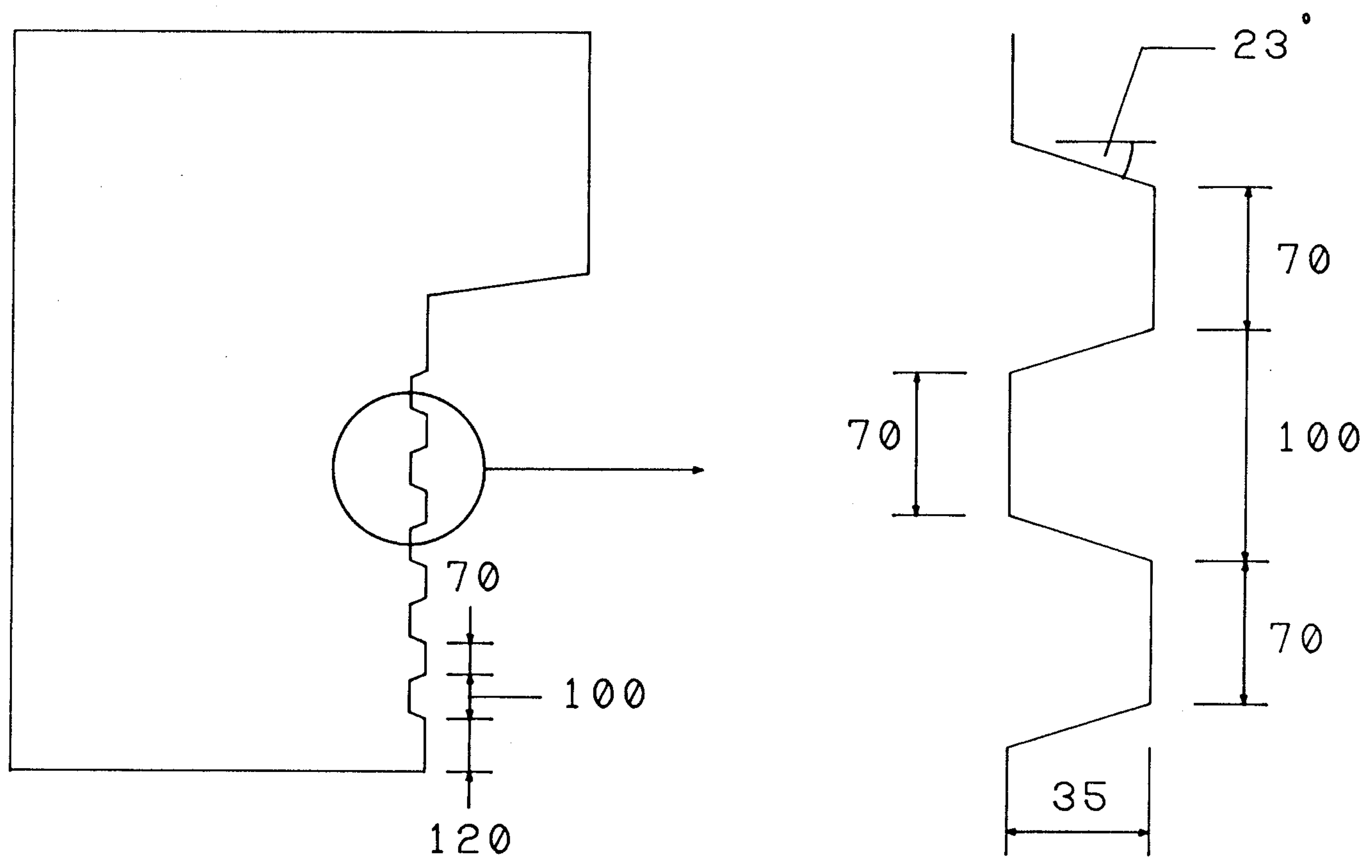

Dimensions in mm.

Figure 3.3 LK or Large-Key Panel Configuration

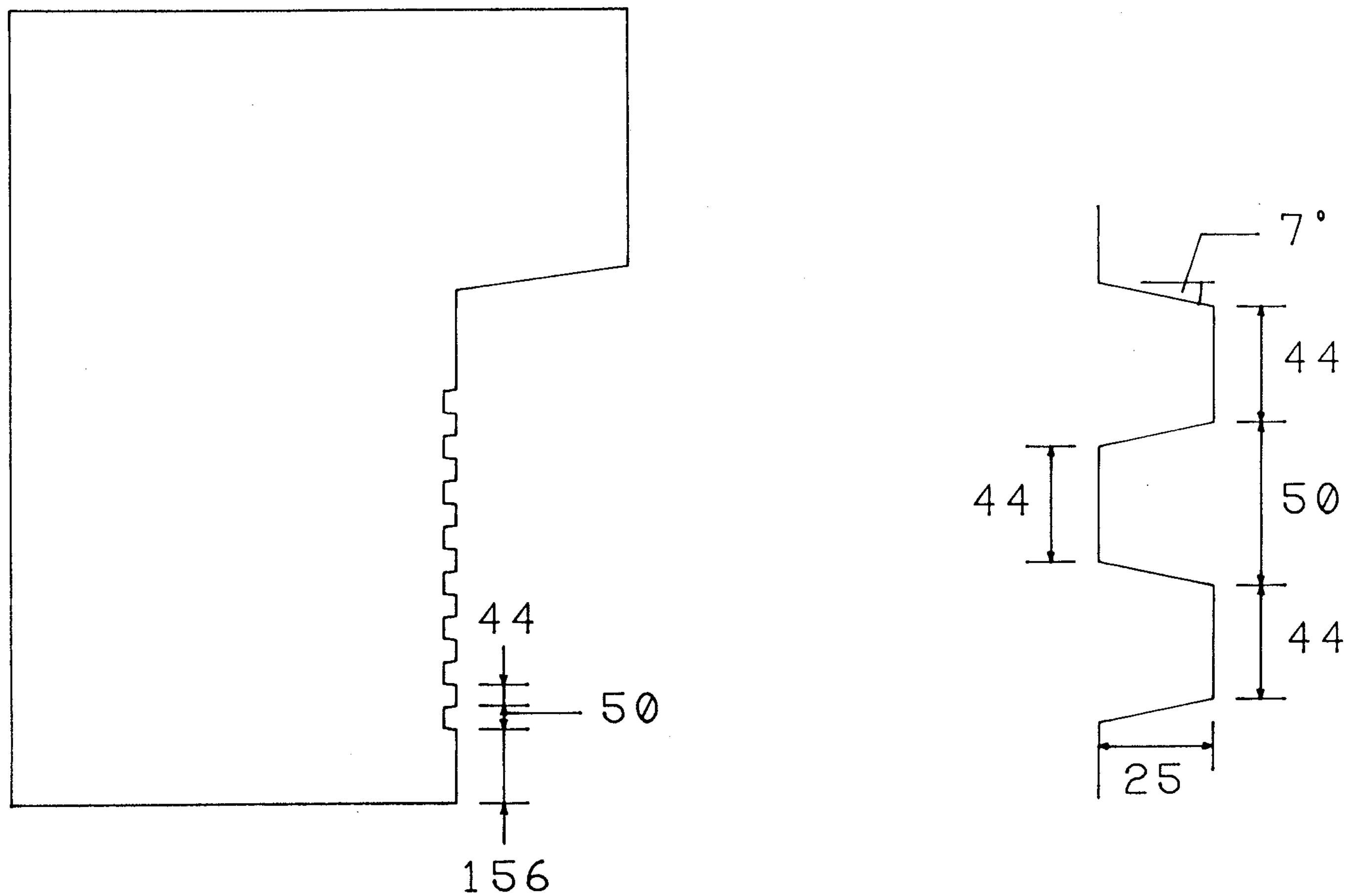

Dimensions in mm.

Figure 3.4 SK or Small-Key Panel Configuration

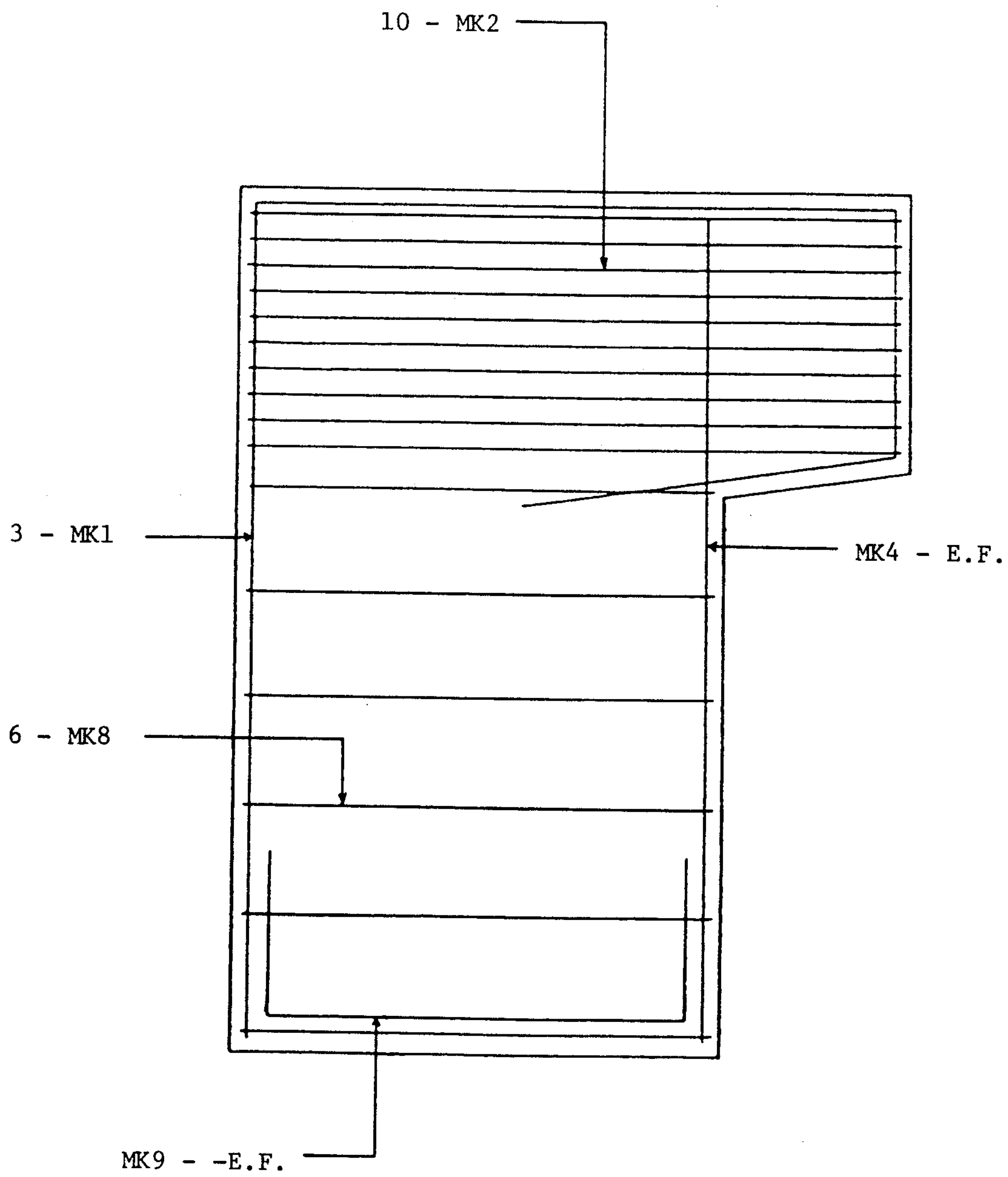

Figure 3.5 No-Key Panel Reinforcement

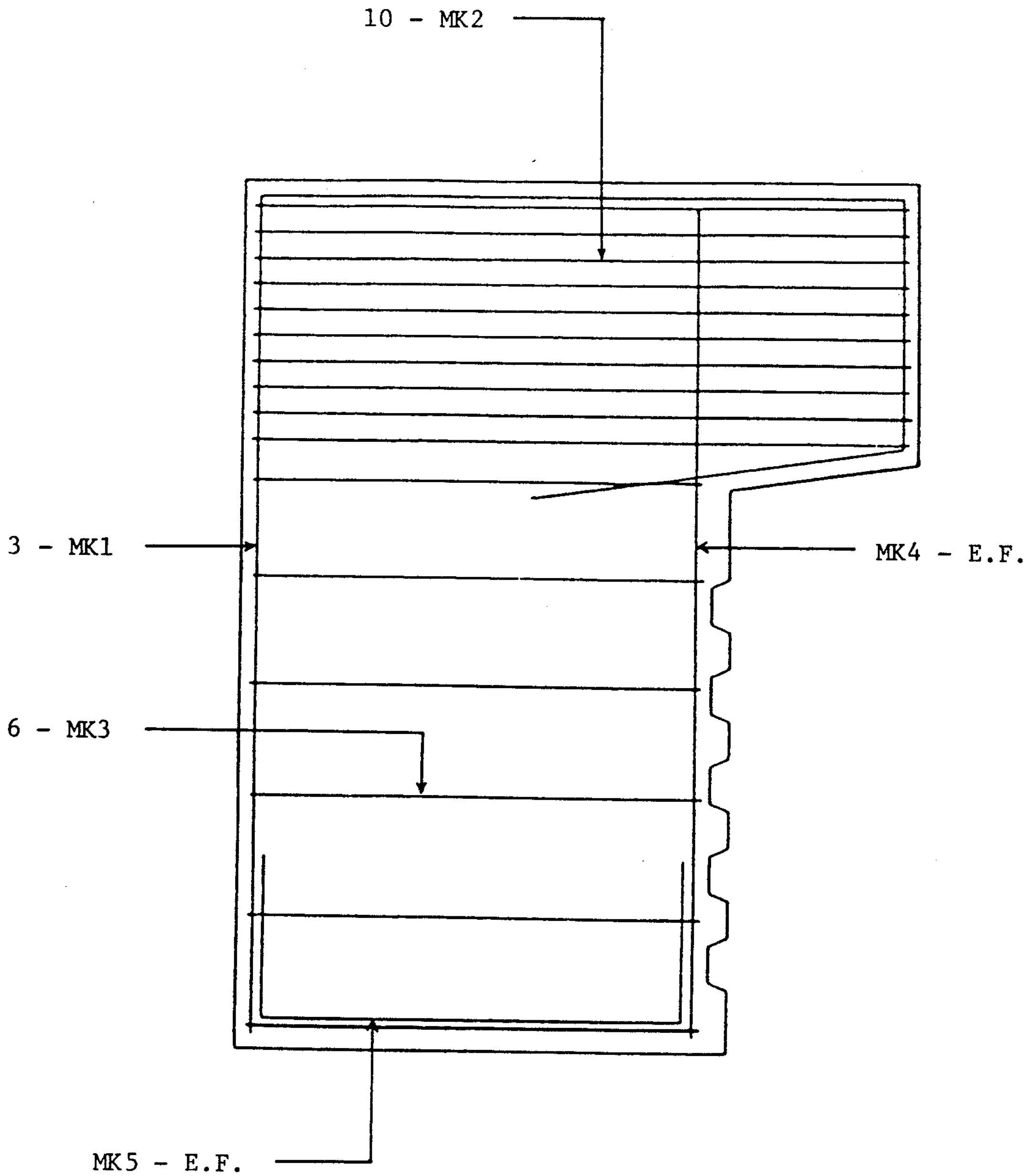

Figure 3.6 Large-Key Panel Reinforcement

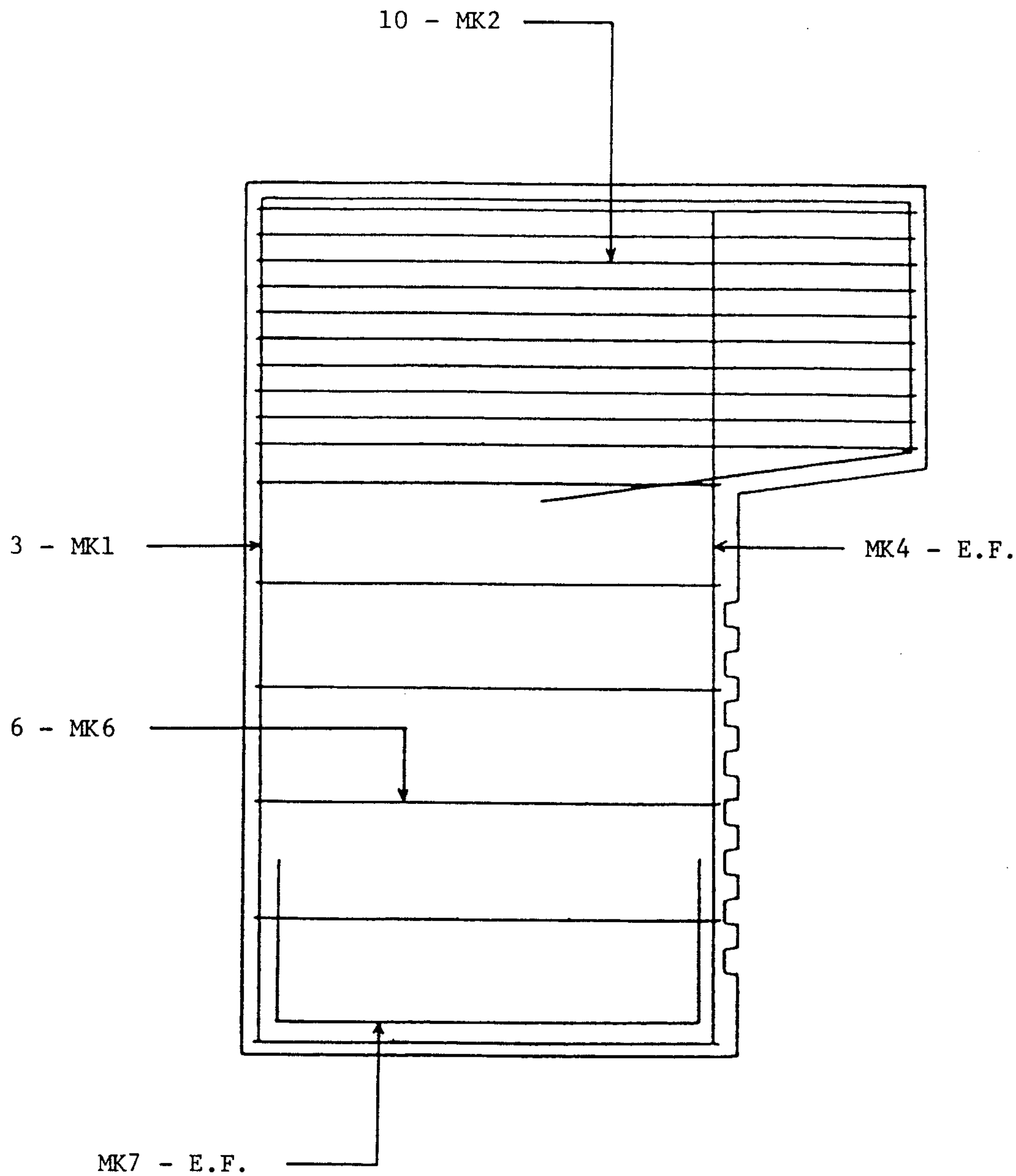

Figure 3.7 Small—Key Panel Reinforcement

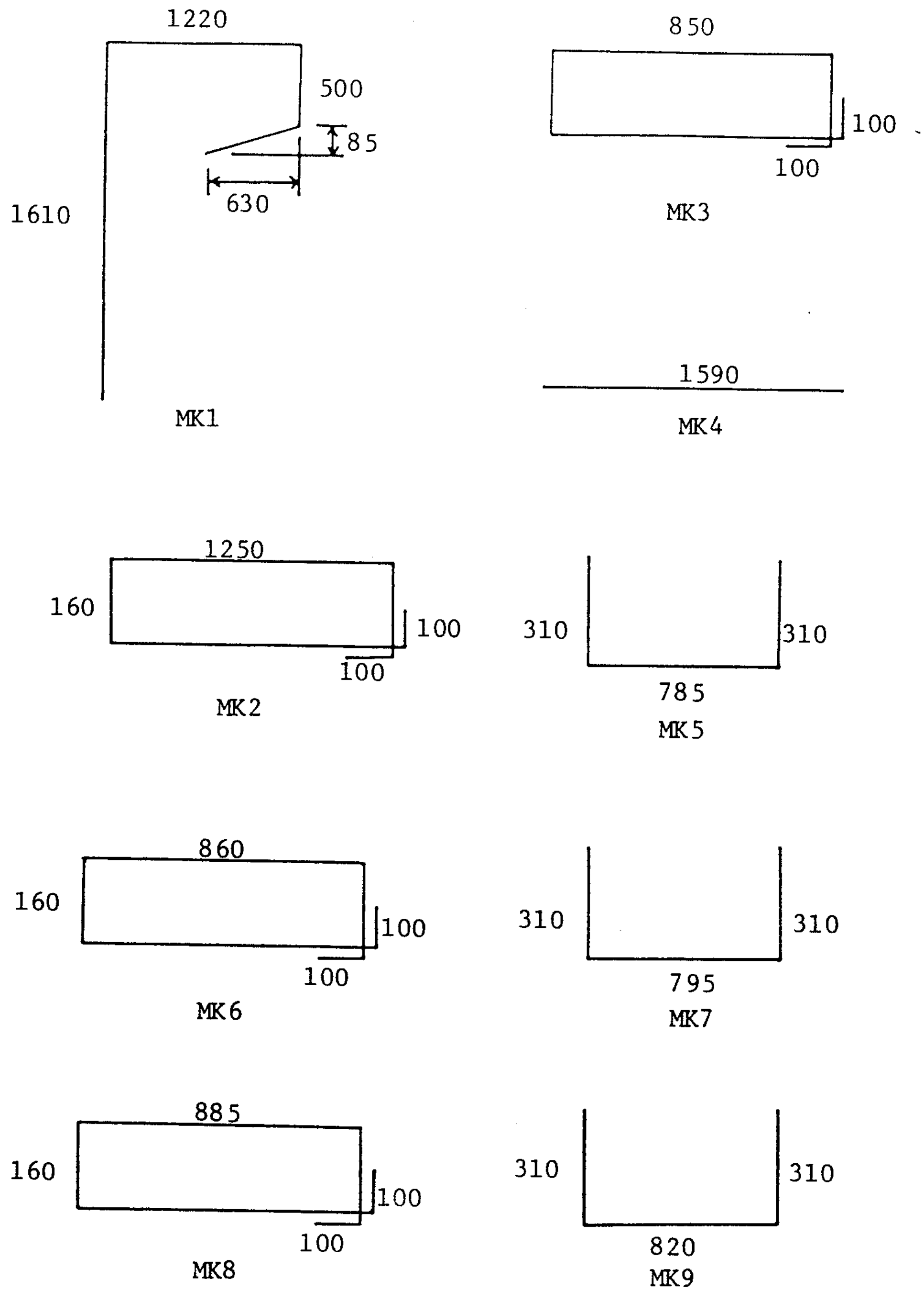

Not to scale
Dimensions in mm.

Figure 3.8   Reinforcement Details

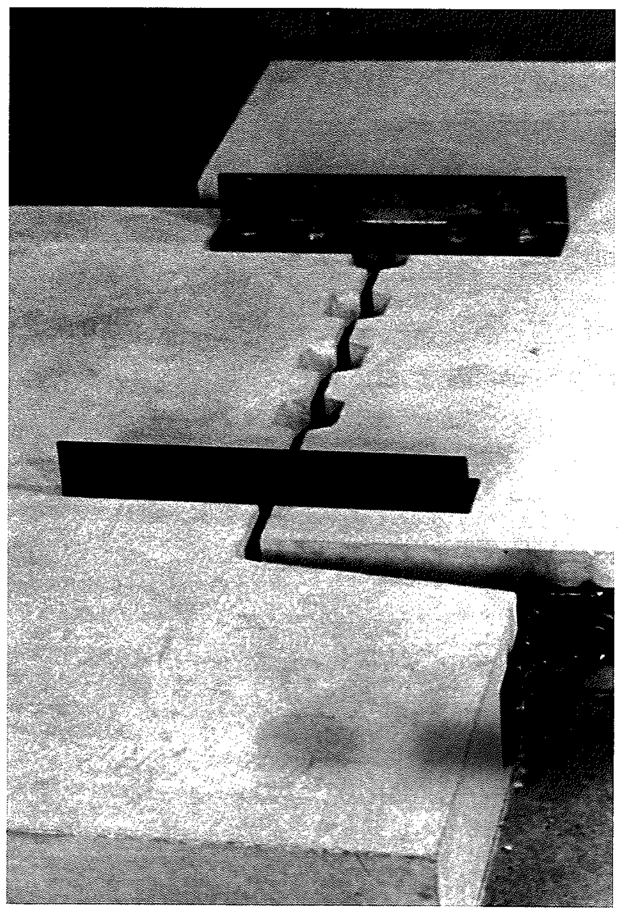

Figure 3.9 Horizontal Assembly of the Specimens

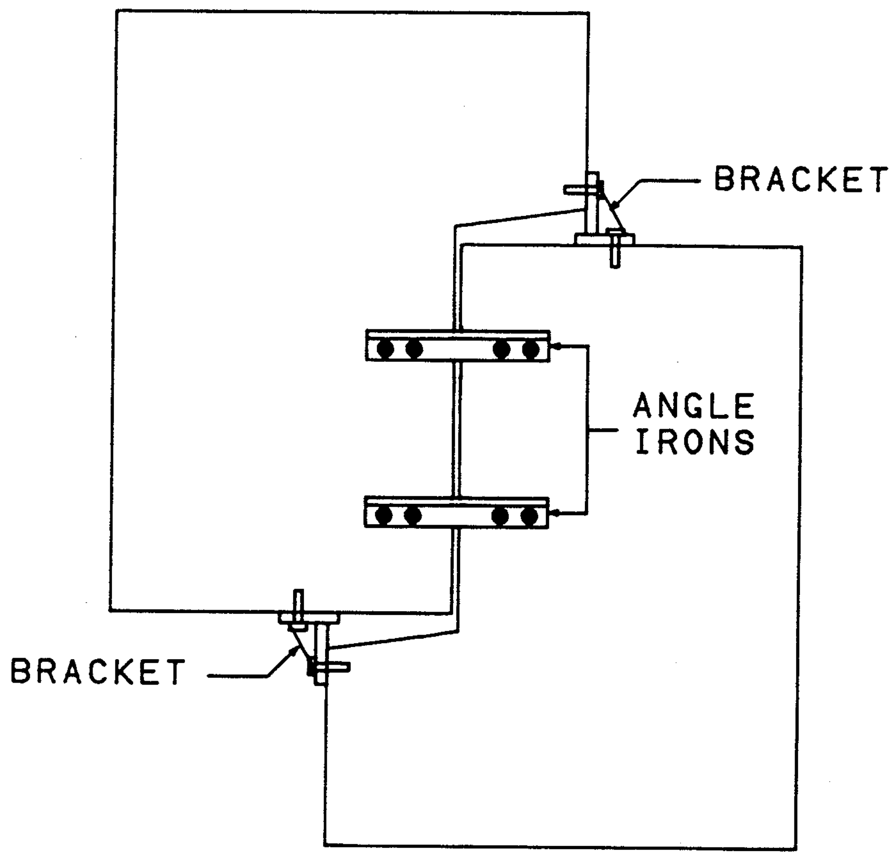

Figure 3.10 Temporary Bracing System

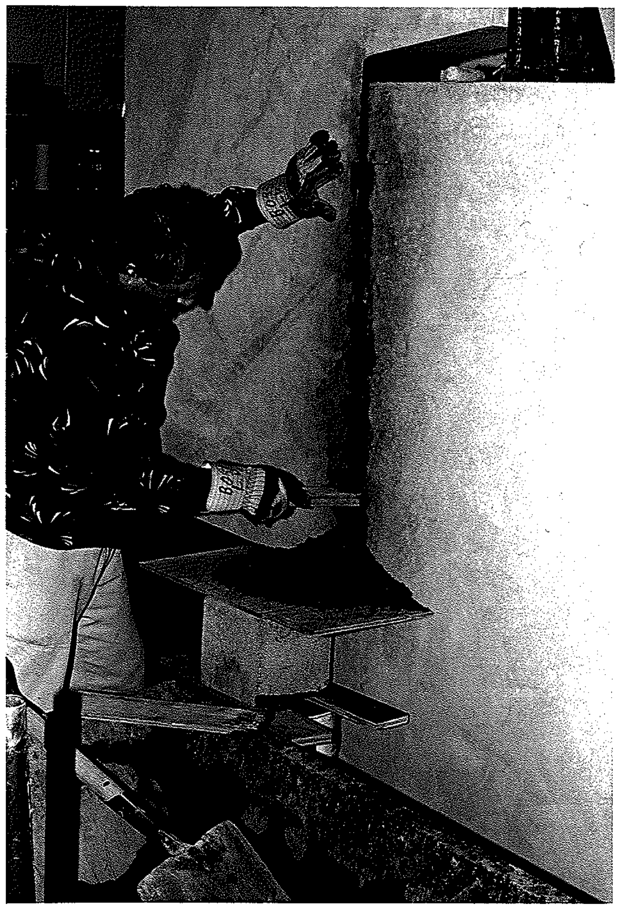

Figure 3.11 Drypacking of the Specimen

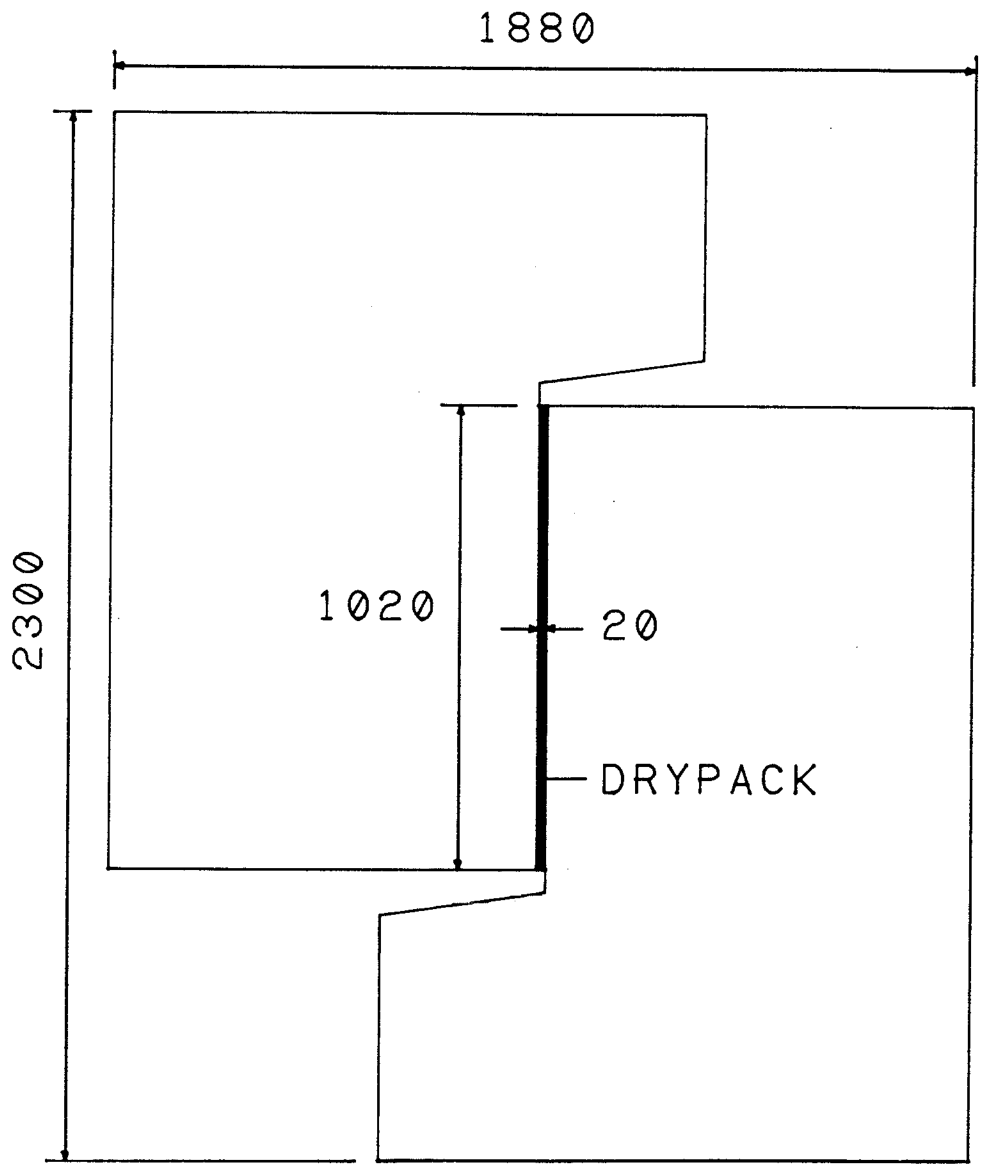

Dimensions in mm.

Figure 3.12 Typical No-Key Specimen

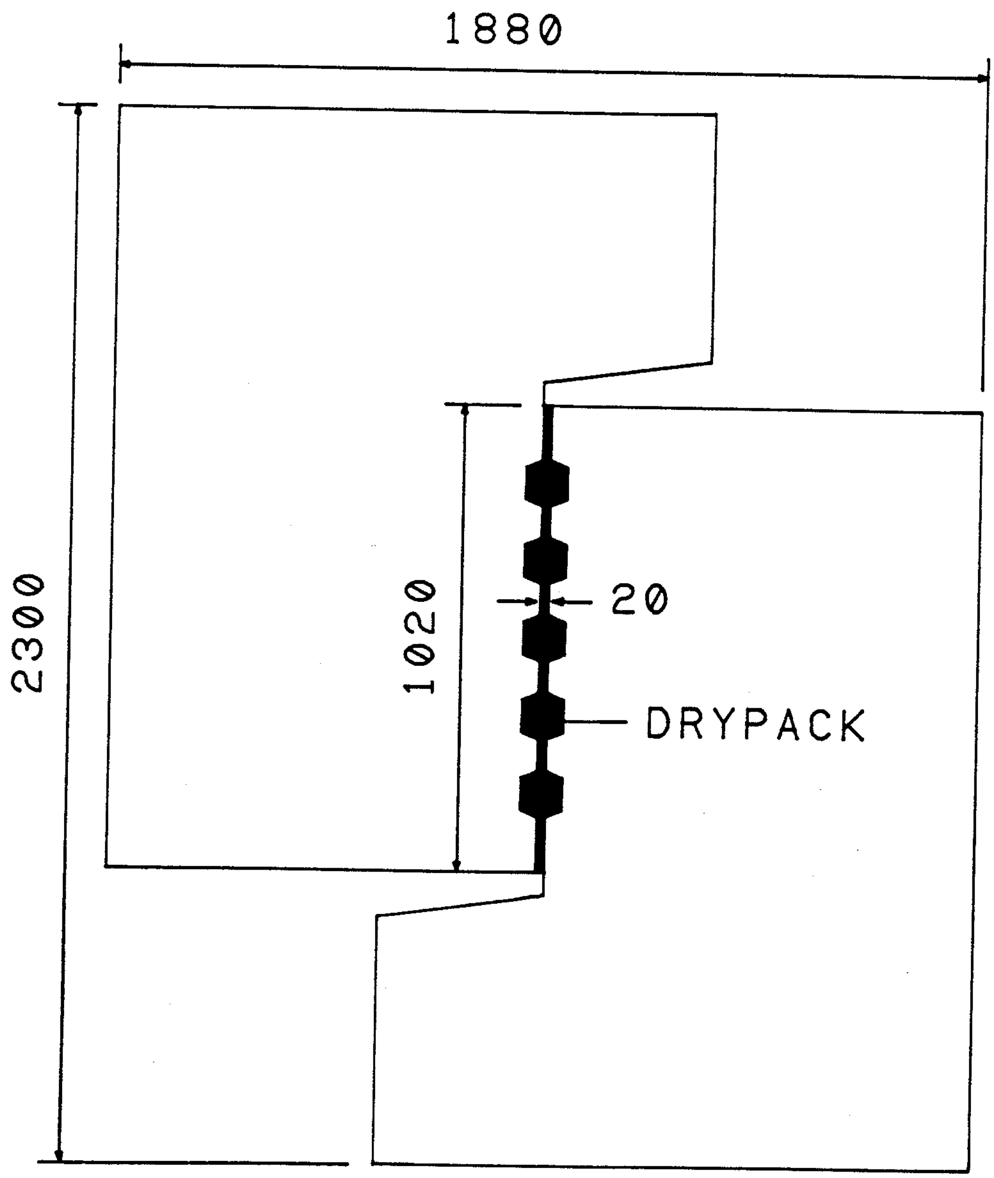

Dimensions in mm.

Figure 3.13 Typical Large-Key Specimen

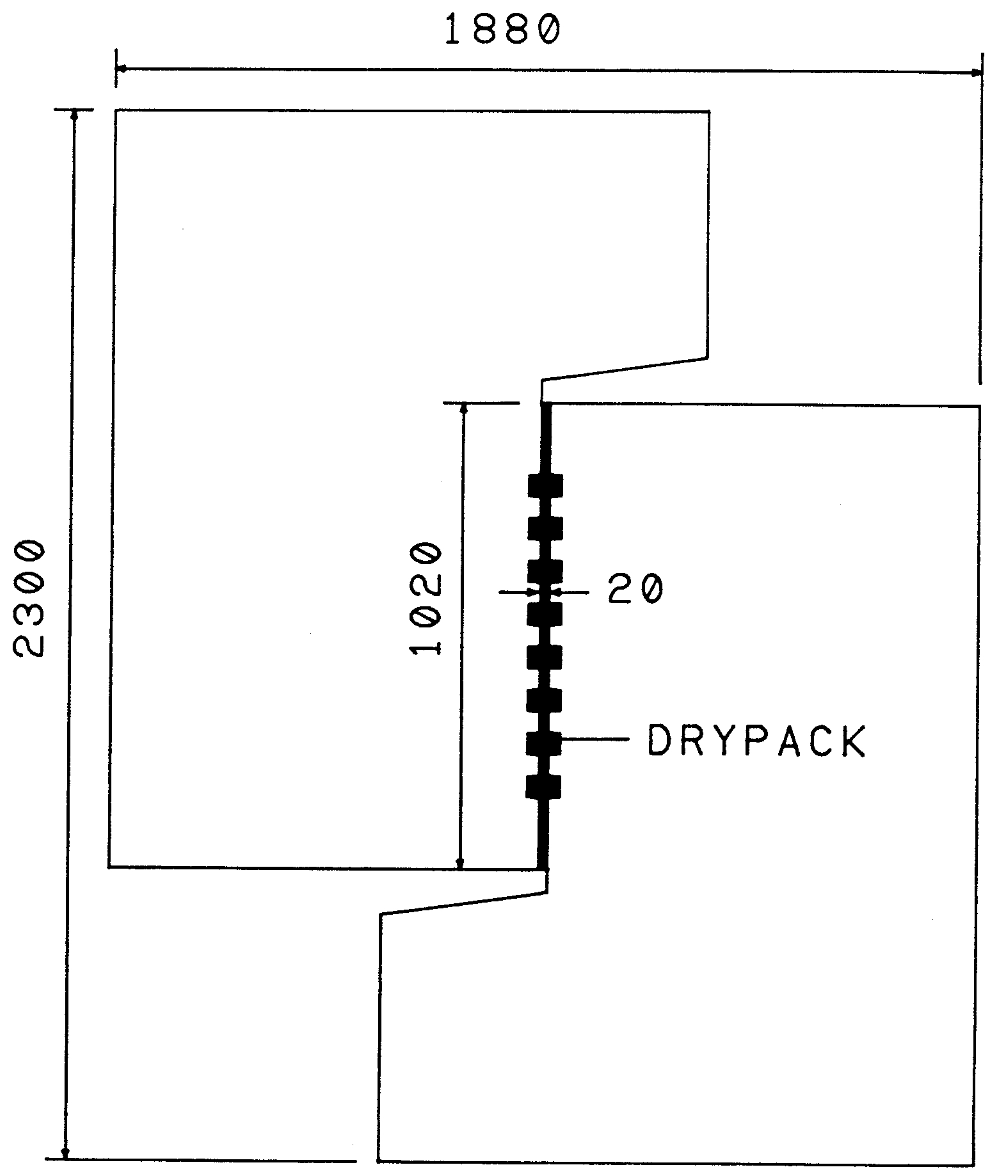

Dimensions in mm.

Figure 3.14 Typical Small-Key Specimen

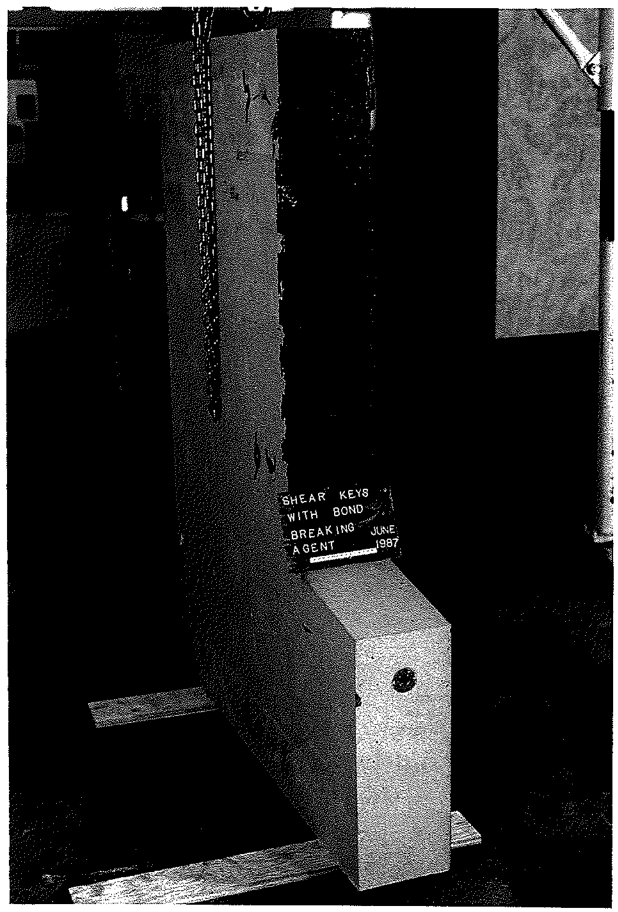

Figure 3.15 Panel with Bond Breaking Agent

Figure 3.16 Drypack Consistency

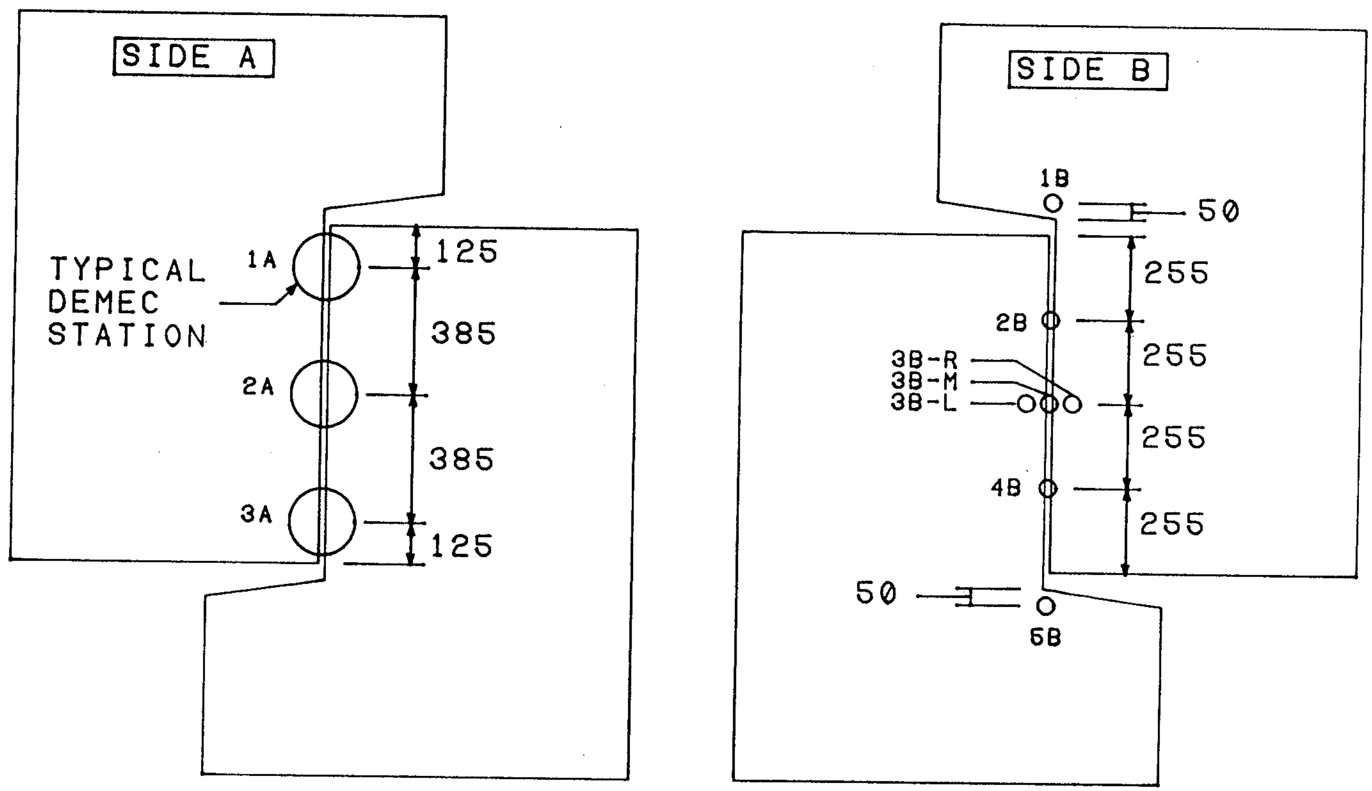

Dimensions in mm.

Figure 3.17 Demec Station Layout for the No-Key Specimen

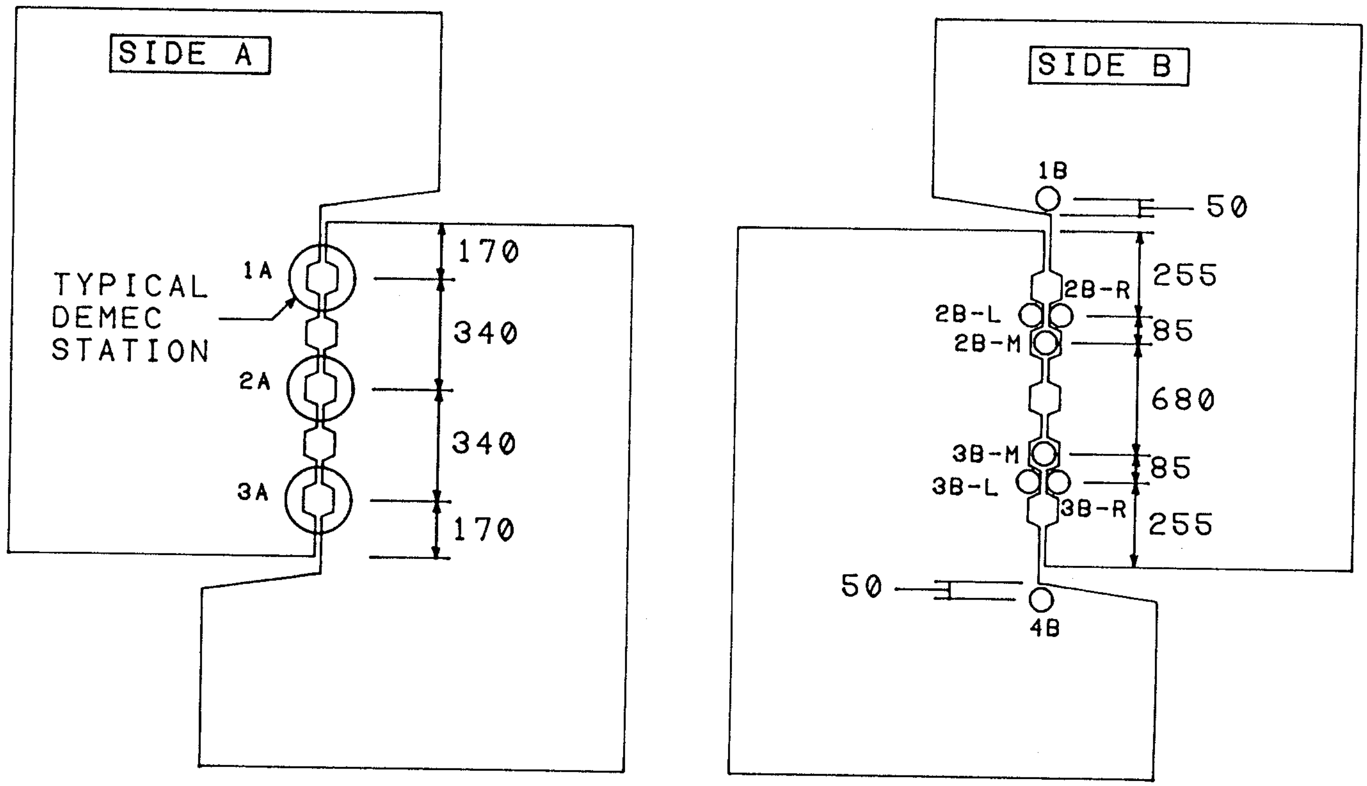

Dimensions in mm.

Figure 3.18 Demec Station Layout for the Large-Key Specimen

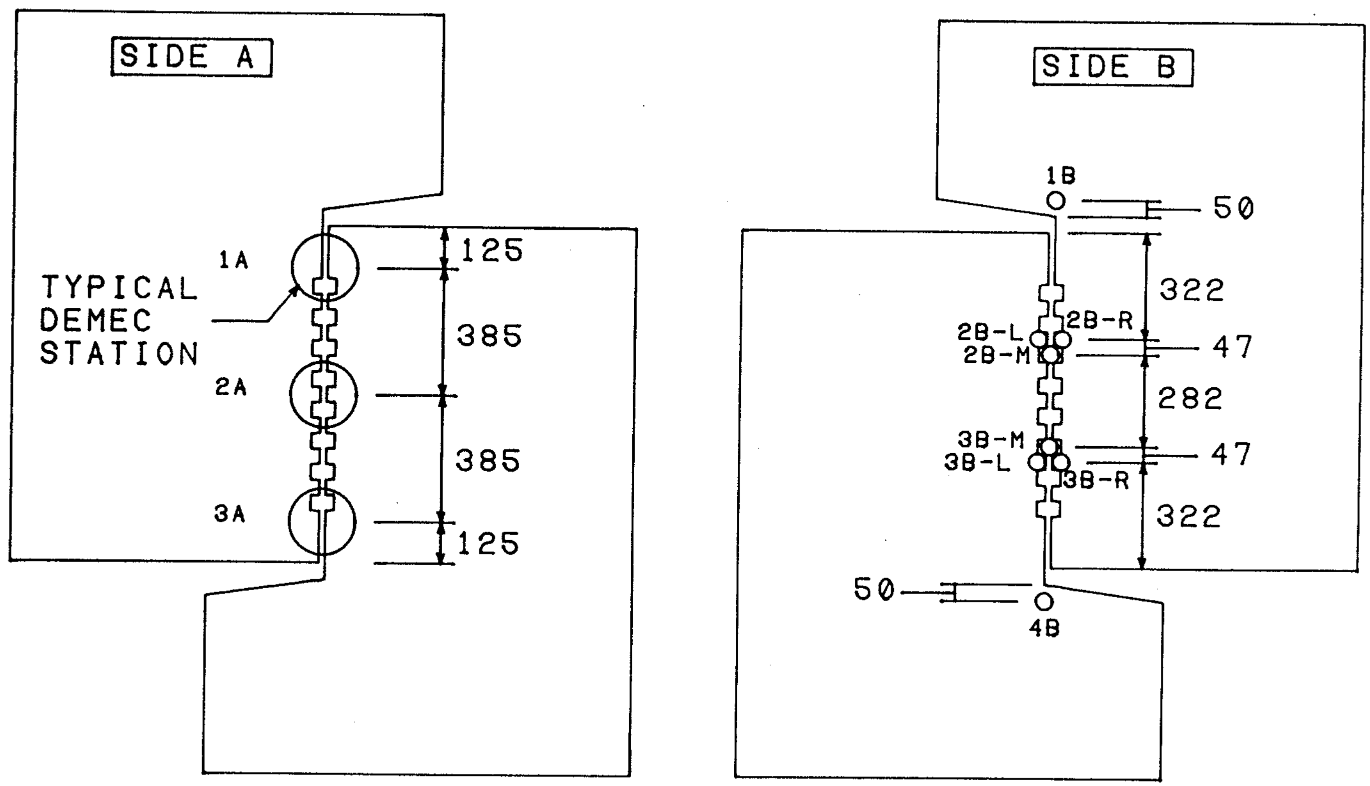

Dimensions in mm.

Figure 3.19 Demec Station Layout for the Small–Key Specimen

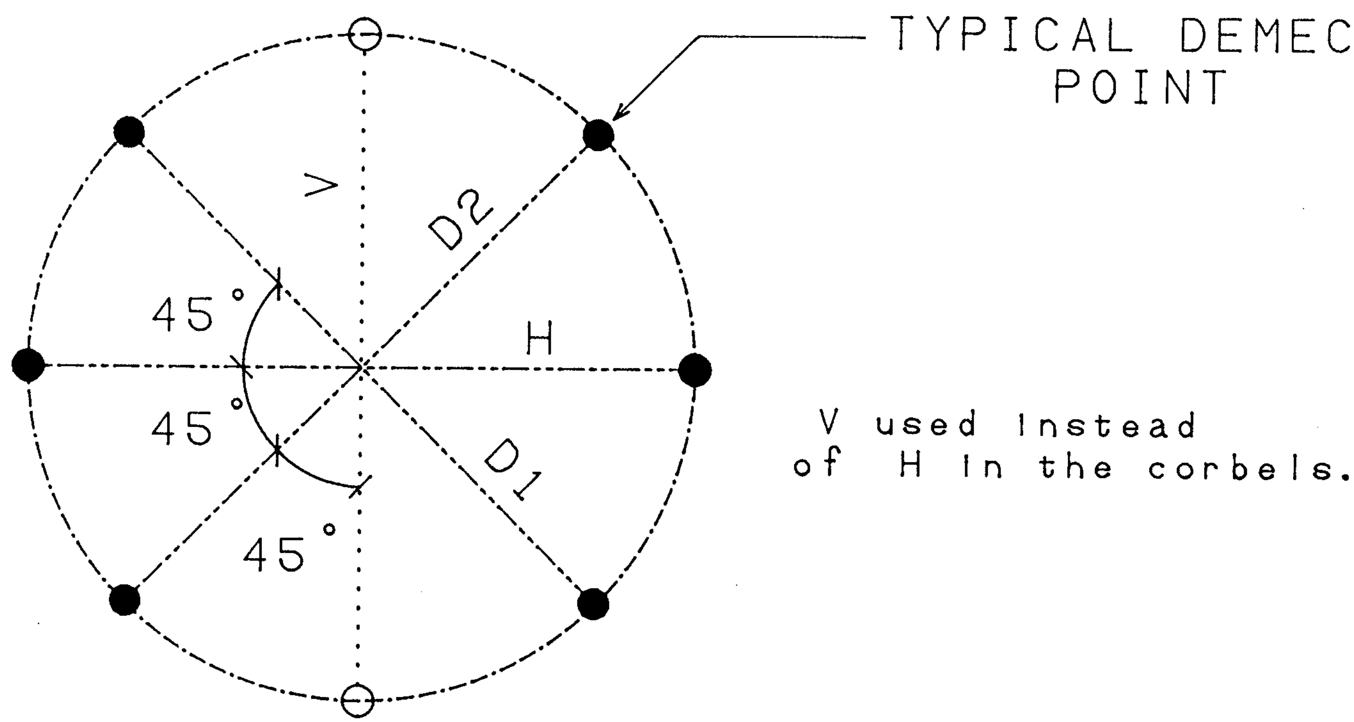

Figure 3.20 Demec Point Layout at Each Station

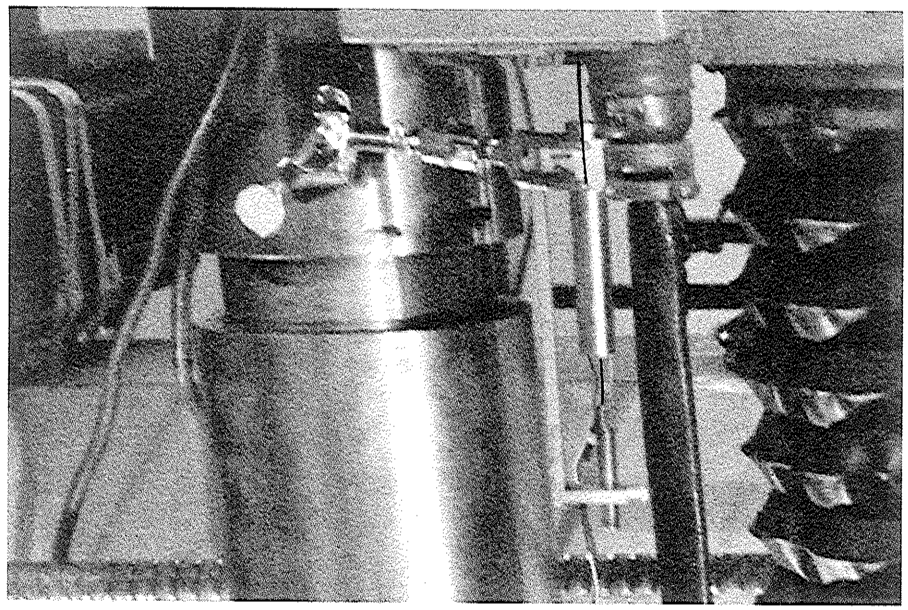

Figure 3.21 LVDT to Measure Stroke Displacement

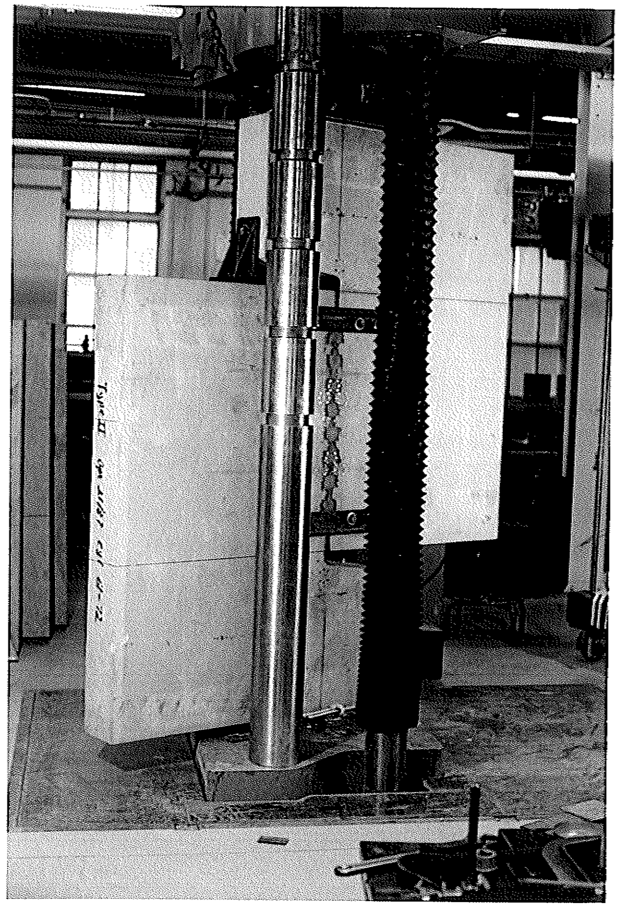

Figure 3.22 Installation of the Specimen in the Testing Machine

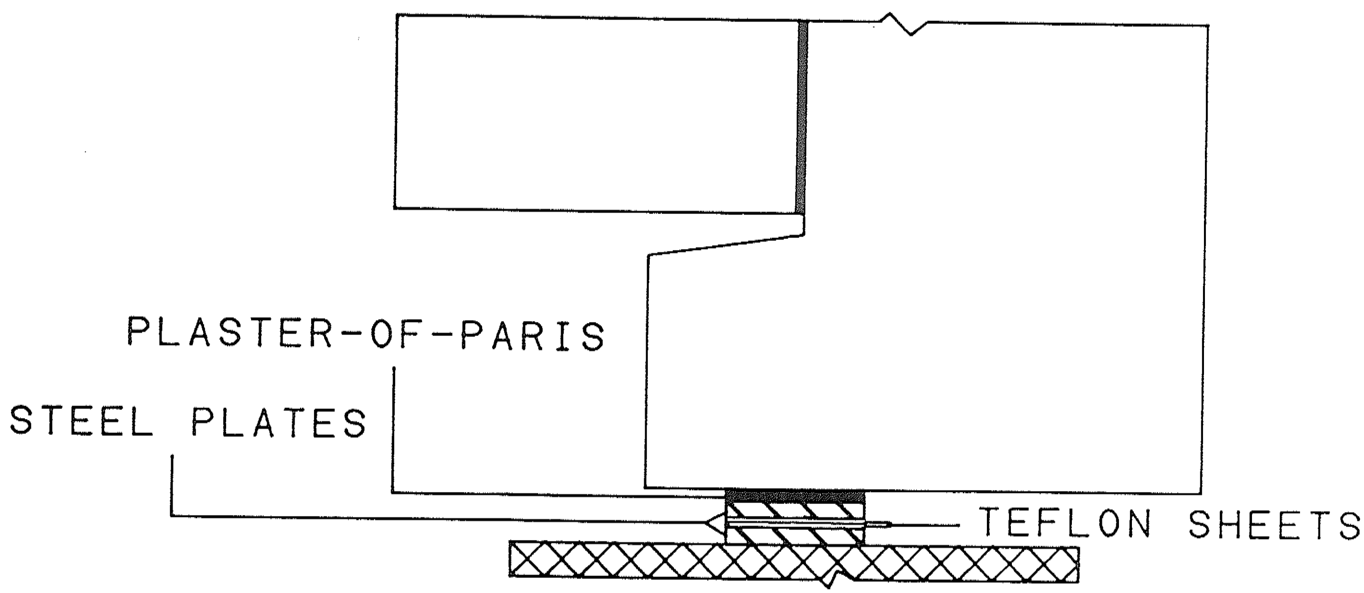

Figure 3.23 Steel Bearing Pad

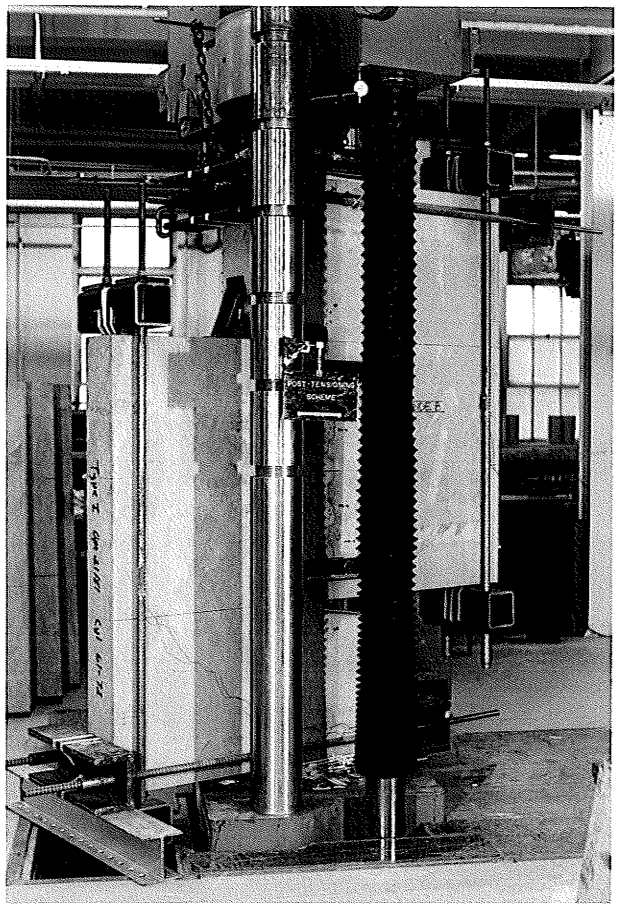

Figure 3.24 Specimen Ends Post-tensioned

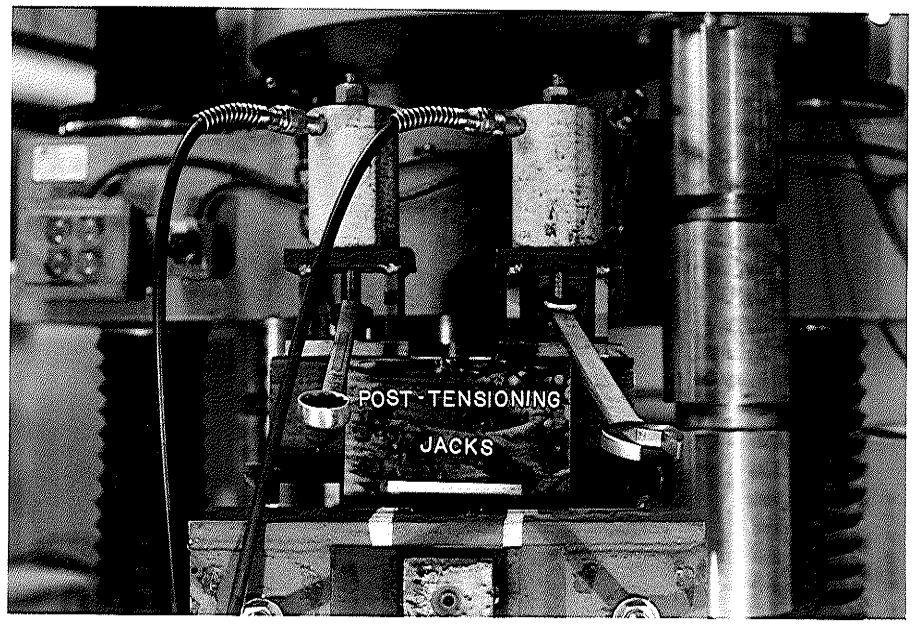

Figure 3.25 Post-tensioning Jacks

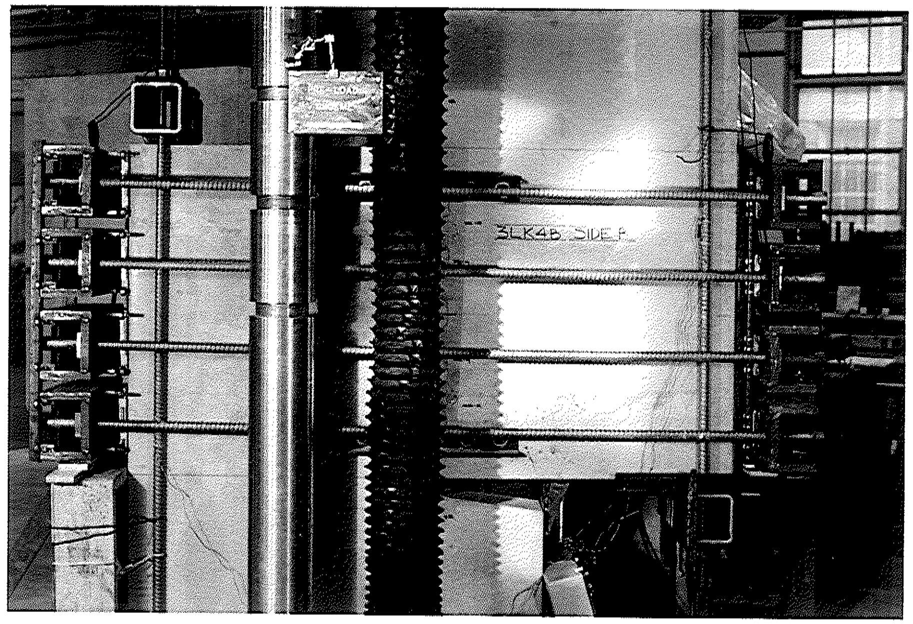

Figure 3.26 Preload System

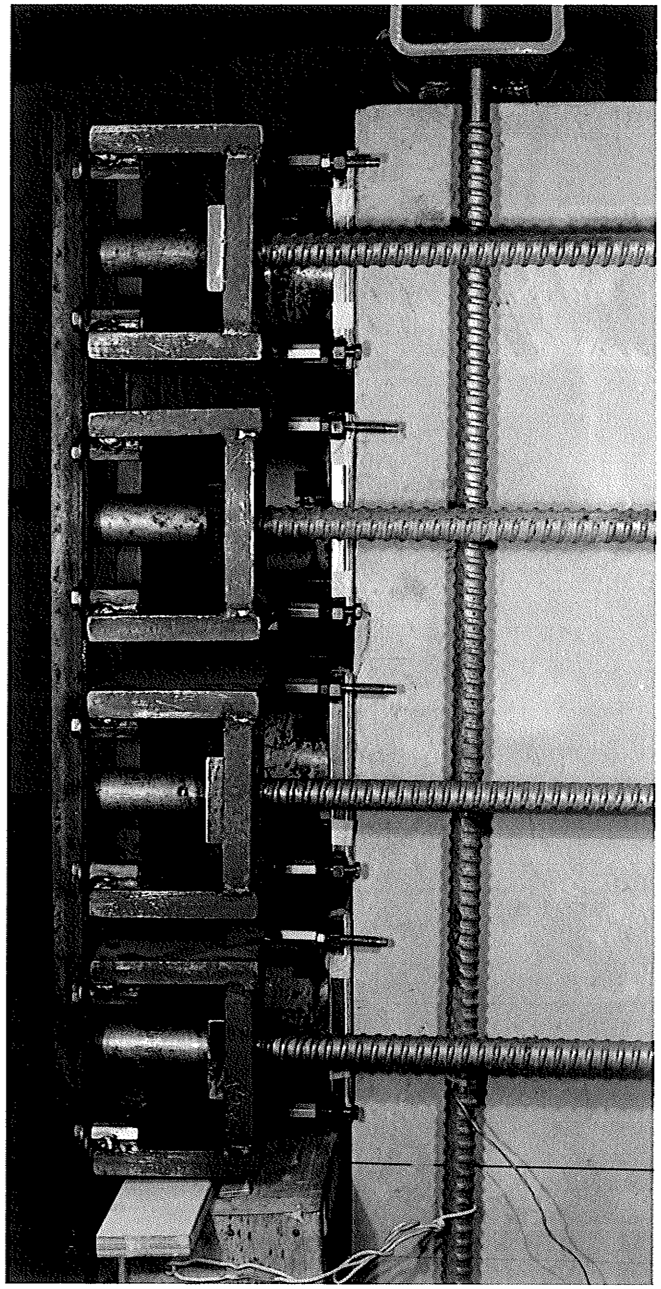

Figure 3.27 Preload Hydraulic Jacking System

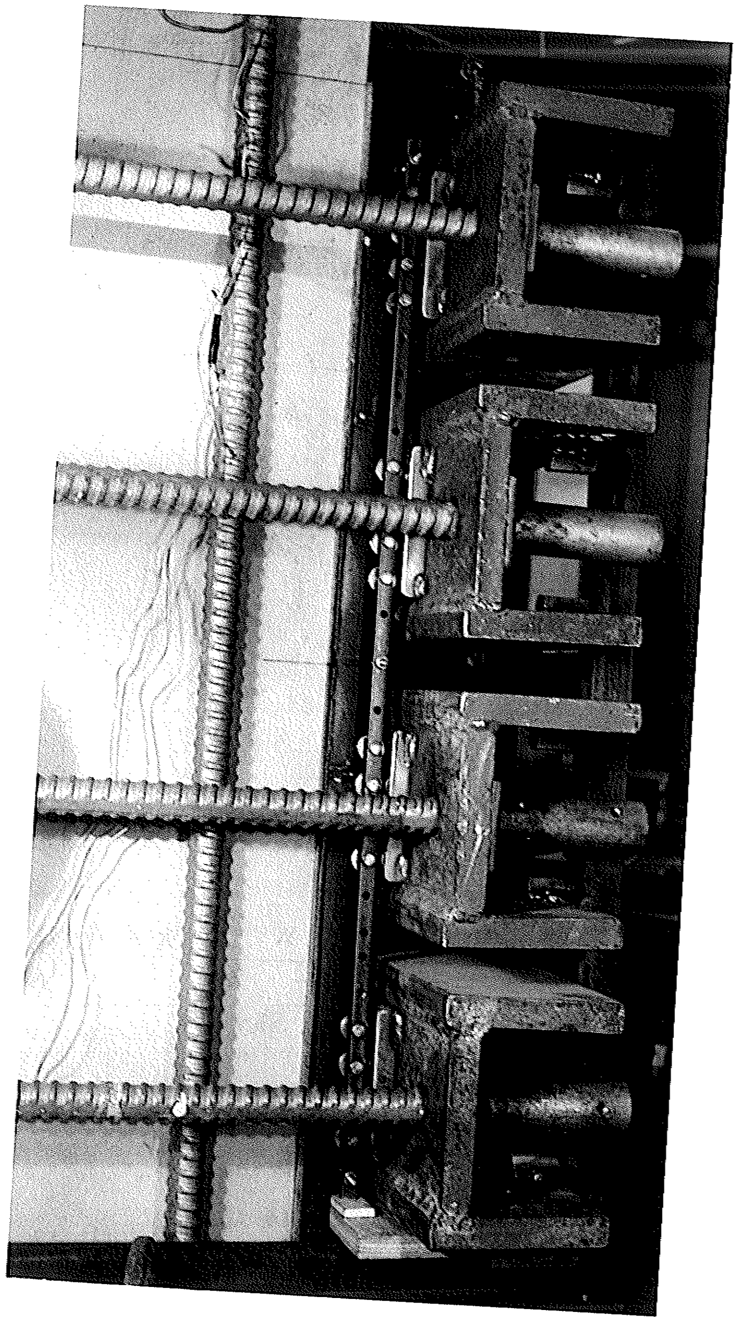

Figure 3.28 Reaction End of the Preload System

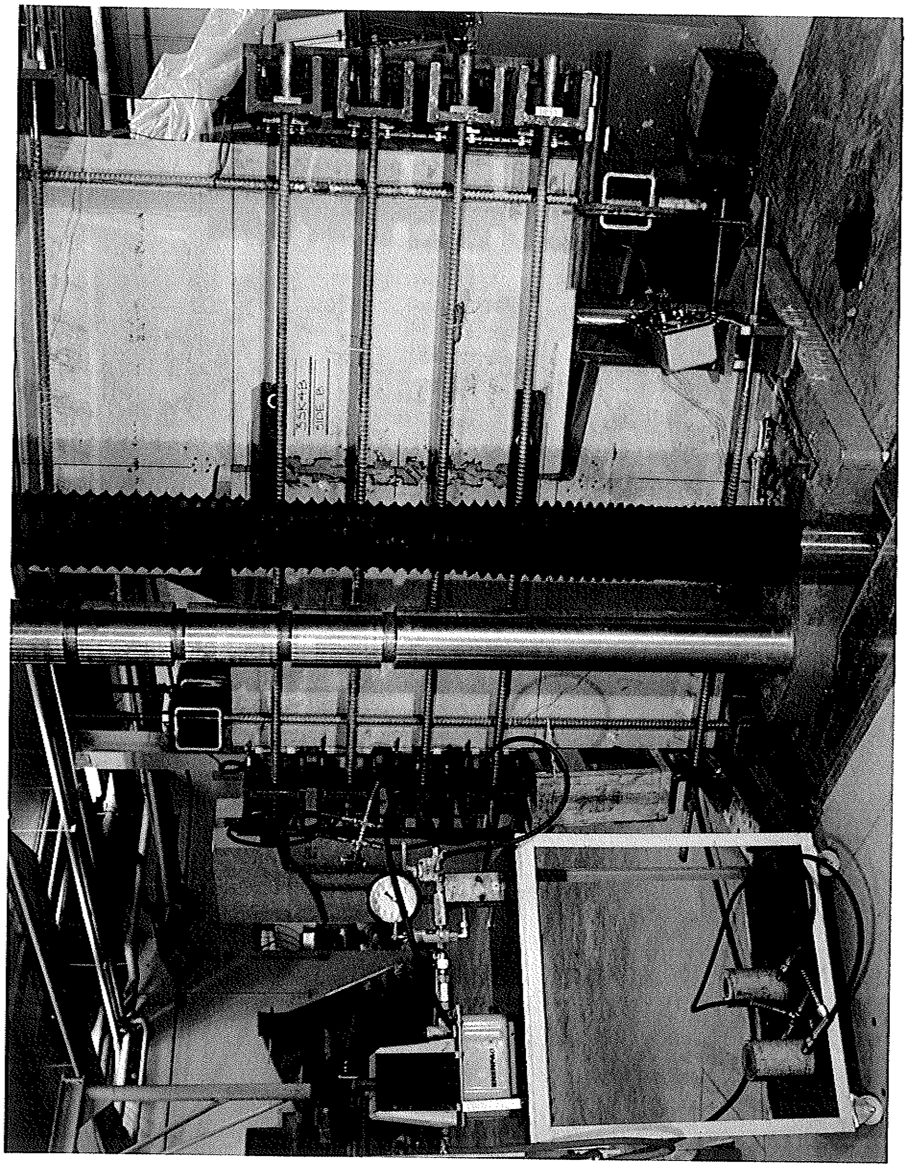

Figure 3.29 Test Setup

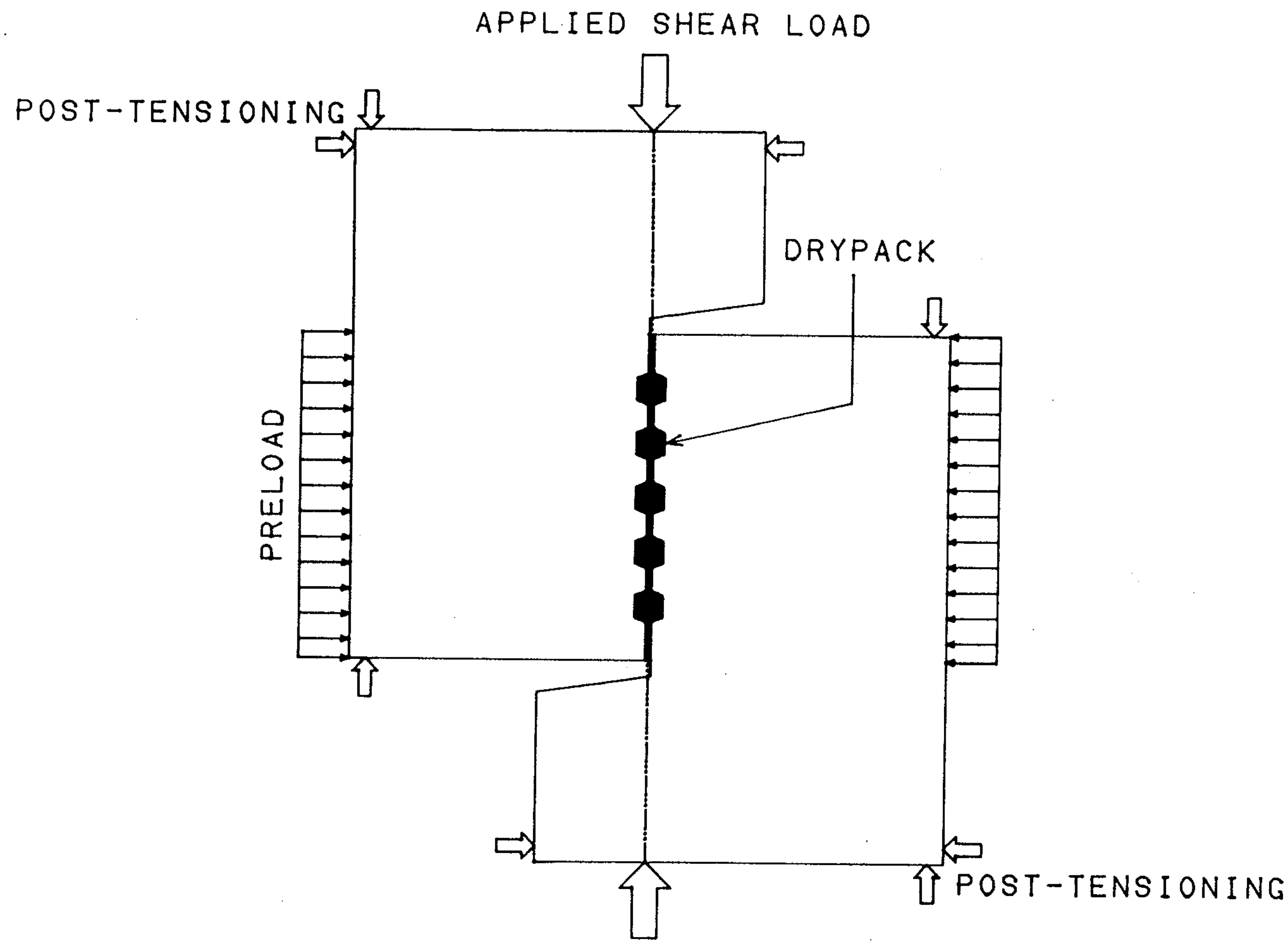

Figure 3.30 Loading Scheme

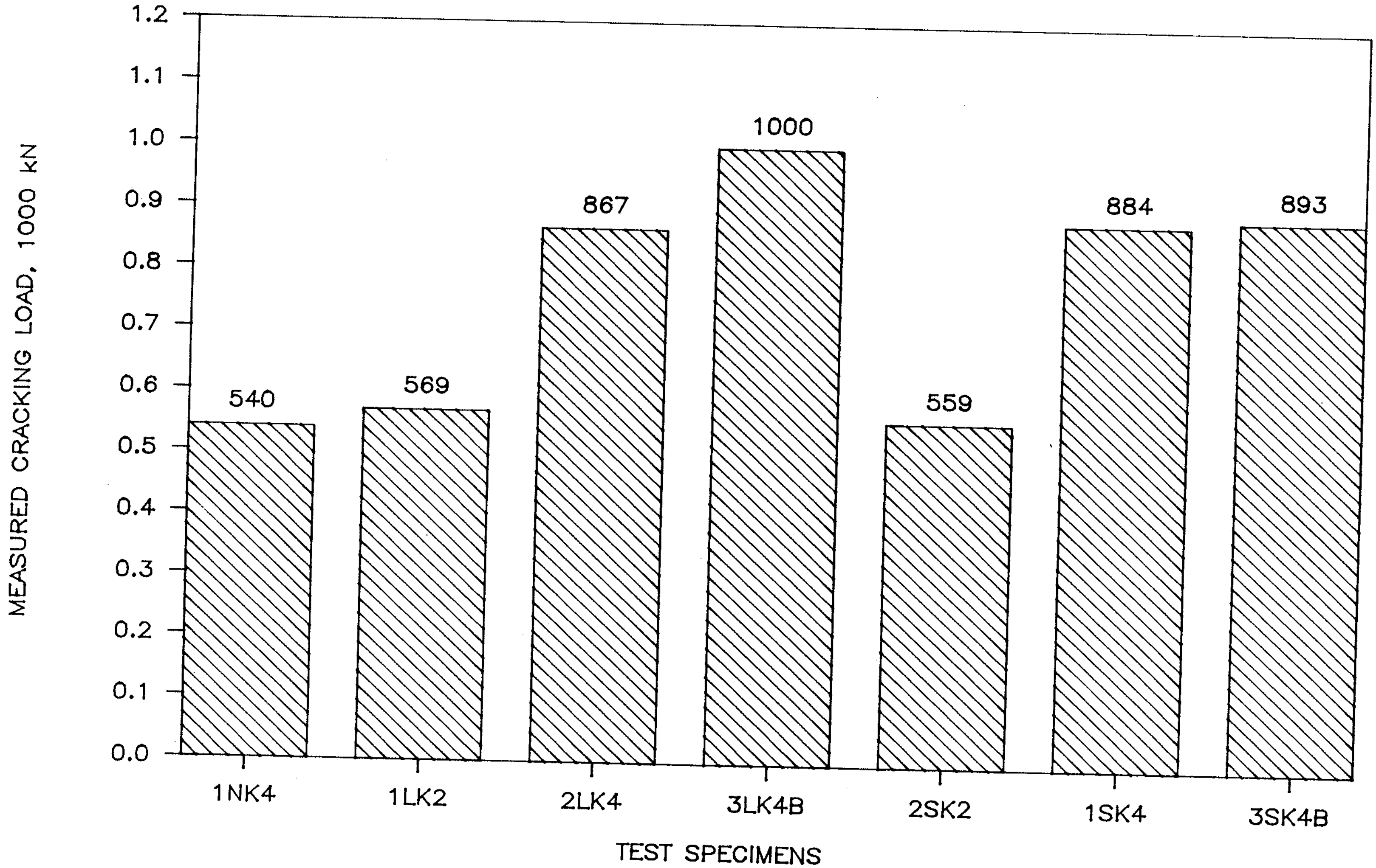

Figure 4.1 Comparison of Cracking Loads

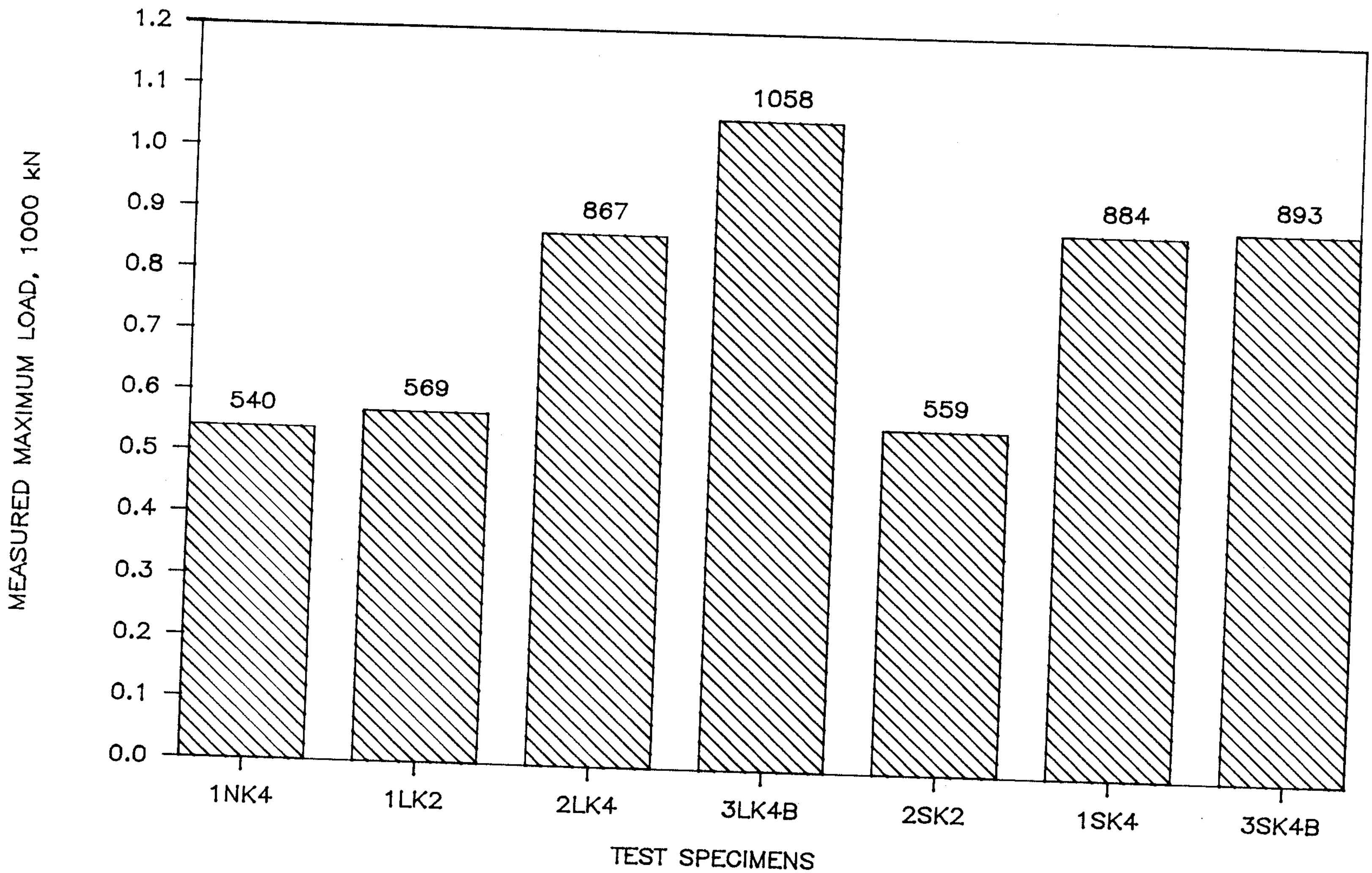

Figure 4.2 Comparison of Maximum Loads

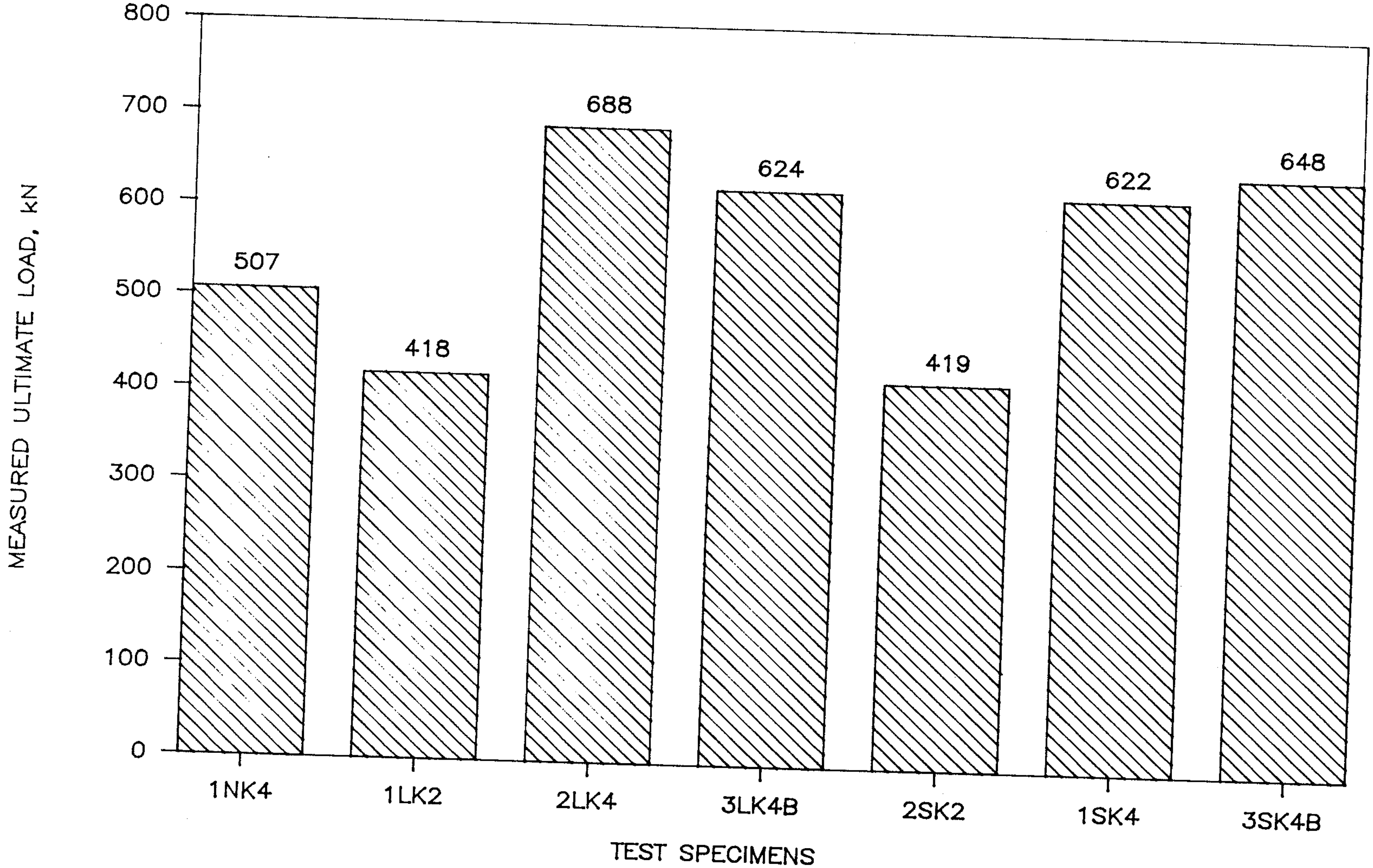

Figure 4.3 Comparison of Ultimate Loads

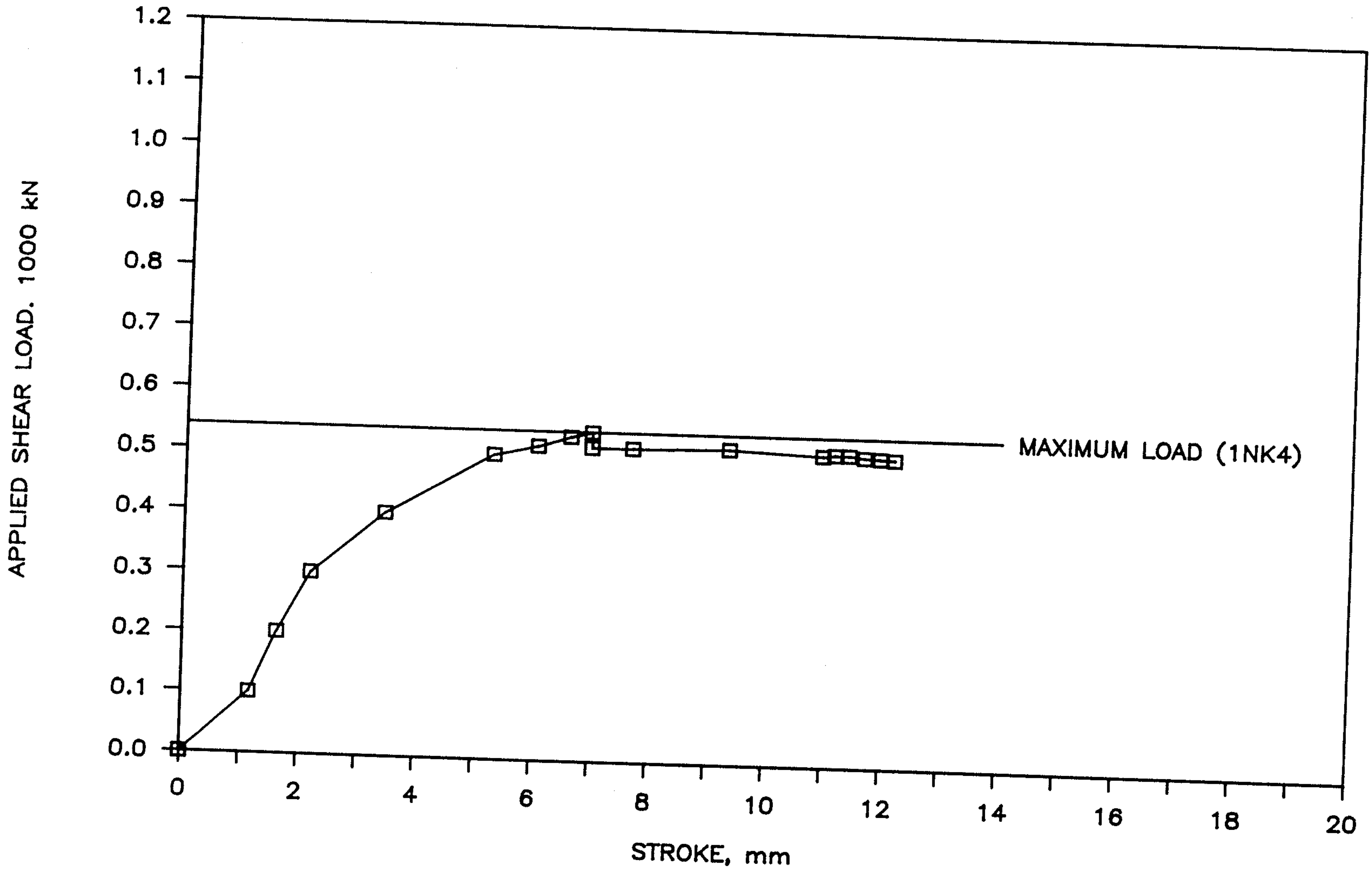

Figure 4.4 Applied Shear Load-Stroke Relationship for Specimen 1NK4

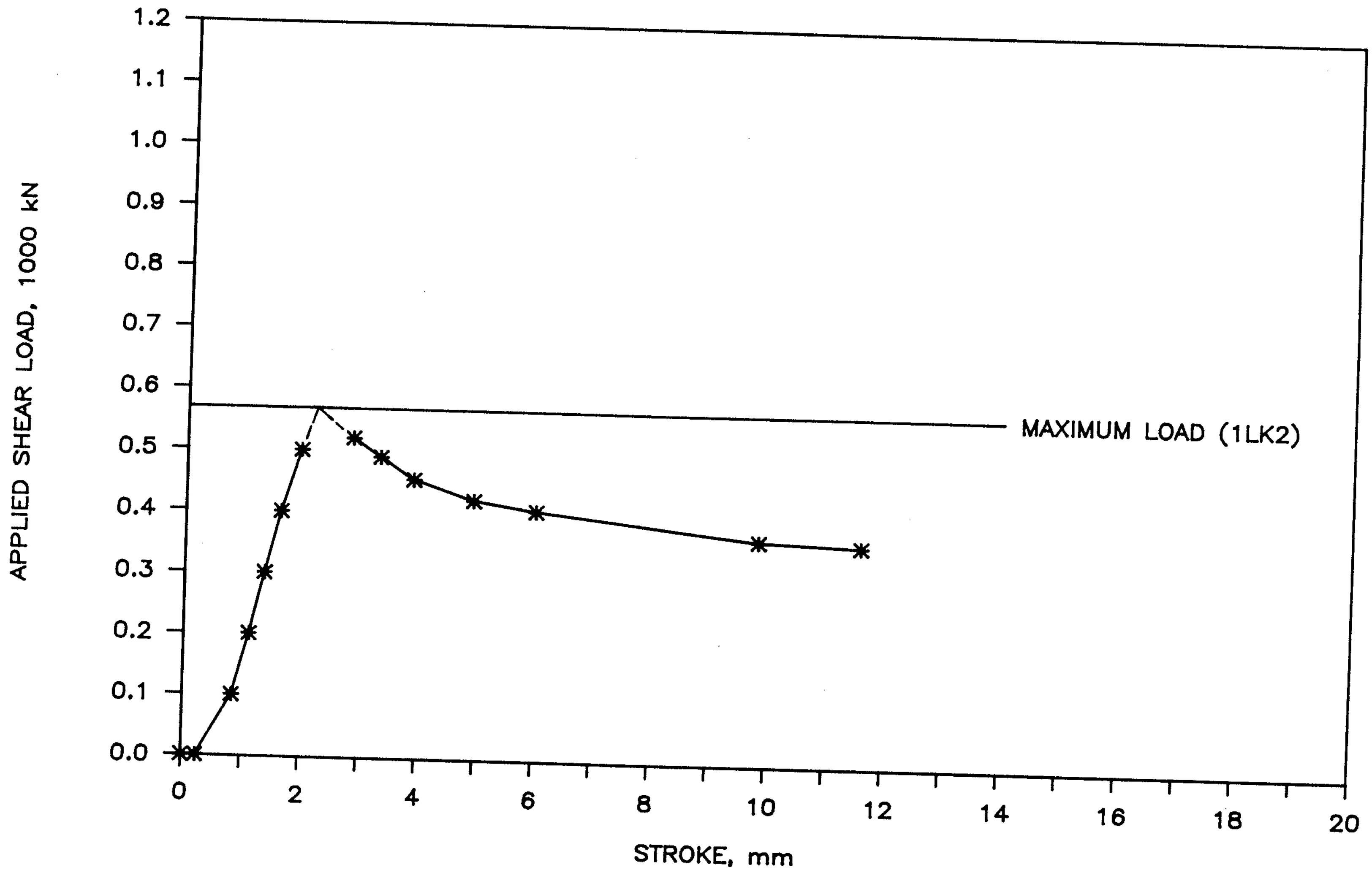

Figure 4.5 Applied Shear Load-Stroke Relationship for Specimen 1LK2

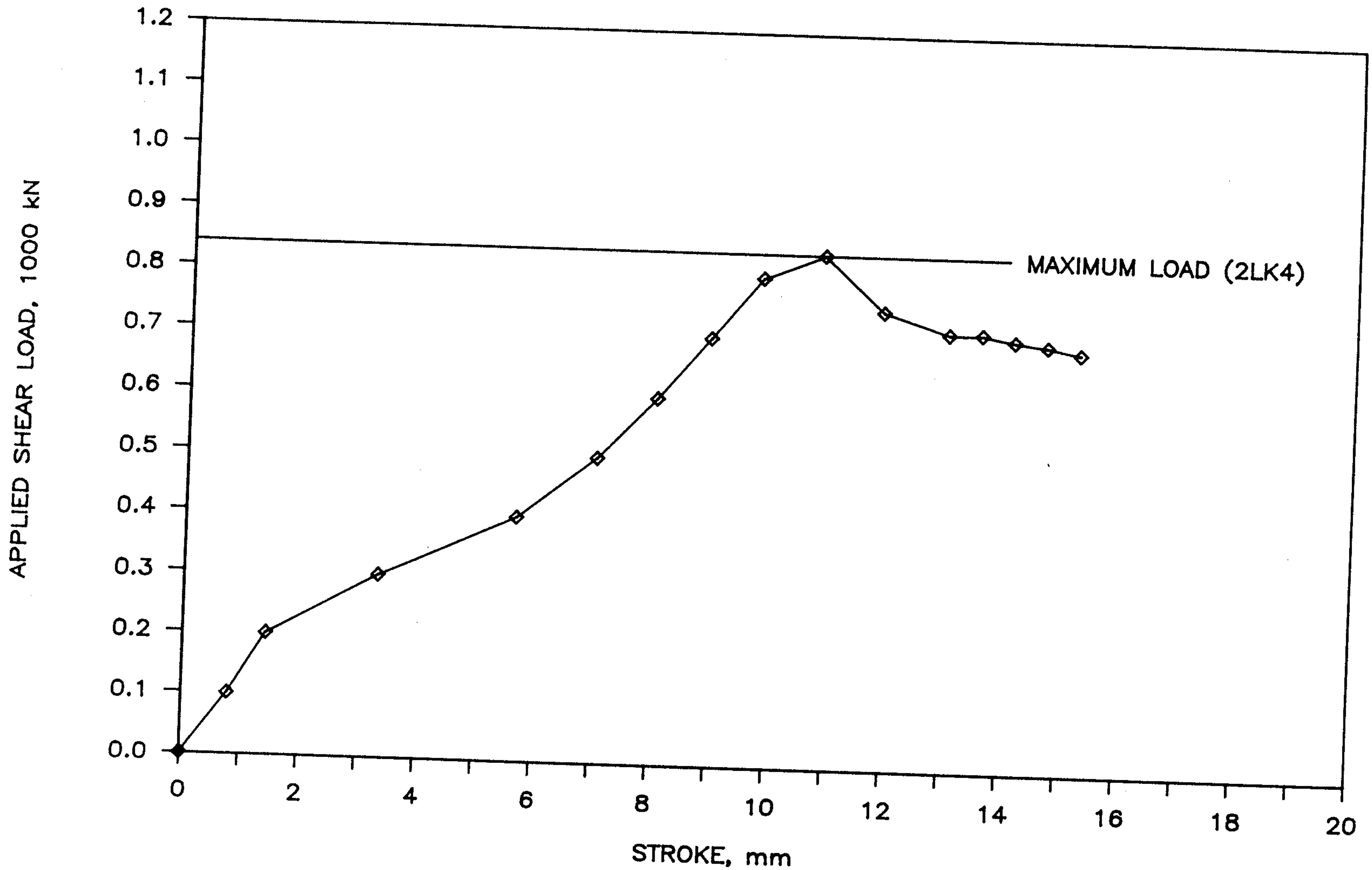

Figure 4.6 Applied Shear Load-Stroke Relationship for Specimen 2LK4

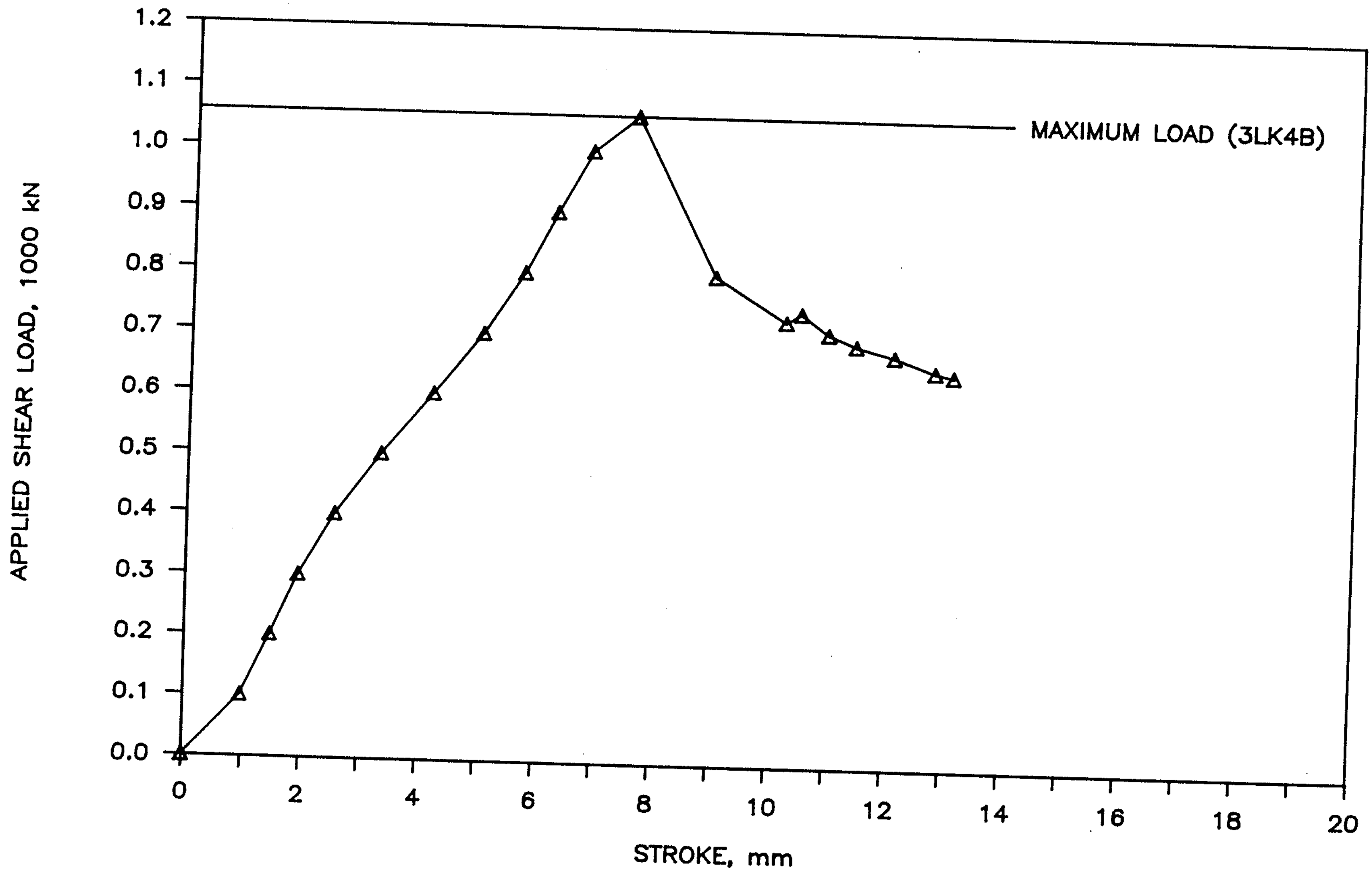

Figure 4.7 Applied Shear Load-Stroke Relationship for Specimen 3LK4B

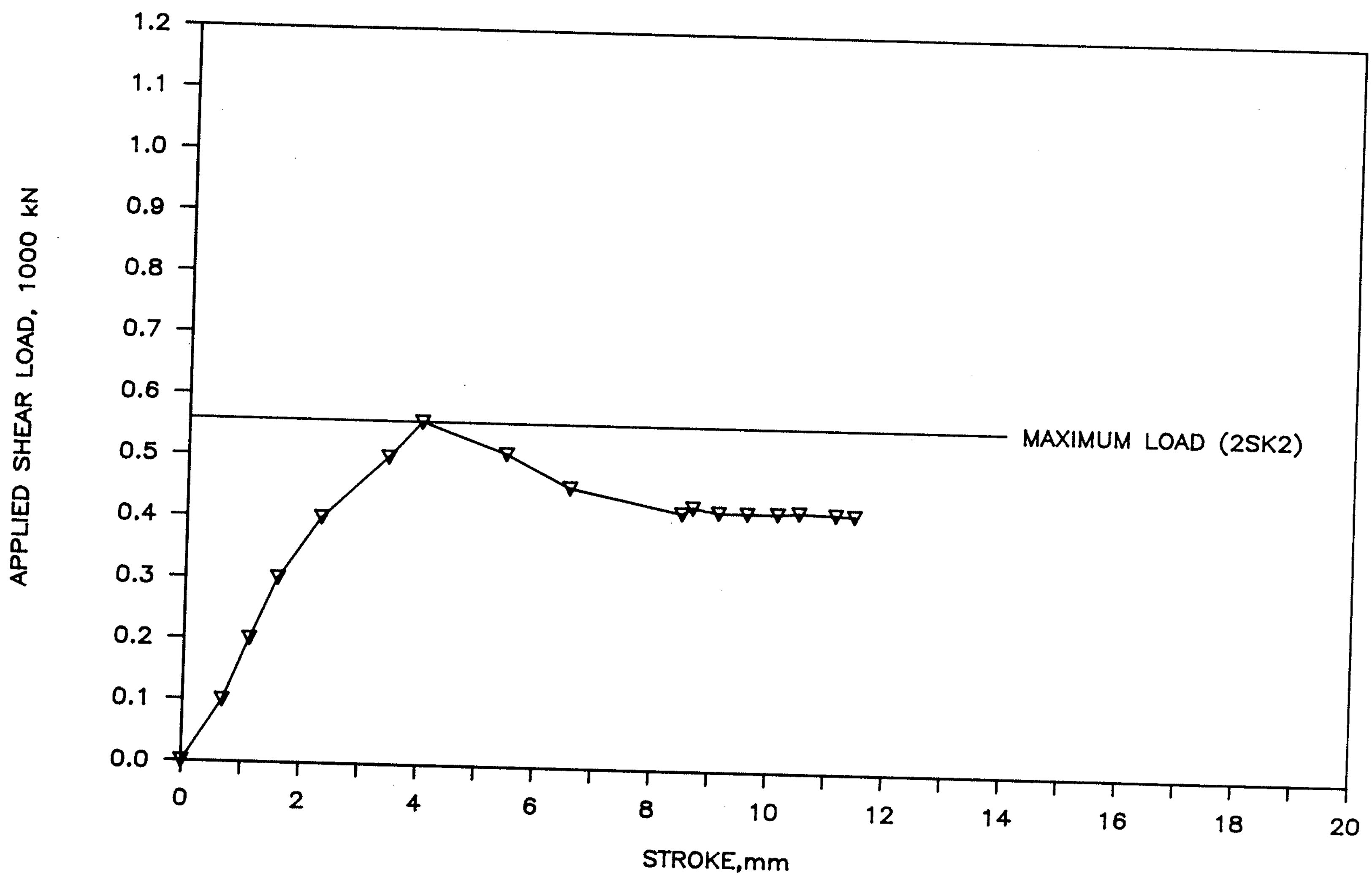

Figure 4.8 Applied Shear Load-Stroke Relationship for Specimen 2SK2

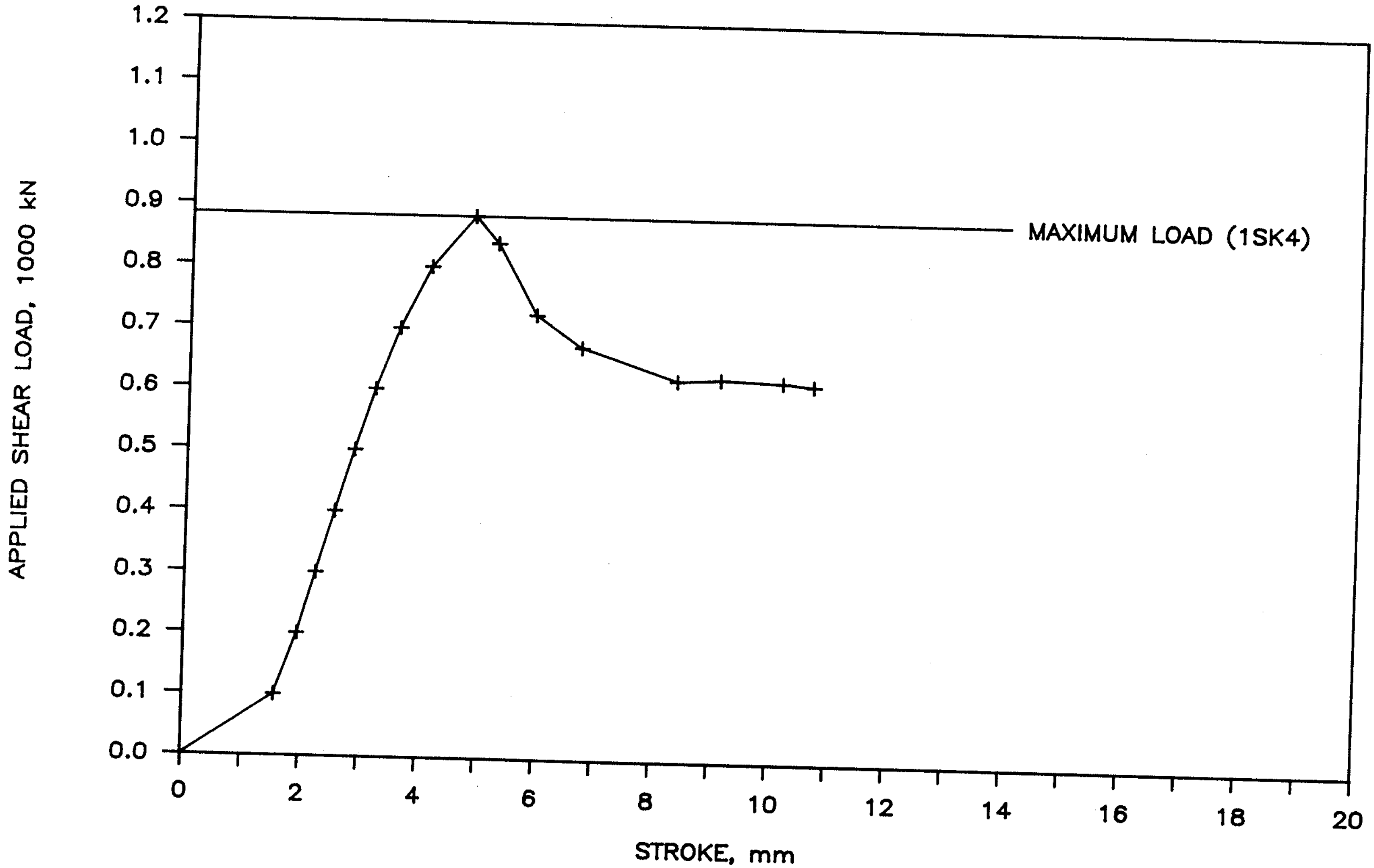

Figure 4.9 Applied Shear Load-Stroke Relationship for Specimen 1SK4

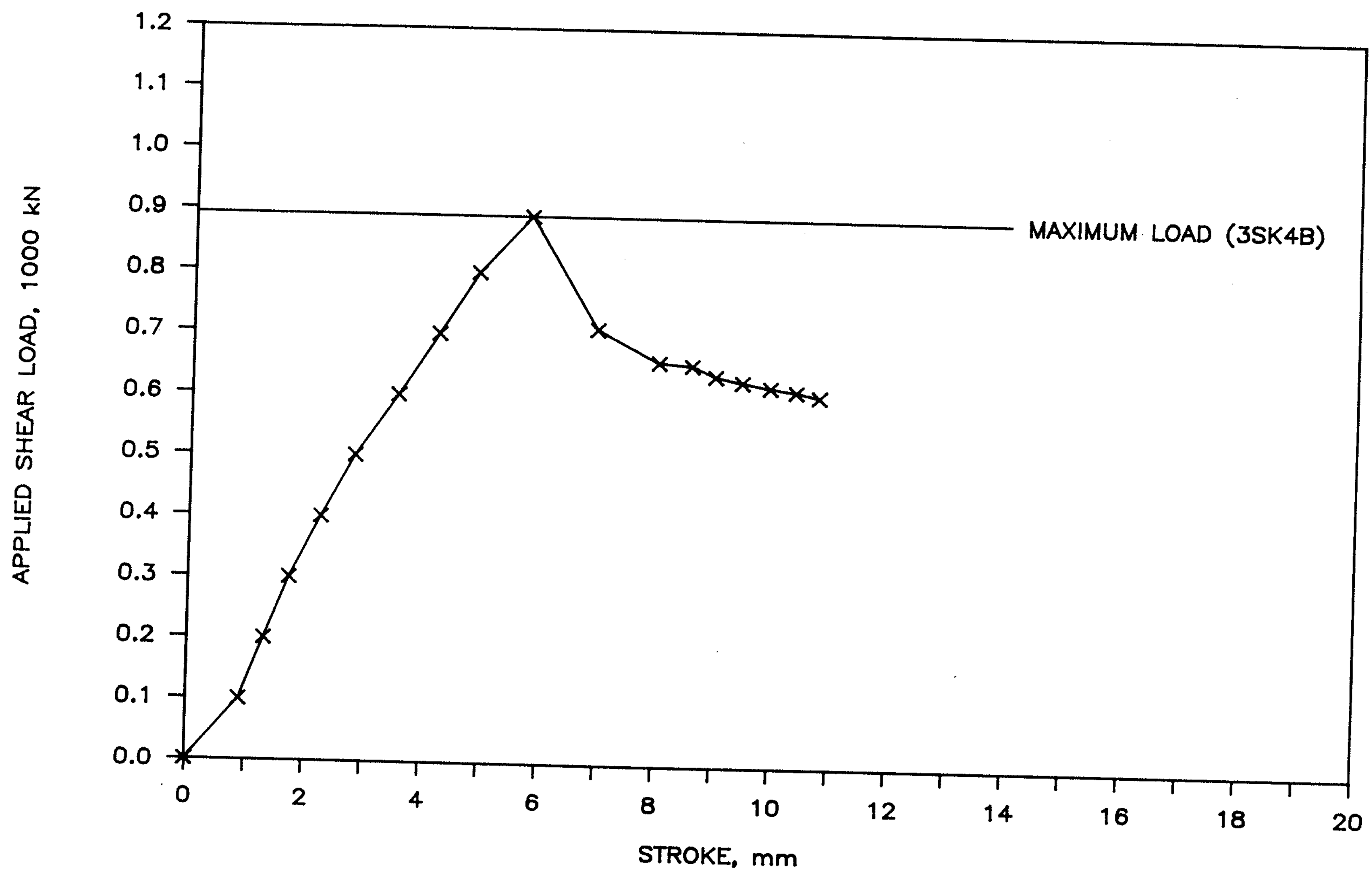

Figure 4.10 Applied Shear Load-Stroke Relationship for Specimen 3SK4B

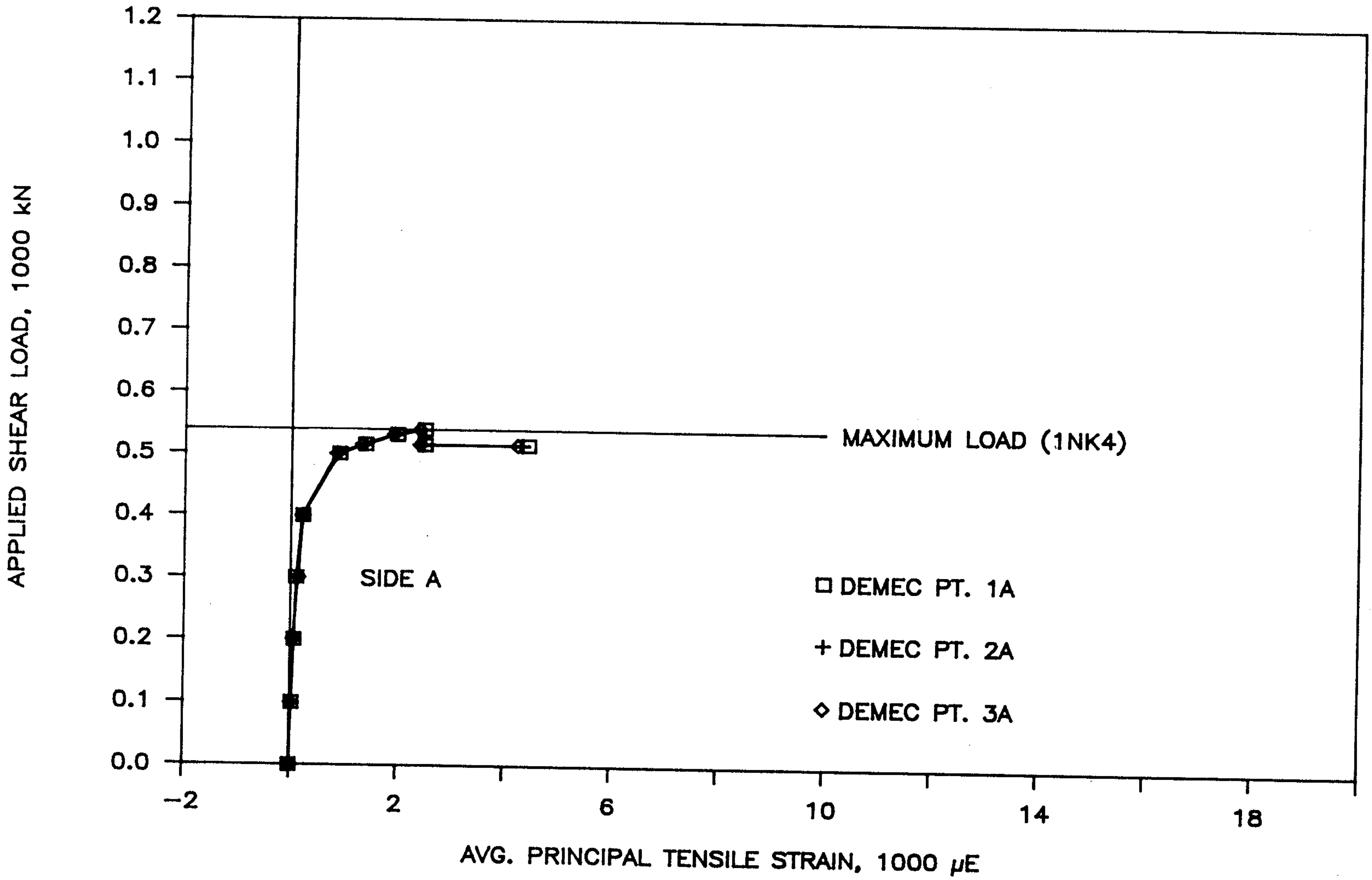

Figure 5.1 Applied Shear Load-Average Principal Tensile Strain Relationship on Side A of Specimen 1NK4

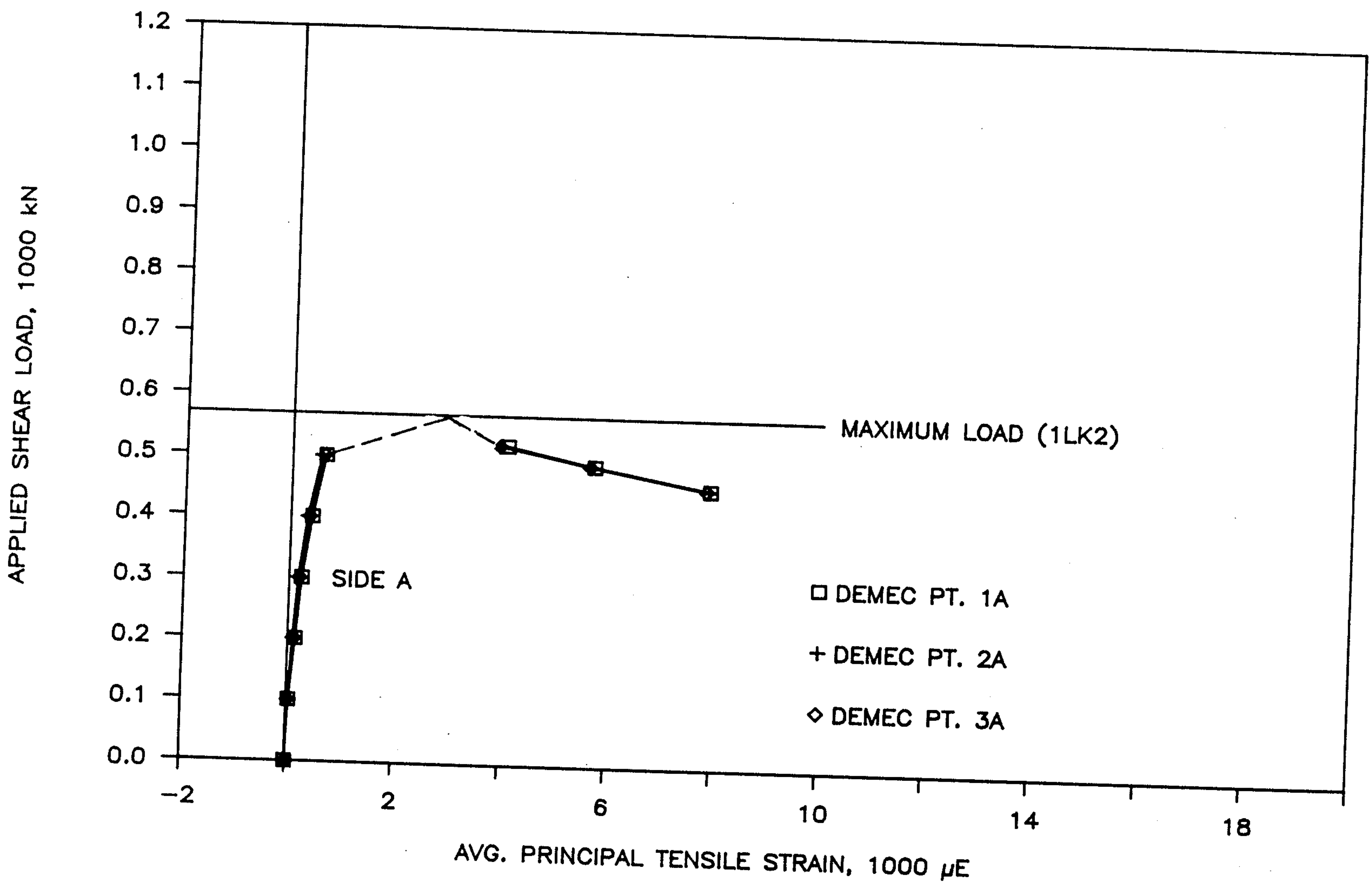

Figure 5.2 Applied Shear Load-Average Principal Tensile Strain Relationship on Side A of Specimen 1LK2

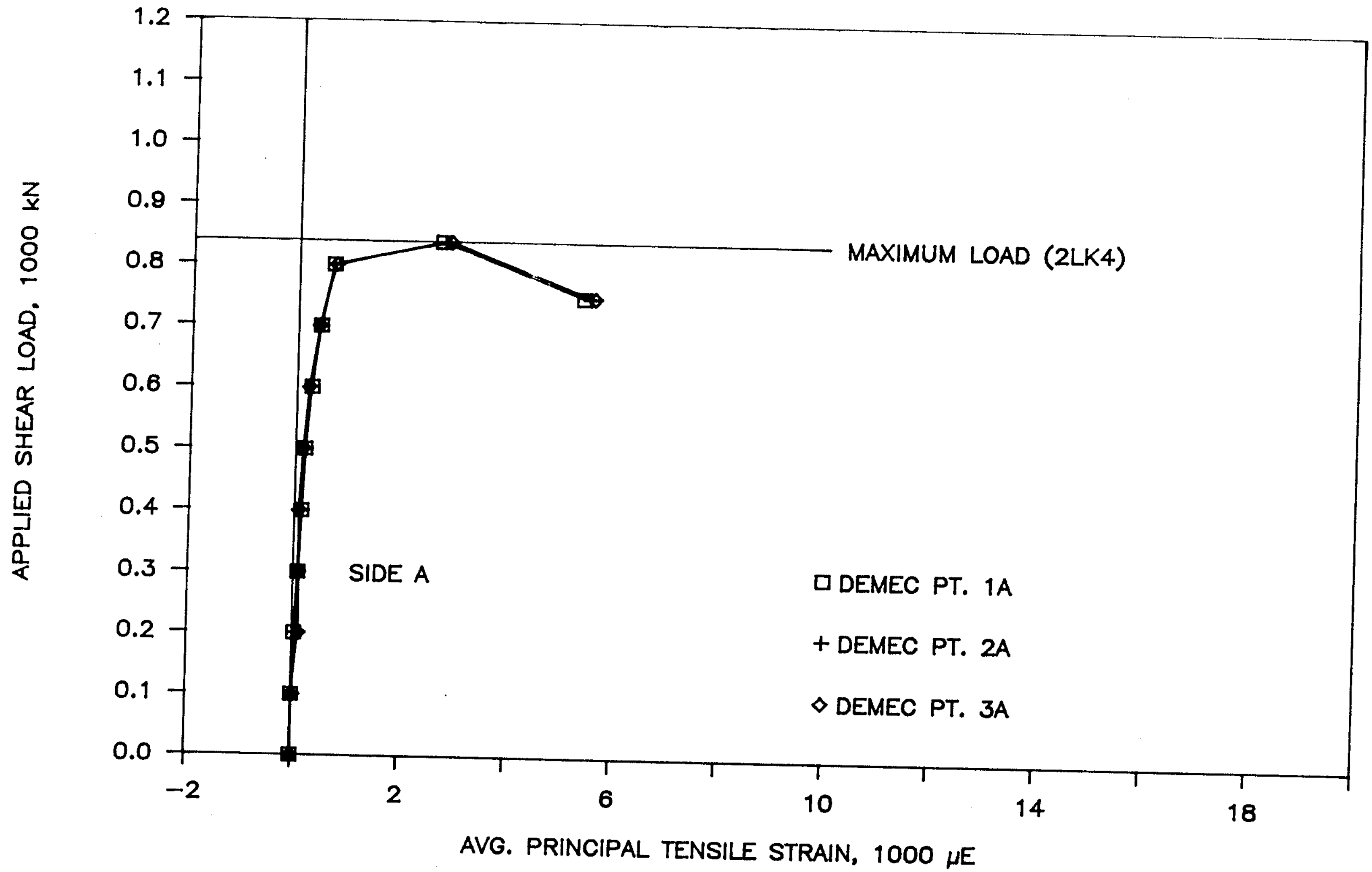

Figure 5.3 Applied Shear Load-Average Principal Tensile Strain Relationship on Side A of Specimen 2LK4

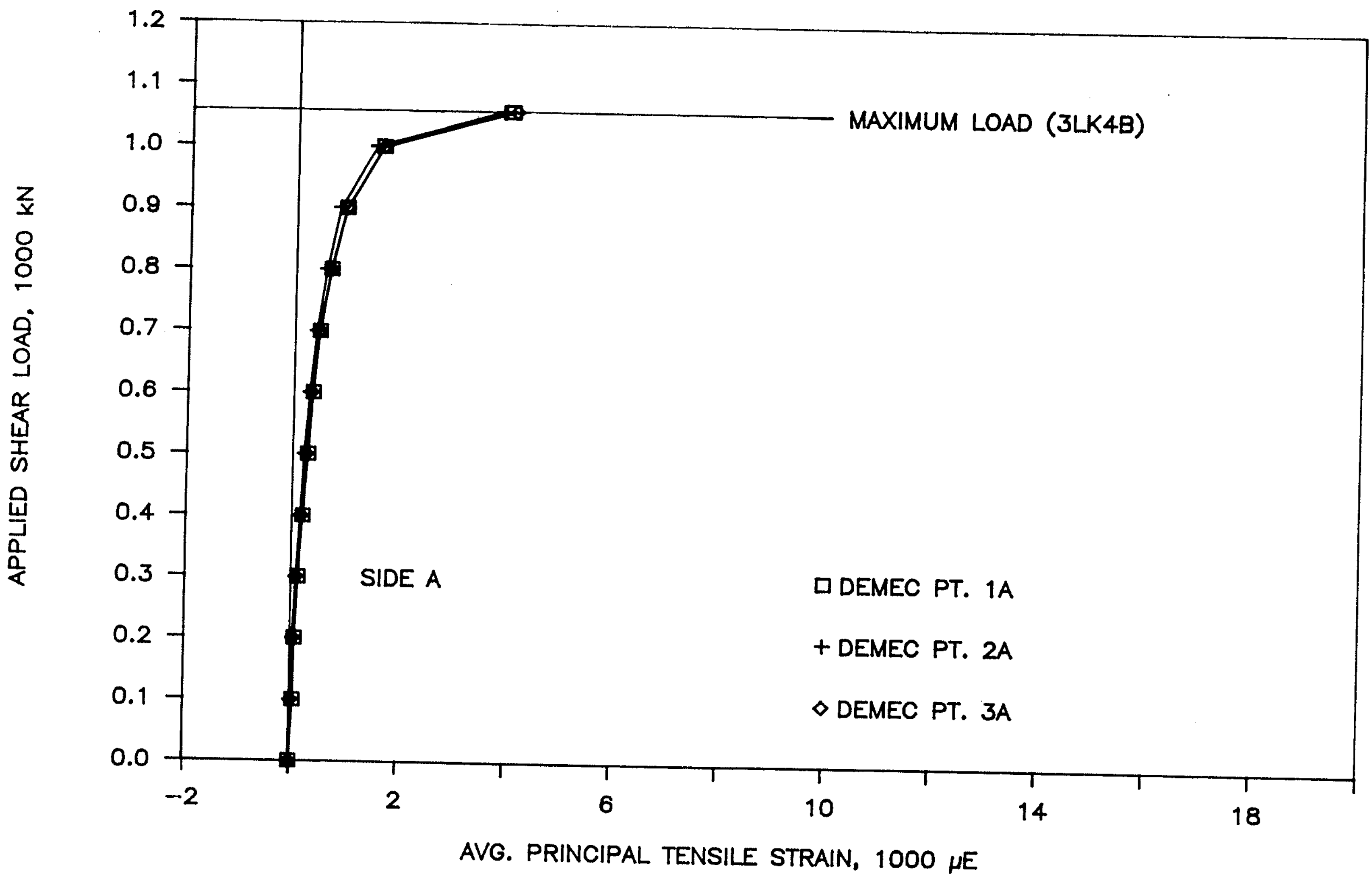

Figure 5.4 Applied Shear Load-Average Principal Tensile Strain Relationship on Side A of Specimen 3LK4B

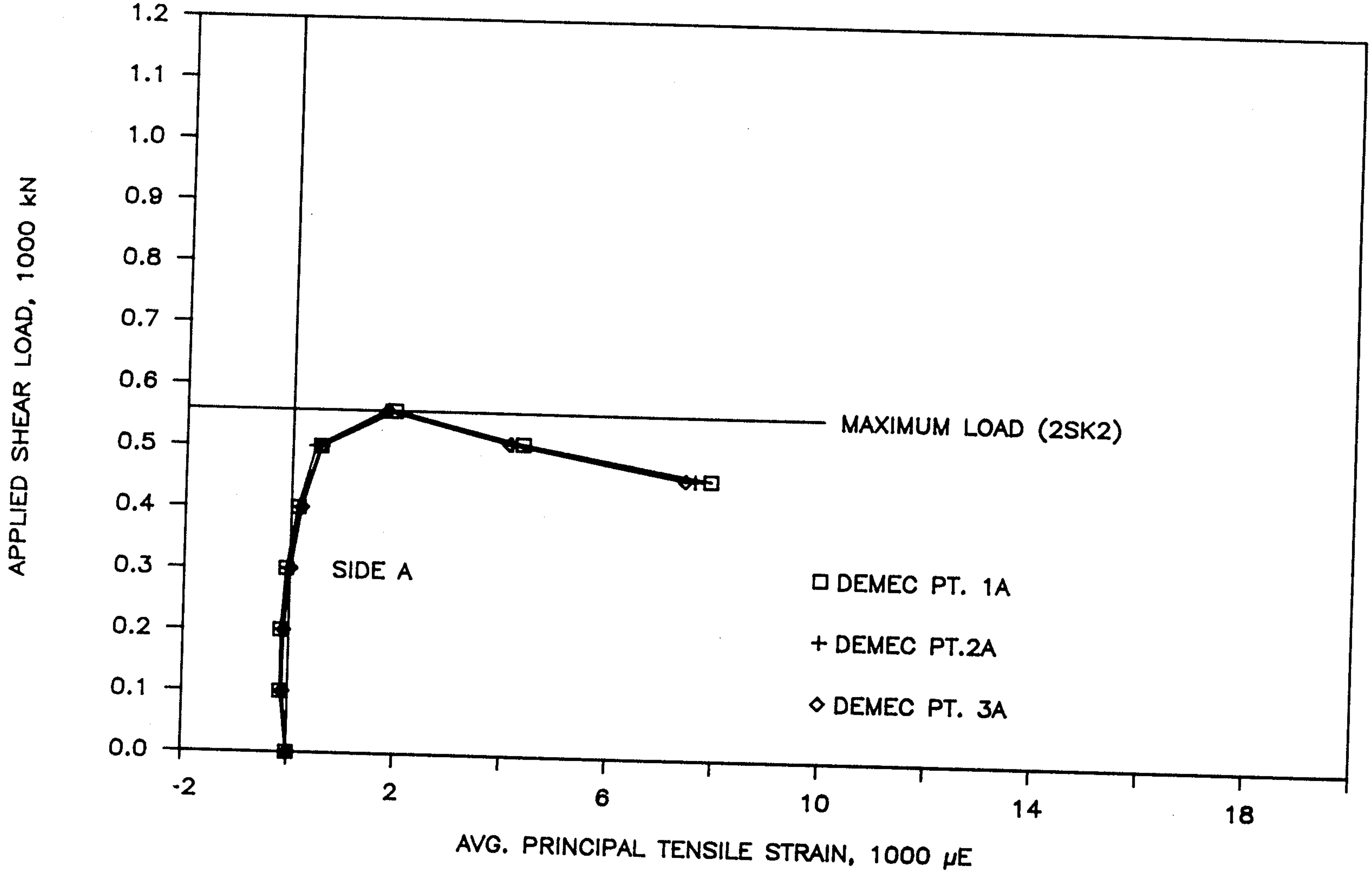

Figure 5.5 Applied Shear Load-Average Principal Tensile Strain Relationship on Side A of Specimen 2SK2

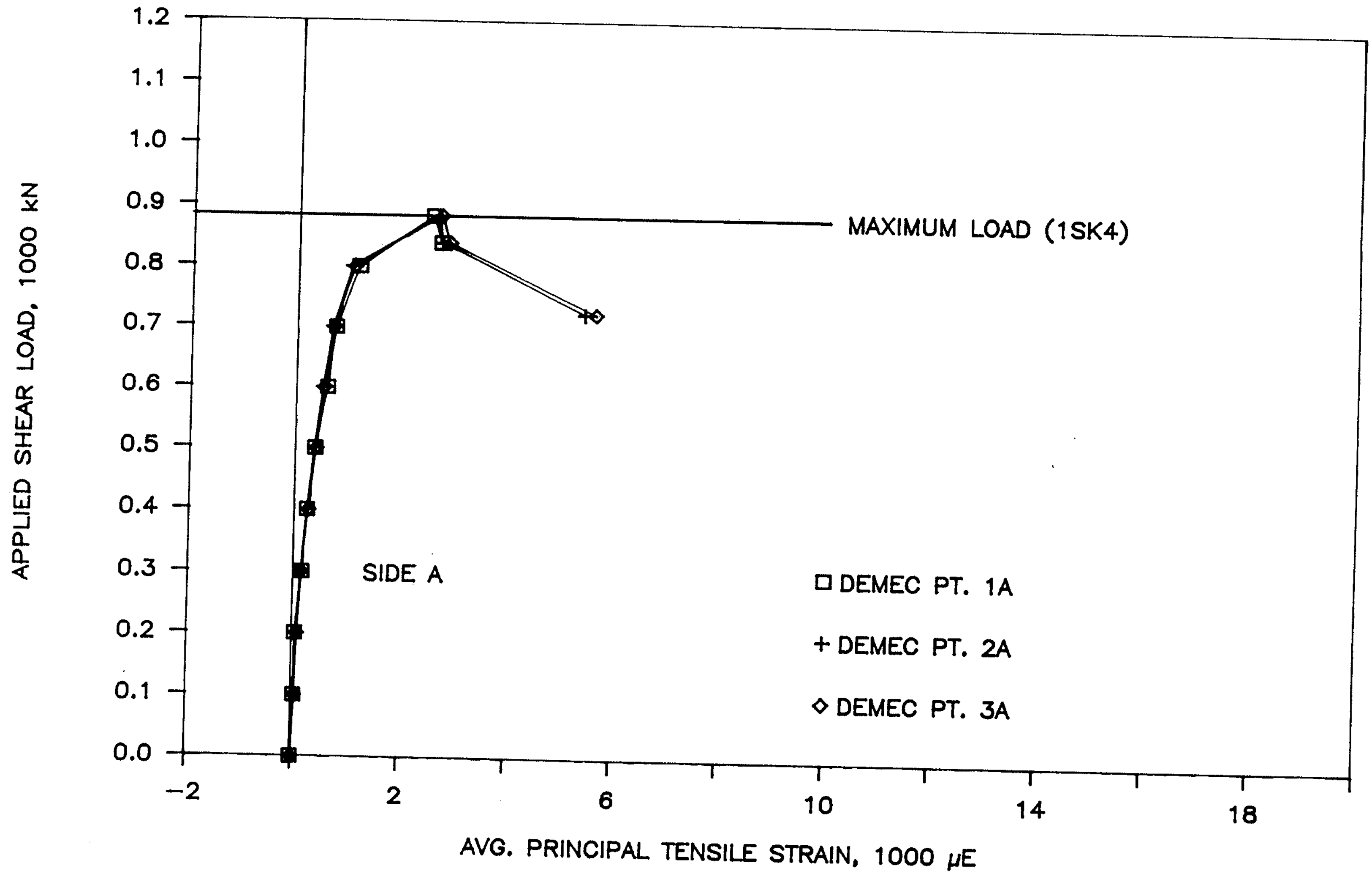

Figure 5.6 Applied Shear Load-Average Principal Tensile Strain Relationship on Side A of Specimen 1SK4

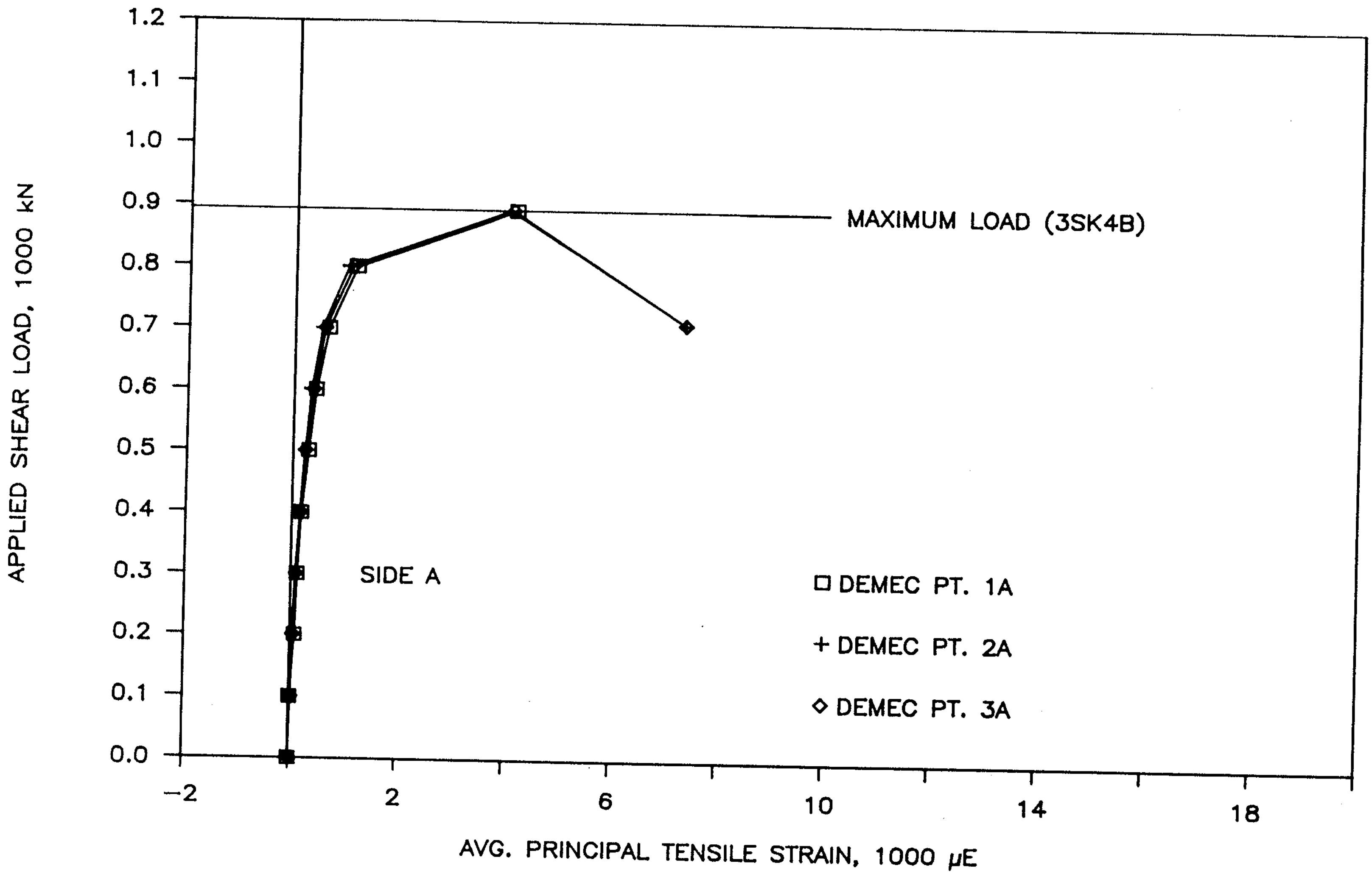

Figure 5.7 Applied Shear Load-Average Principal Tensile Strain Relationship on Side A of Specimen 3SK4B

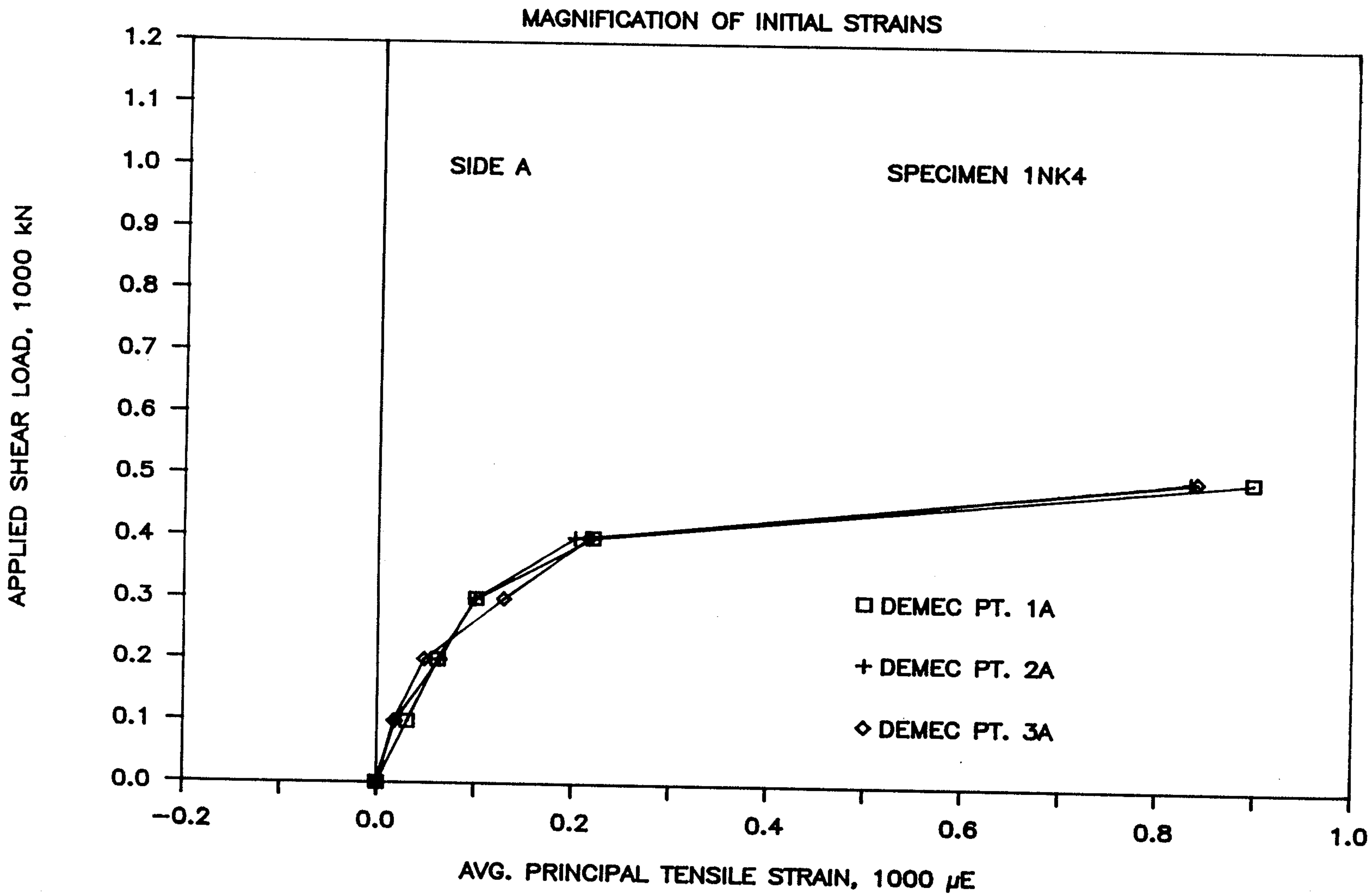

Figure 5.8 Magnification of the Applied Shear Load-Average Principal Tensile Strain Relationship on Side A of Specimen 1NK4

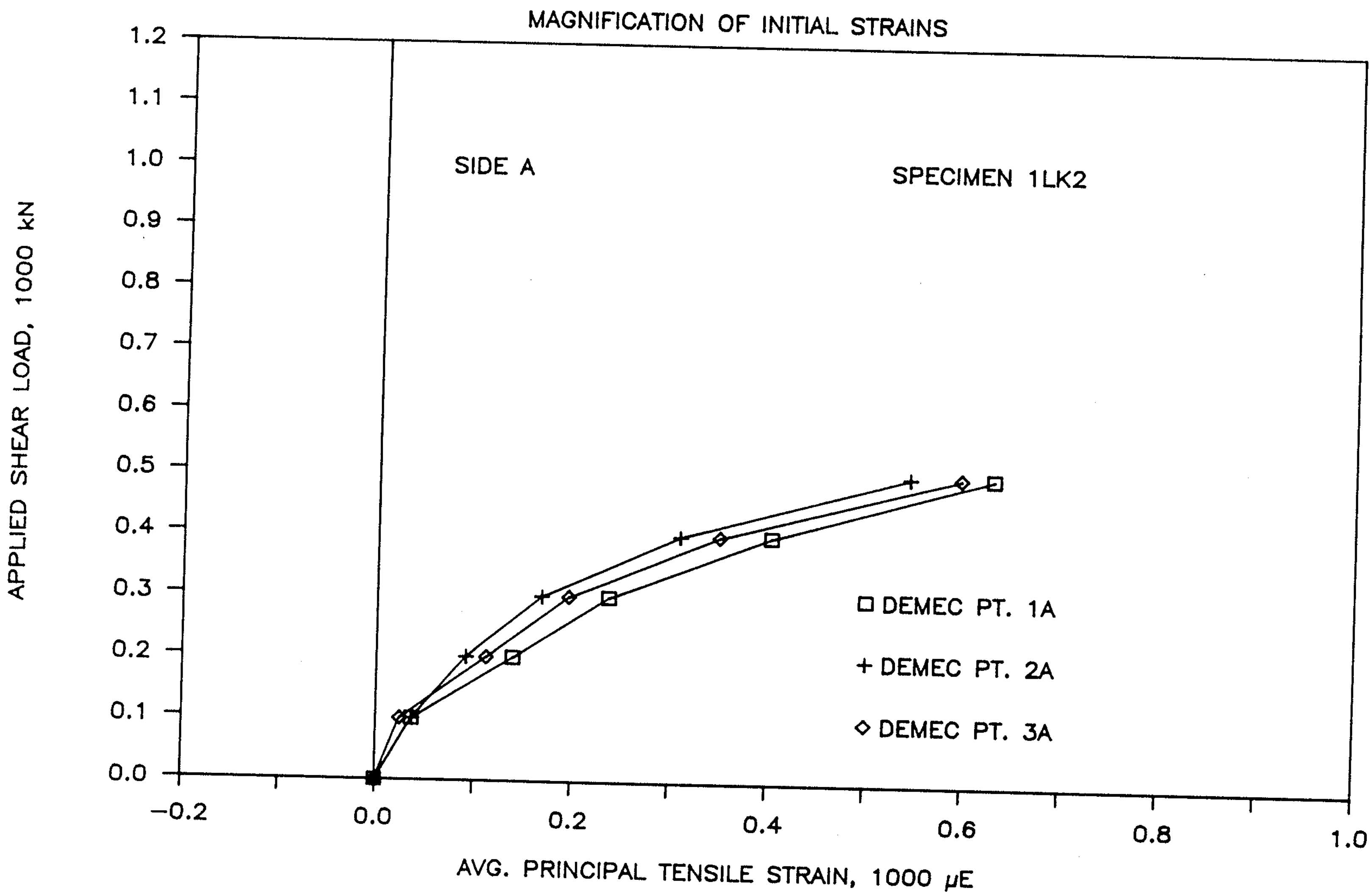

Figure 5.9 Magnification of the Applied Shear Load-Average Principal Tensile Strain Relationship on Side A of Specimen 1LK2

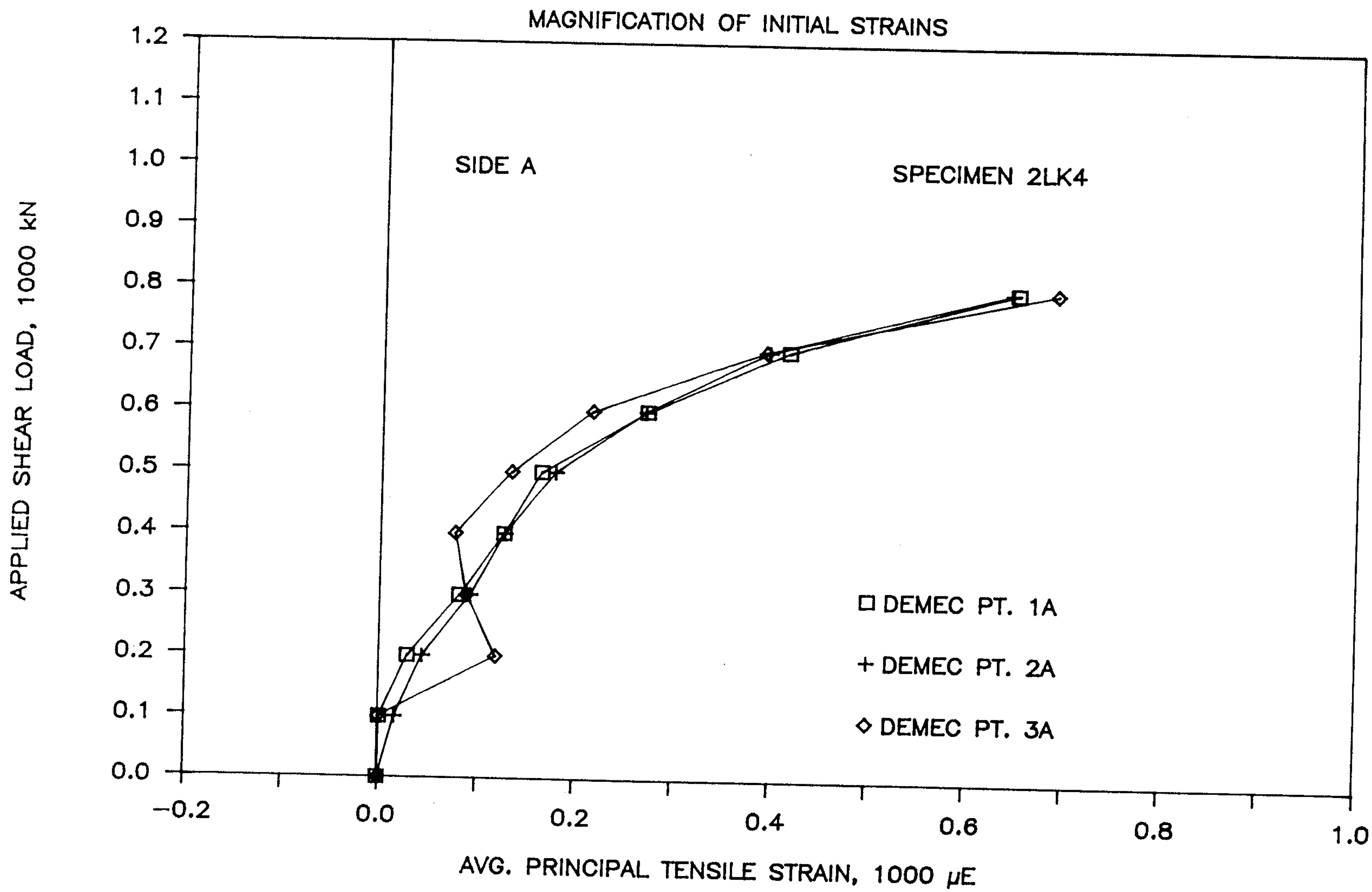

Figure 5.10 Magnification of the Applied Shear Load-Average Principal Tensile Strain Relationship on Side A of Specimen 2LK4

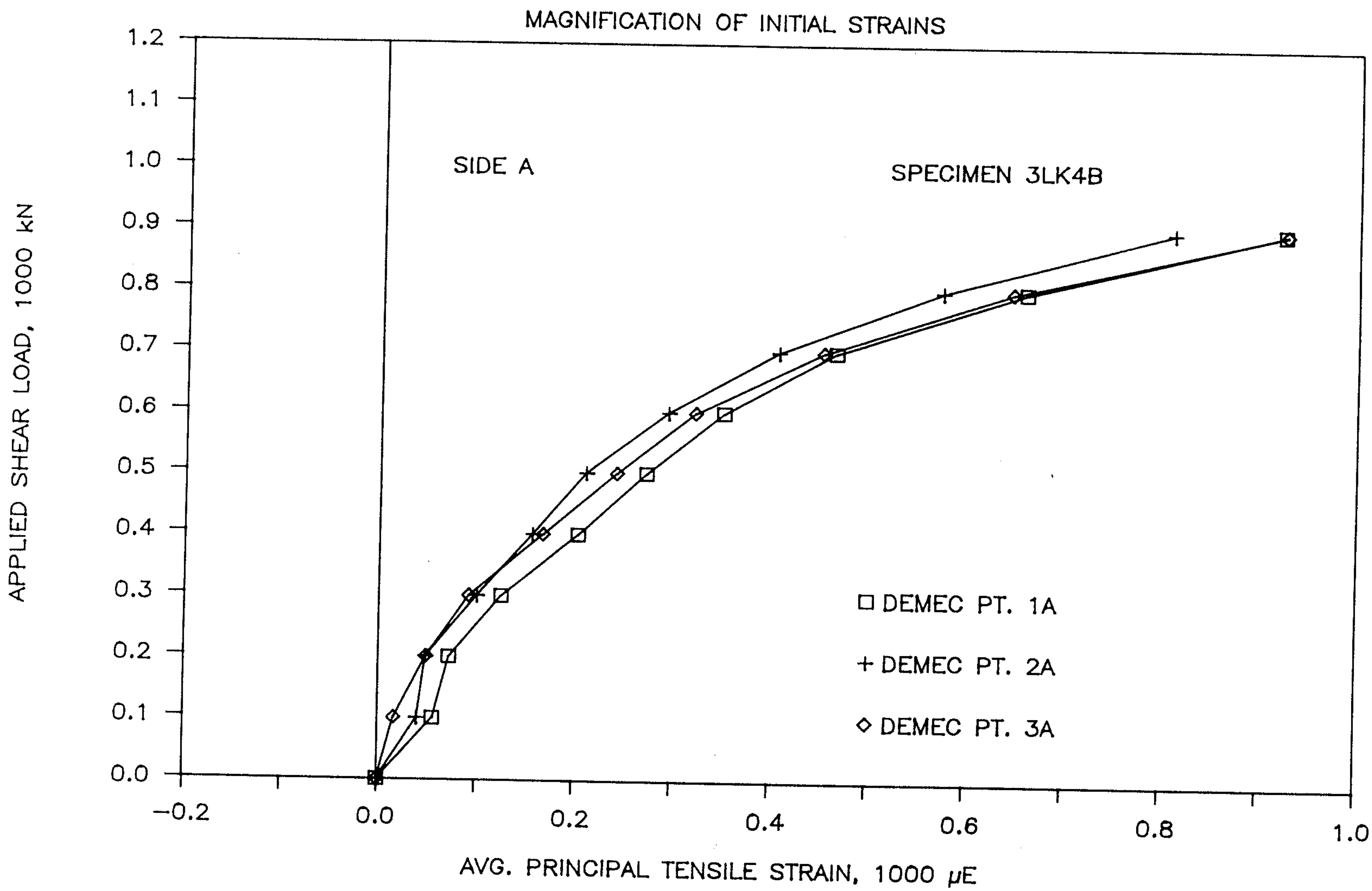

Figure 5.11 Magnification of the Applied Shear Load-Average Principal Tensile Strain Relationship on Side A of Specimen 3LK4B

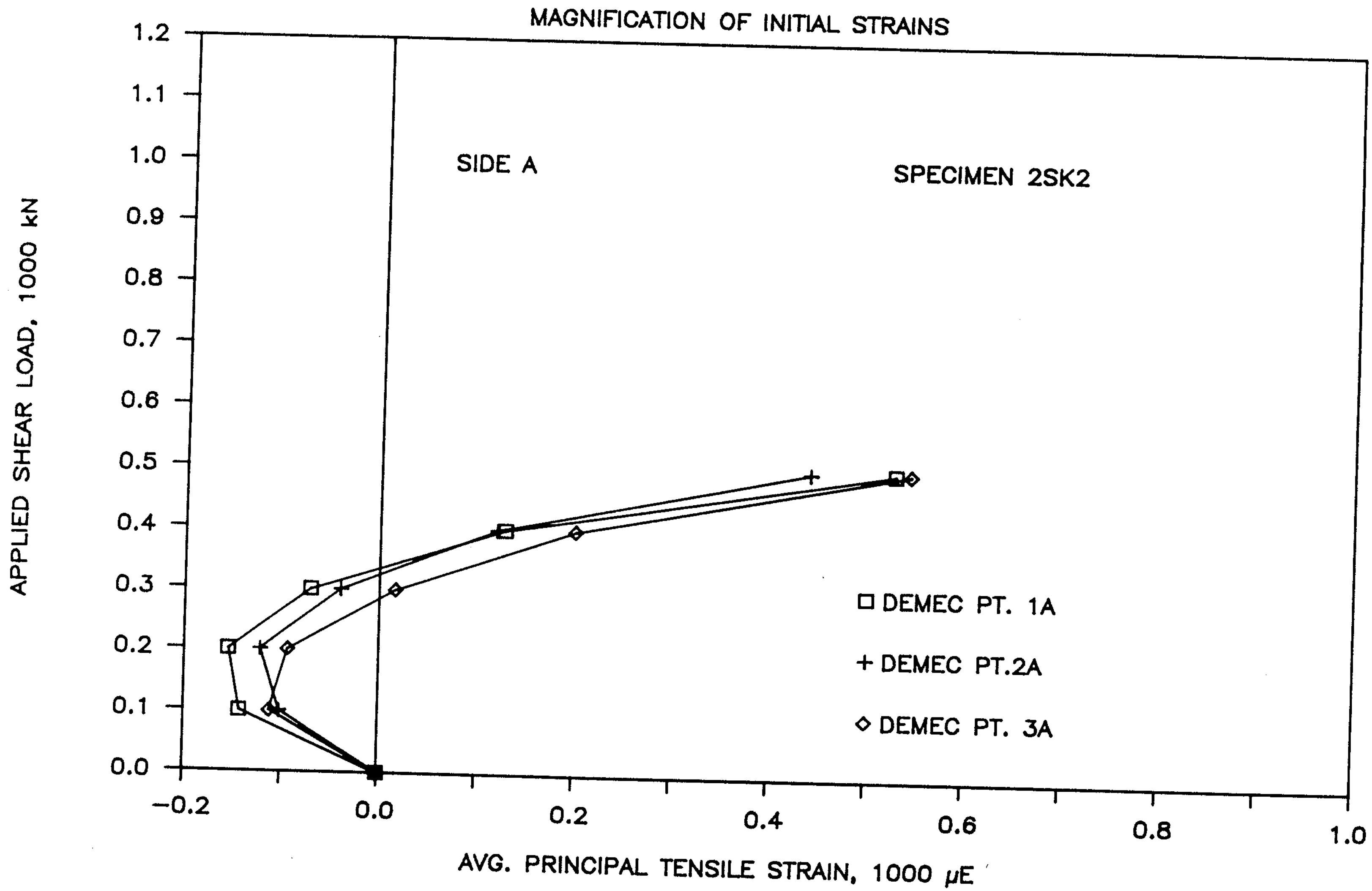

Figure 5.12 Magnification of the Applied Shear Load-Average Principal Tensile Strain Relationship on Side A of Specimen 2SK2

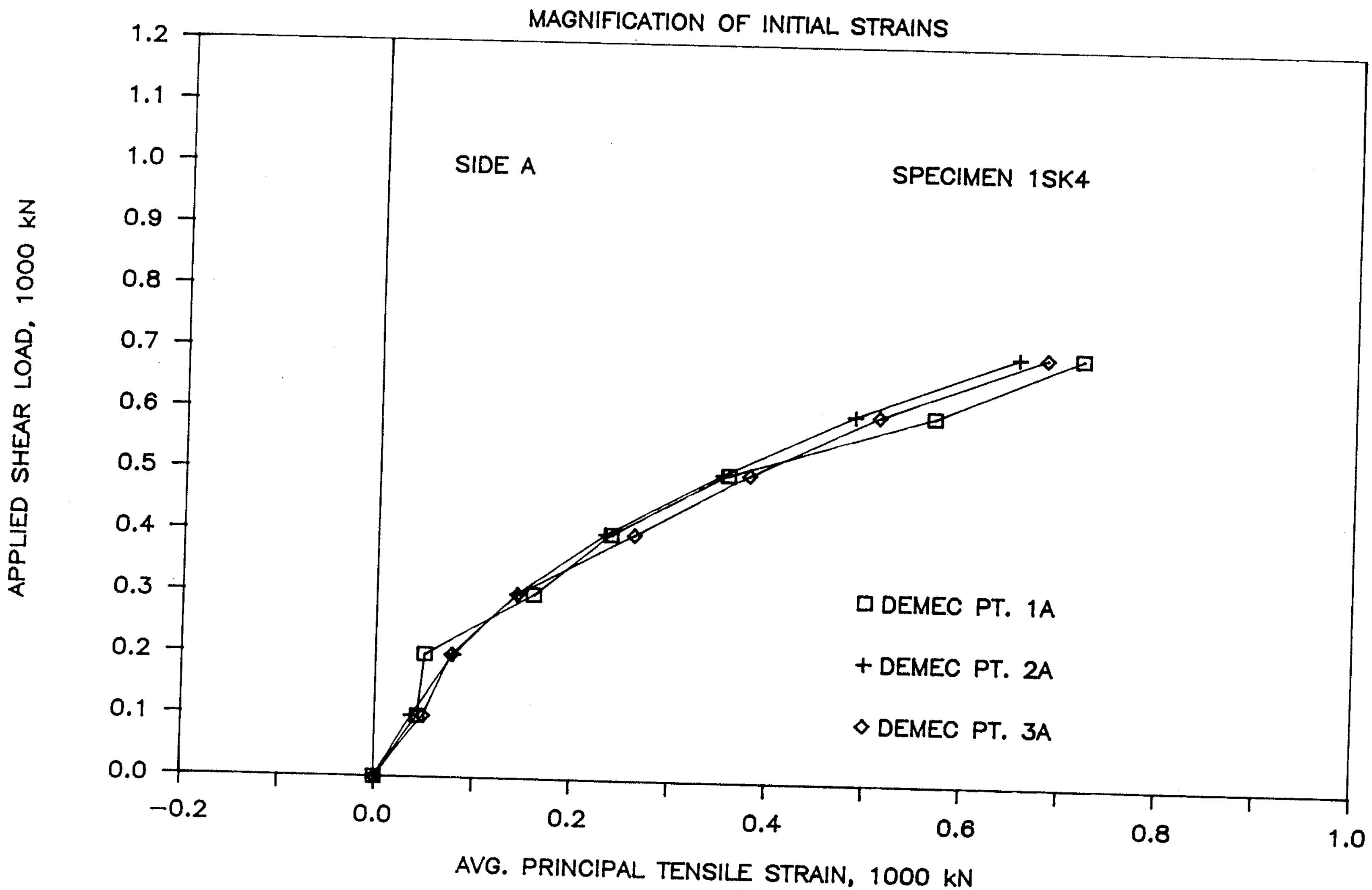

Figure 5.13 Magnification of the Applied Shear Load-Average Principal Tensile Strain Relationship on Side A of Specimen 1SK4

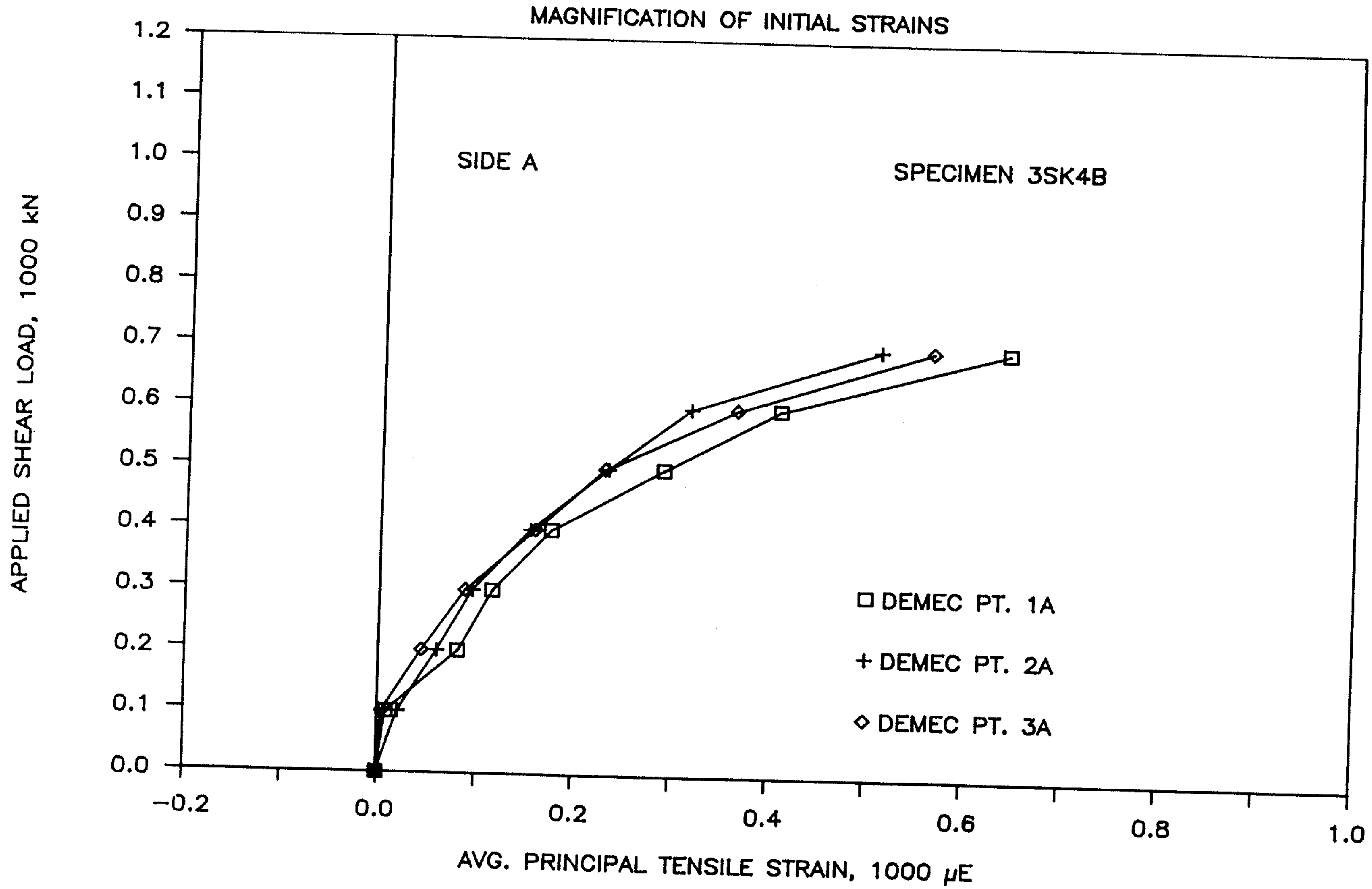

Figure 5.14 Magnification of the Applied Shear Load-Average Principal Tensile Strain Relationship on Side A of Specimen 3SK4B

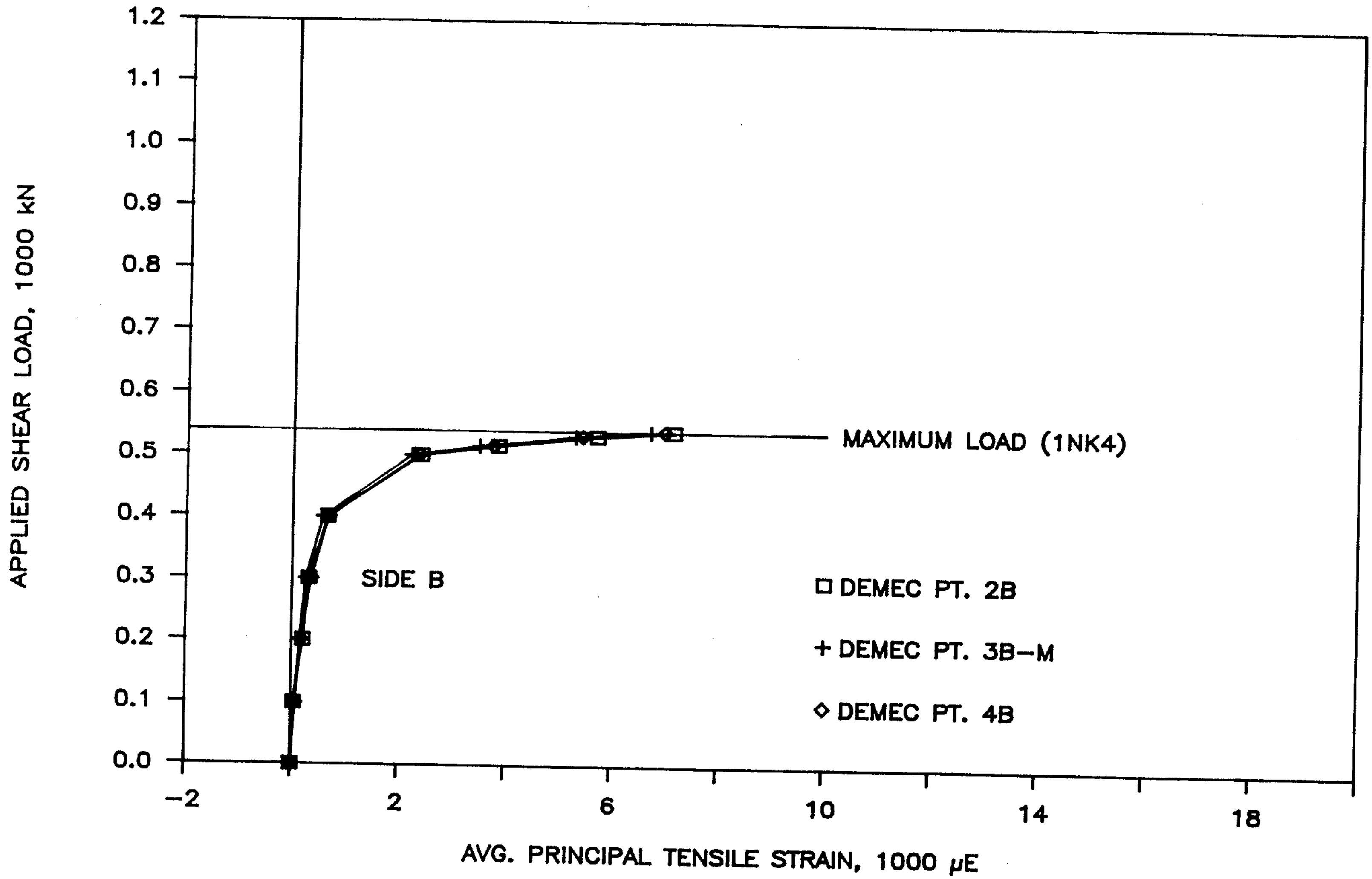

Figure 5.15 Applied Shear Load-Concrete and Drypack Principal Tensile Strain Relationships on Side B of Specimen 1NK4

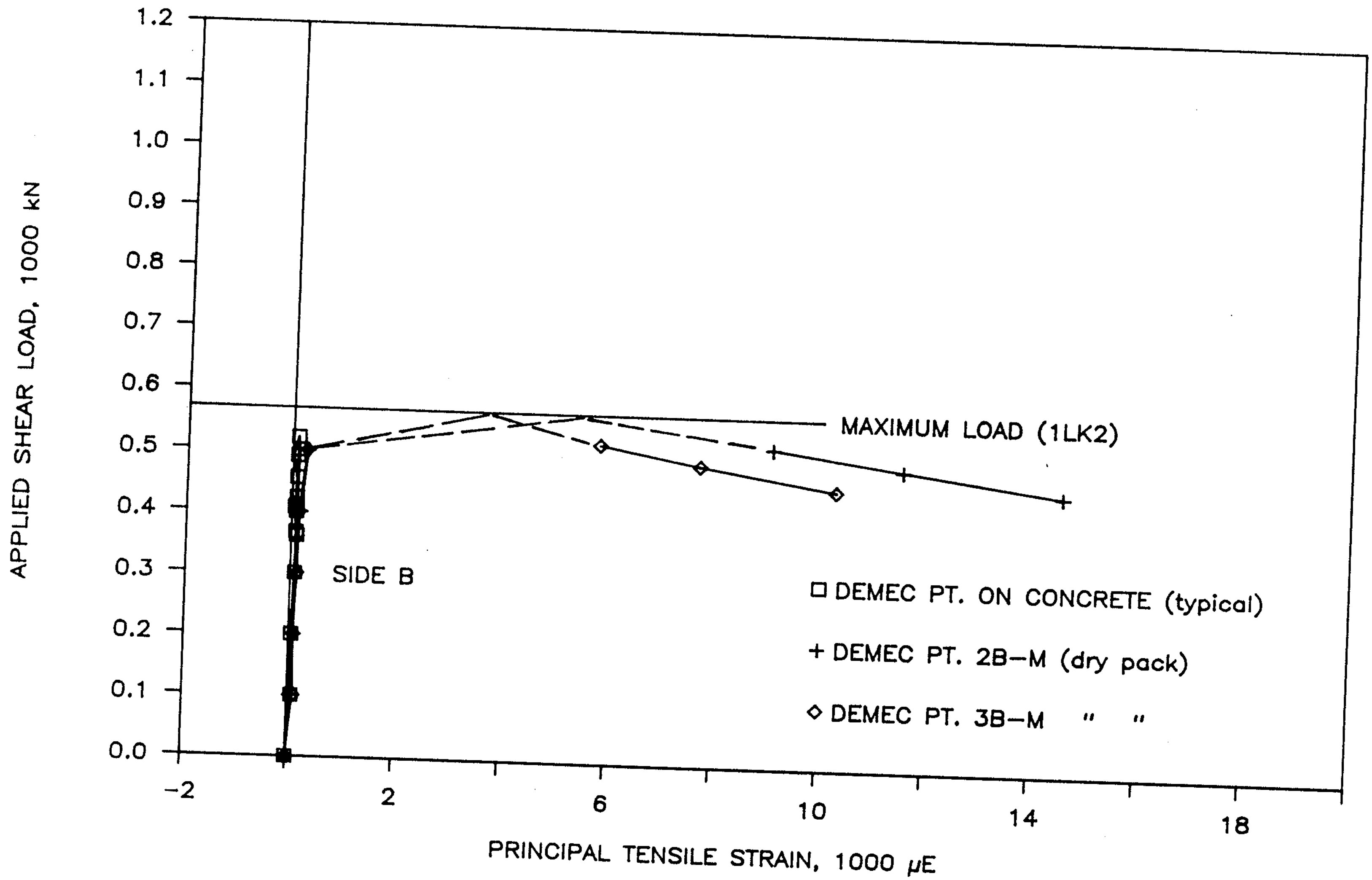

Figure 5.16 Applied Shear Load-Concrete and Drypack Principal Tensile Strain Relationships on Side B of Specimen 1LK2

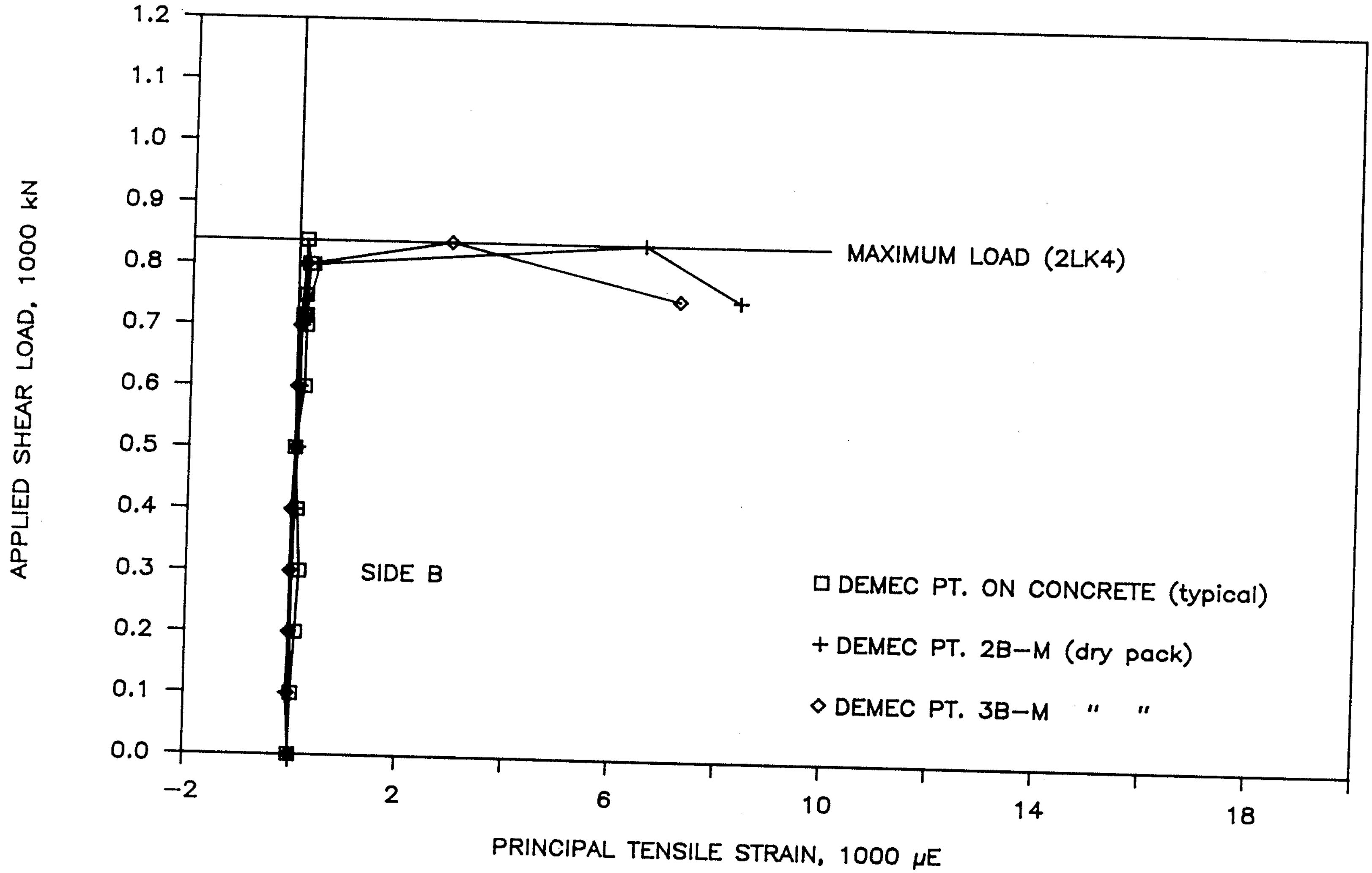

Figure 5.17 Applied Shear Load-Concrete and Drypack Principal Tensile Strain Relationships on Side B of Specimen 2LK4

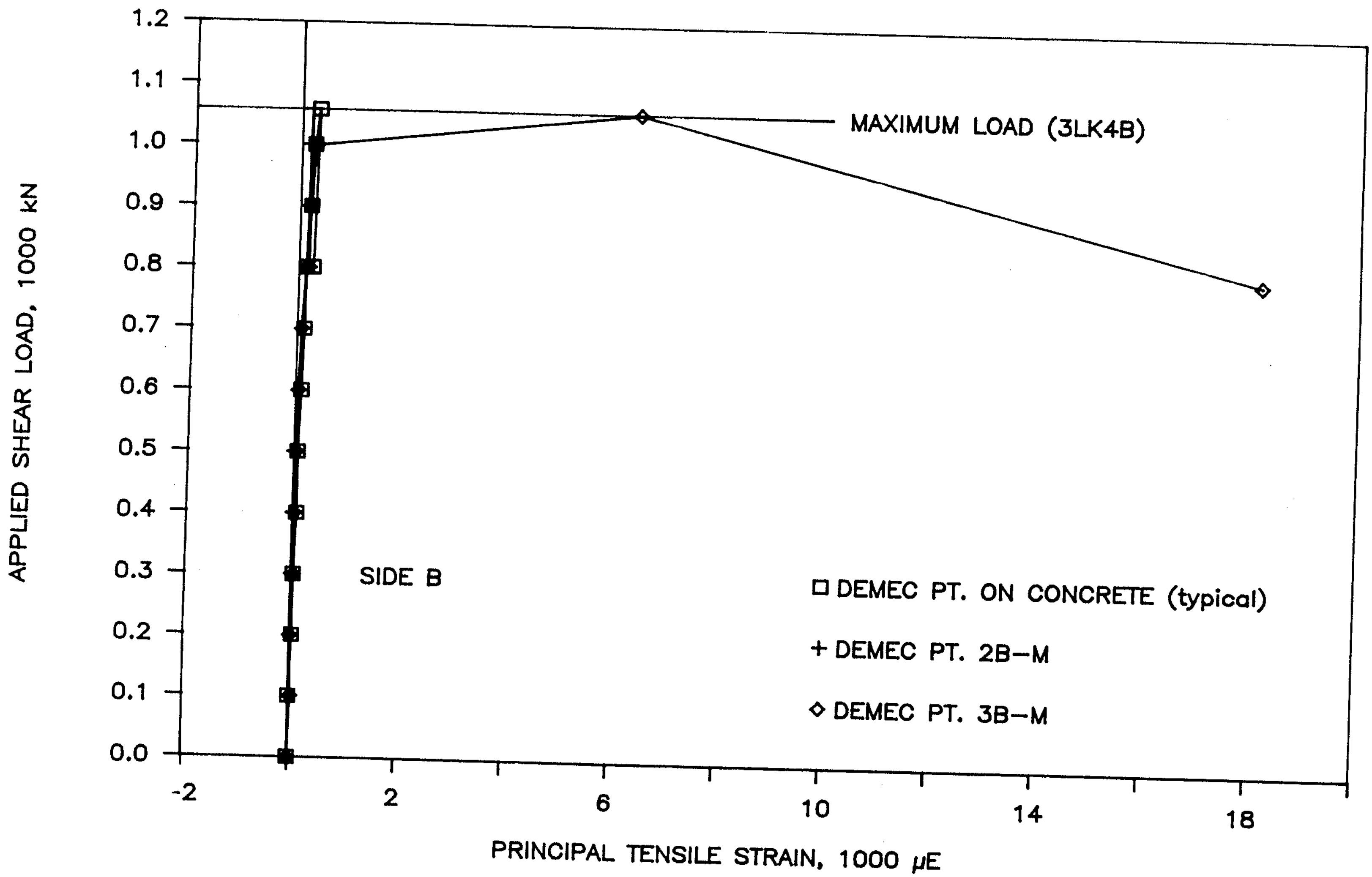

Figure 5.18 Applied Shear Load-Concrete and Drypack Principal Tensile Strain Relationships on Side B of Specimen 3LK4B

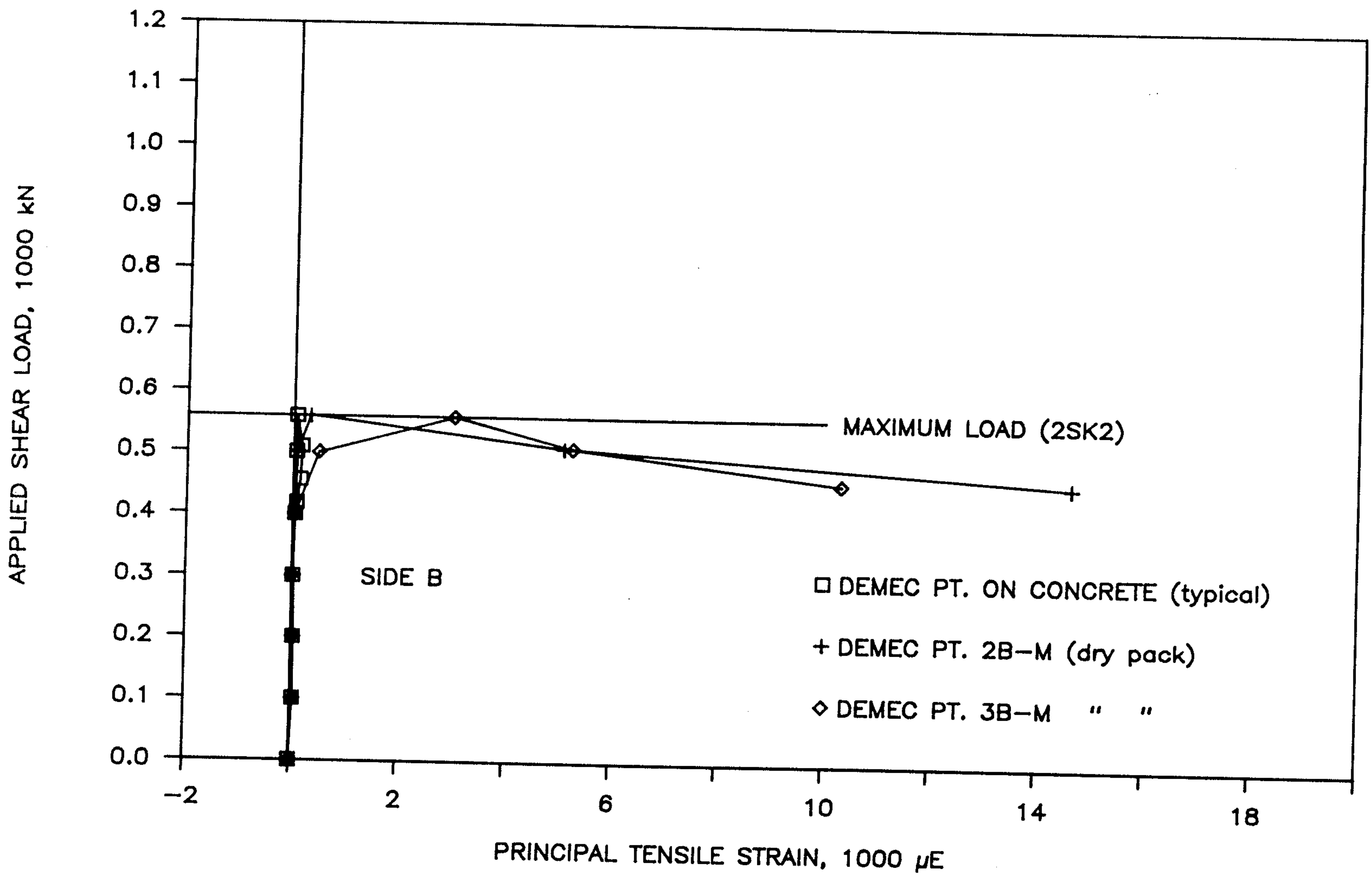

Figure 5.19 Applied Shear Load-Concrete and Drypack Principal Tensile Strain Relationships on Side B of Specimen 2SK2

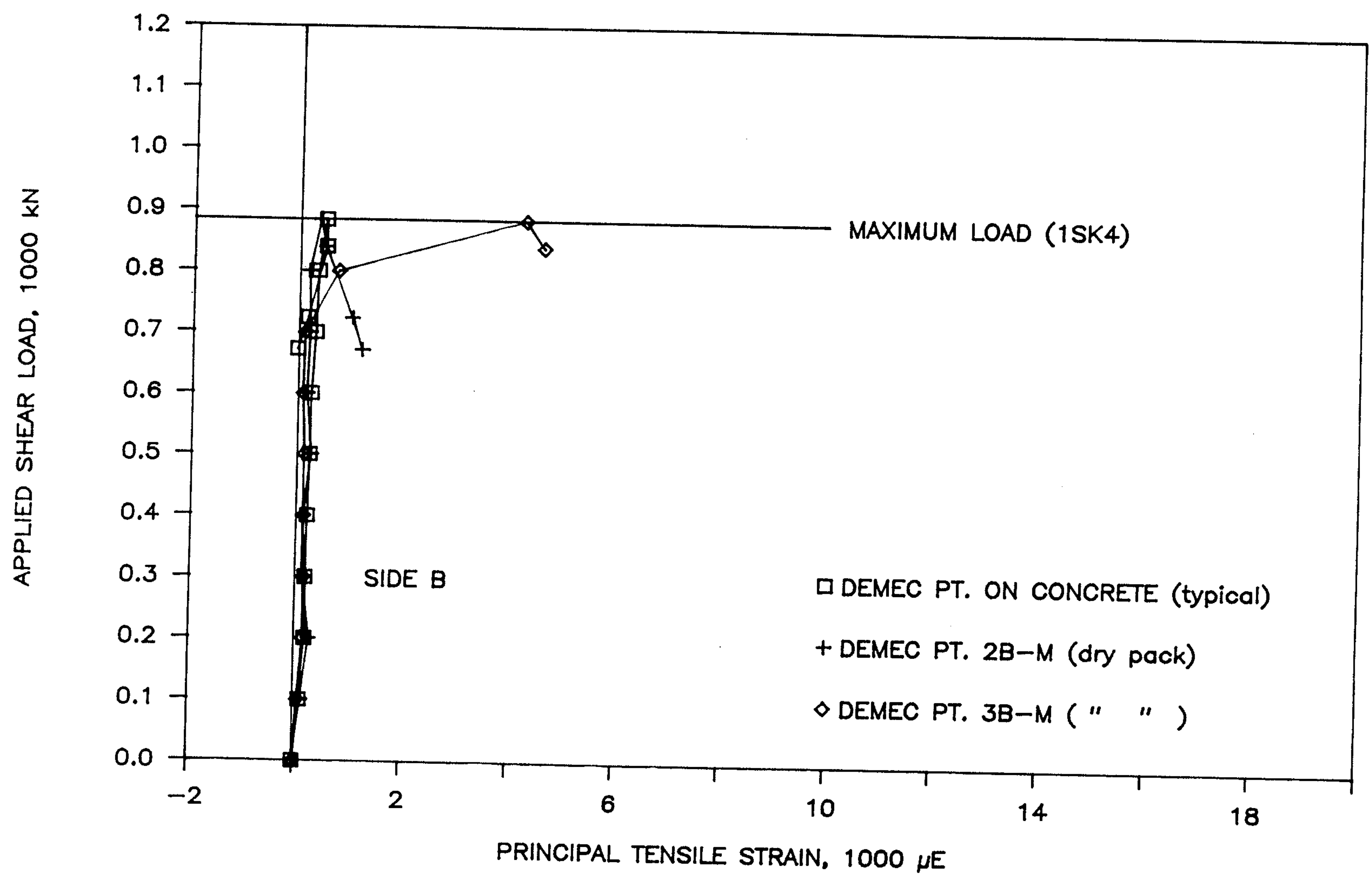

Figure 5.20 Applied Shear Load-Concrete and Drypack Principal Tensile Strain Relationships on Side B of Specimen 1SK4

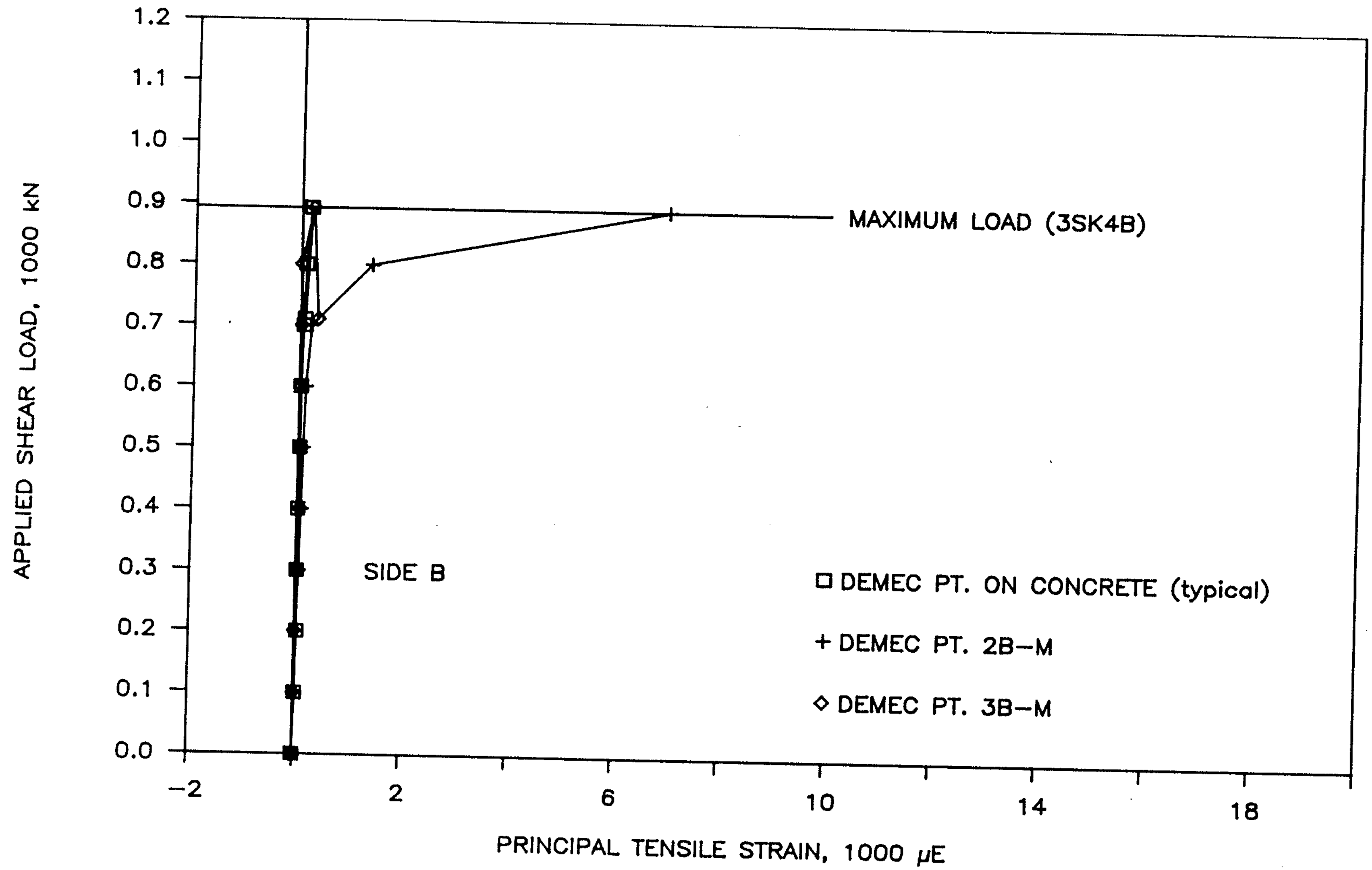

Figure 5.21 Applied Shear Load-Concrete and Drypack Principal Tensile Strain Relationships on Side B of Specimen 3SK4B

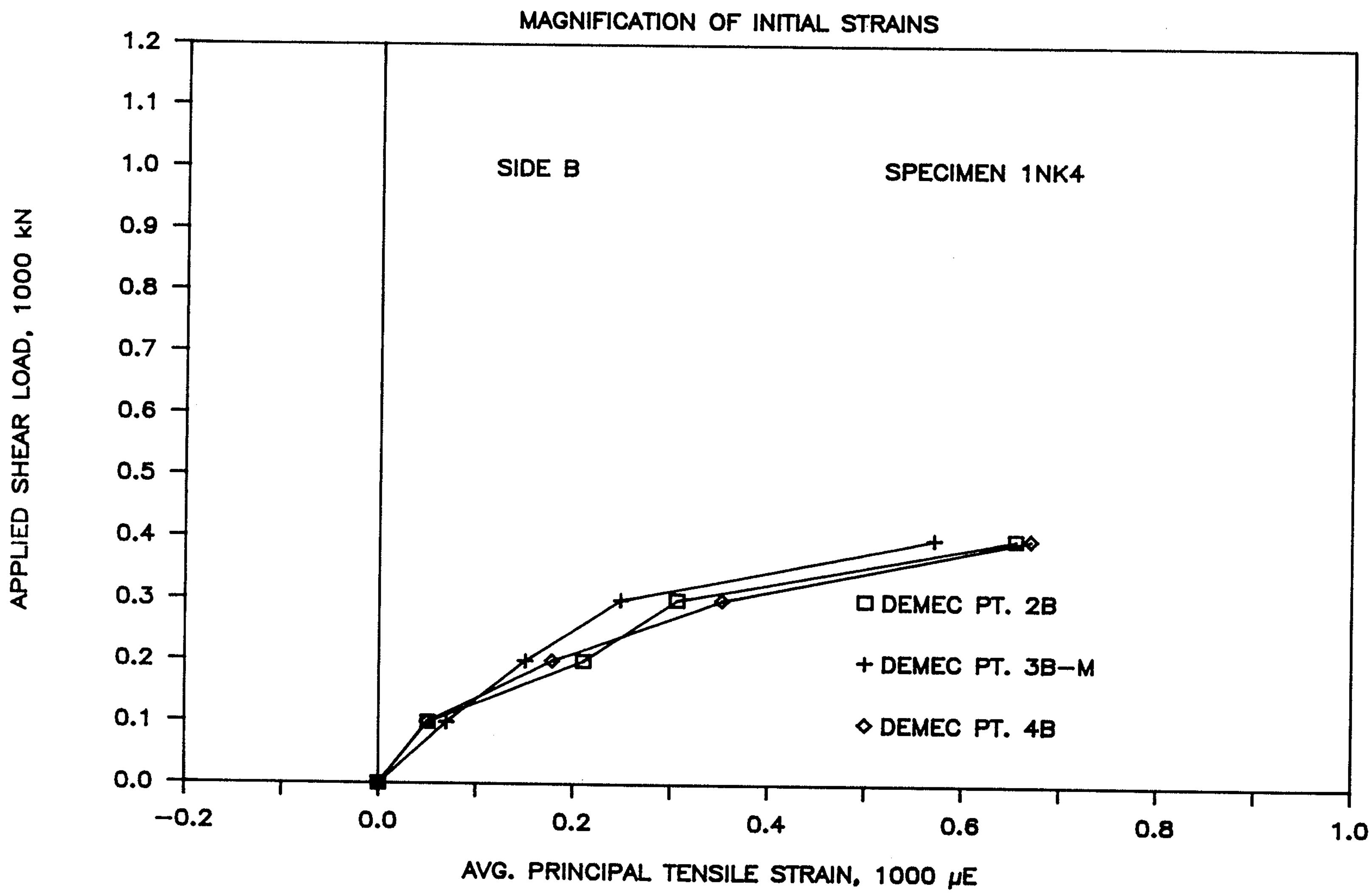

Figure 5.22 Magnification of the Applied Shear Load - Concrete and Drypack Principal Tensile Strain Relationships on Side B of Specimen 1NK4

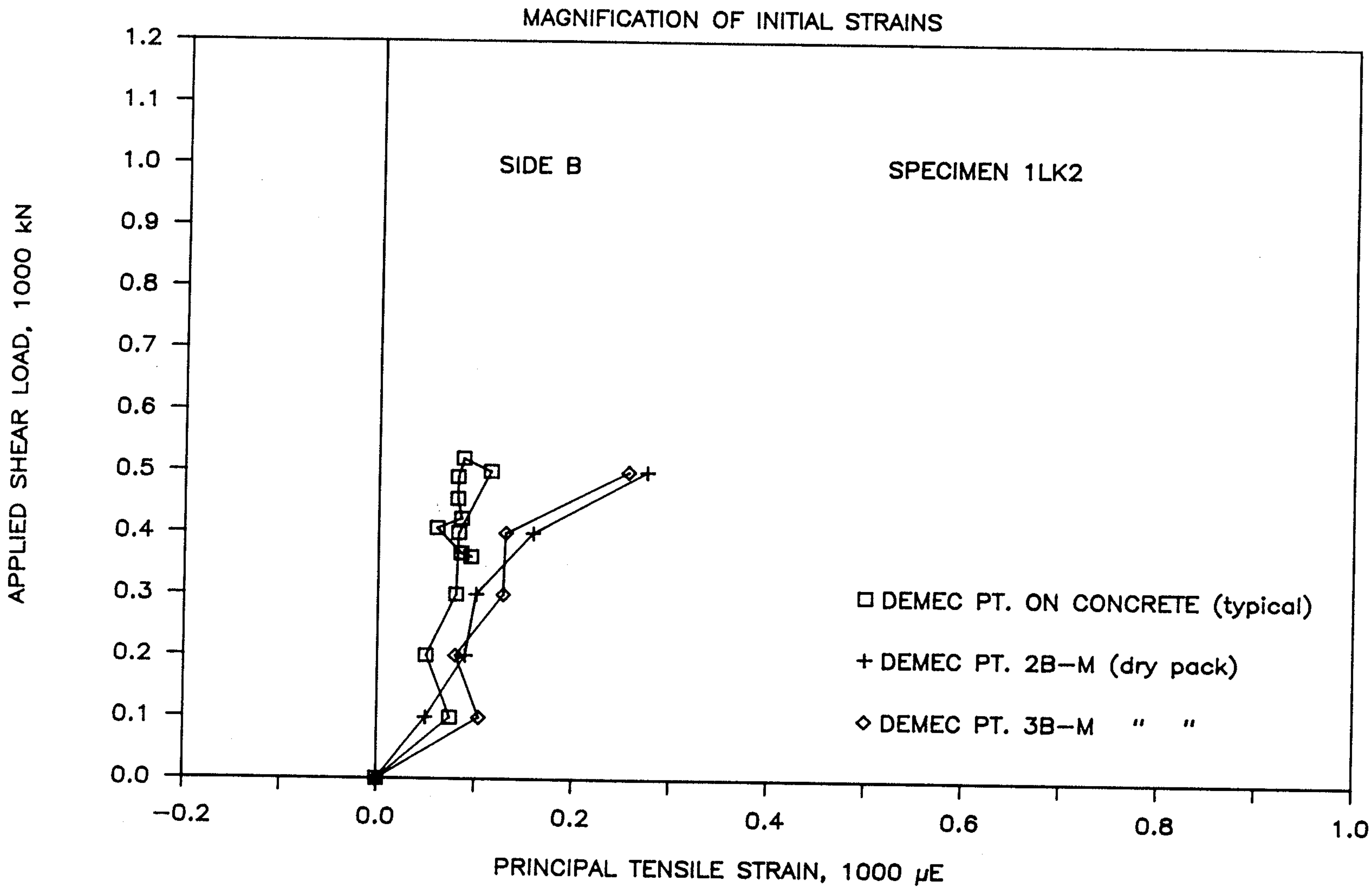

Figure 5.23 Magnification of the Applied Shear Load - Concrete and Drypack Principal Tensile Strain Relationships on Side B of Specimen 1LK2

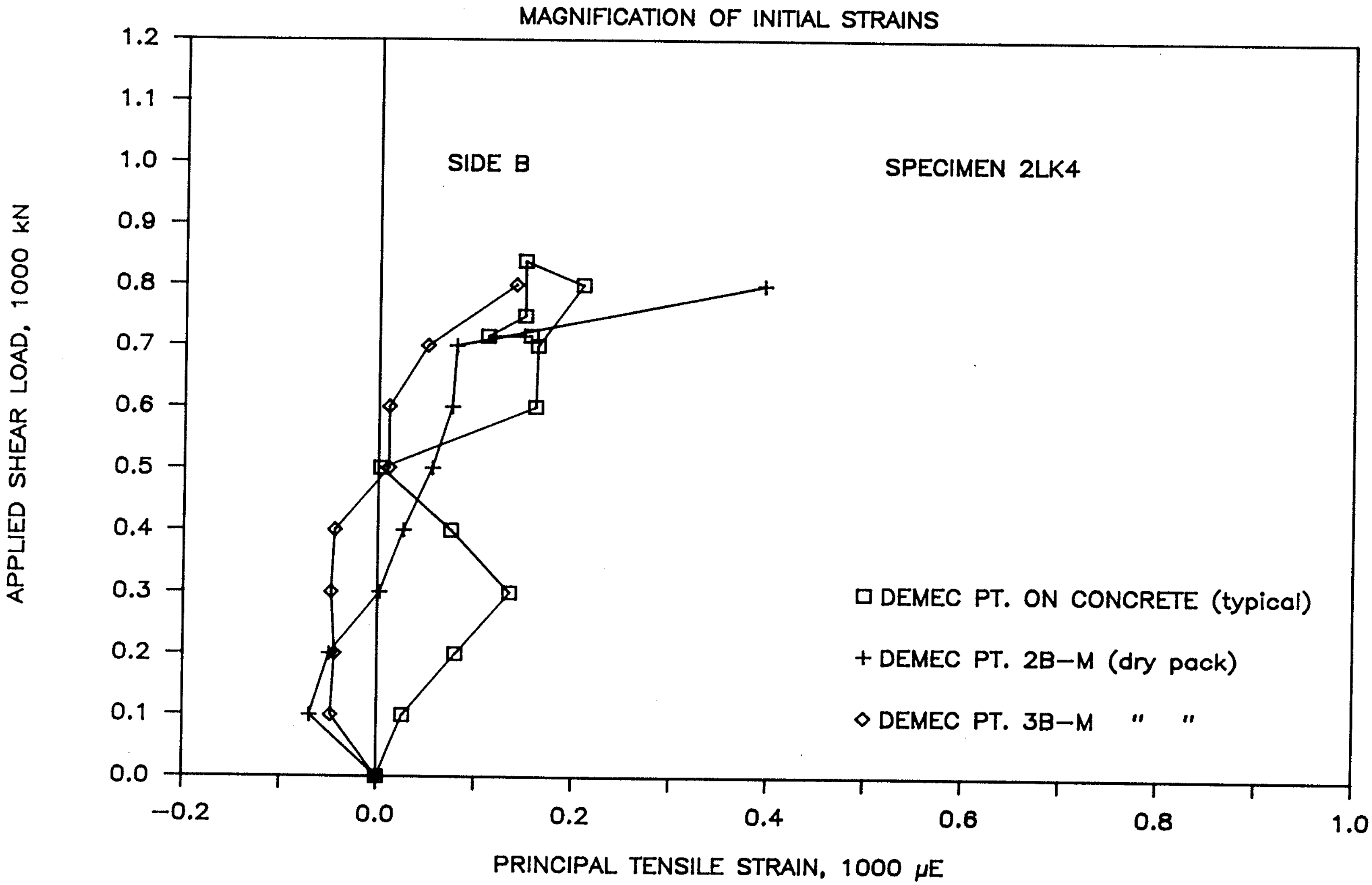

Figure 5.24 Magnification of the Applied Shear Load - Concrete and Drypack Principal Tensile Strain Relationships on Side B of Specimen 2LK4

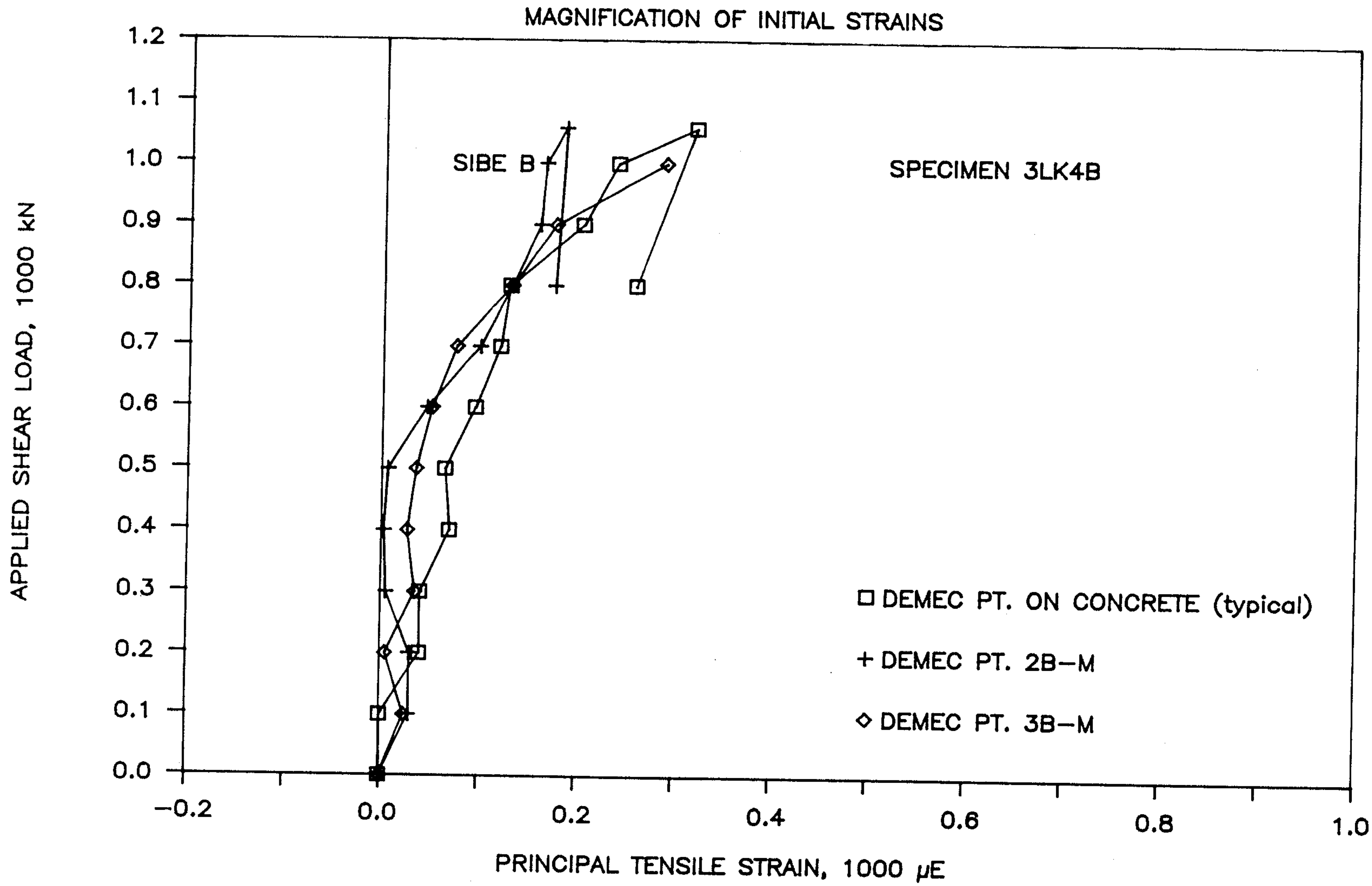

Figure 5.25 Magnification of the Applied Shear Load - Concrete and Drypack Principal Tensile Strain Relationships on Side B of Specimen 3LK4B

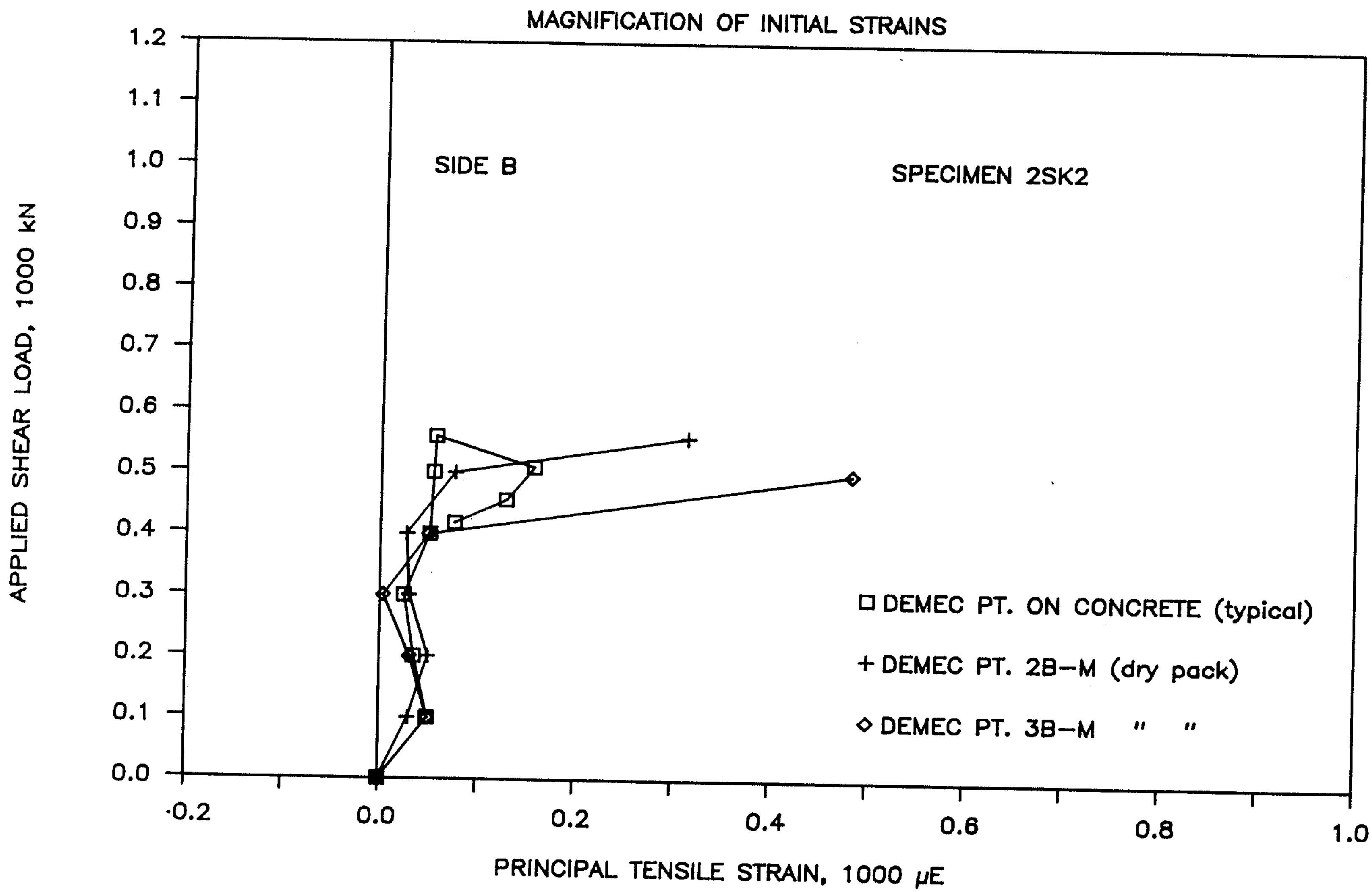

Figure 5.26 Magnification of the Applied Shear Load - Concrete and Drypack Principal Tensile Strain Relationships on Side B of Specimen 2SK2

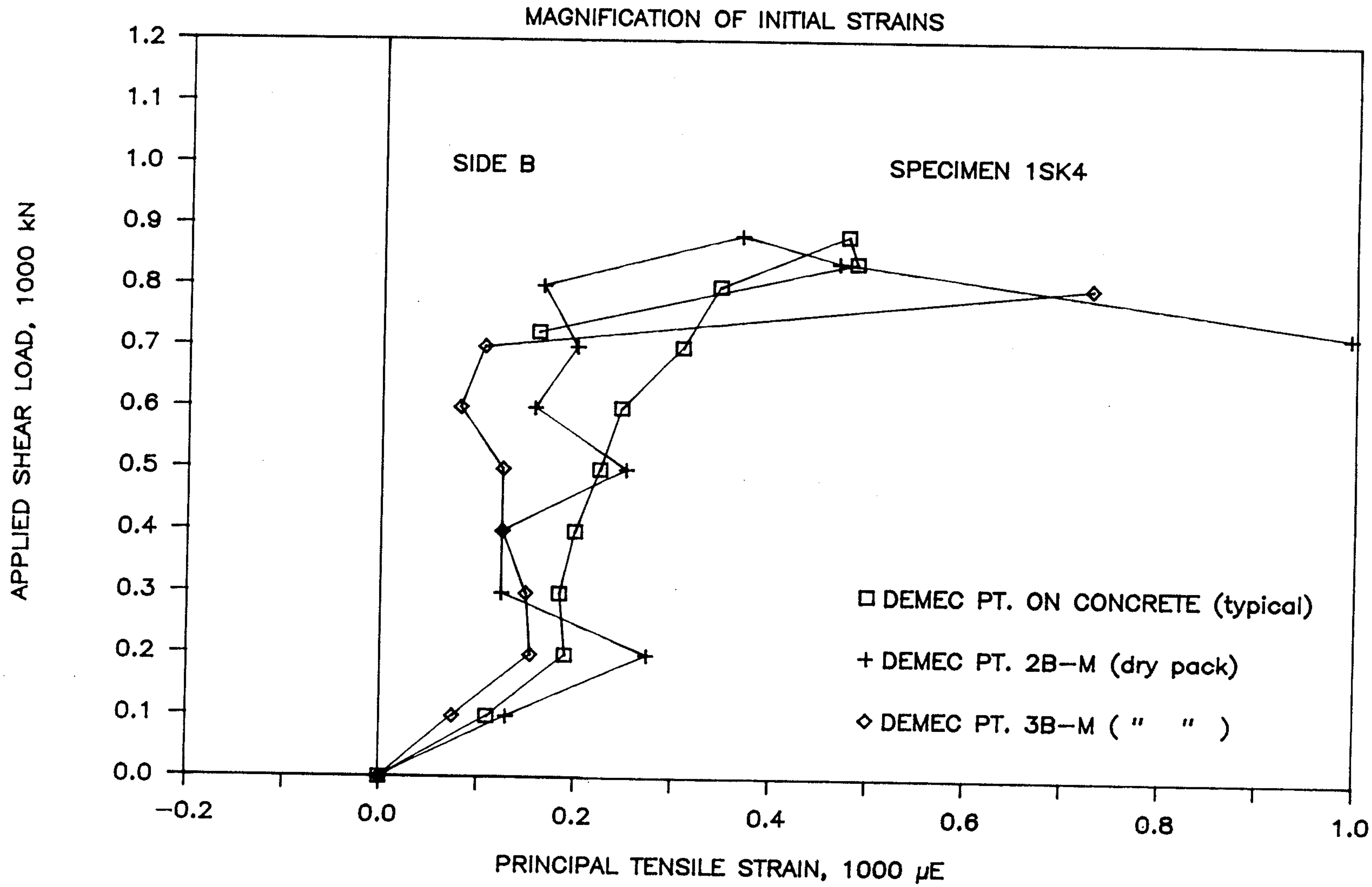

Figure 5.27 Magnification of the Applied Shear Load - Concrete and Drypack Principal Tensile Strain Relationships on Side B of Specimen 1SK4

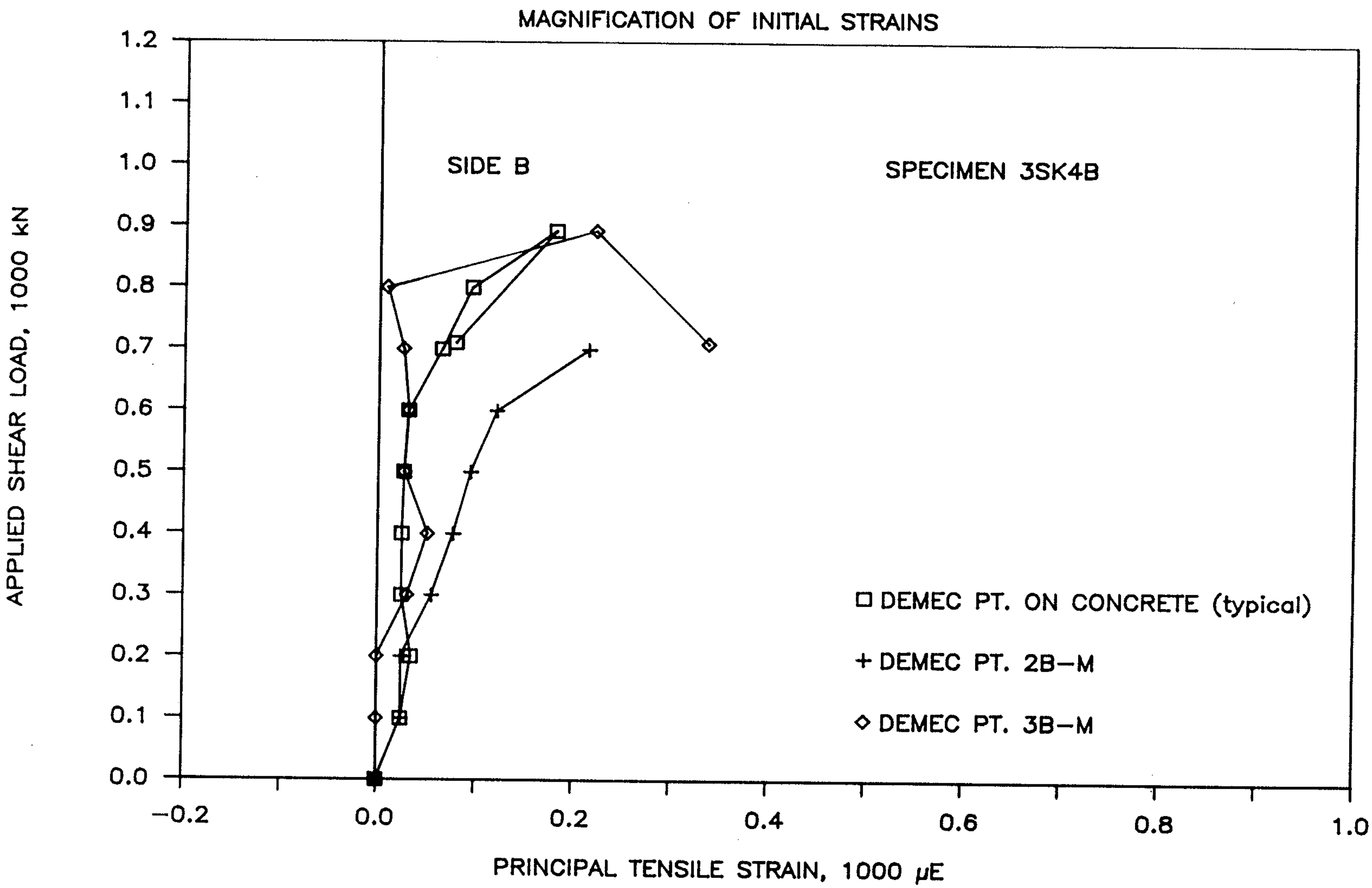

Figure 5.28 Magnification of the Applied Shear Load - Concrete and Drypack Principal Tensile Strain Relationships on Side B of Specimen 3SK4B

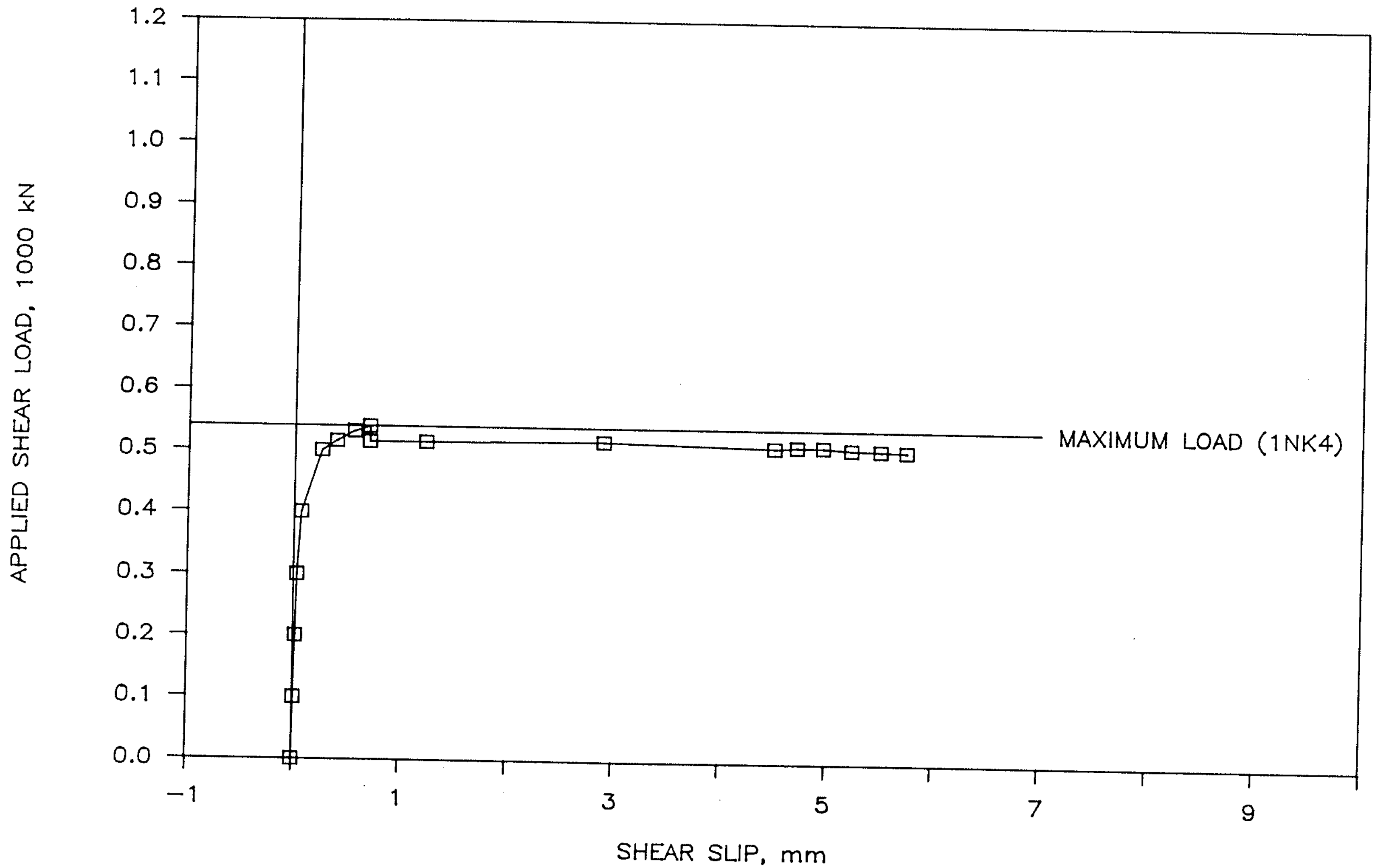

Figure 5.29 Applied Shear Load-Slip Relationship for Specimen 1NK4

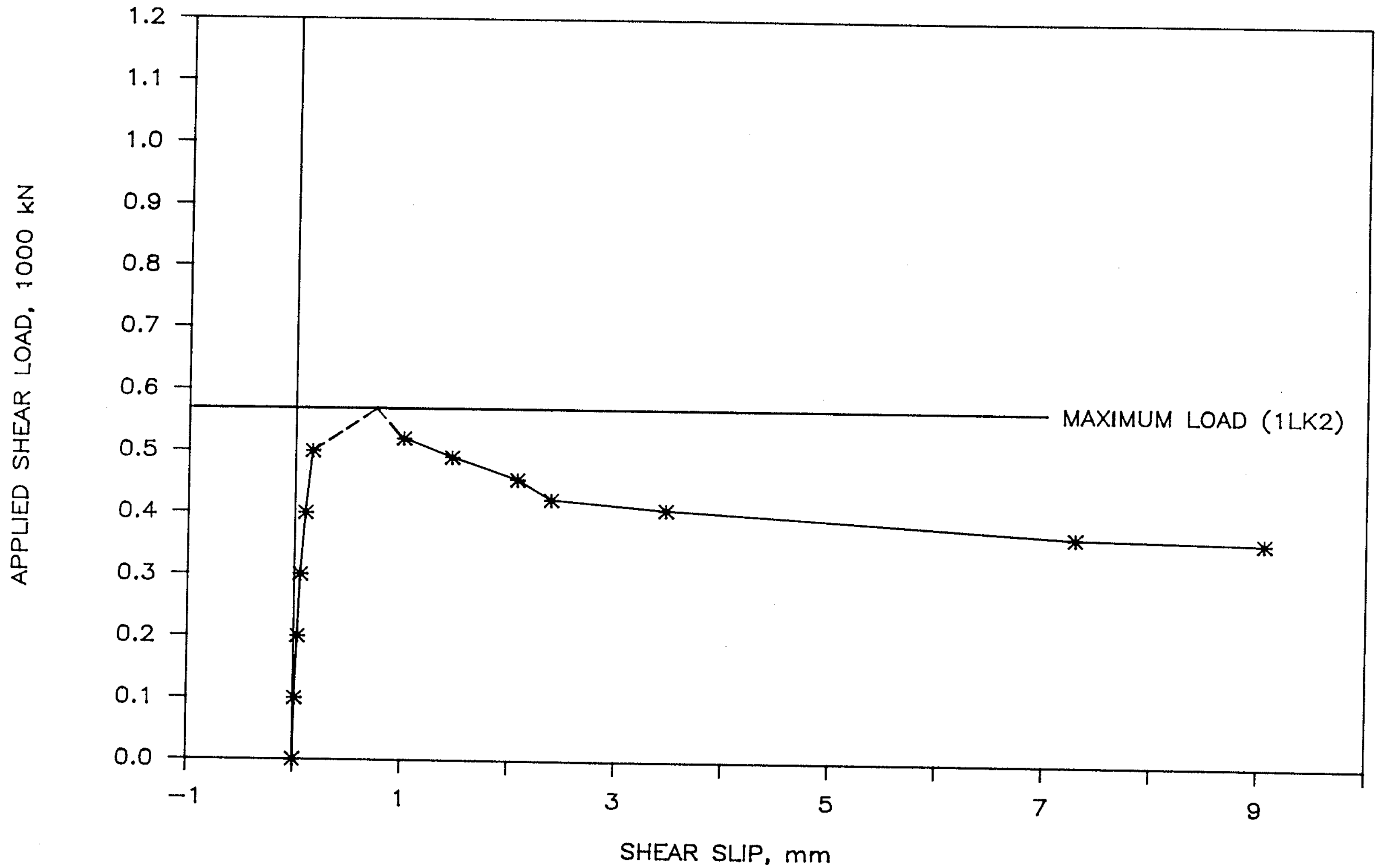

Figure 5.30 Applied Shear Load-Slip Relationship for Specimen 1LK2

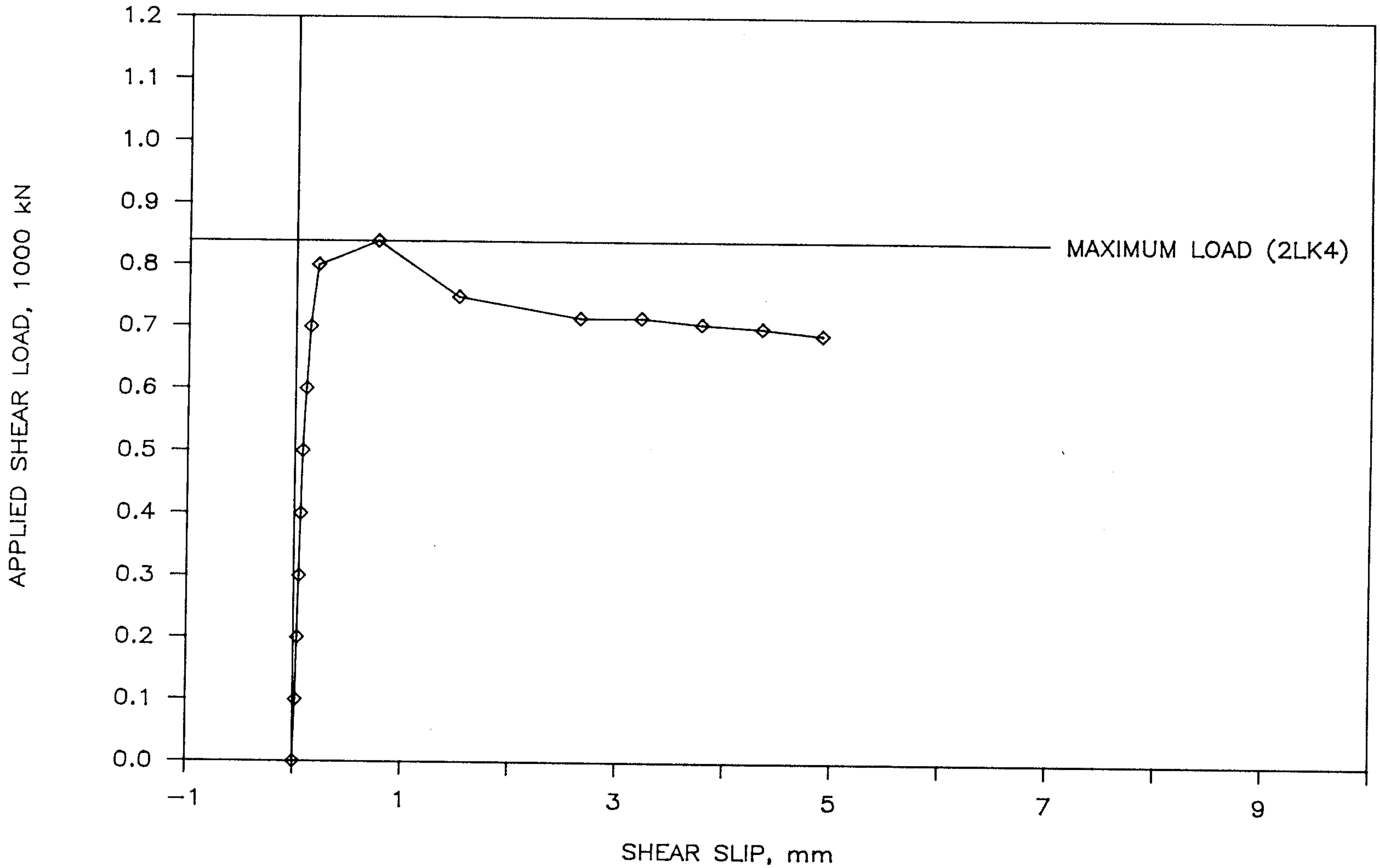

Figure 5.31 Applied Shear Load-Slip Relationship for Specimen 2LK4

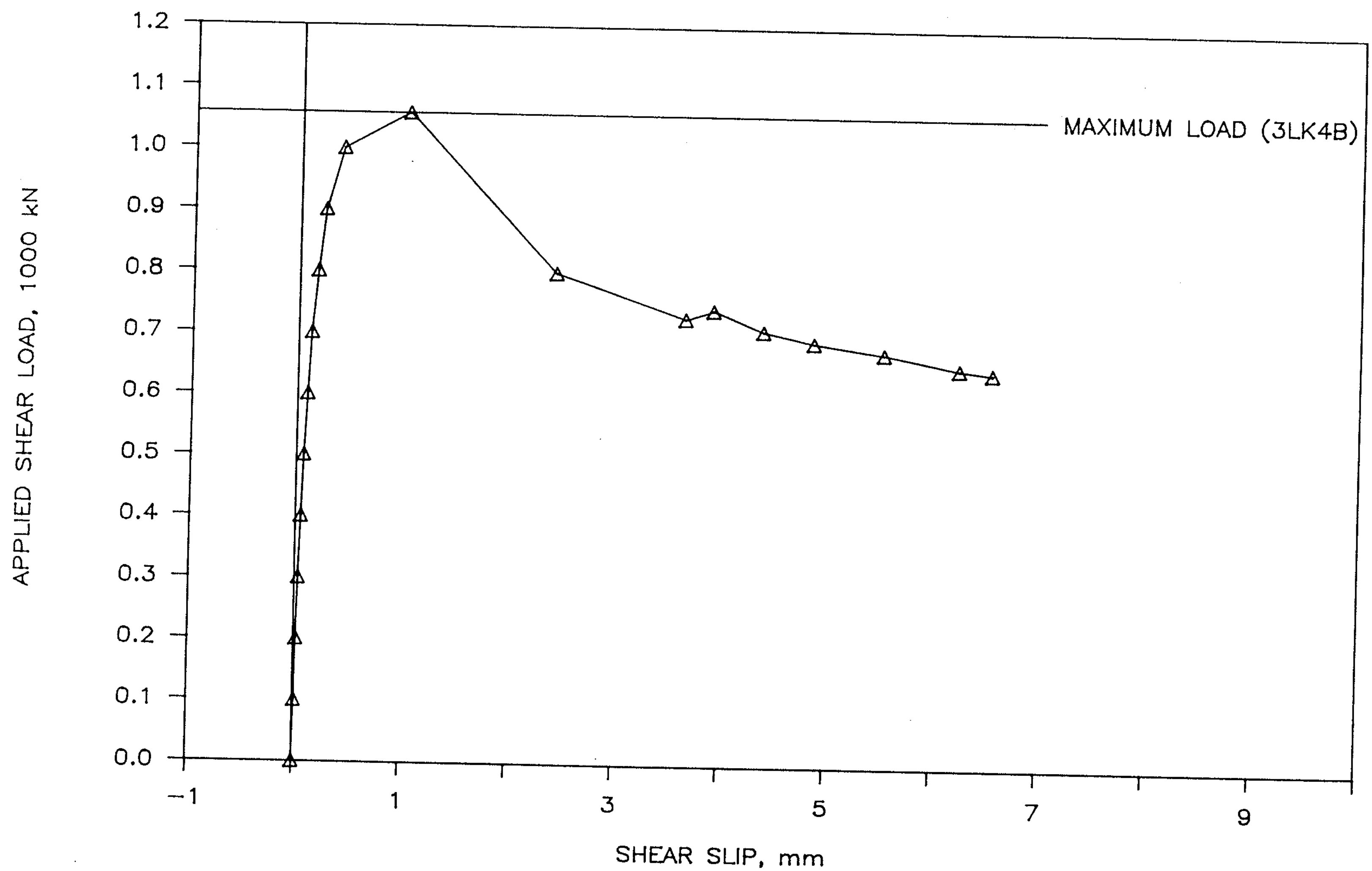

Figure 5.32 Applied Shear Load-Slip Relationship for Specimen 3LK4B

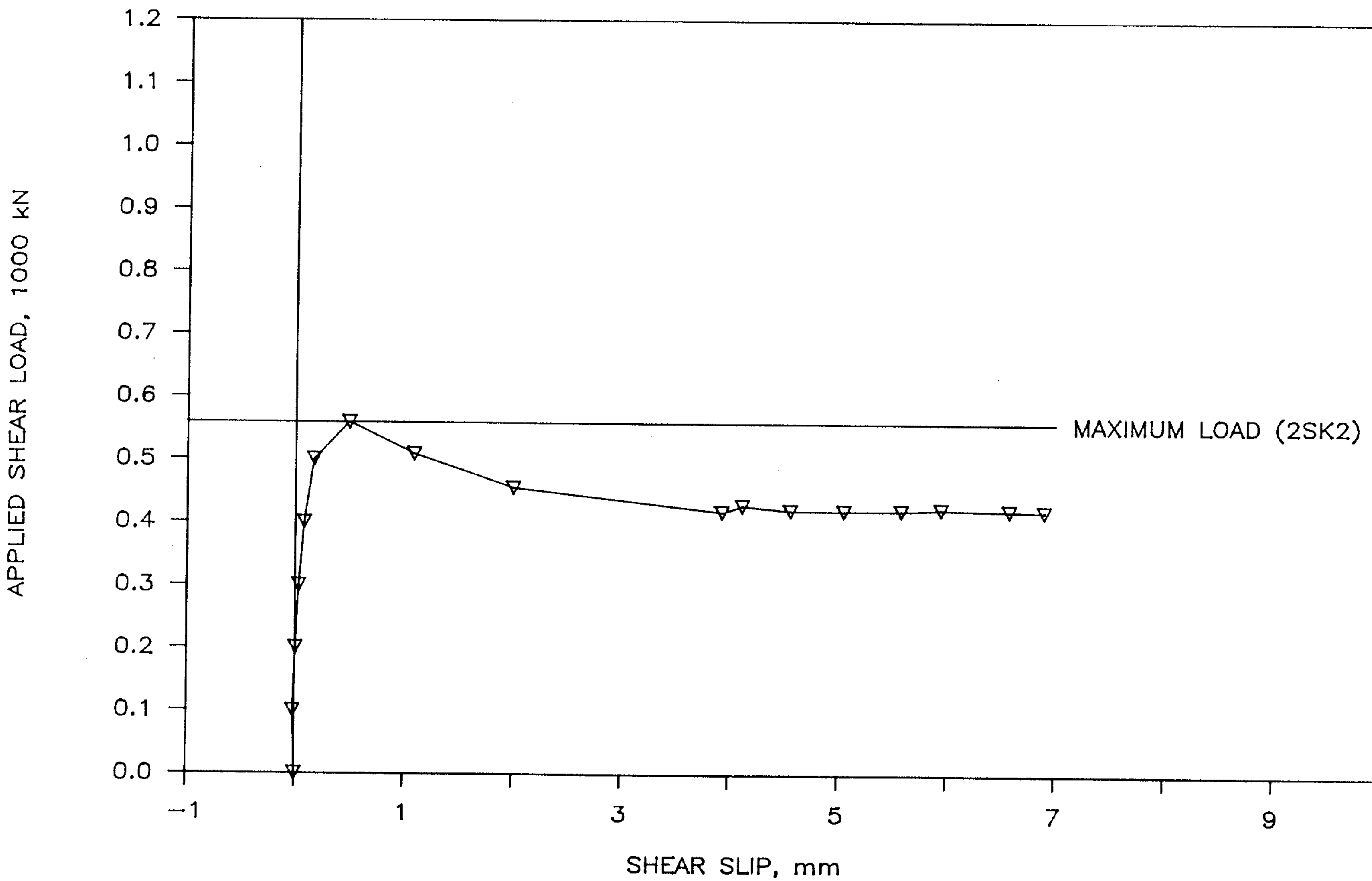

Figure 5.33 Applied Shear Load-Slip Relationship for Specimen 2SK2

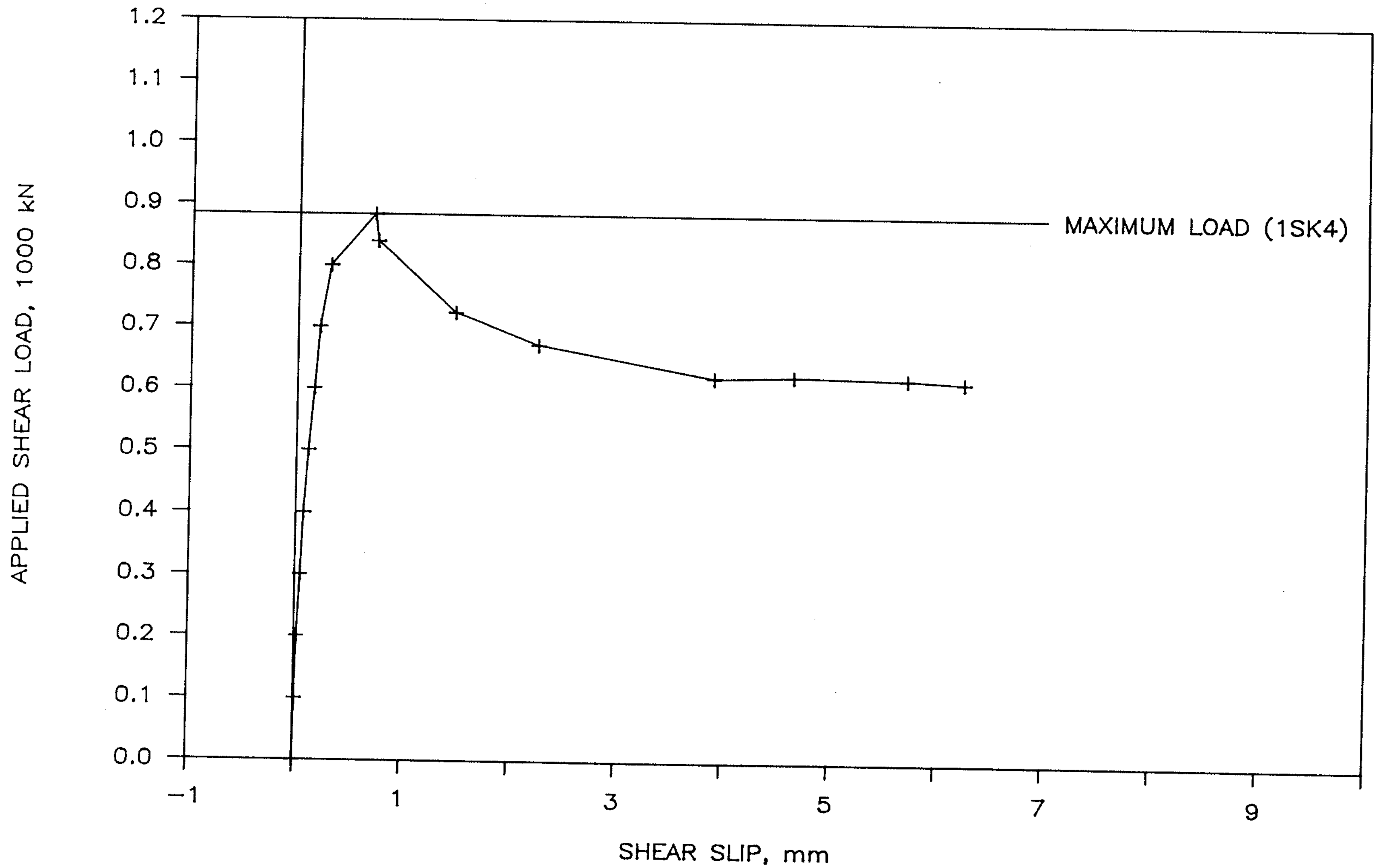

Figure 5.34 Applied Shear Load-Slip Relationship for Specimen 1SK4

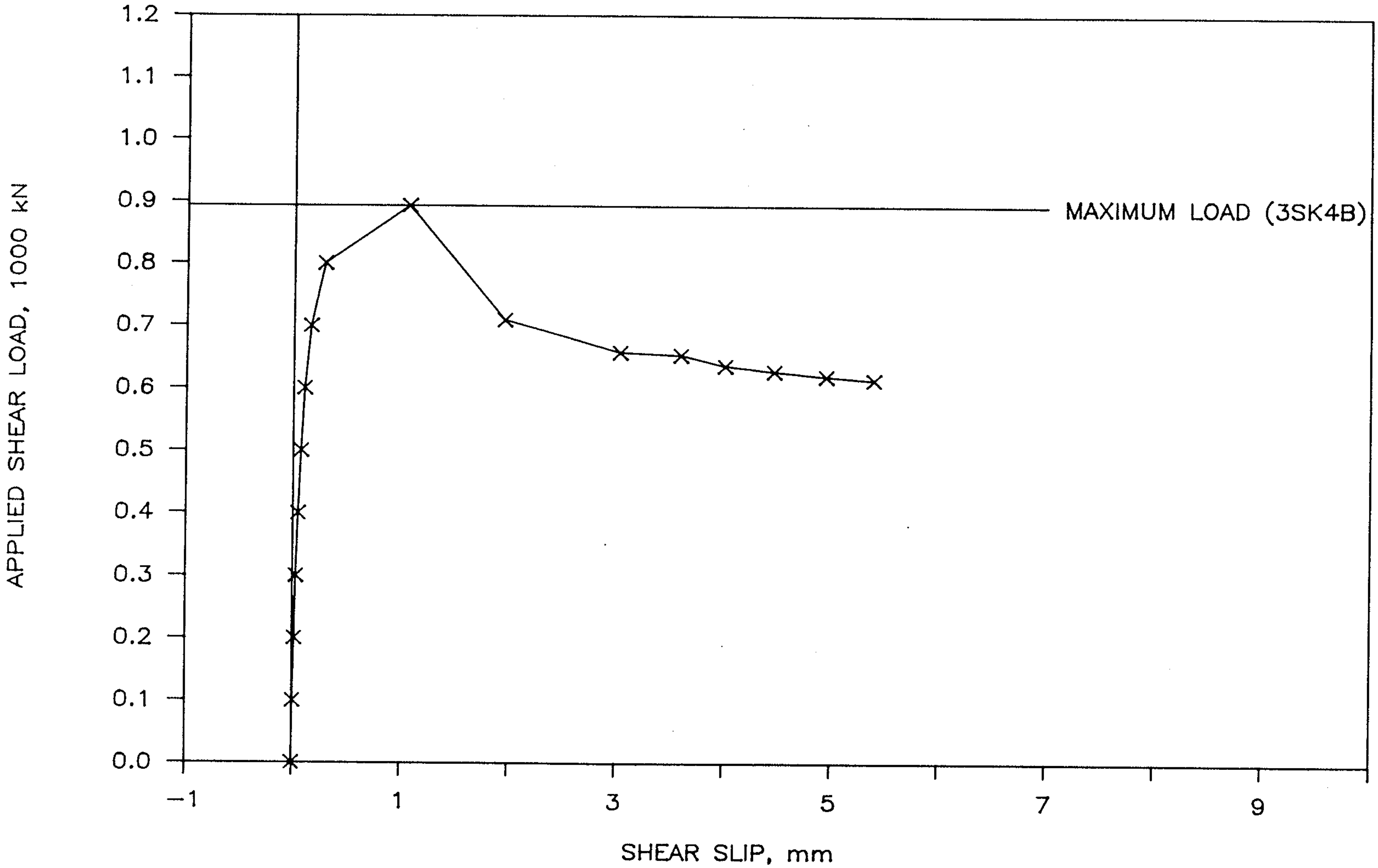

Figure 5.35 Applied Shear Load-Slip Relationship for Specimen 3SK4B

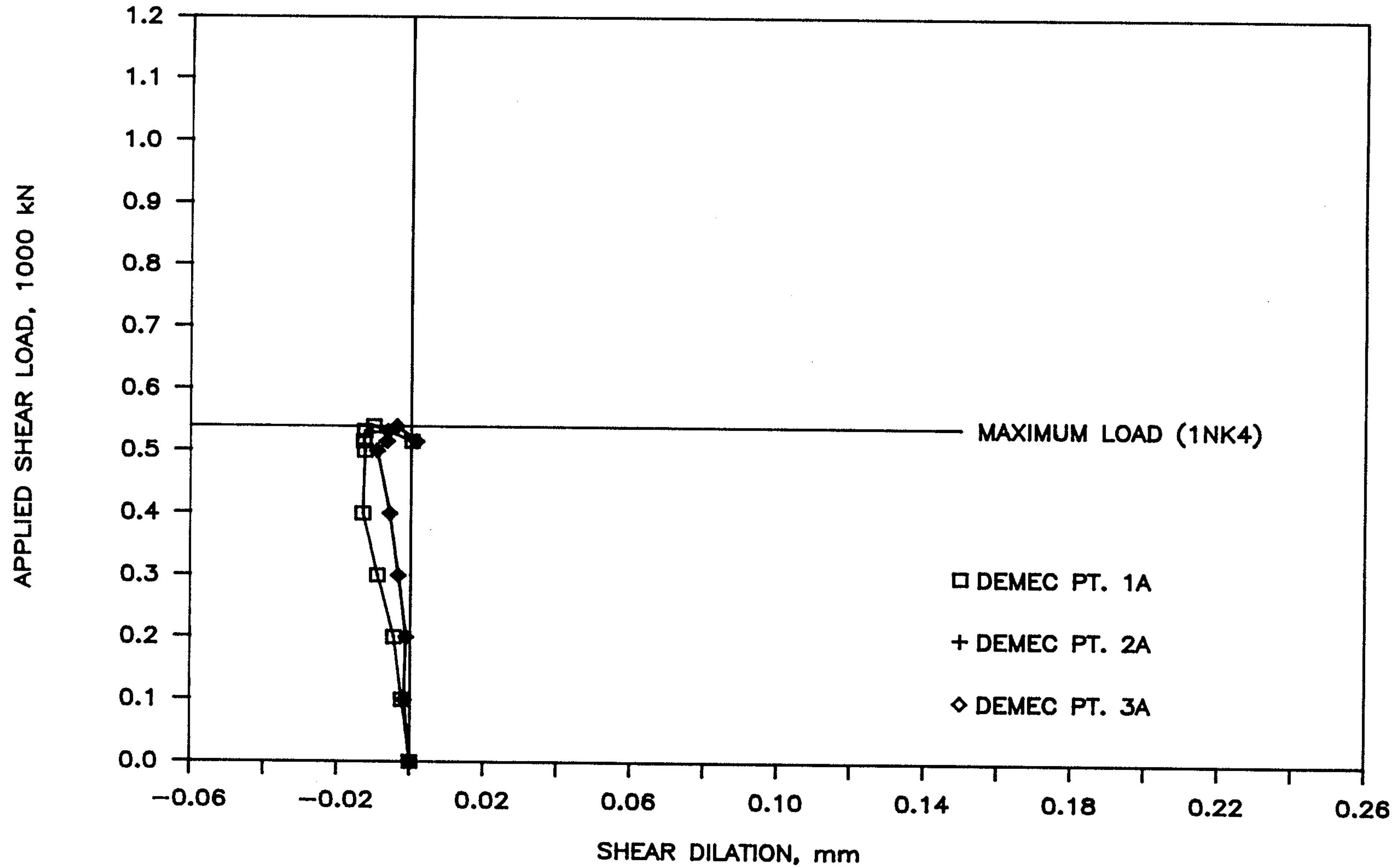

Figure 5.36 Applied Shear Load-Dilation Relationship for Specimen 1NK4

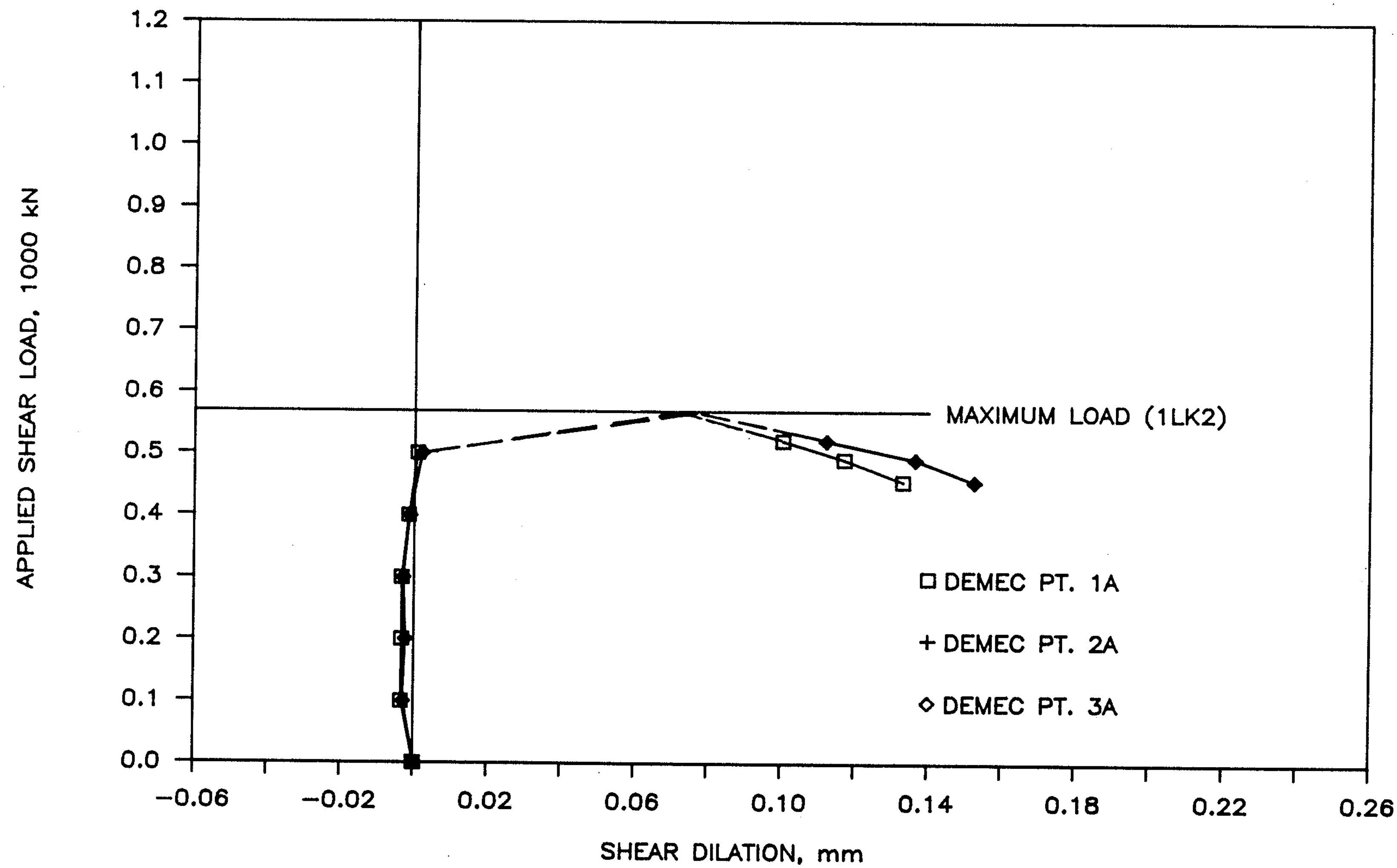

Figure 5.37 Applied Shear Load-Dilation Relationship for Specimen 1LK2

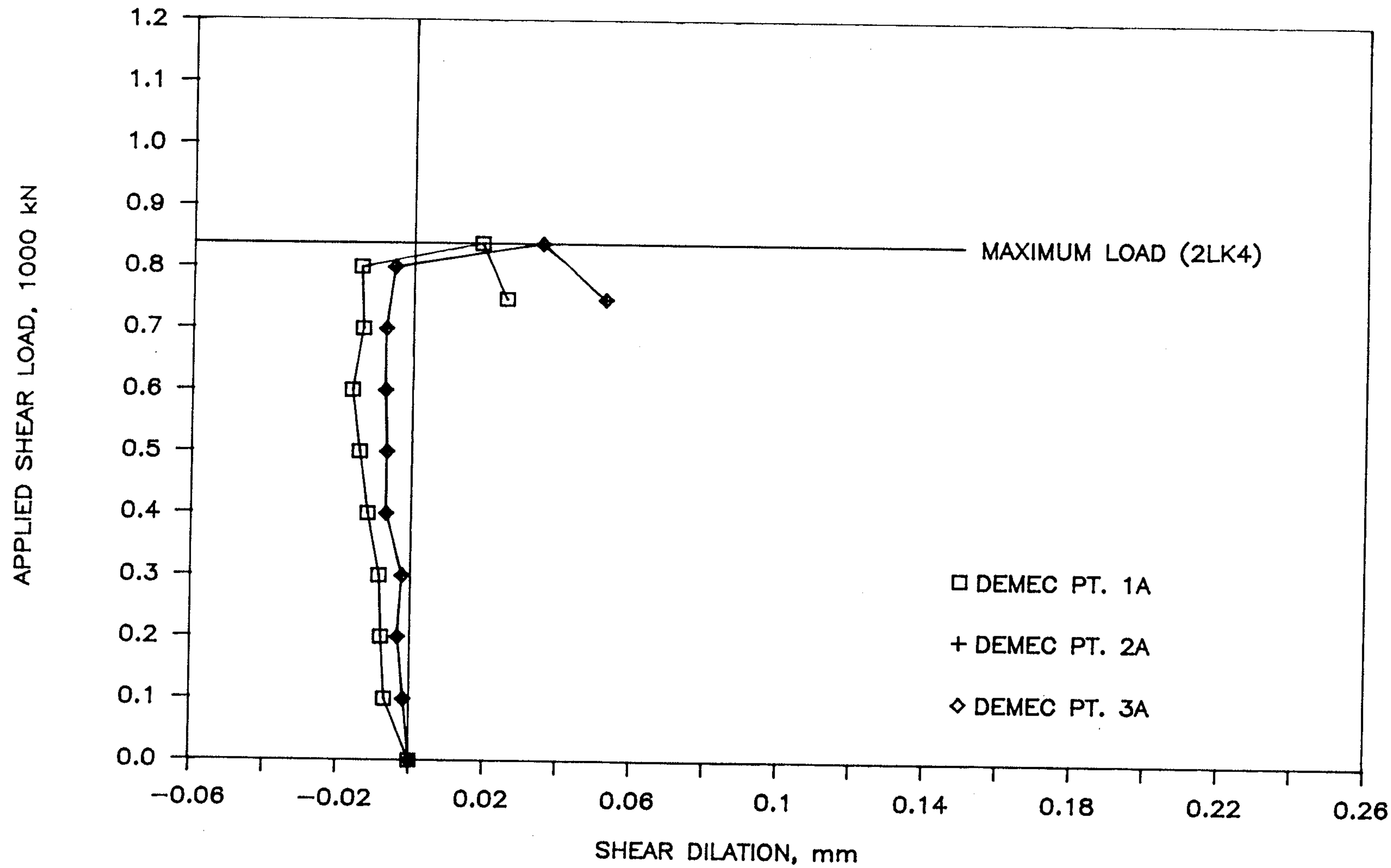

Figure 5.38 Applied Shear Load-Dilation Relationship for Specimen 2LK4

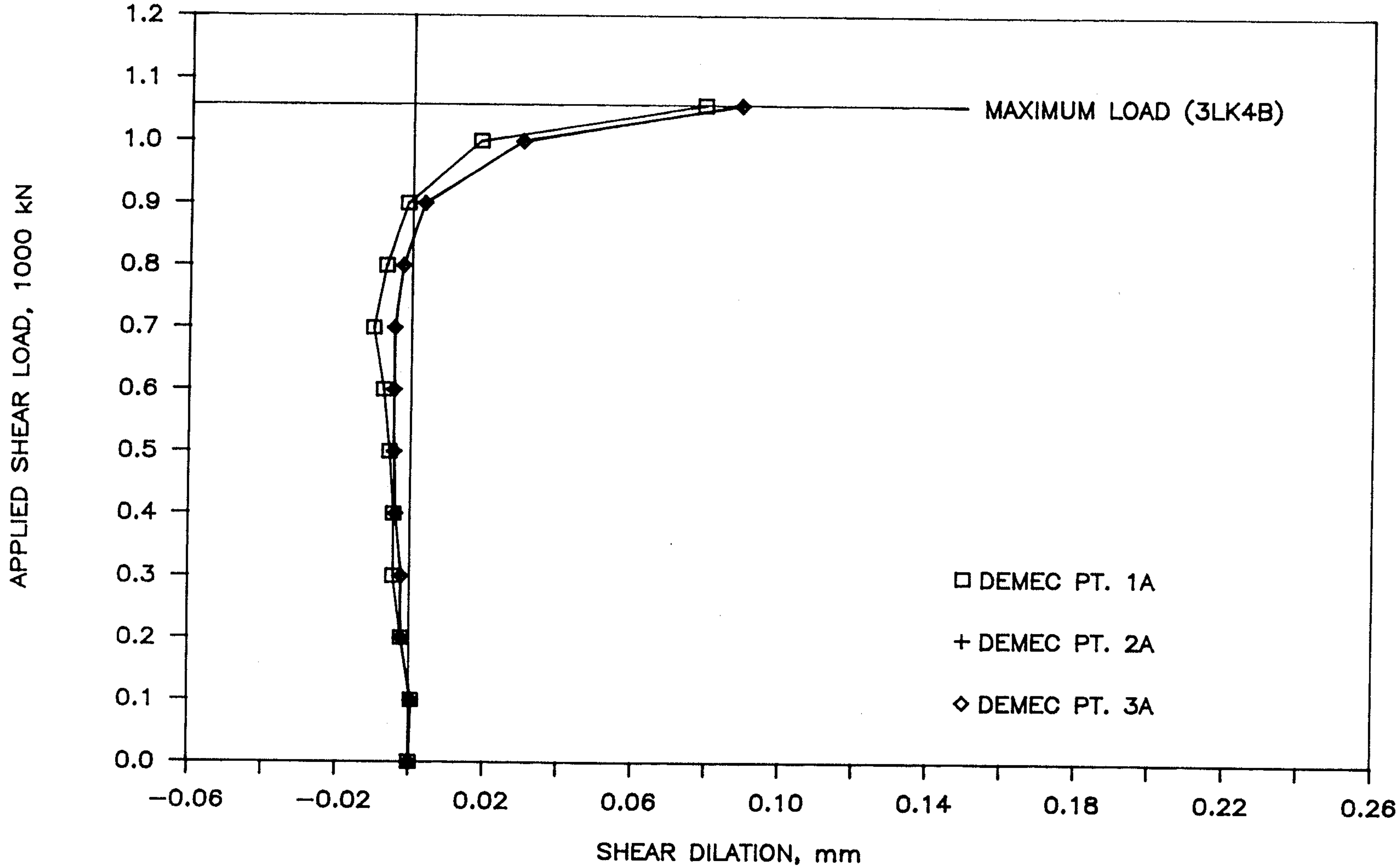

Figure 5.39 Applied Shear Load-Dilation Relationship for Specimen 3LK4B

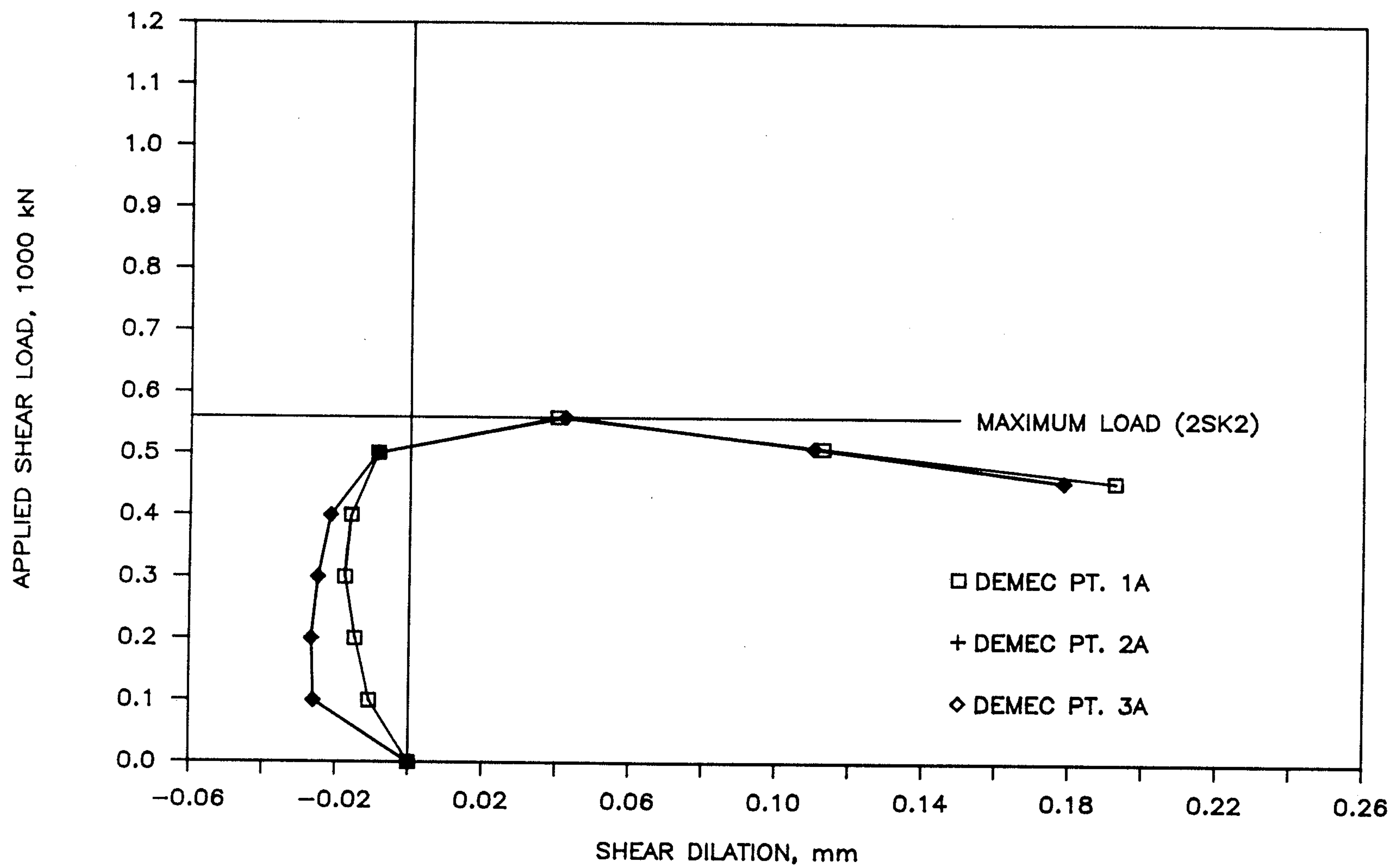

Figure 5.40 Applied Shear Load-Dilation Relationship for Specimen 2SK2

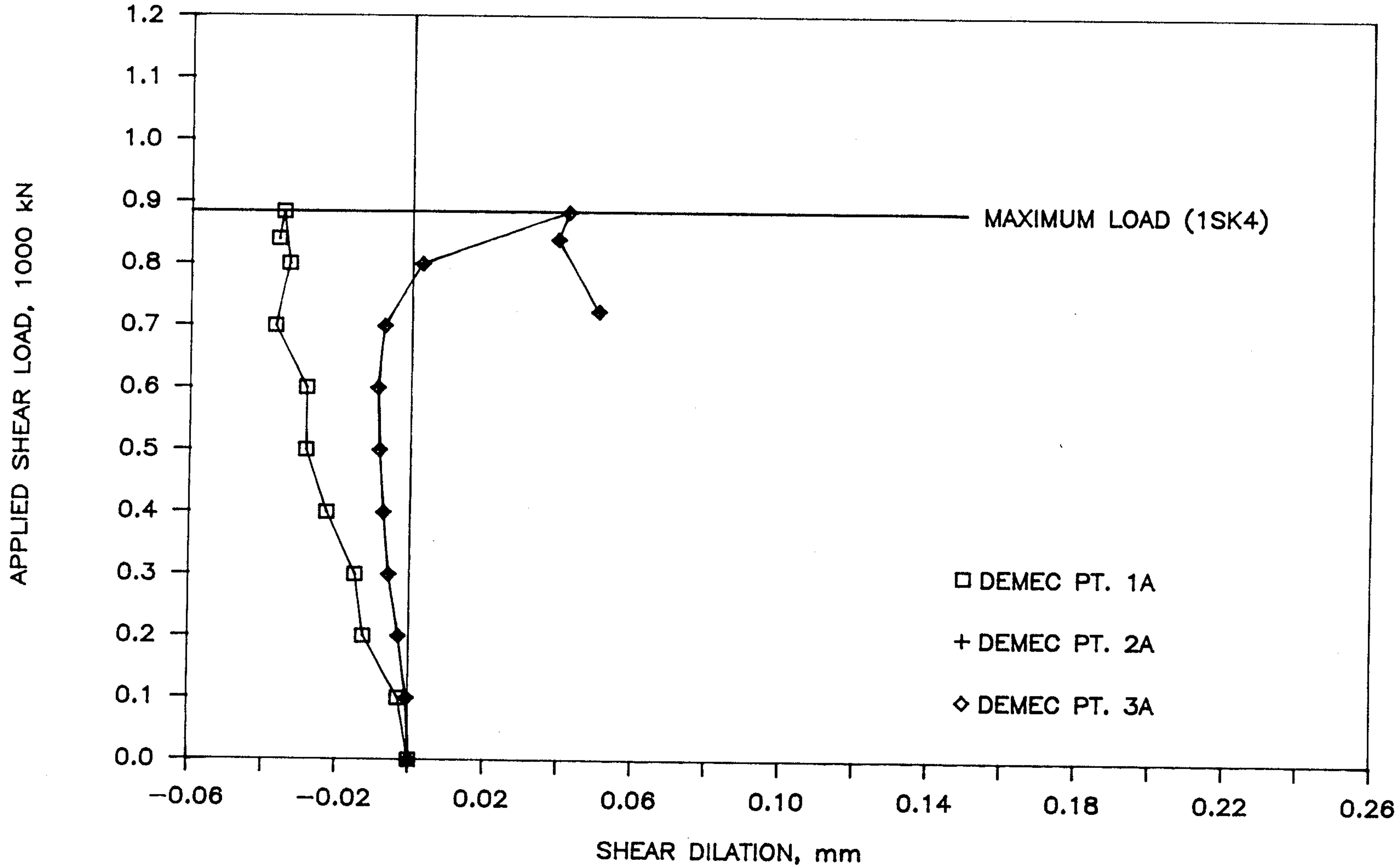

Figure 5.41 Applied Shear Load-Dilation Relationship for Specimen 1SK4

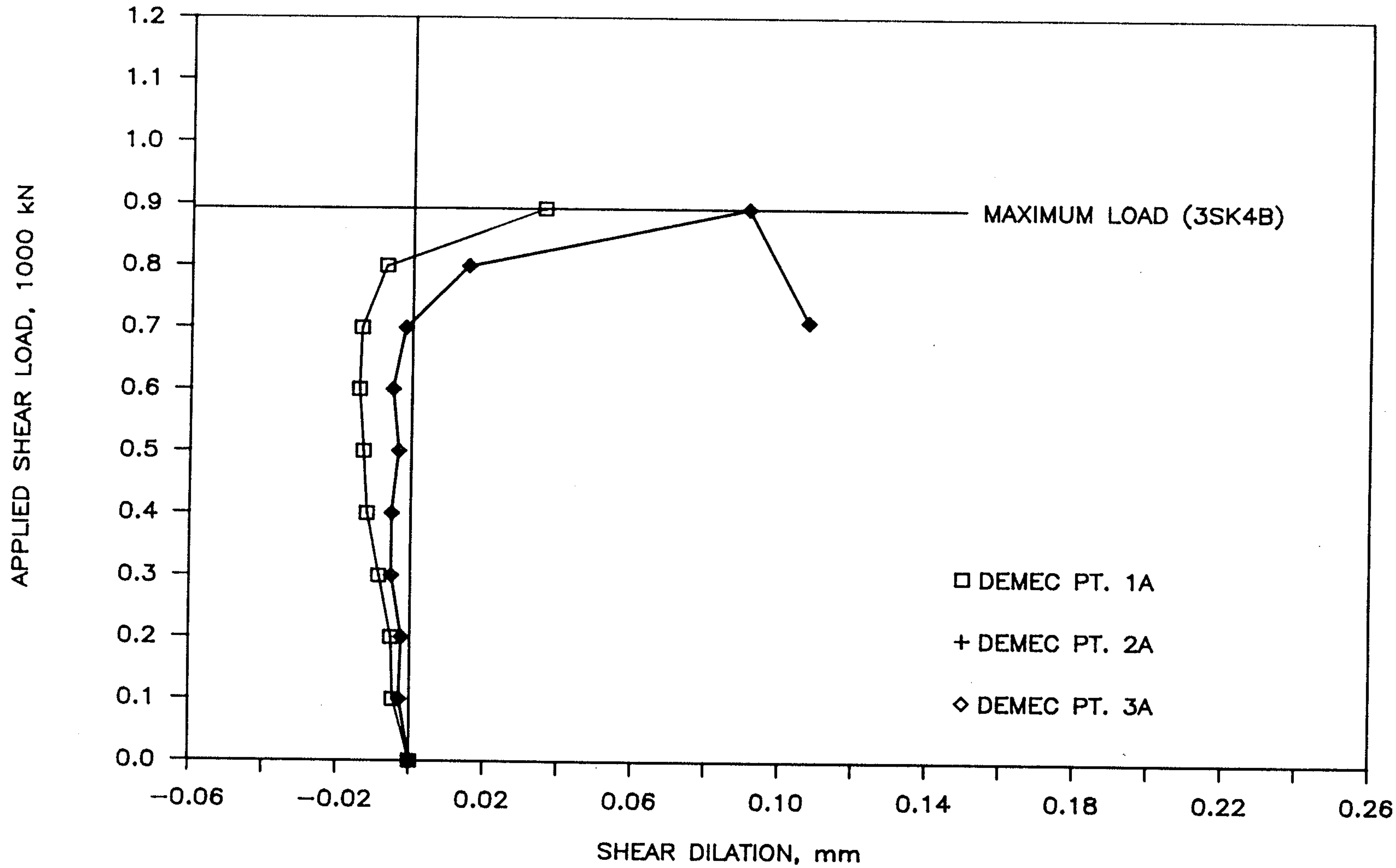

Figure 5.42 Applied Shear Load-Dilation Relationship for Specimen 3SK4B

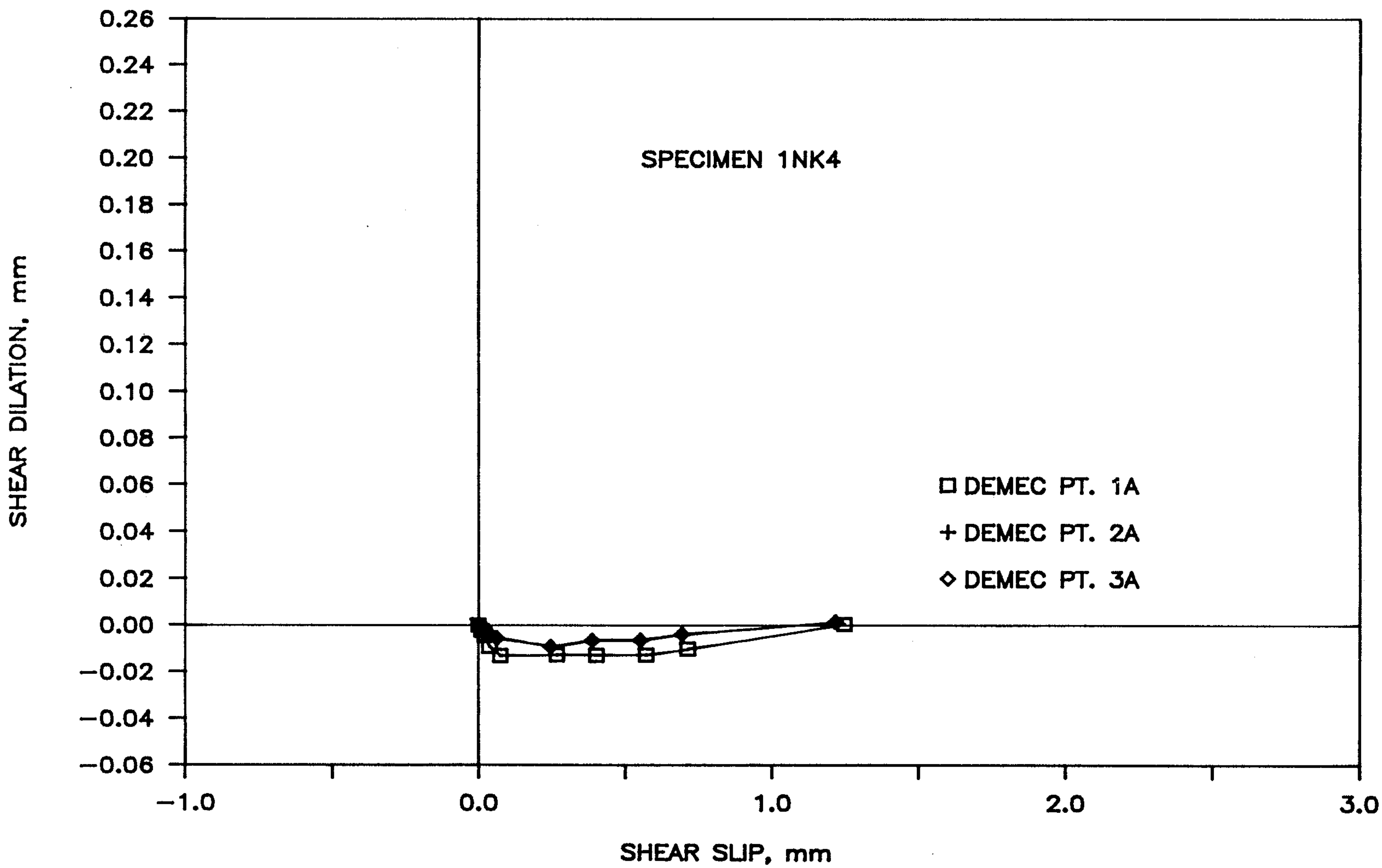

Figure 5.43 Dilation-Slip Relationship for Specimen 1NK4

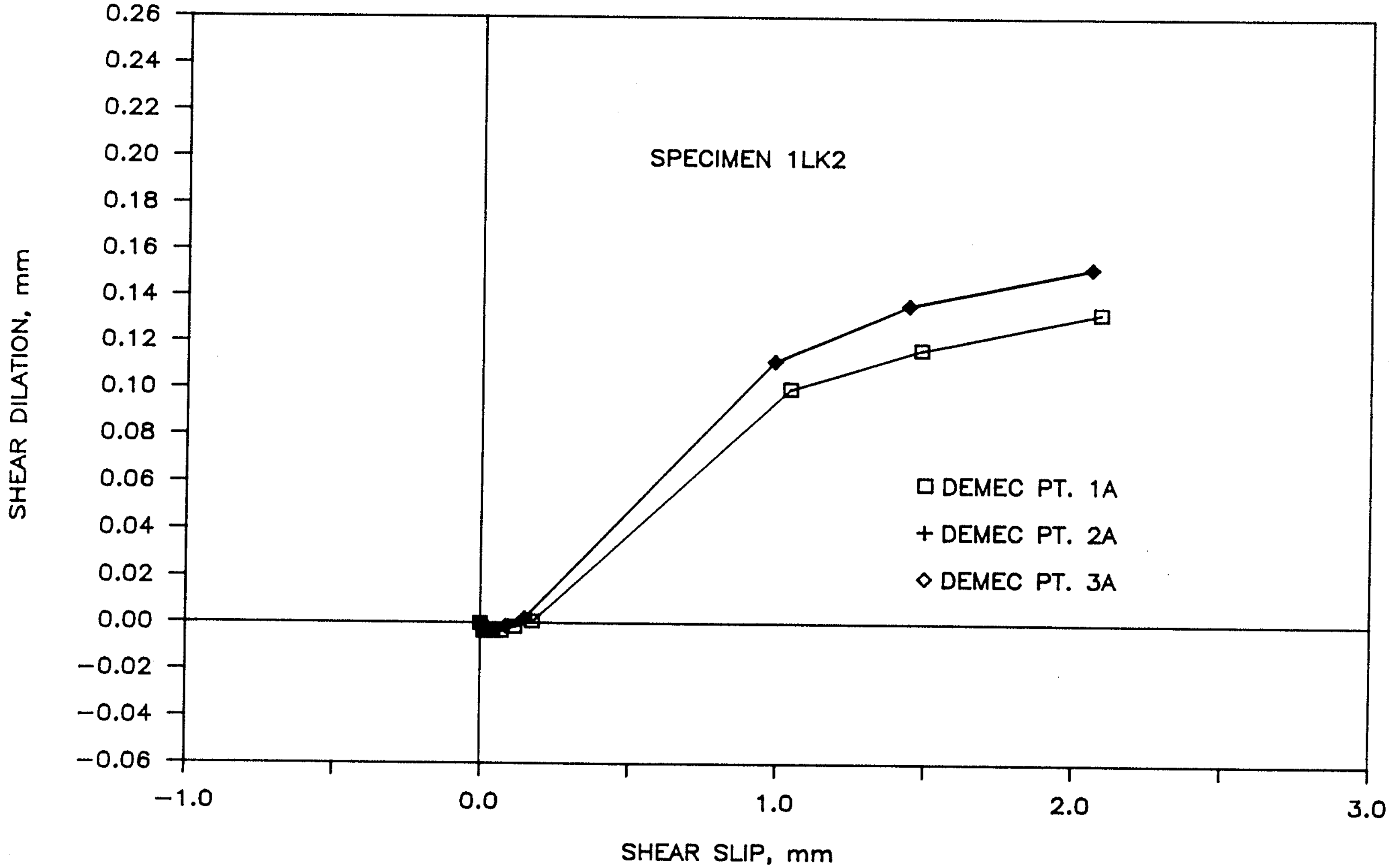

Figure 5.44 Dilation-Slip Relationship for Specimen 1LK2

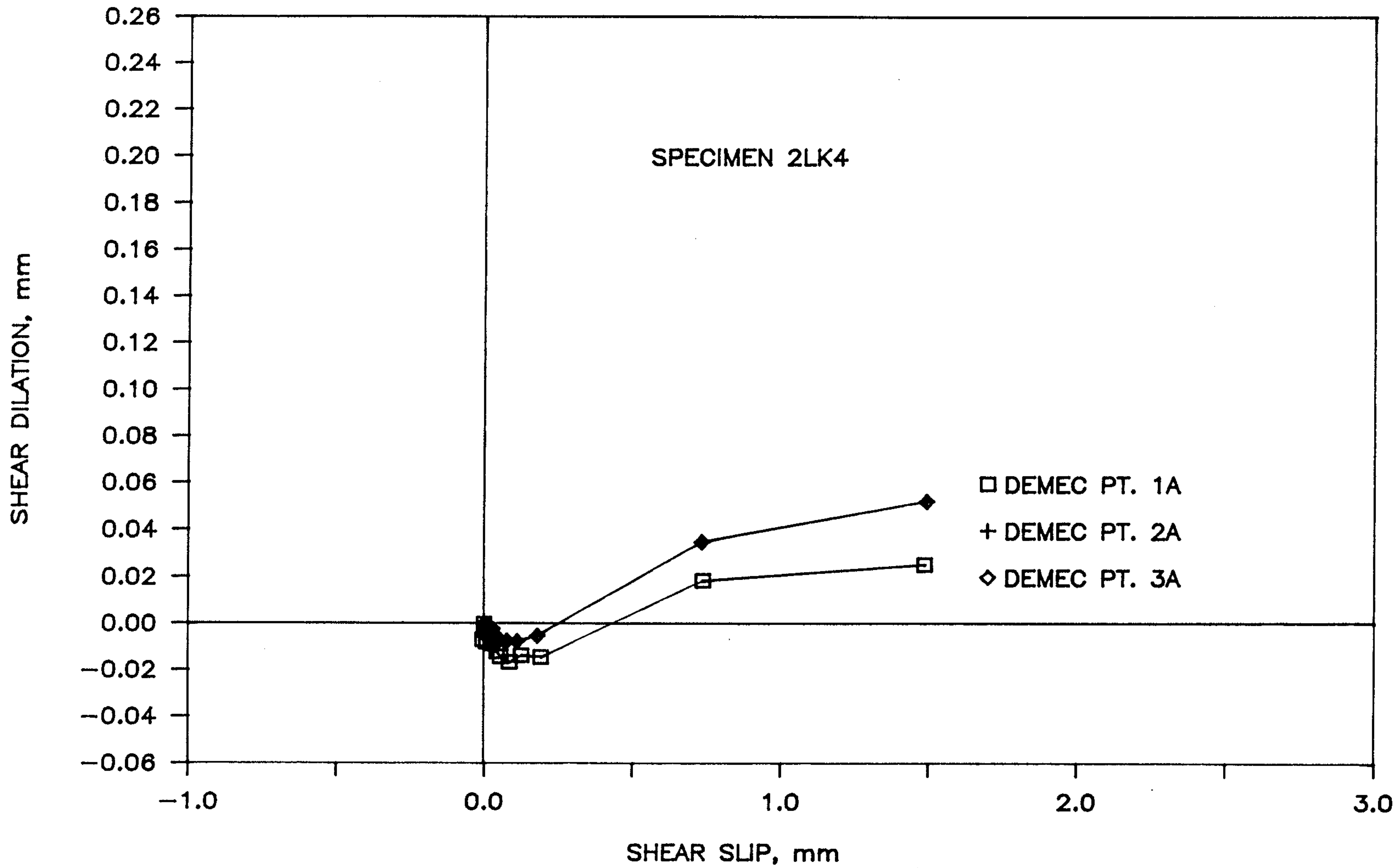

Figure 5.45 Dilation-Slip Relationship for Specimen 2LK4

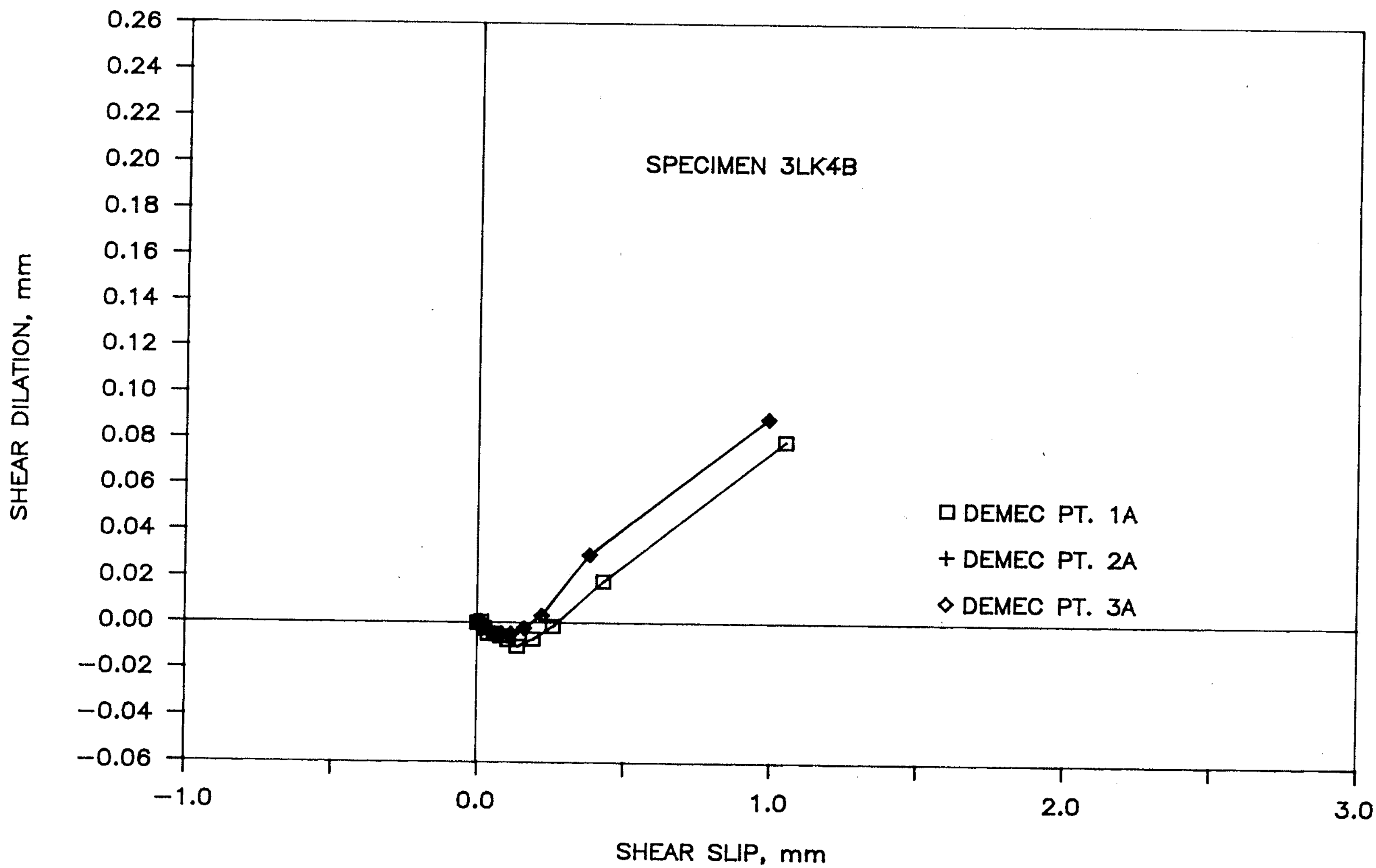

Figure 5.46 Dilation-Slip Relationship for Specimen 3LK4B

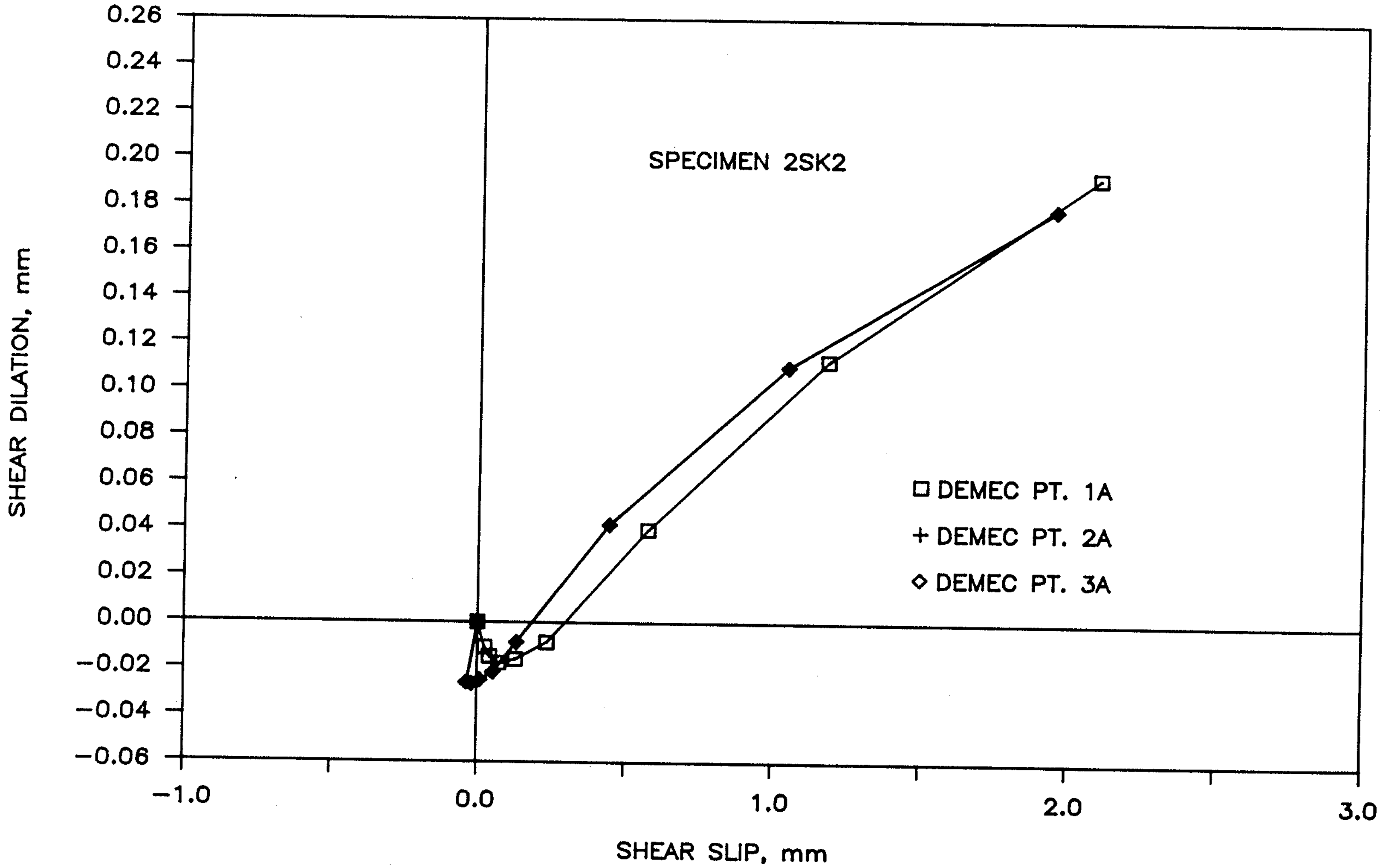

Figure 5.47 Dilation-Slip Relationship for Specimen 2SK2

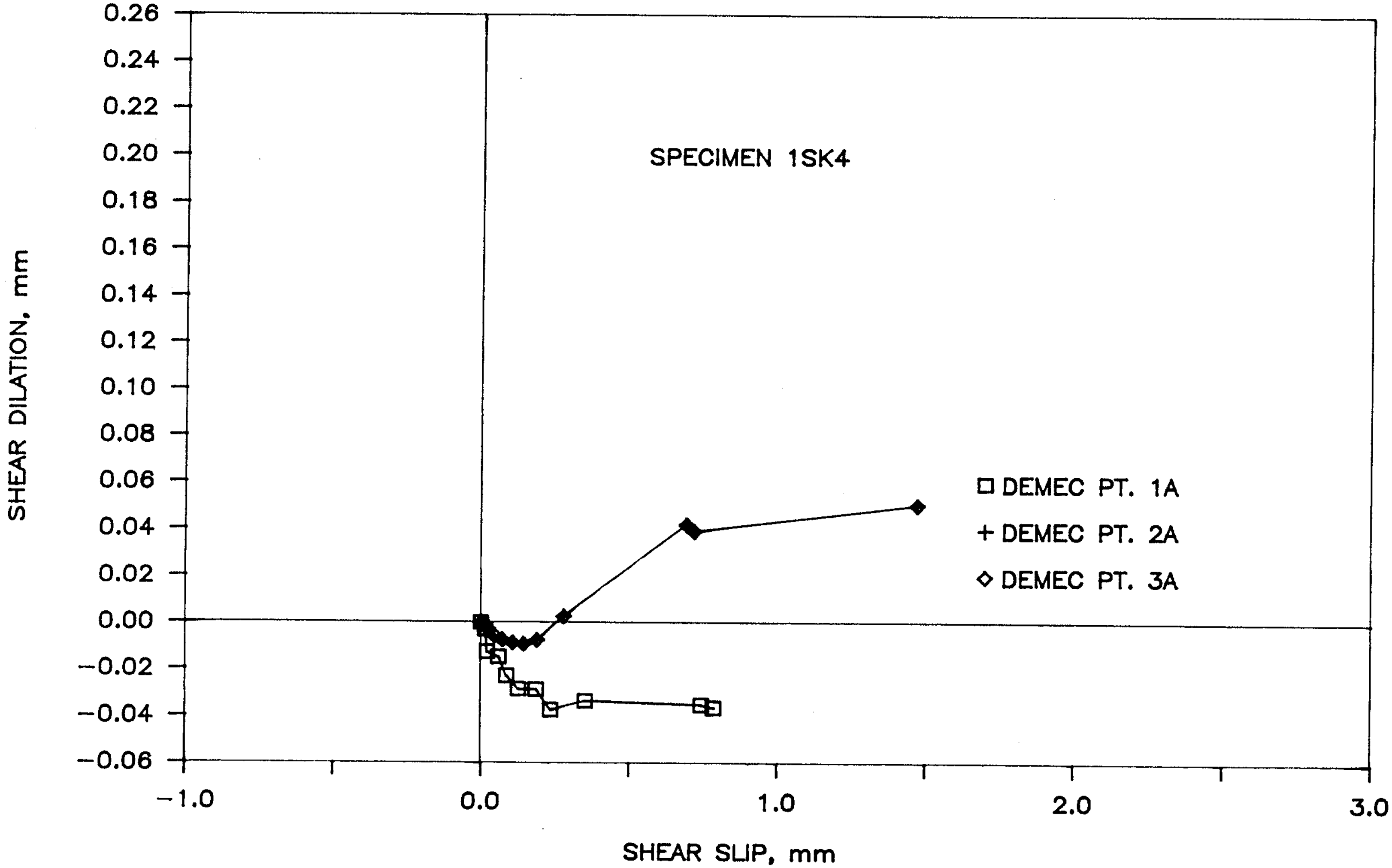

Figure 5.48 Dilation-Slip Relationship for Specimen 1SK4

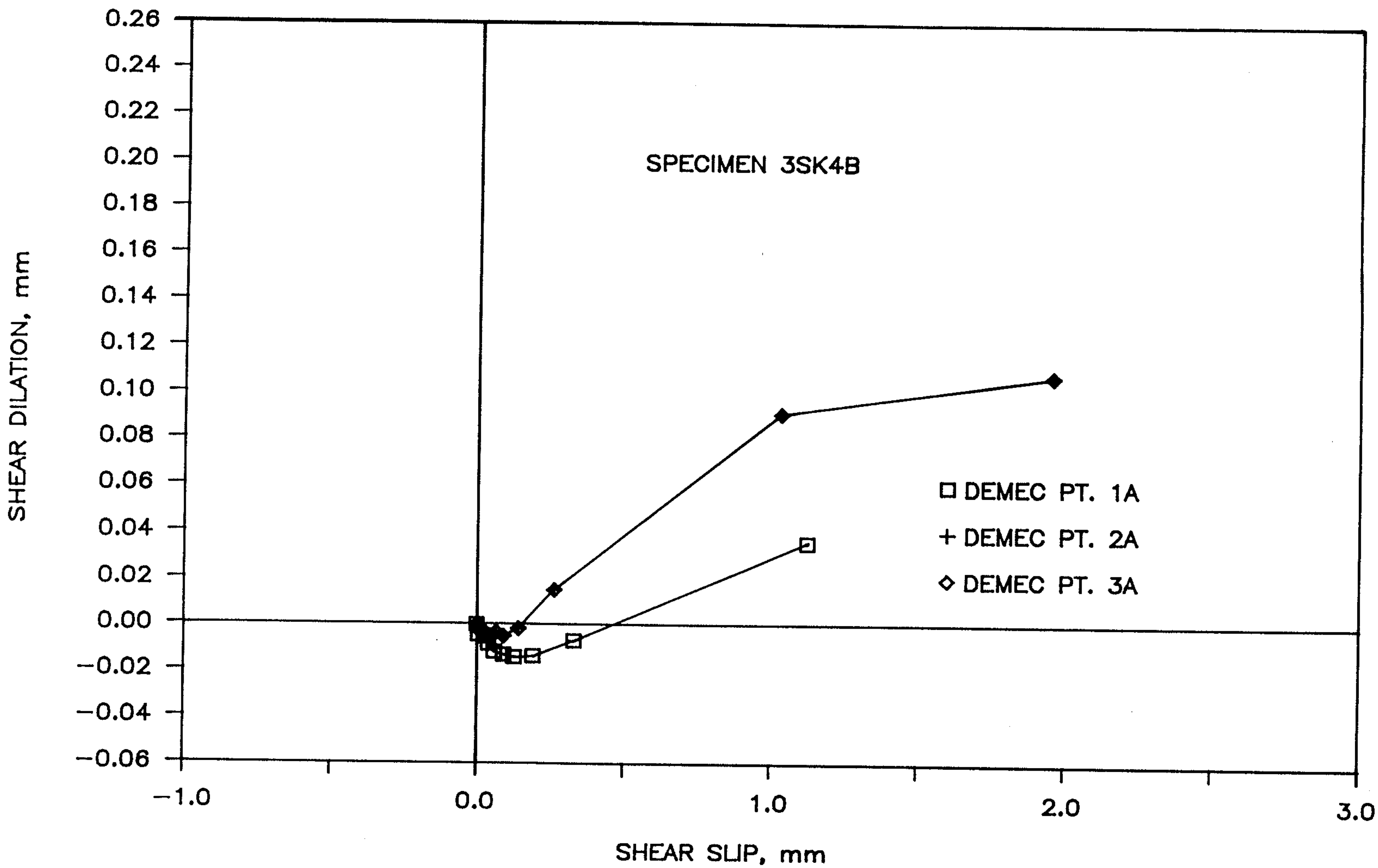

Figure 5.49 Dilation-Slip Relationship for Specimen 3SK4B

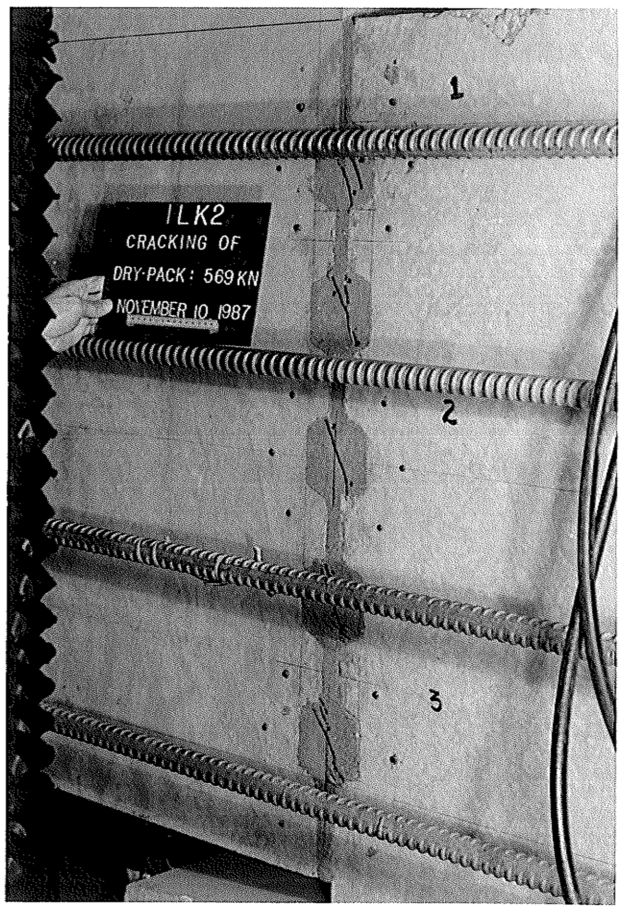

Figure 5.50   Crack Pattern at Maximum Load for Specimen 1LK2

Figure 5.51 Crack Pattern at Maximum Load for Specimen 2LK4

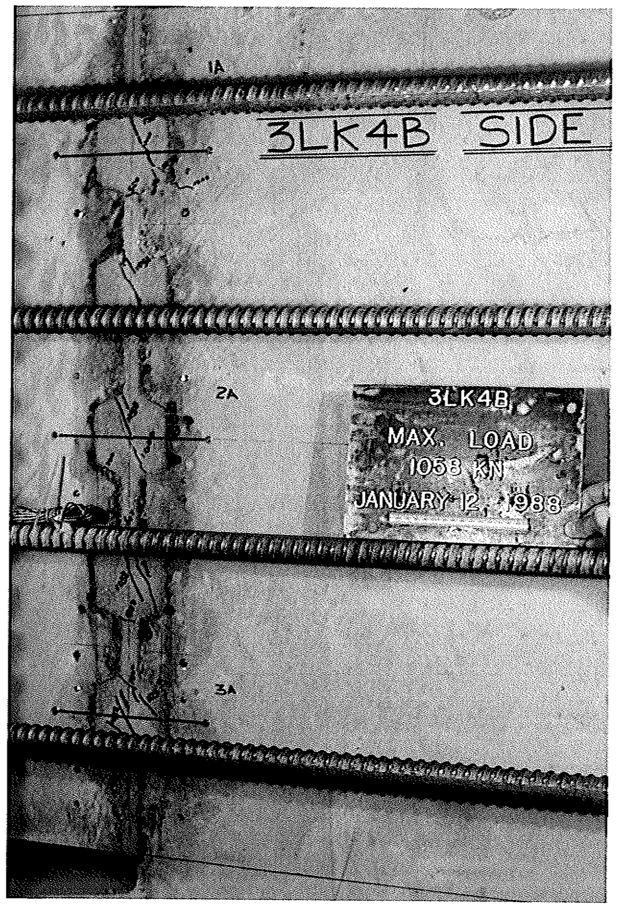

Figure 5.52 Crack Pattern at Maximum Load for Specimen 3LK4B

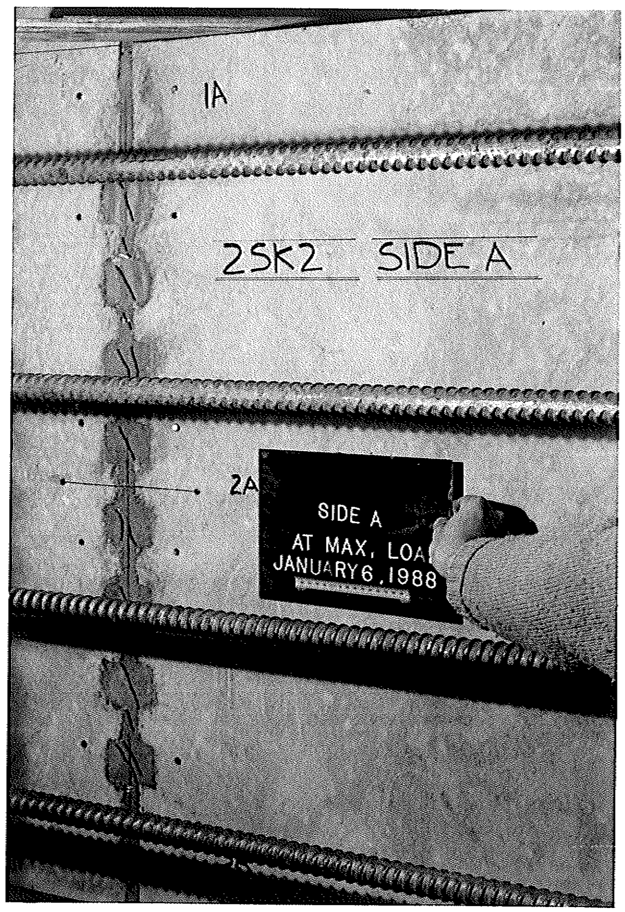

Figure 5.53 Crack Pattern at Maximum Load for Specimen 2SK2

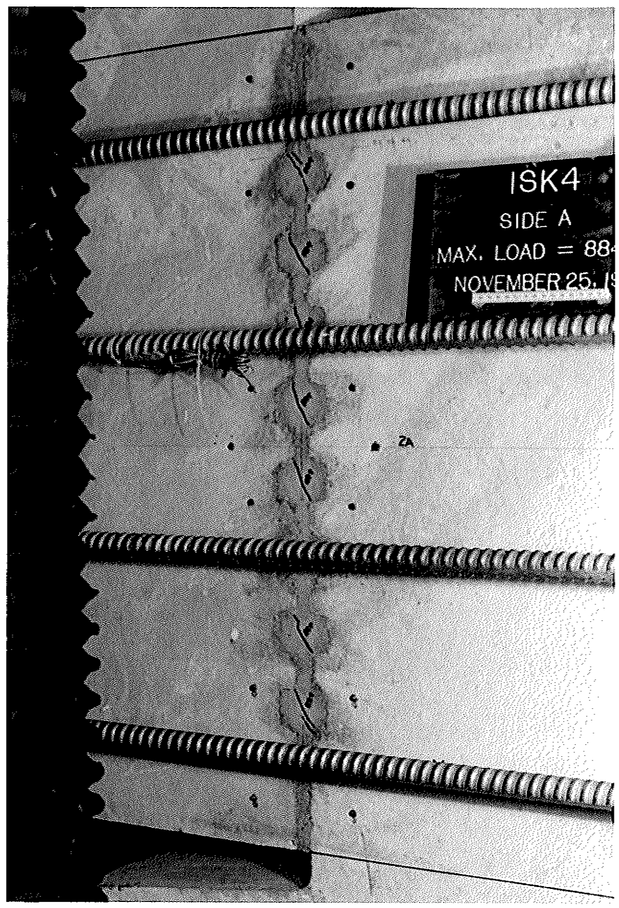

Figure 5.54 Crack Pattern at Maximum Load for Specimen 1SK4

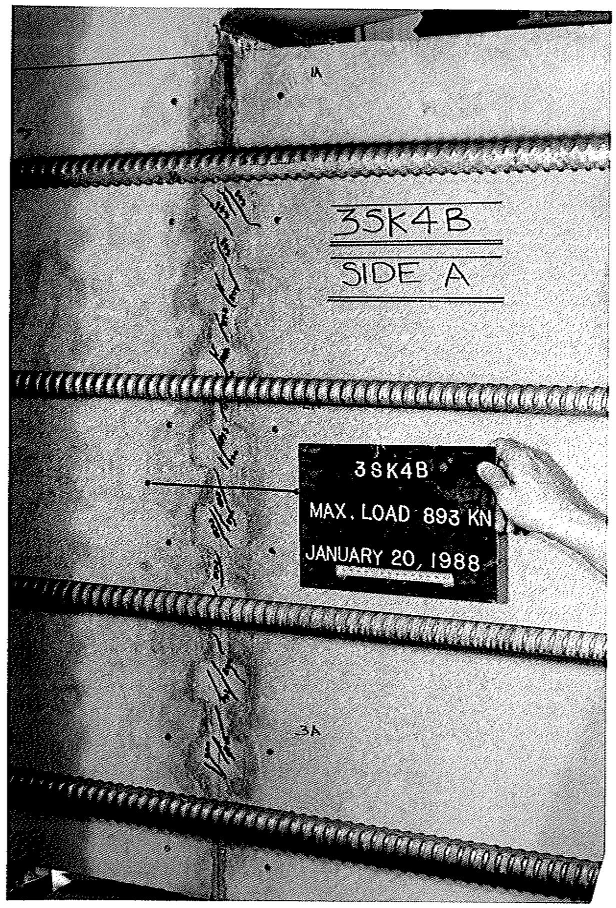

Figure 5.55 Crack Pattern at Maximum Load for Specimen 3SK4B

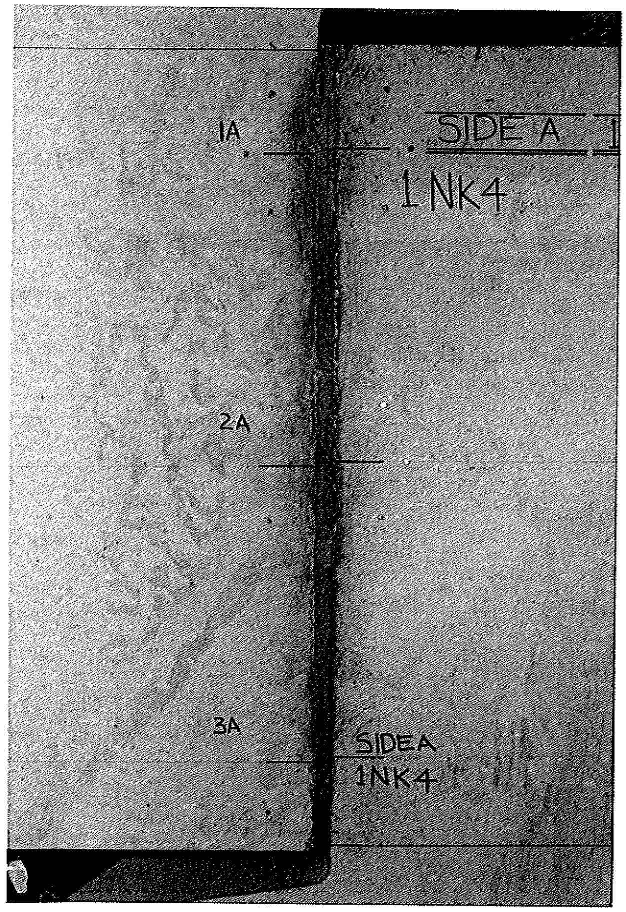

Figure 5.56 Crack Pattern at Ultimate Load for Specimen 1NK4

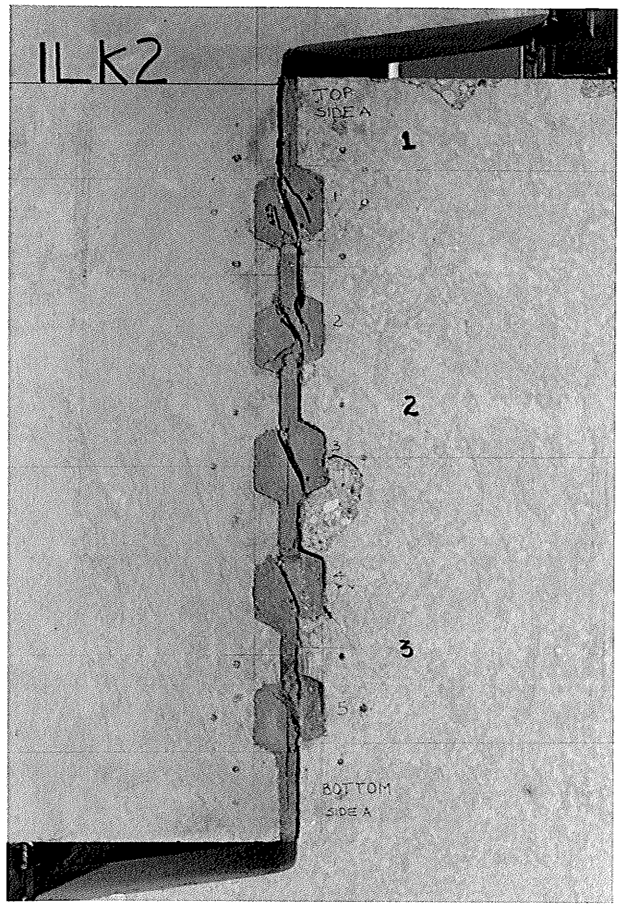

Figure 5.57 Crack Pattern at Ultimate Load for Specimen 1LK2

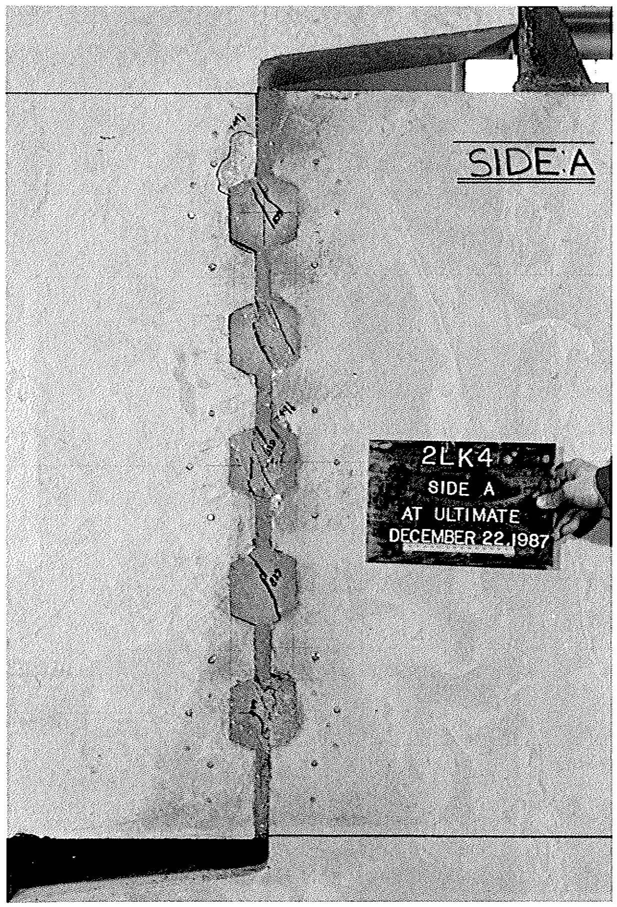

Figure 5.58   Crack Pattern at Ultimate Load for Specimen 2LK4

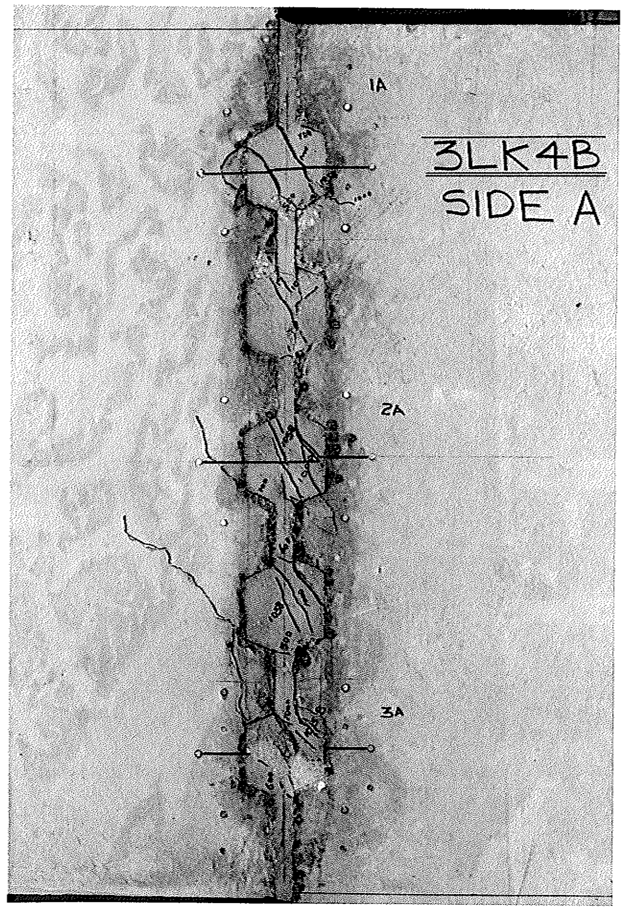

Figure 5.59 Crack Pattern at Ultimate Load for Specimen 3LK4B

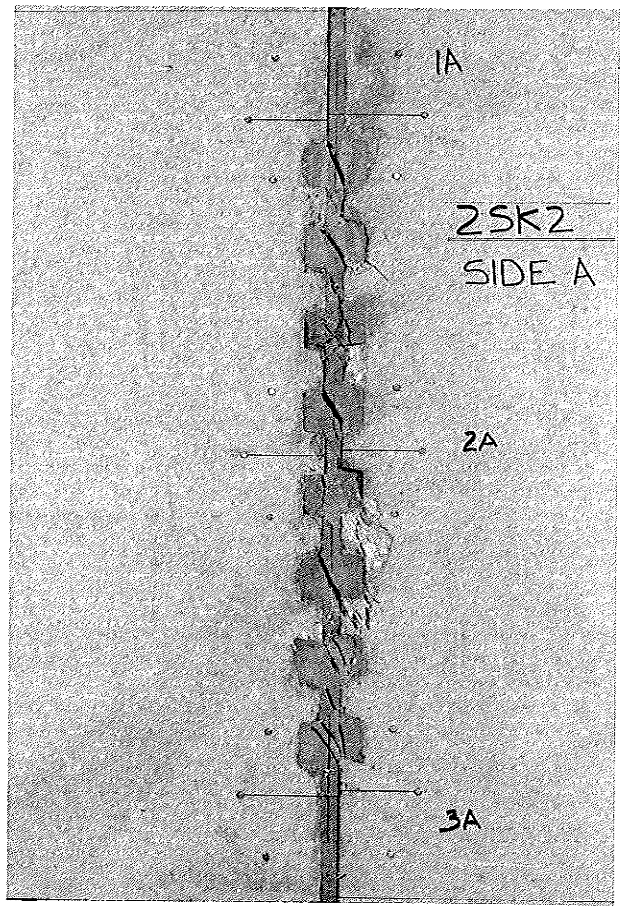

Figure 5.60 Crack Pattern at Ultimate Load for Specimen 2SK2

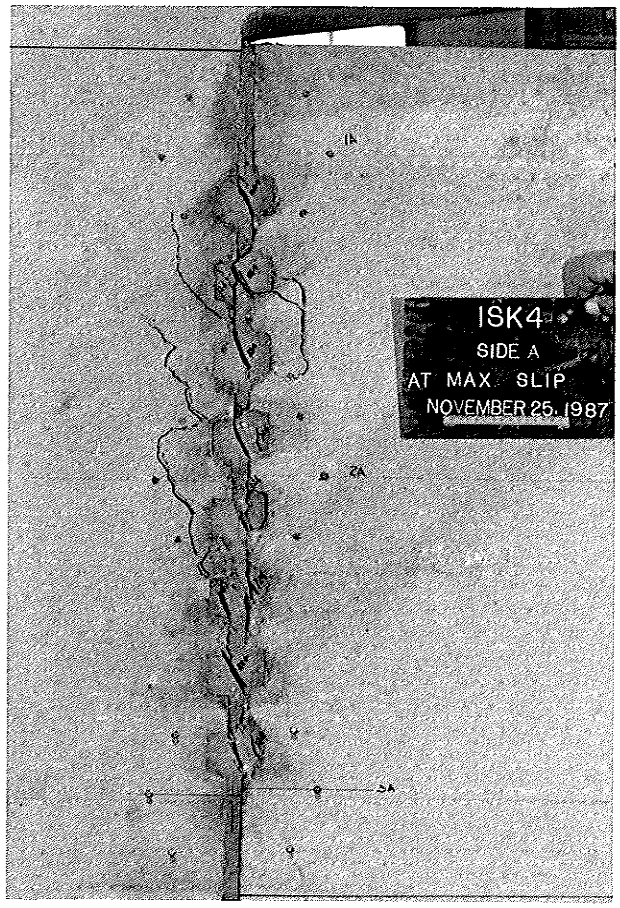

Figure 5.61 Crack Pattern at Ultimate Load for Specimen 1SK4

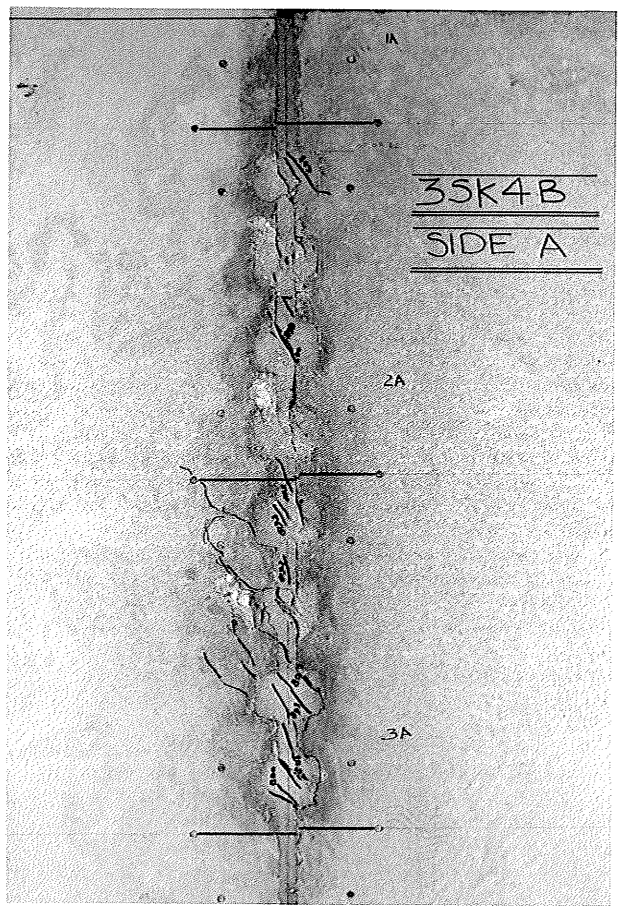

Figure 5.62 Crack Pattern at Ultimate Load for Specimen 3SK4B

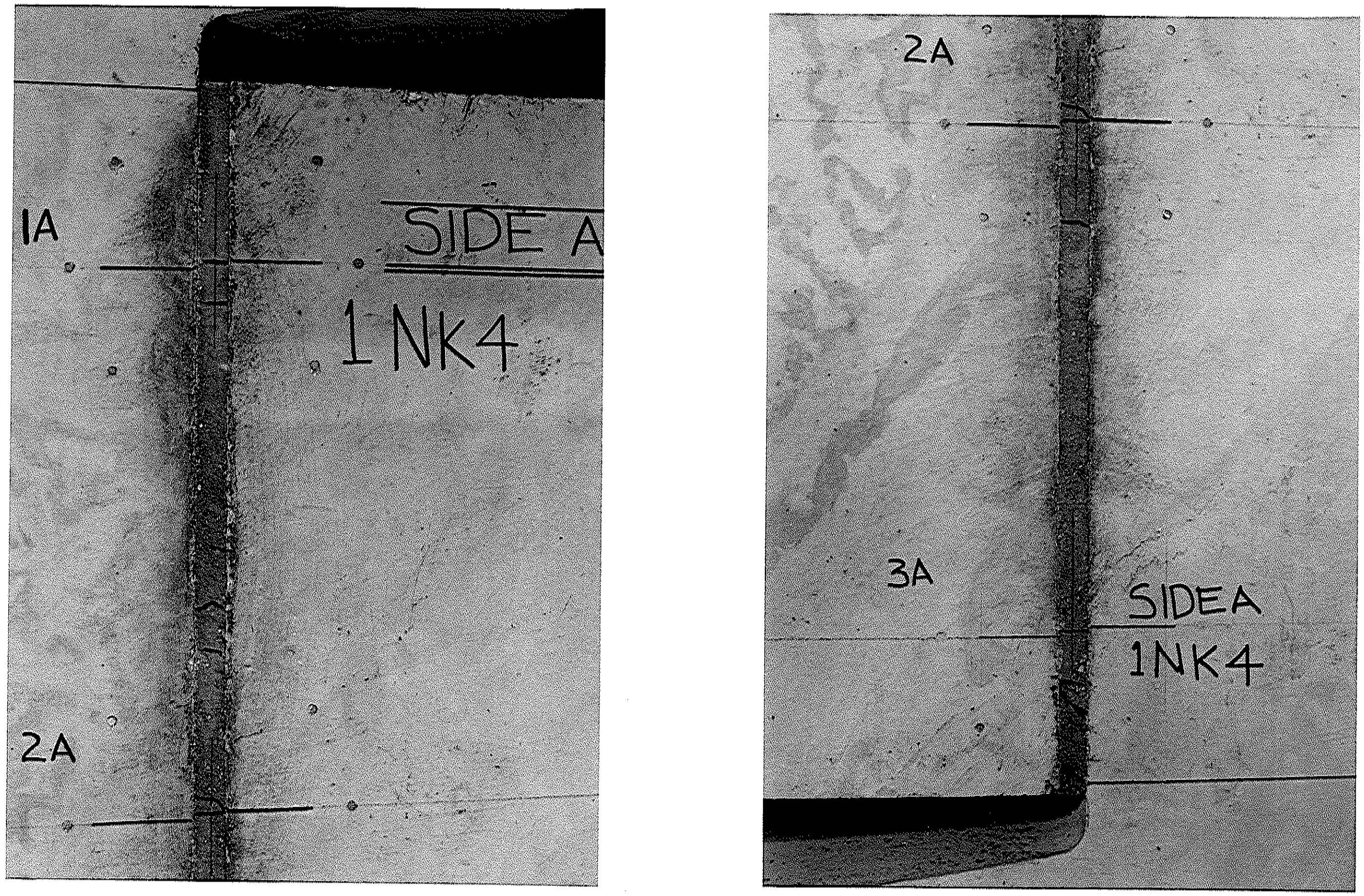

Figure 5.63 Magnification of Crack Pattern at Ultimate Load for Specimen 1NK4

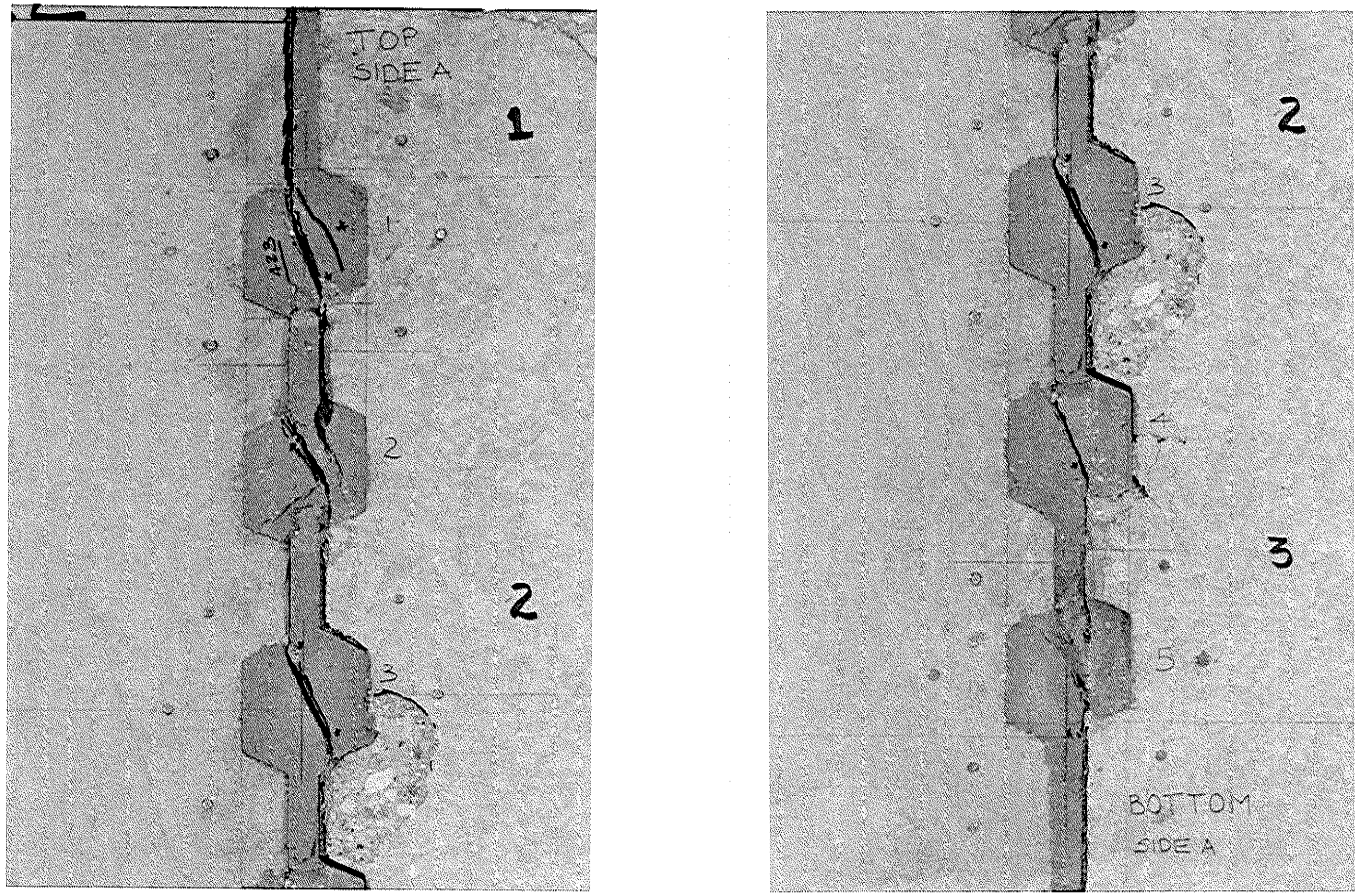

Figure 5.64 Magnification of Crack Pattern at Ultimate Load for Specimen 1LK2

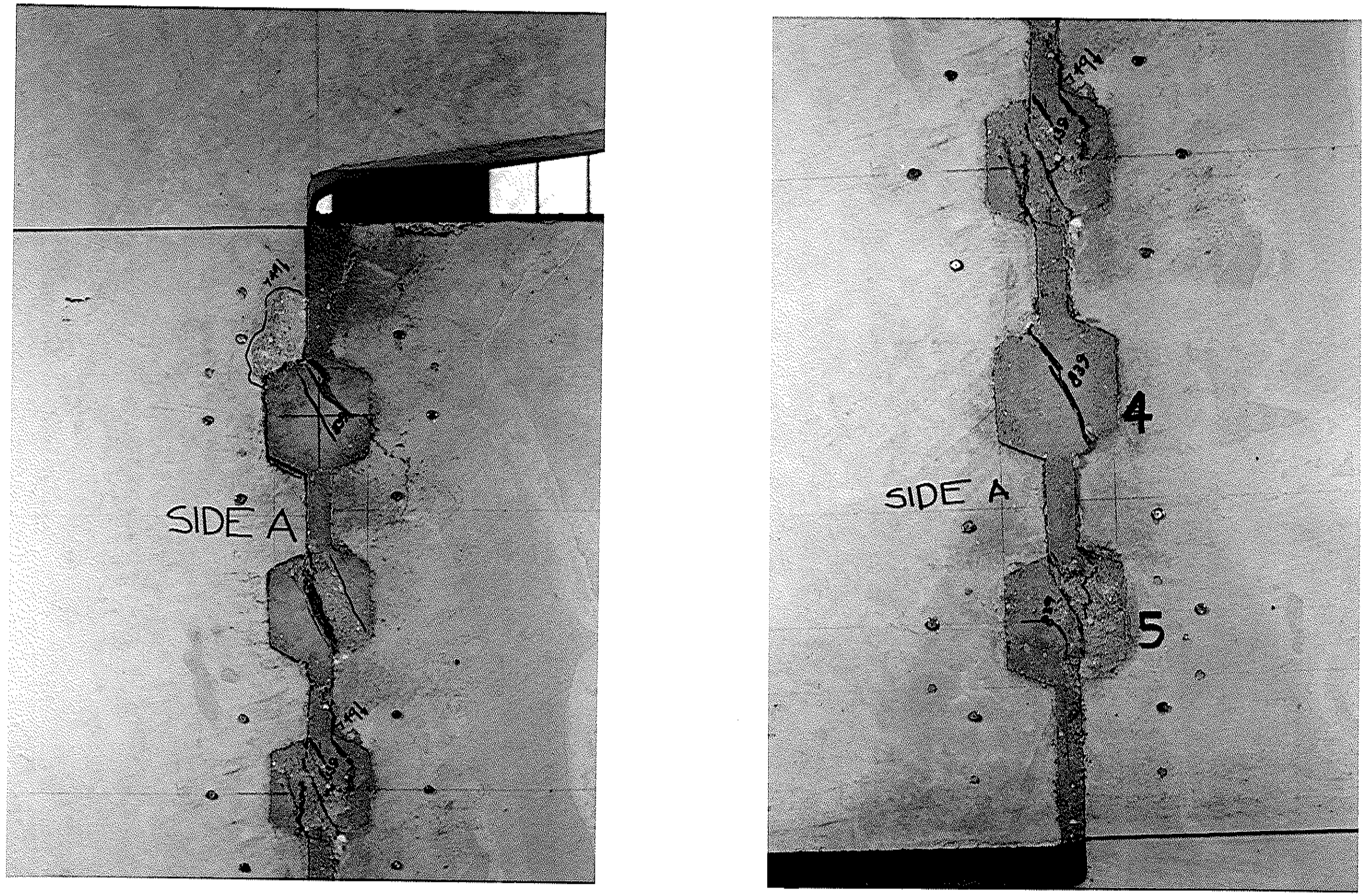

Figure 5.65 Magnification of Crack Pattern at Ultimate Load for Specimen 2LK4

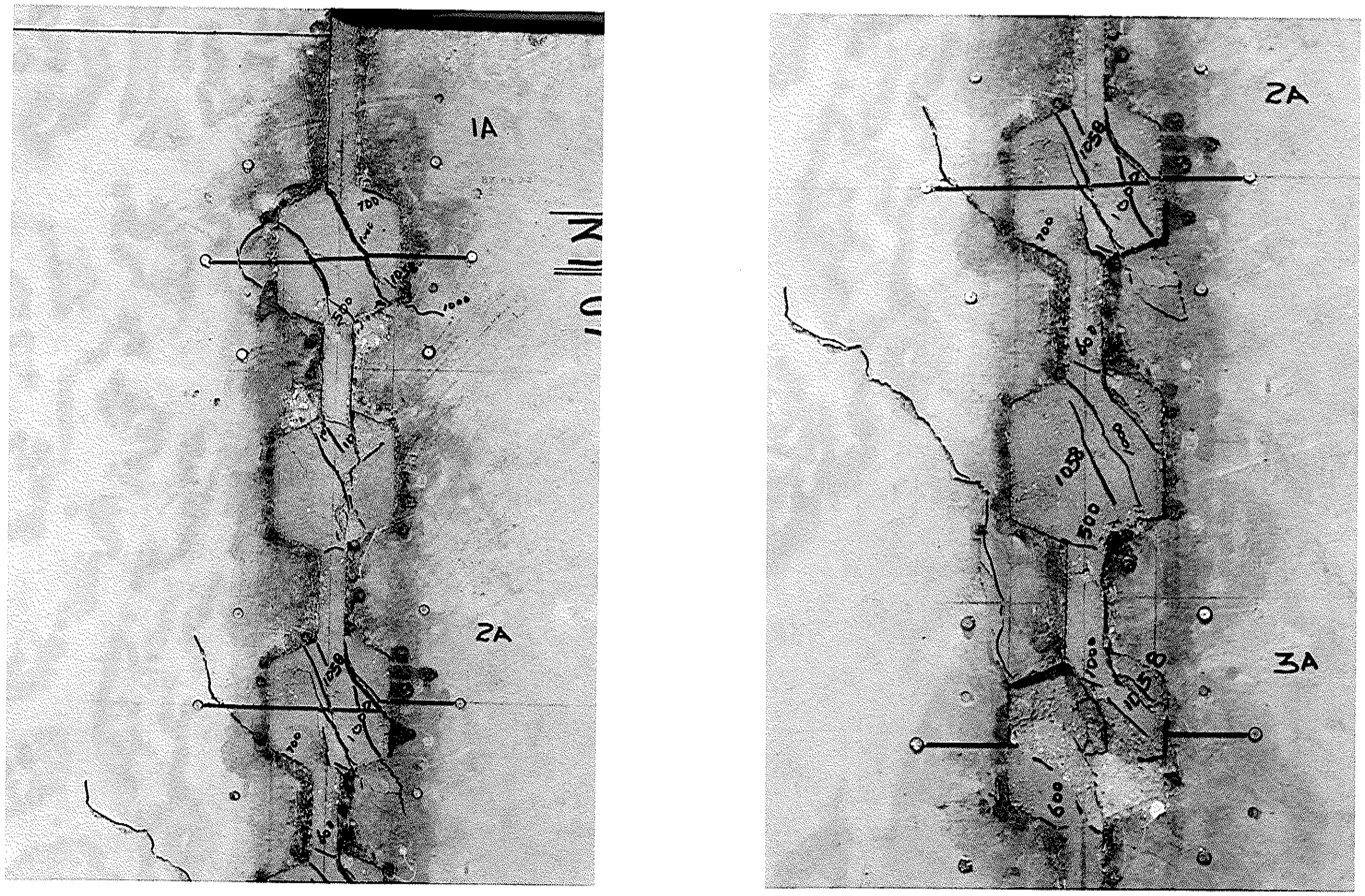

Figure 5.66 Magnification of Crack Pattern at Ultimate Load for Specimen 3LK4B

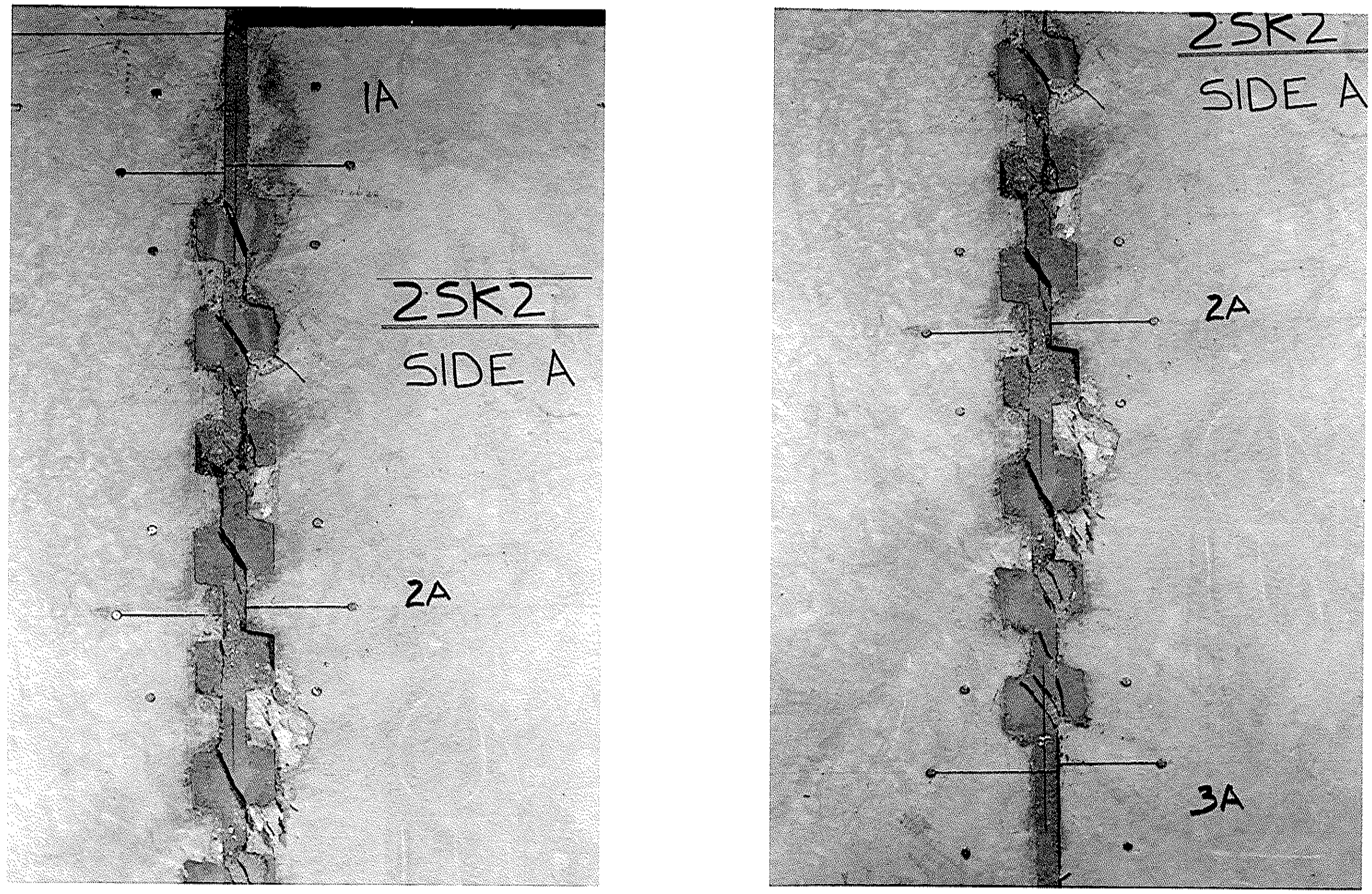

Figure 5.67 Magnification of Crack Pattern at Ultimate Load for Specimen 2SK2

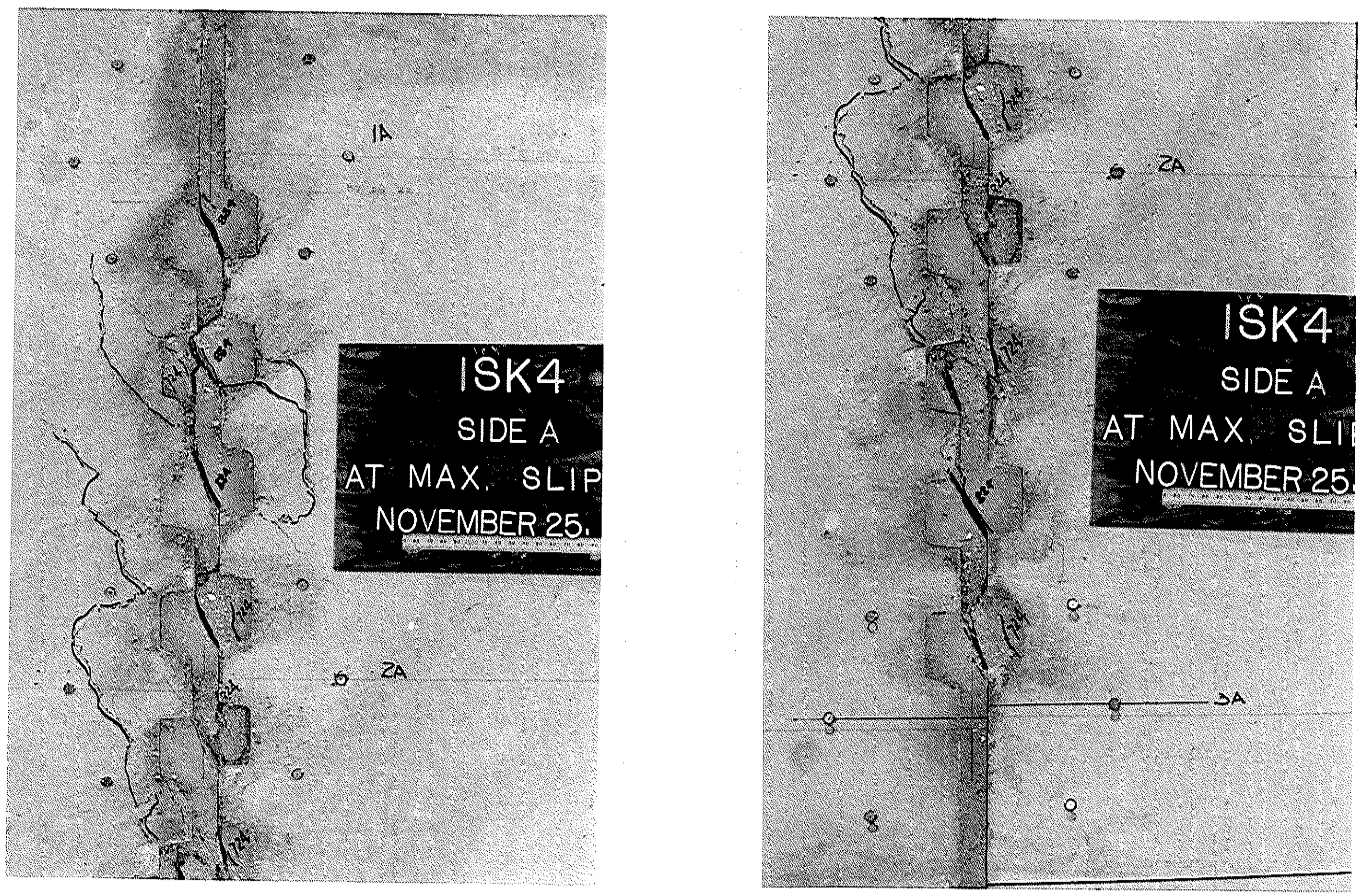

Figure 5.68 Magnification of Crack Pattern at Ultimate Load for Specimen 1SK4

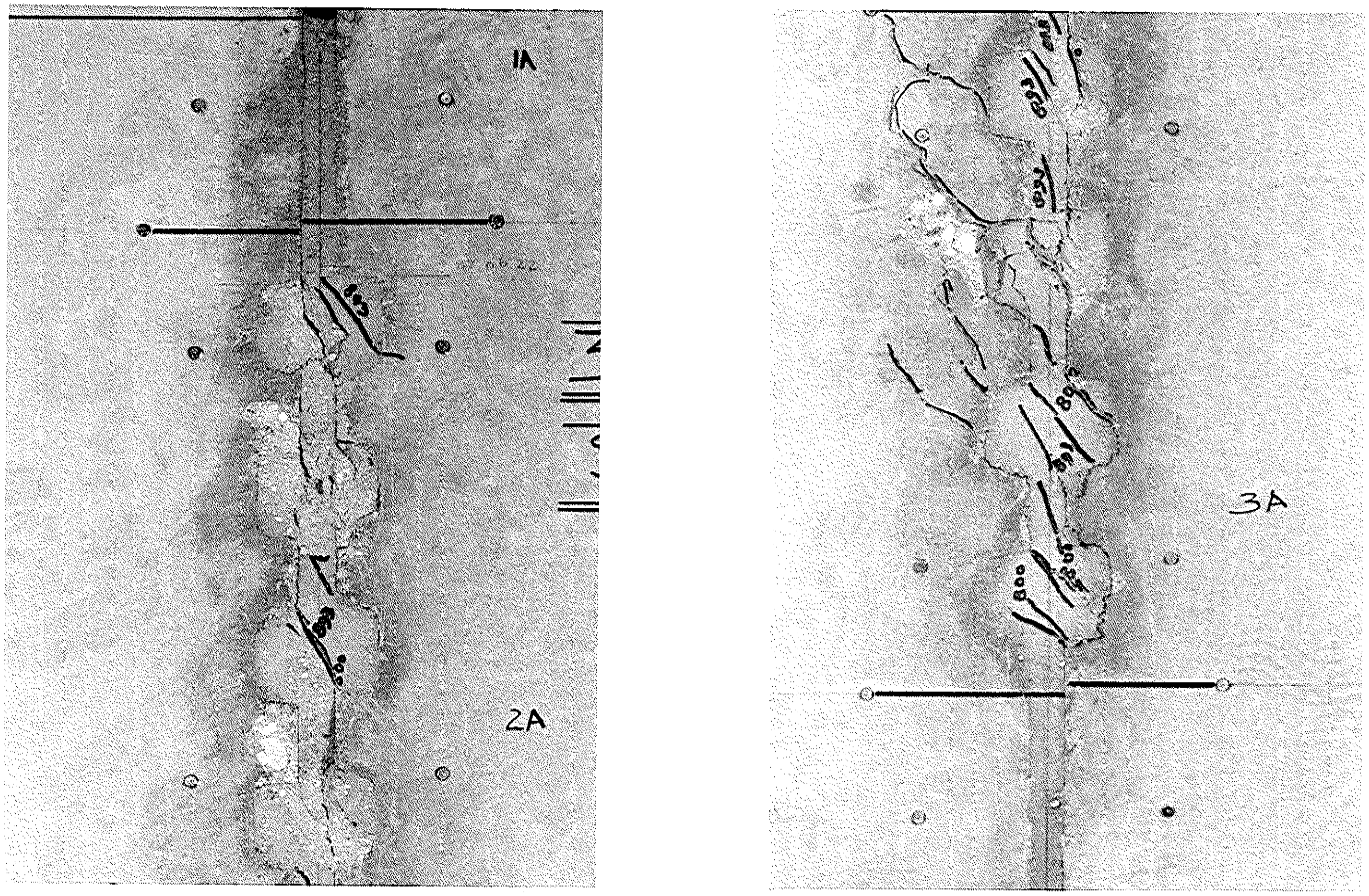

Figure 5.69 Magnification of Crack Pattern at Ultimate Load for Specimen 3SK4B

Figure 5.70 Specimen 1NK4 Taken Apart at Ultimate

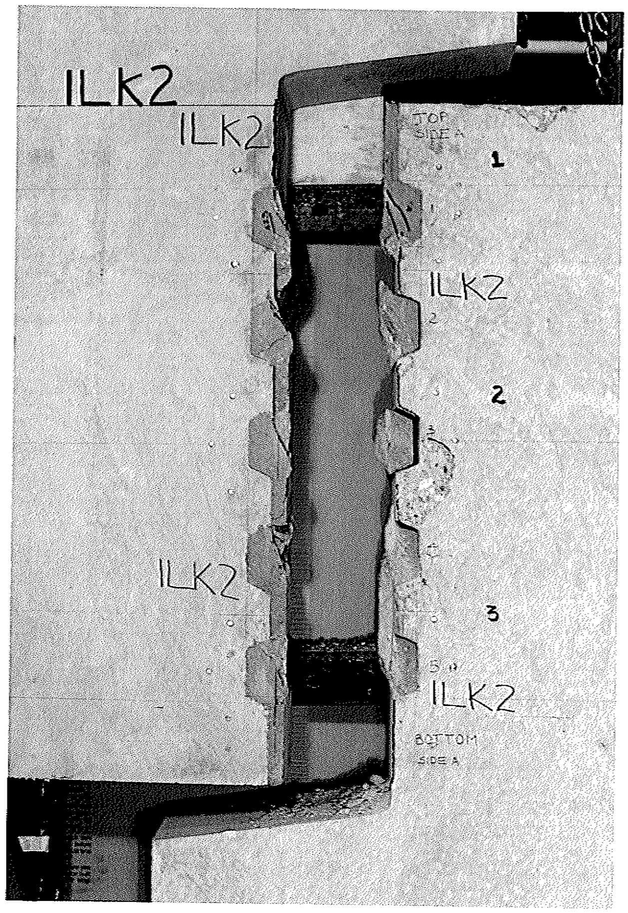

Figure 5.71 Specimen 1LK2 Taken Apart at Ultimate

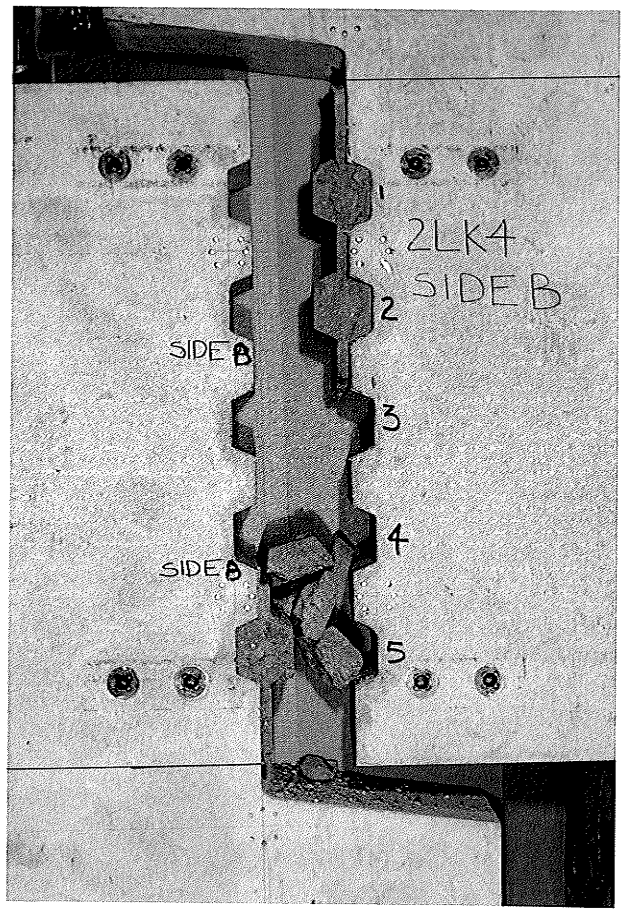

Figure 5.72 Specimen 2LK4 Taken Apart at Ultimate

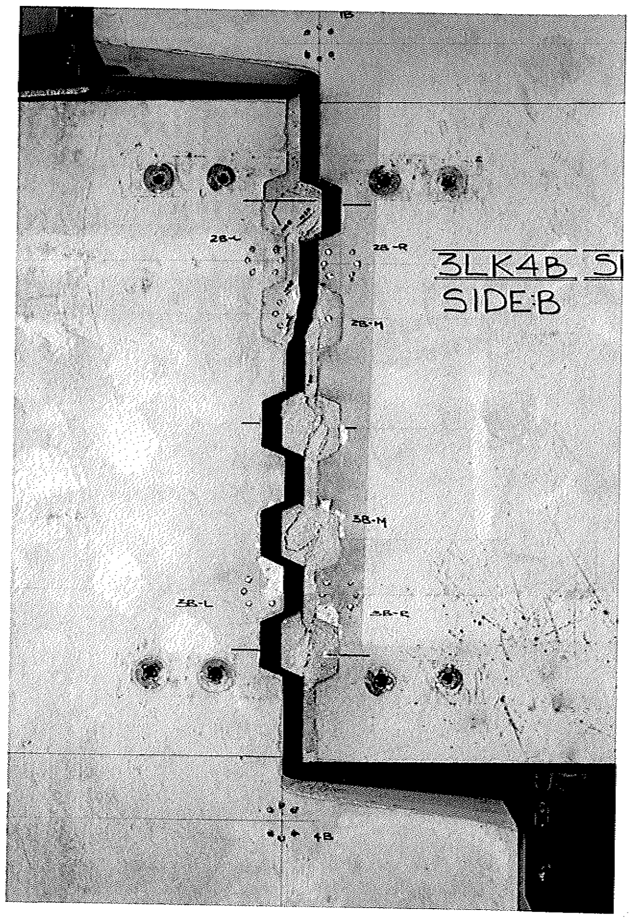

Figure 5.73 Specimen 3LK4B Taken Apart at Ultimate

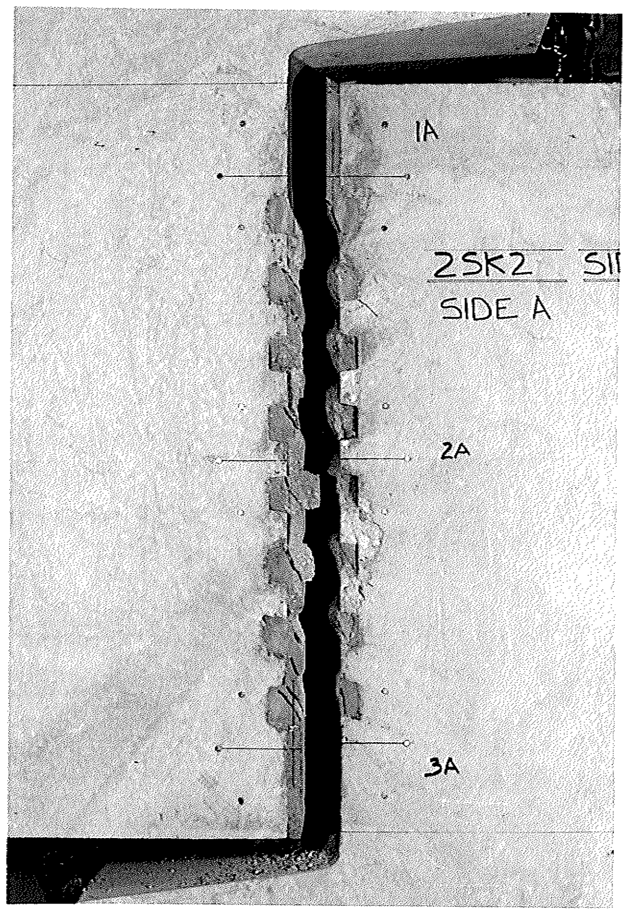

Figure 5.74 Specimen 2SK2 Taken Apart at Ultimate

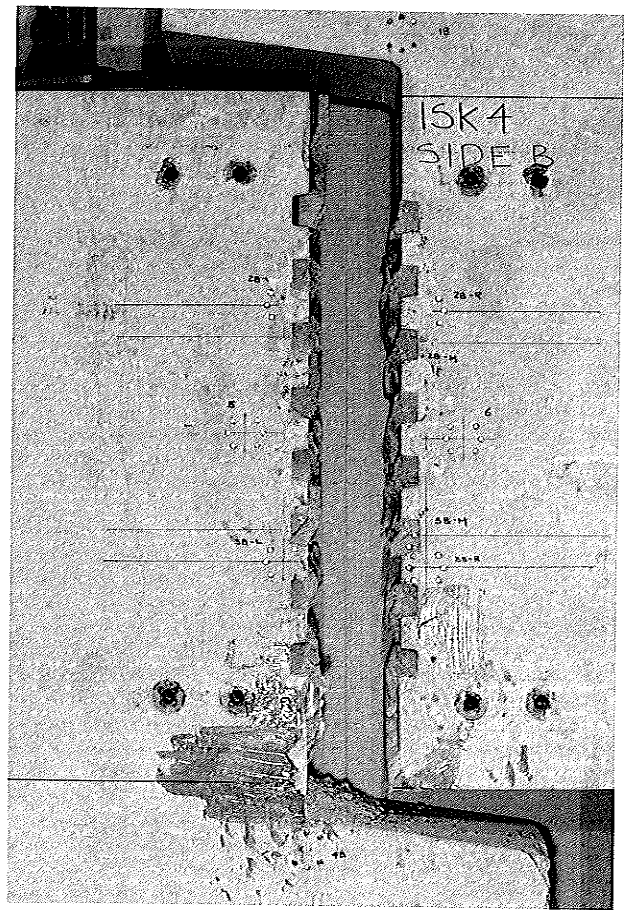

Figure 5.75 Specimen 1SK4 Taken Apart at Ultimate

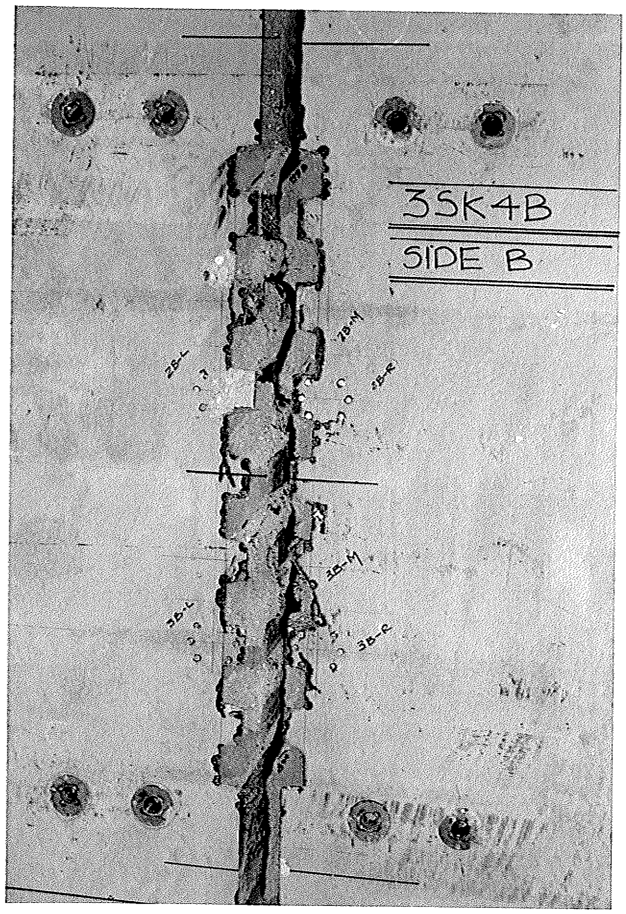

Figure 5.76 Specimen 3SK4B Taken Apart at Ultimate

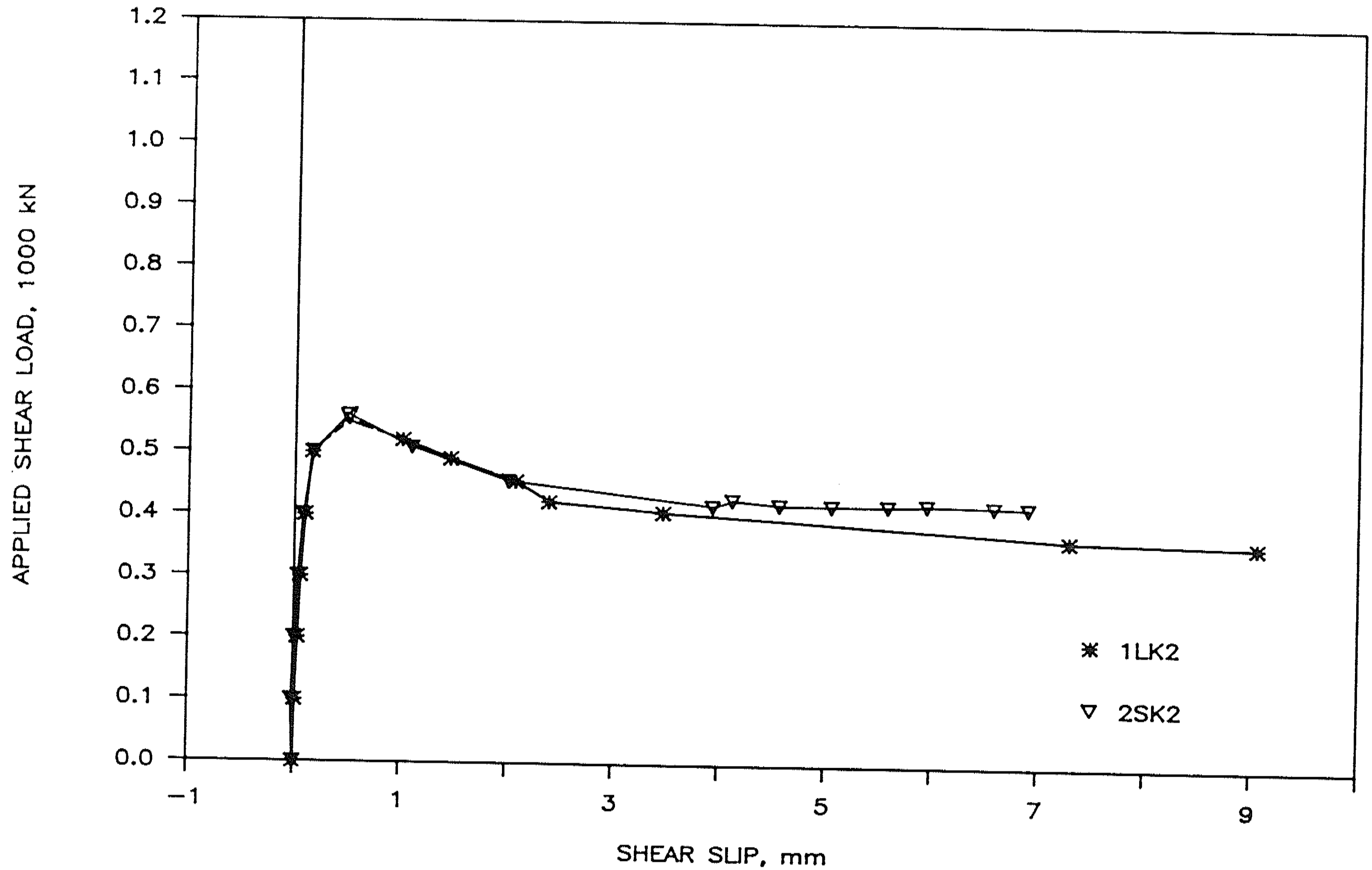

Figure 6.1 Comparison of the Applied Shear Load-Slip Relationship for Specimens 1LK2 and 2SK2

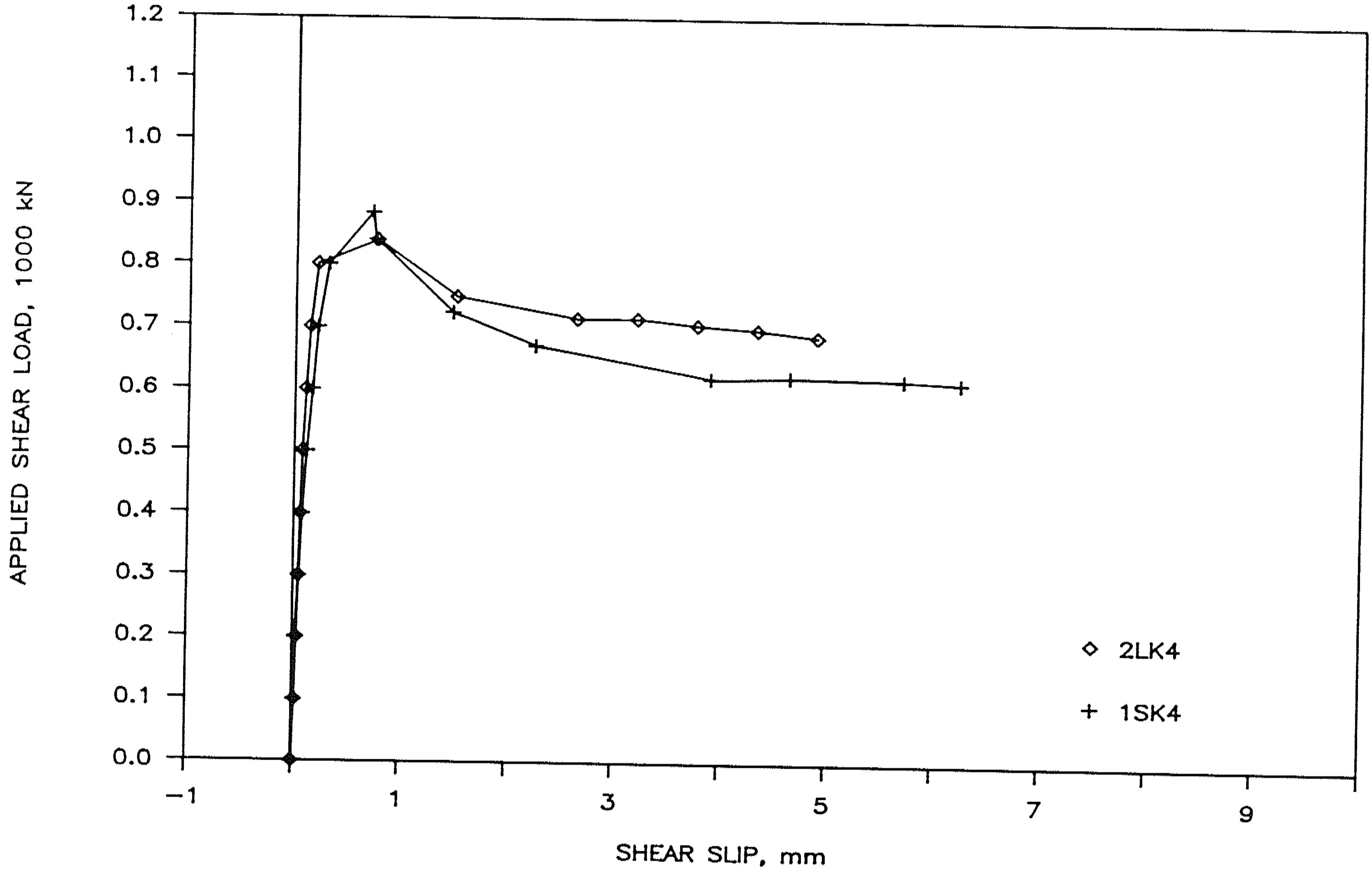

Figure 6.2 Comparison of the Applied Shear Load-Slip Relationship for Specimens 2LK4 and 1SK4

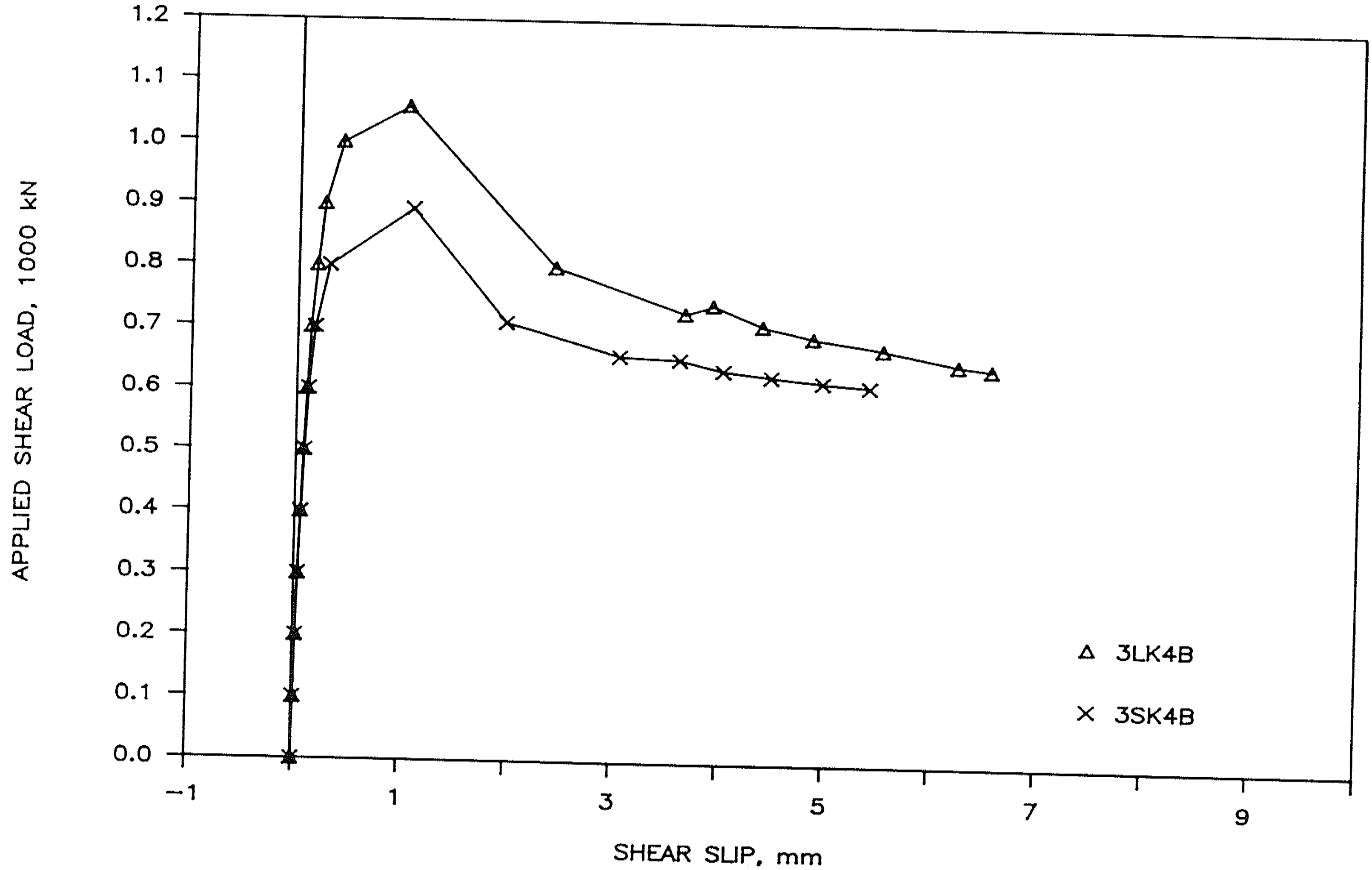

Figure 6.3 Comparison of the Applied Shear Load-Slip Relationship for Specimens 3LK4B and 3SK4B

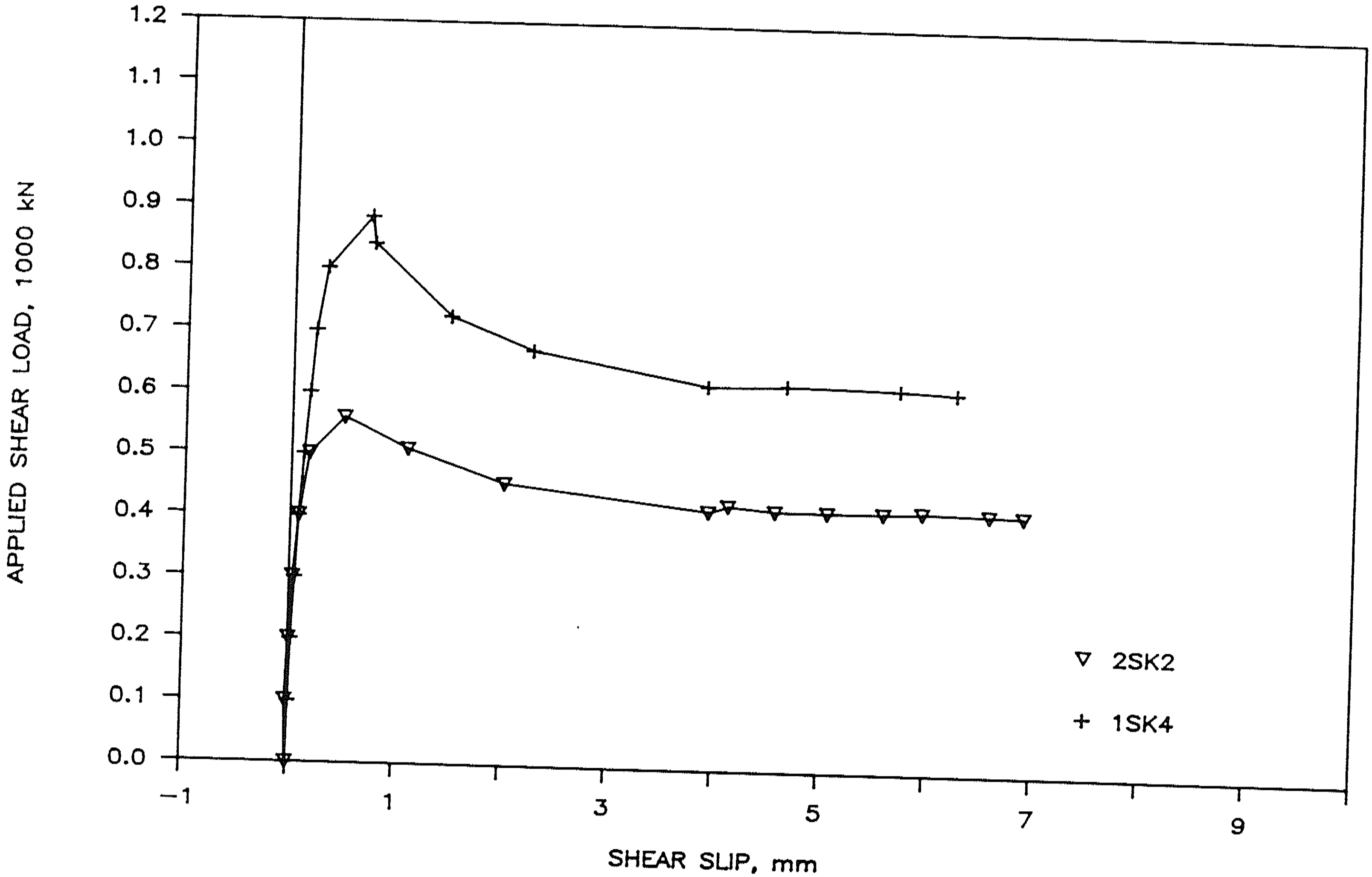

Figure 6.4 Effect of Preload on the Behaviour of the Small Multiple Shear Key Connection

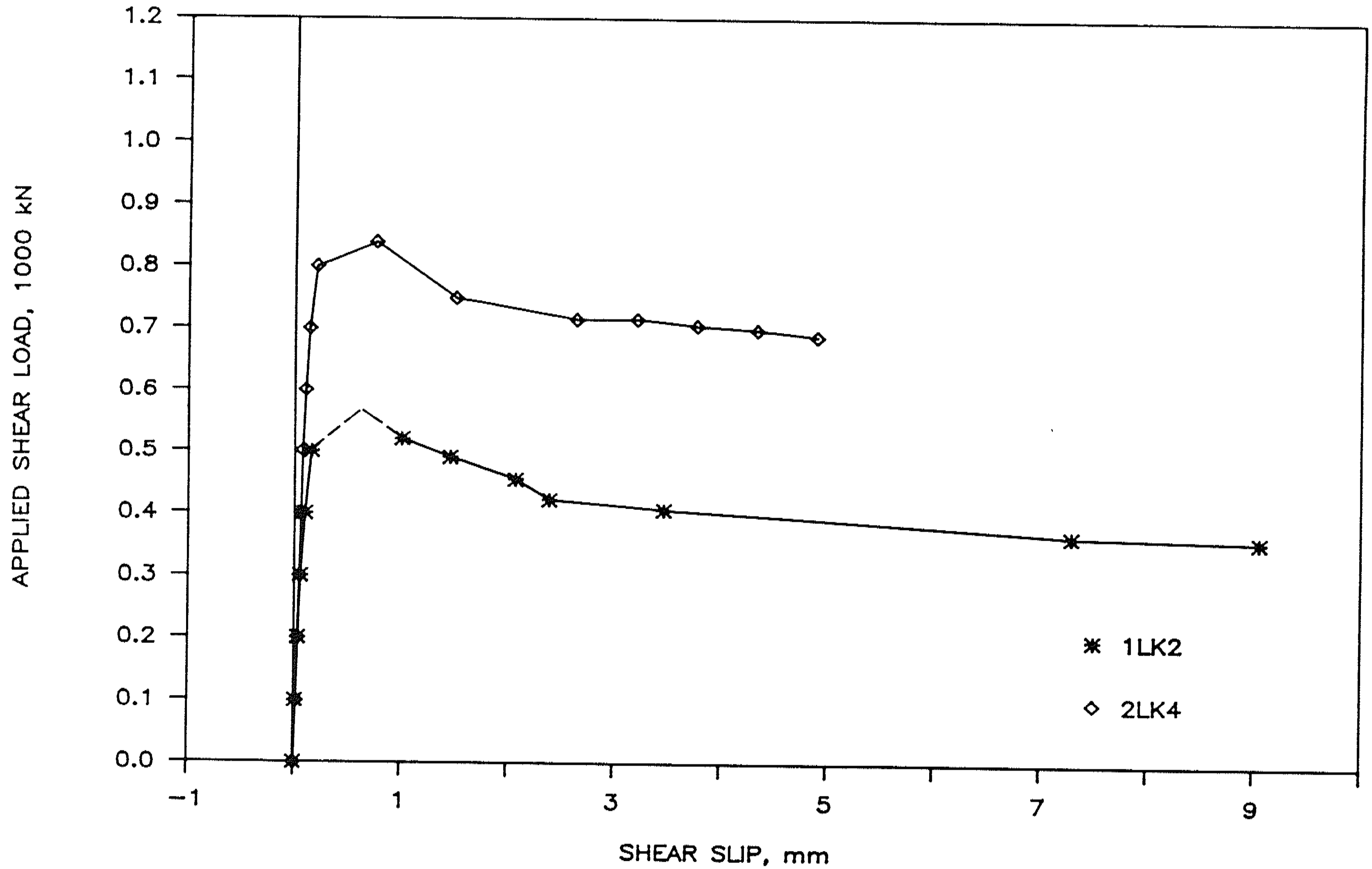

Figure 6.5 Effect of Preload on the Behaviour of the Large Multiple Shear Key Connection

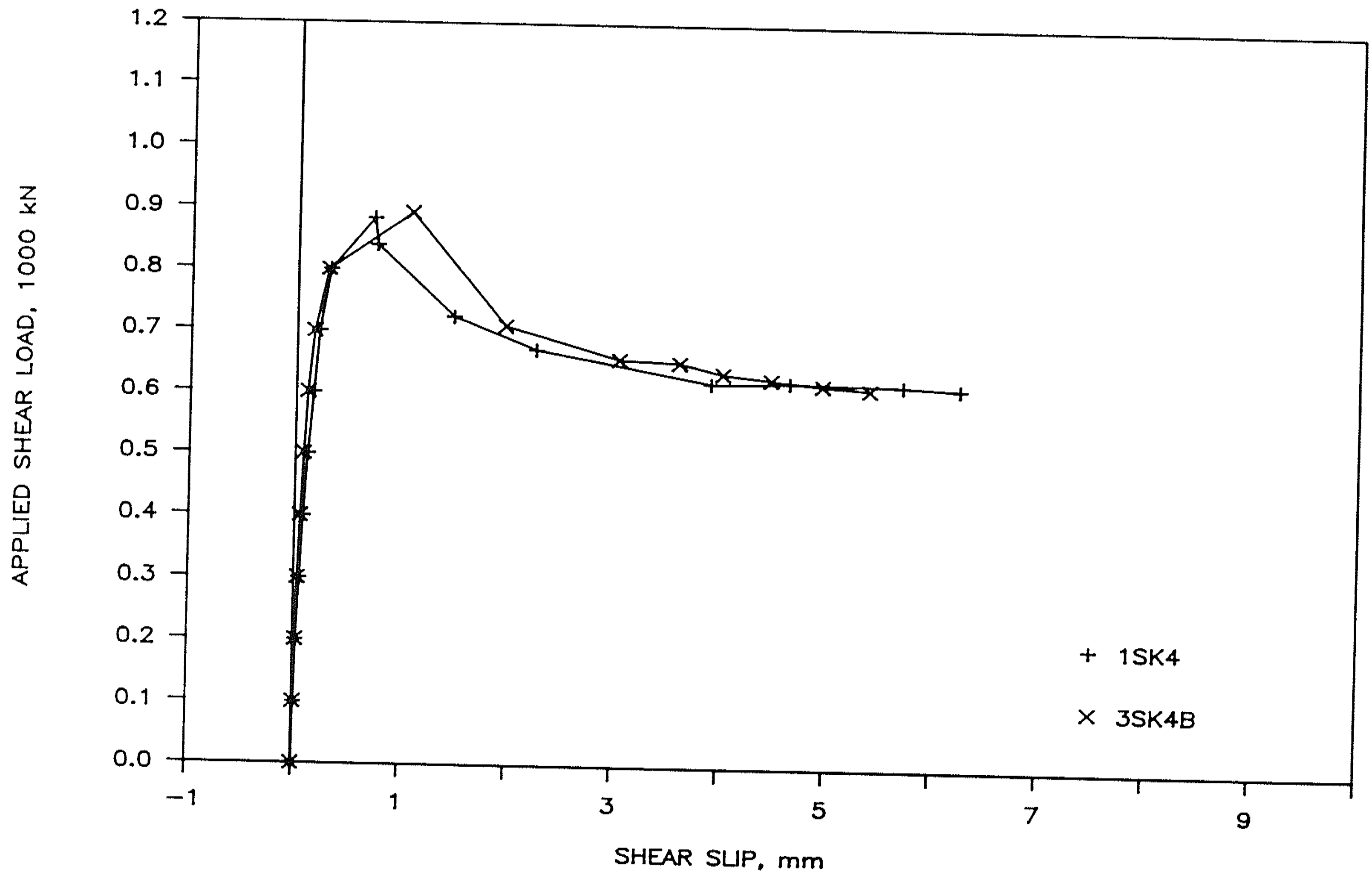

Figure 6.6 Effect of Bond at the Joint Interface of the Small Multiple Shear Key Connection

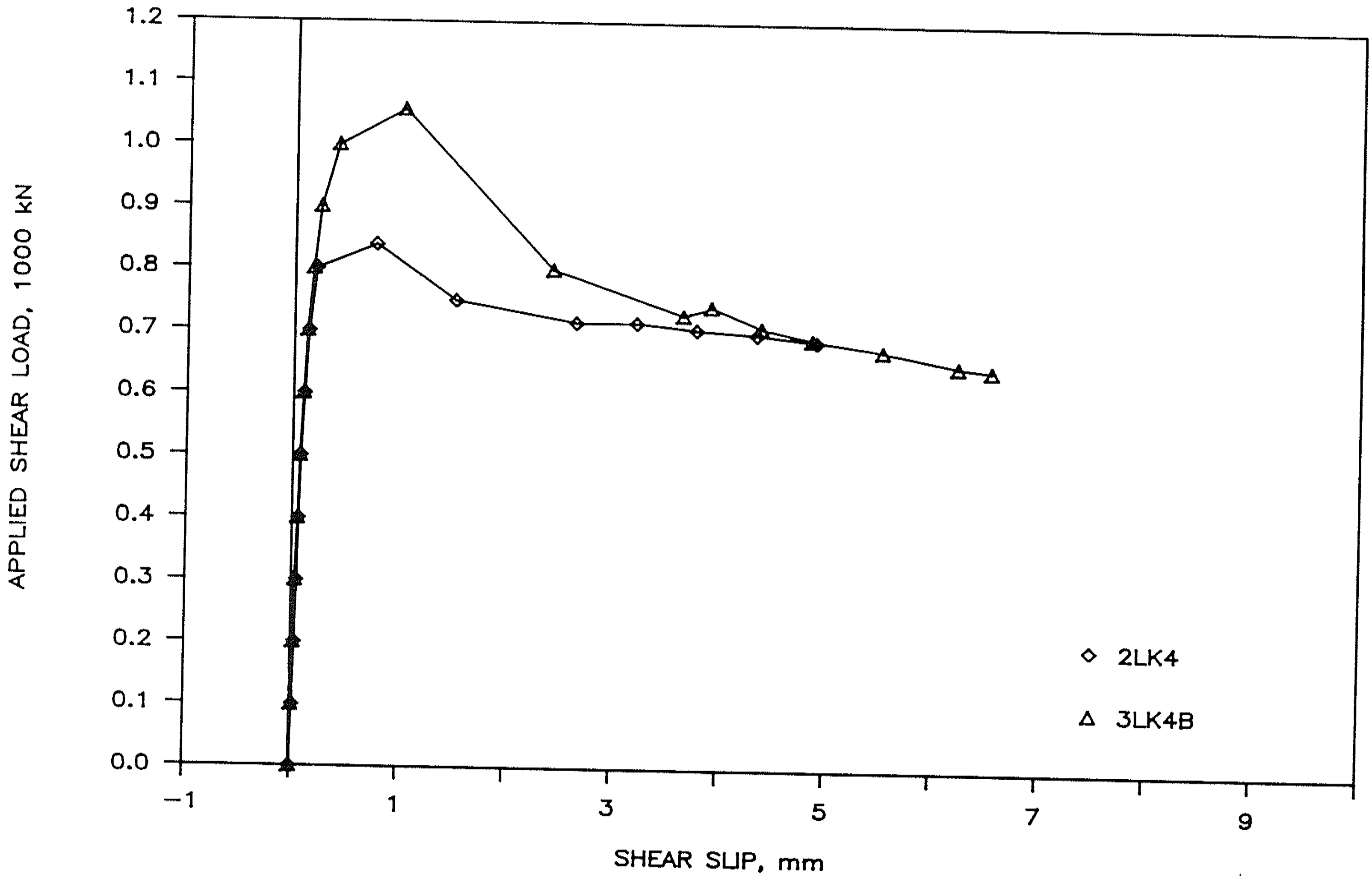

Figure 6.7 Effect of Bond at the Joint Interface of the Large Multiple Shear Key Connection

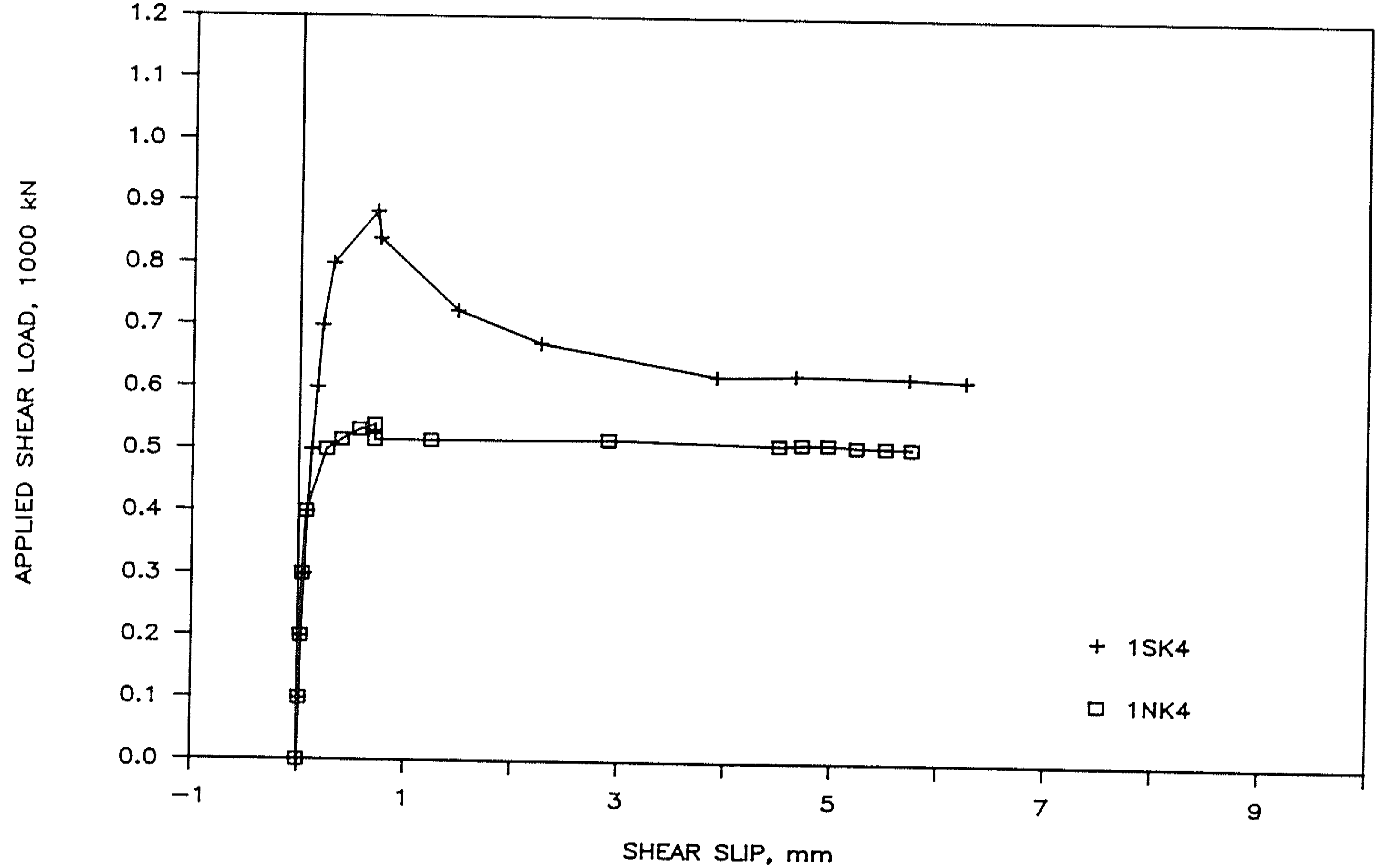

Figure 6.8 Effect of the Presence of the Small Shear Keys at the Connection

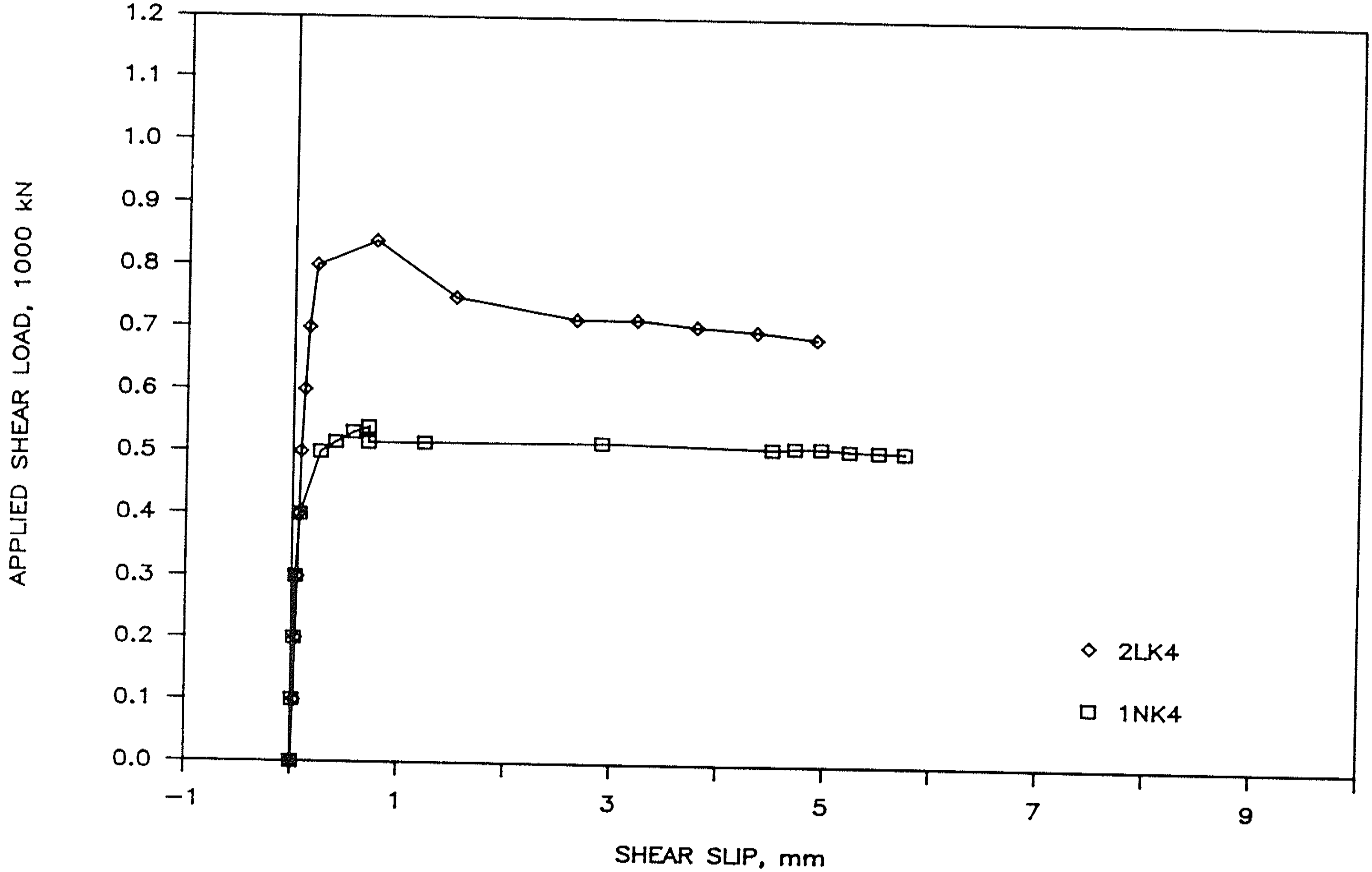

Figure 6.9 Effect of the Presence of the Large Shear Keys at the Connection

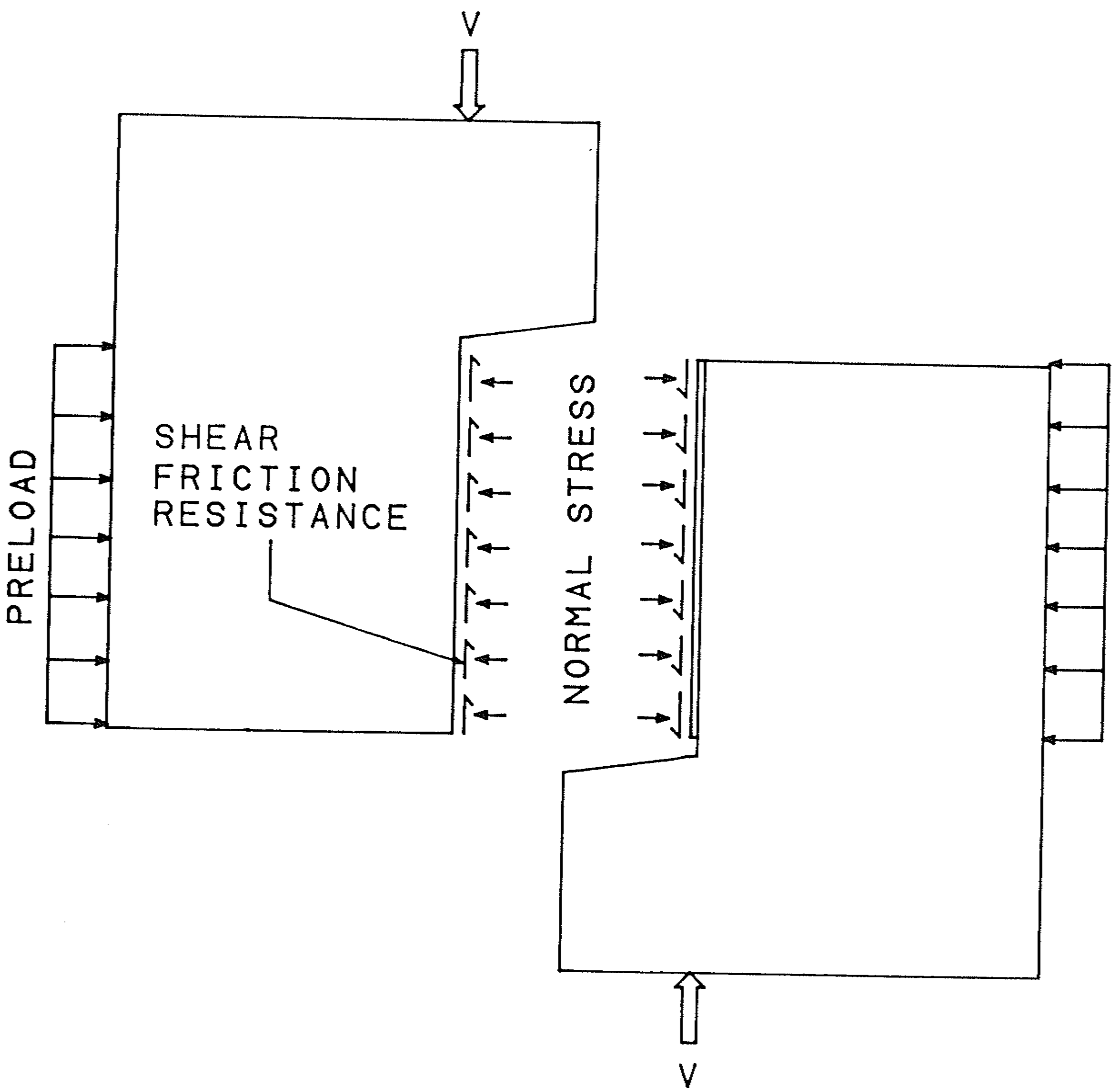

Figure 6.10 Mechanism of Shear Transfer for the Plain Surface Connection

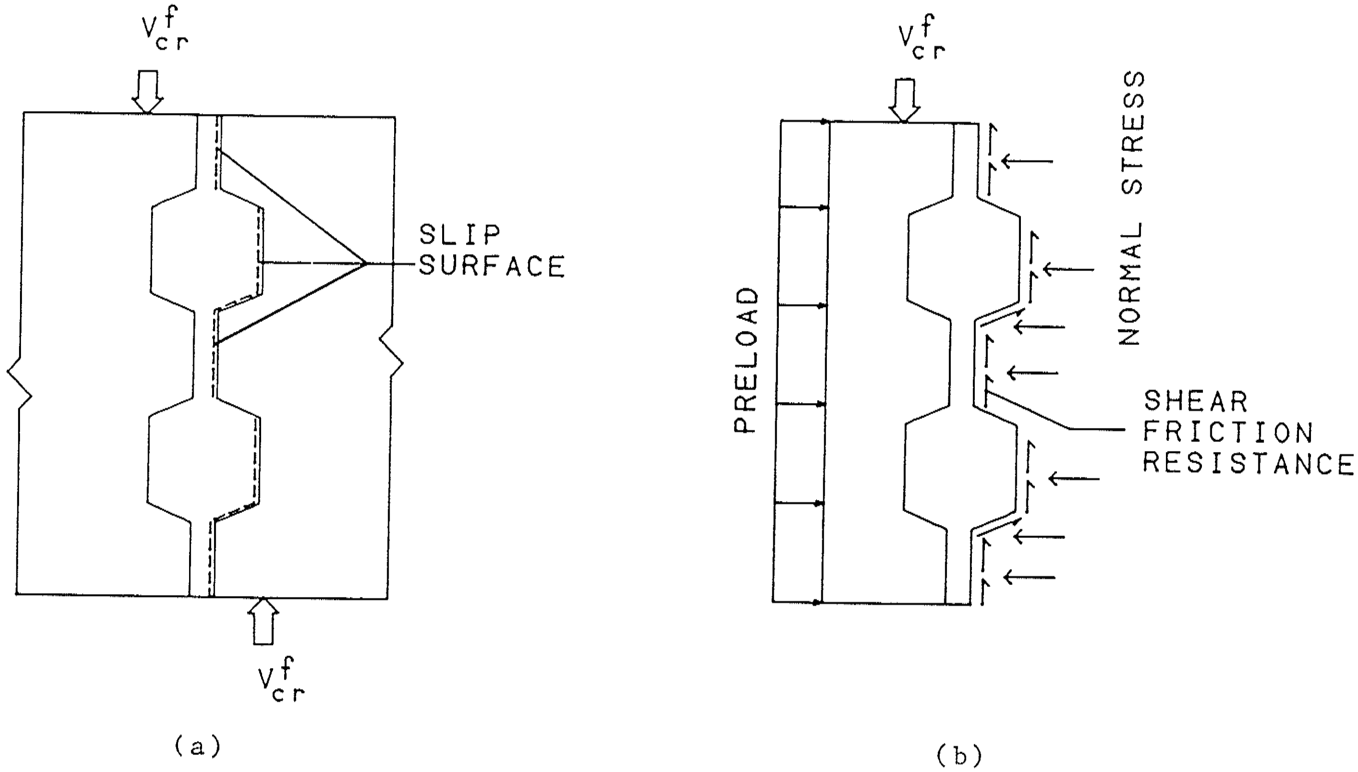

Figure 6.11 (a) Possible Slip Surface for the Multiple Shear Key Connection

(b) Mechanism of Shear Transfer

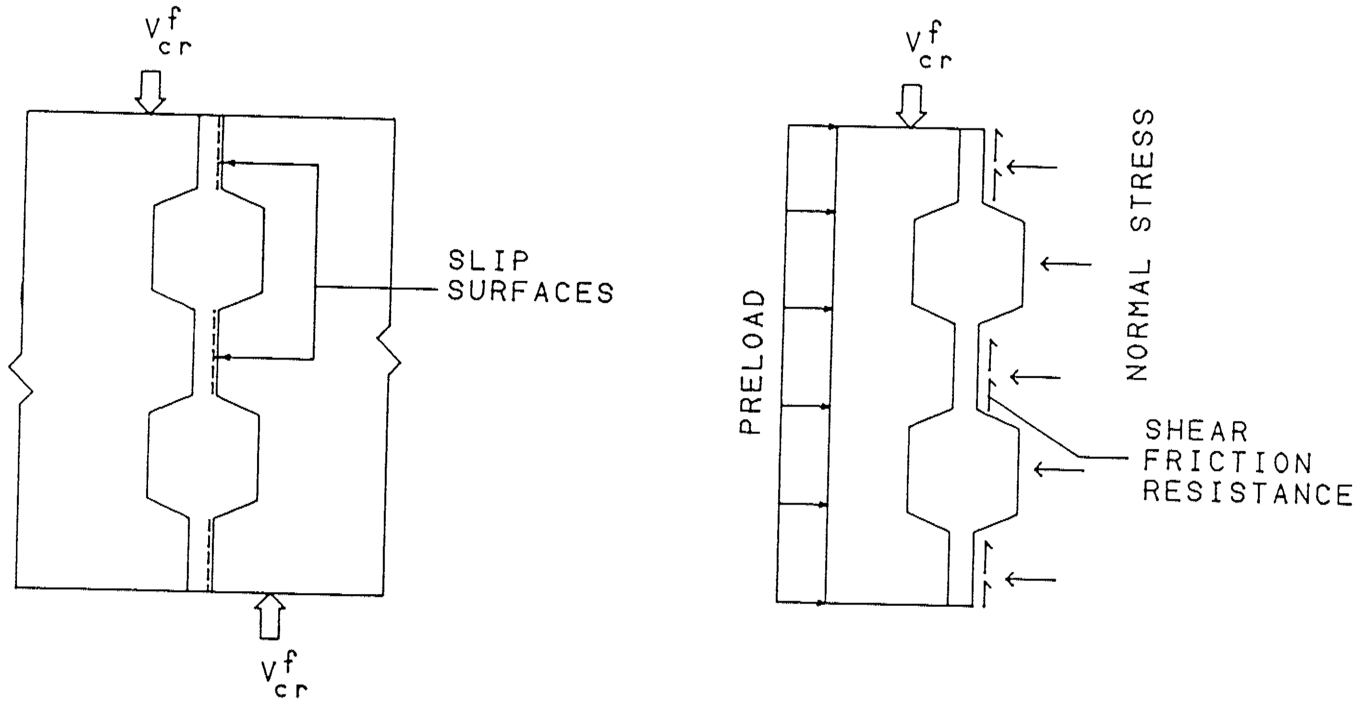

(a) (b)

Figure 6.12 (a) Possible Slip Surface for the Multiple Shear Key Connection

(b) Mechanism of Shear Transfer

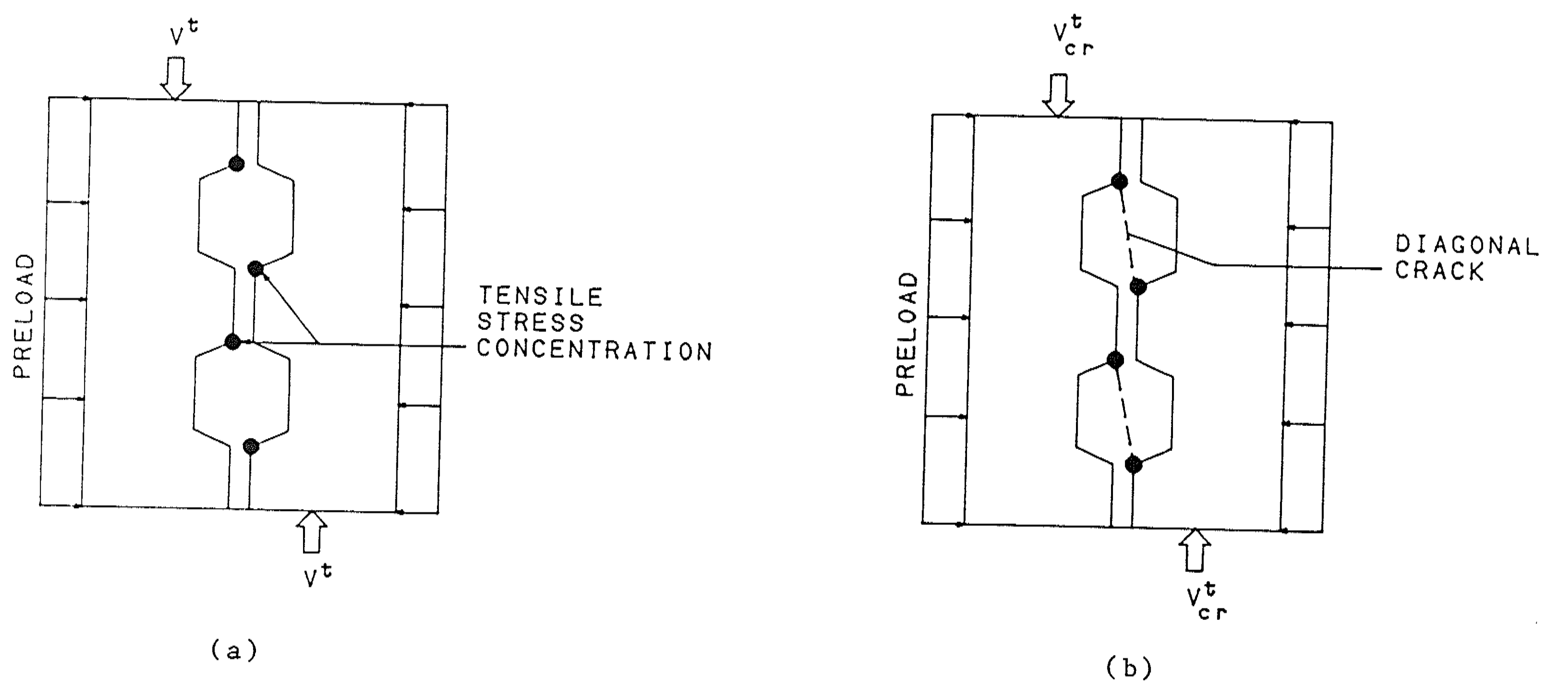

Figure 6.13 (a) Region of High Tensile Stress Concentrations

(b) Mode of Crack Initiation

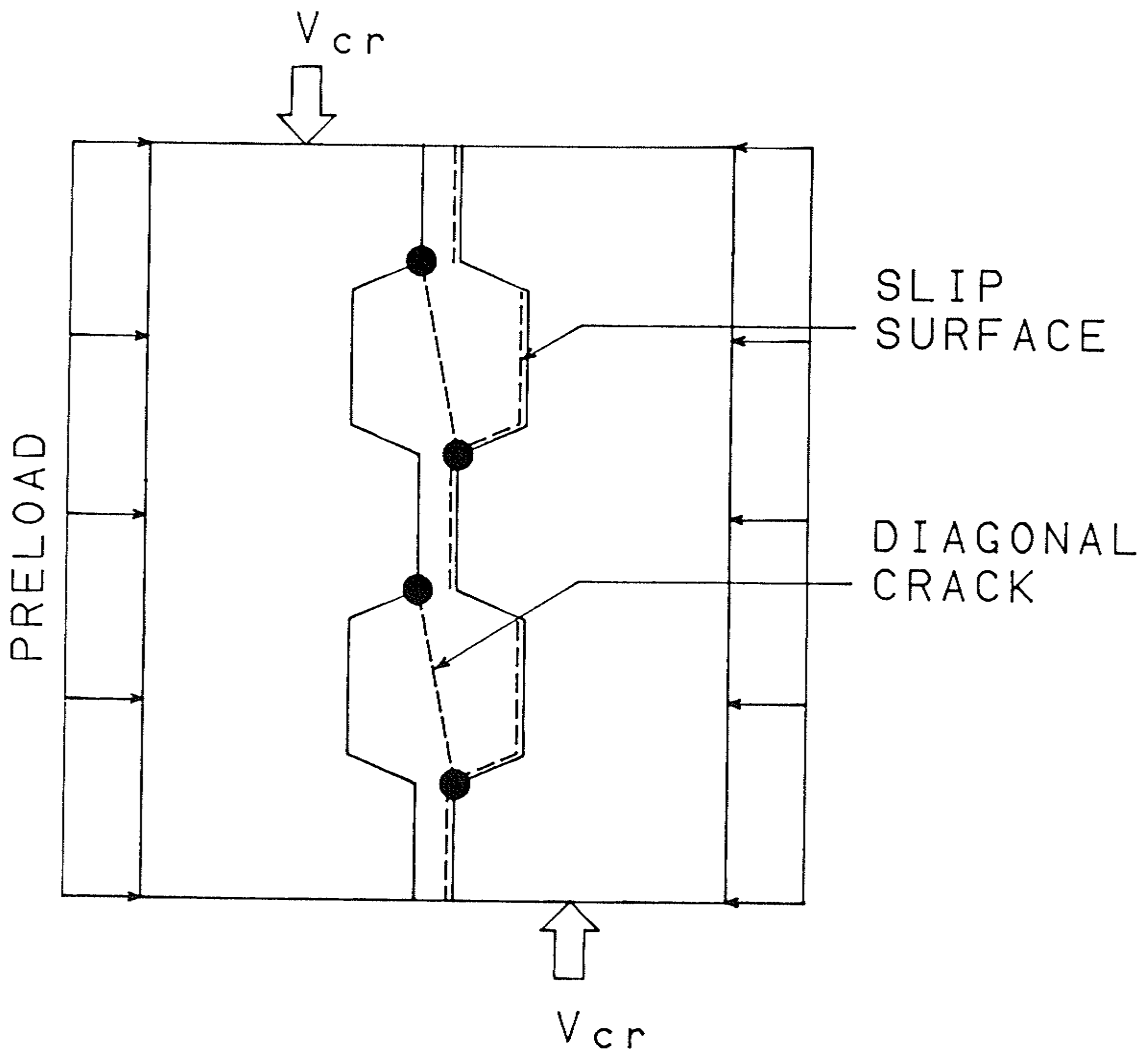

Figure 6.14 Model I - Cracking Load

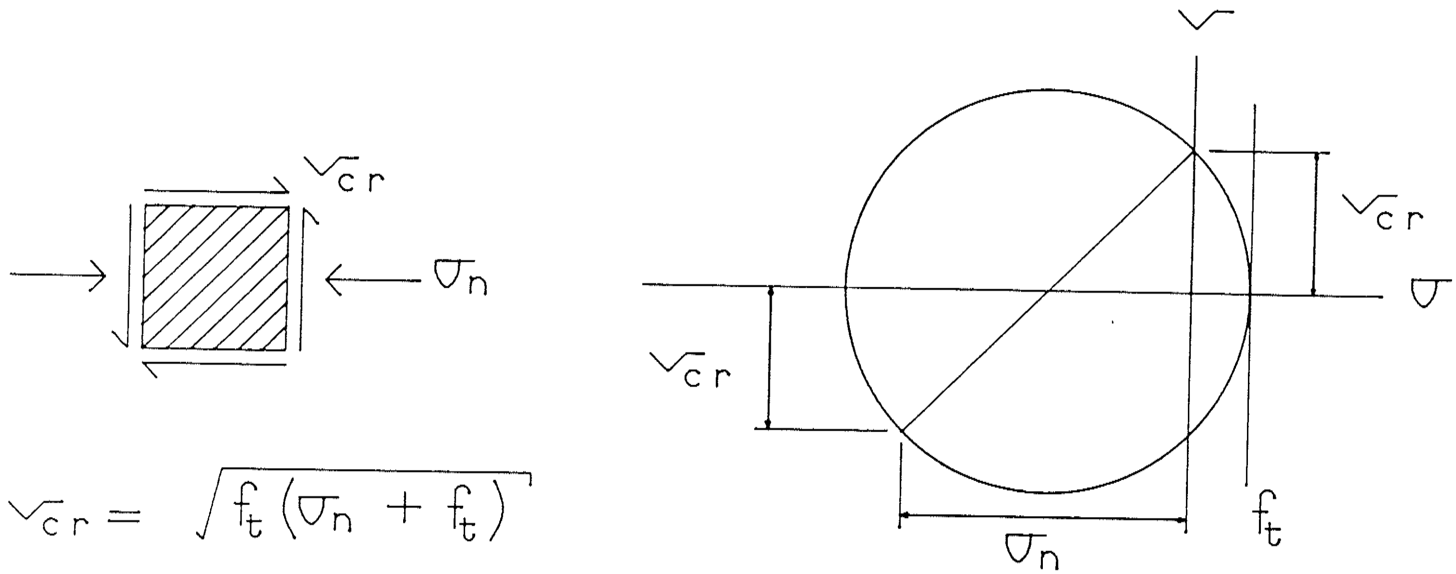

$$v_{cr} = \sqrt{f_t(\sigma_n + f_t)}$$

Figure 6.15 Assumed Stress State in the Drypack

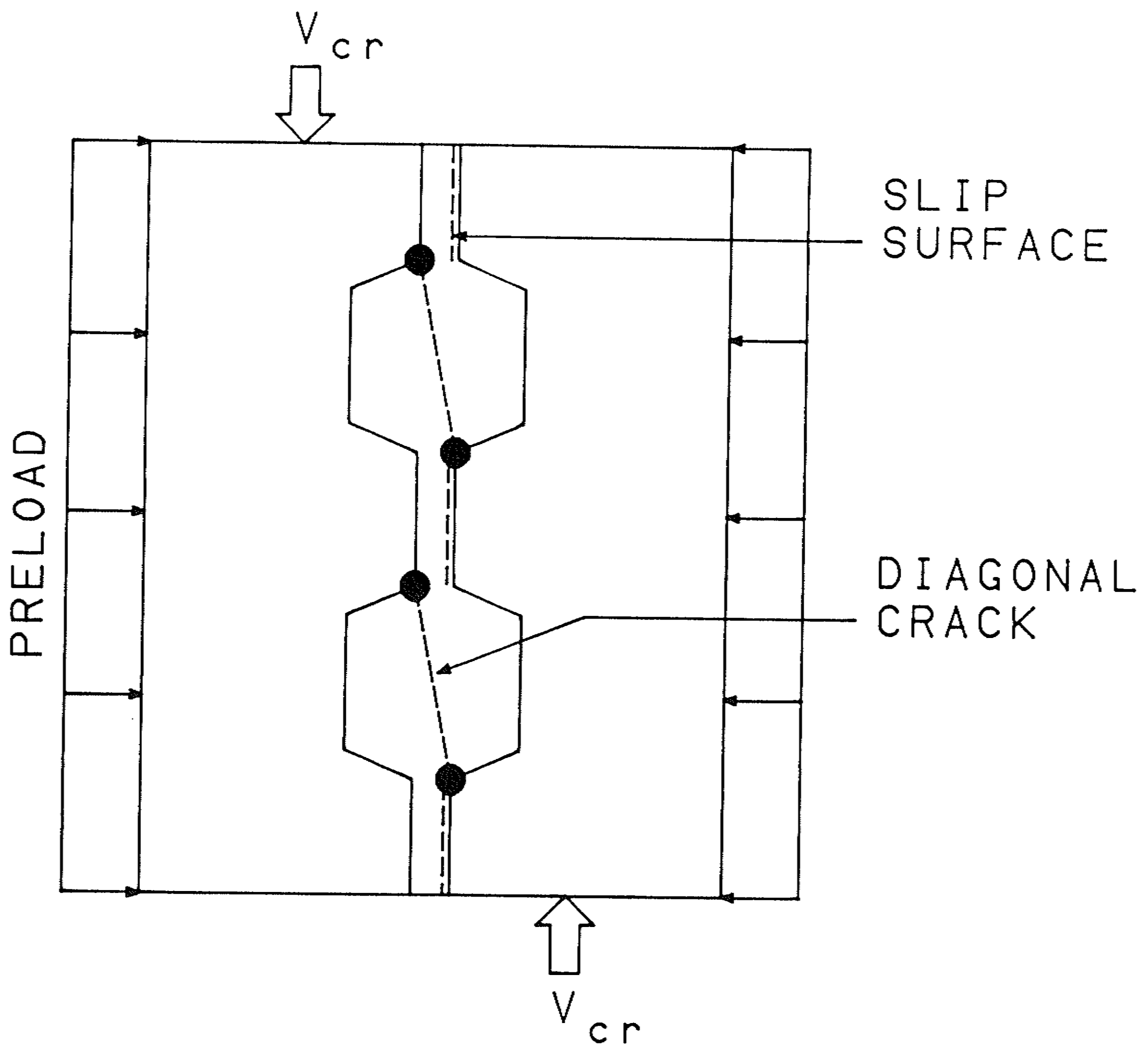

Figure 6.16 Model II - Cracking Load

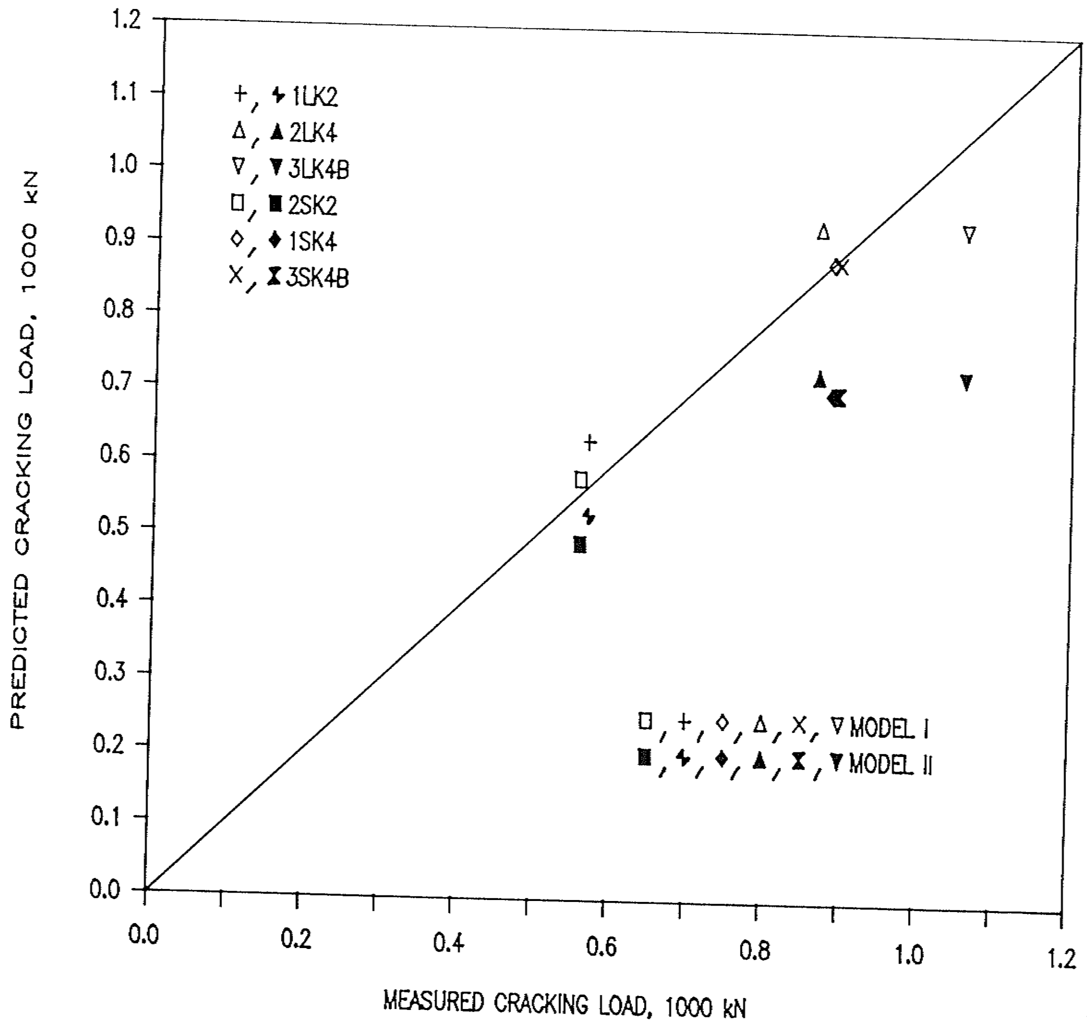

Figure 6.17 Comparison of the Predicted Cracking Load with the Experimental Results

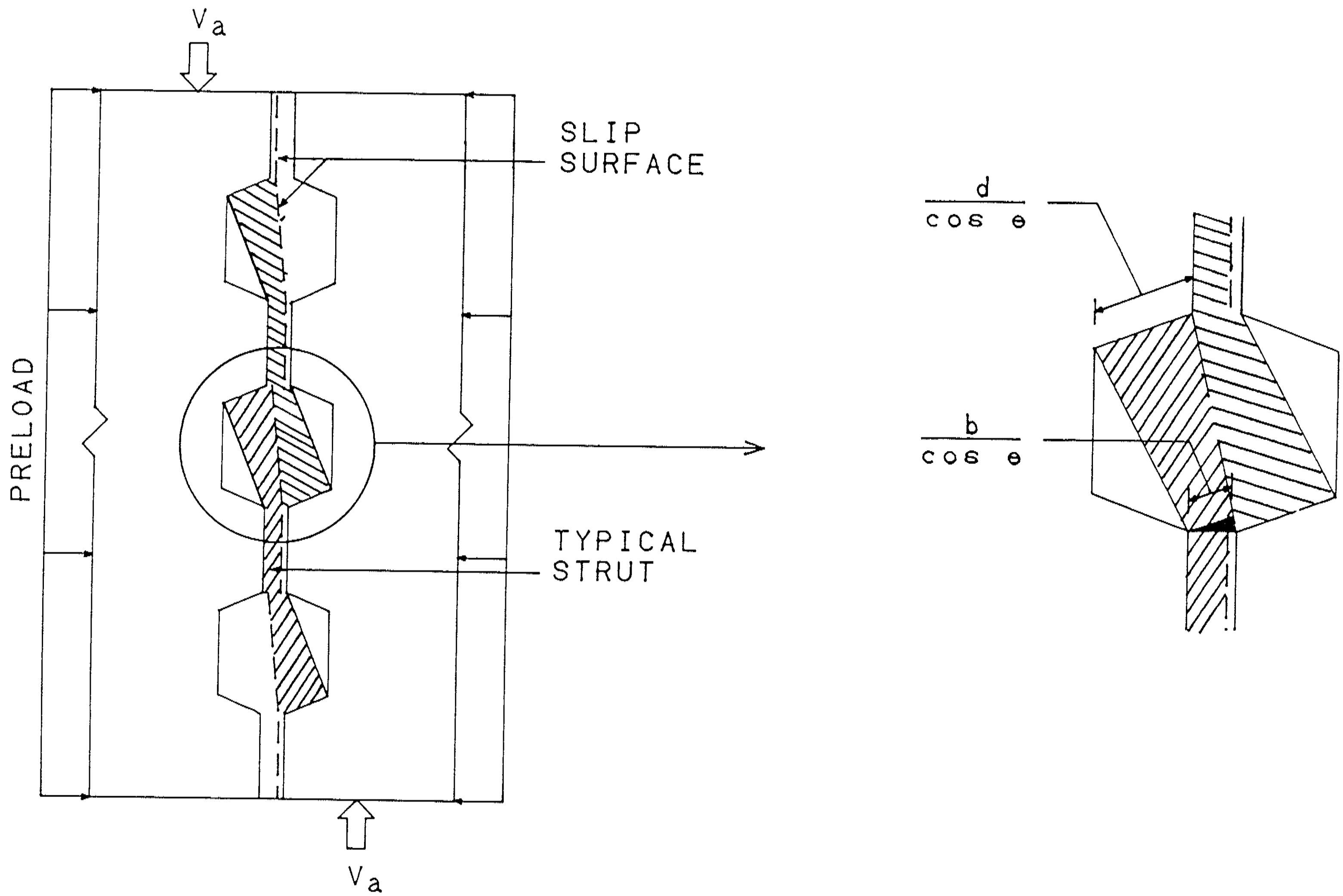

Figure 6.18 Mechanism of Shear Transfer Immediately After Cracking

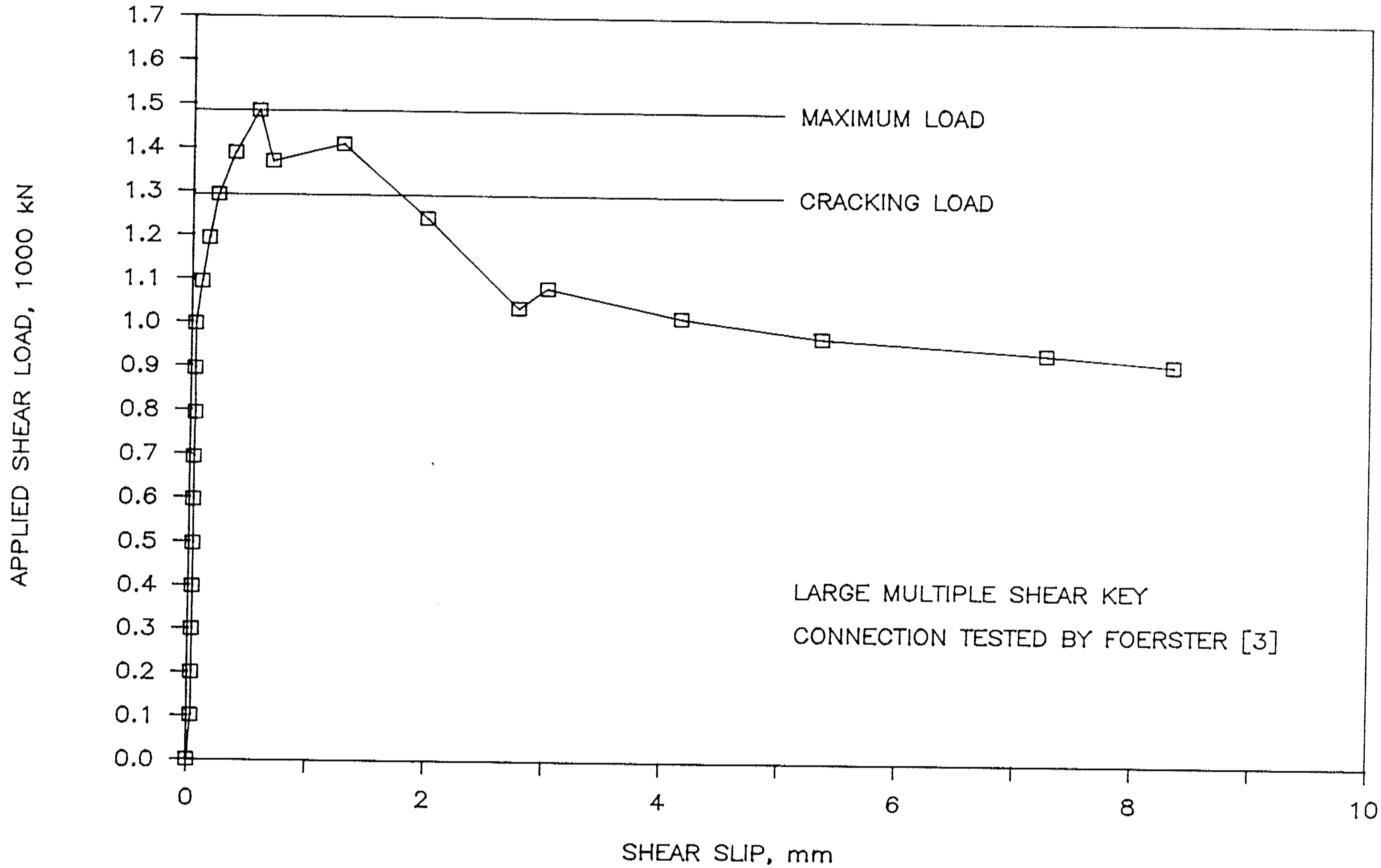

Figure 6.19 Applied Shear Load - Slip Relationship for a Large Multiple Tested in a Previous Study [3]

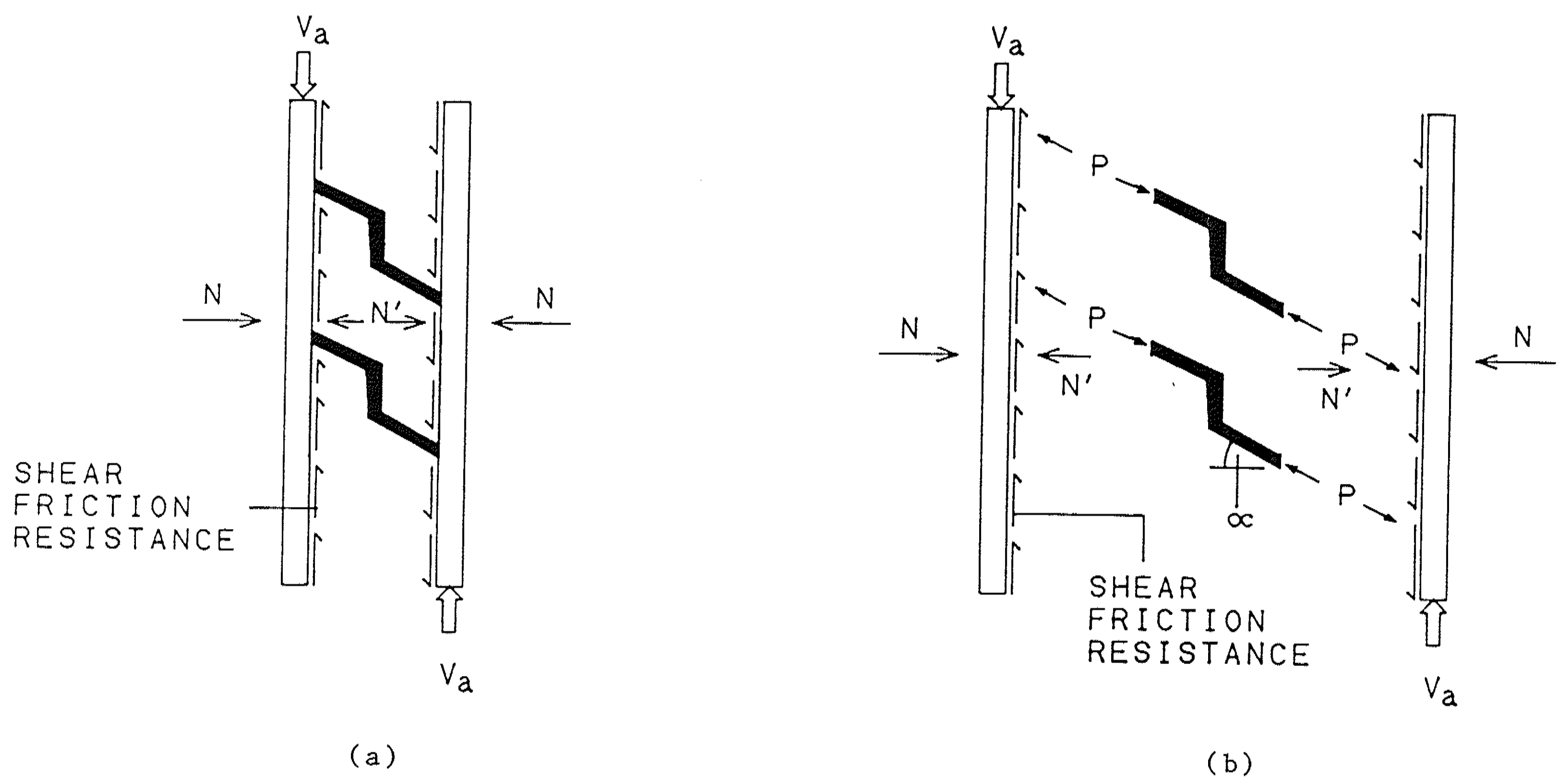

Figure 6.20 (a) Idealization of the Mechanism of Shear Transfer After Cracking

(b) Free Body of the Strut Mechanism

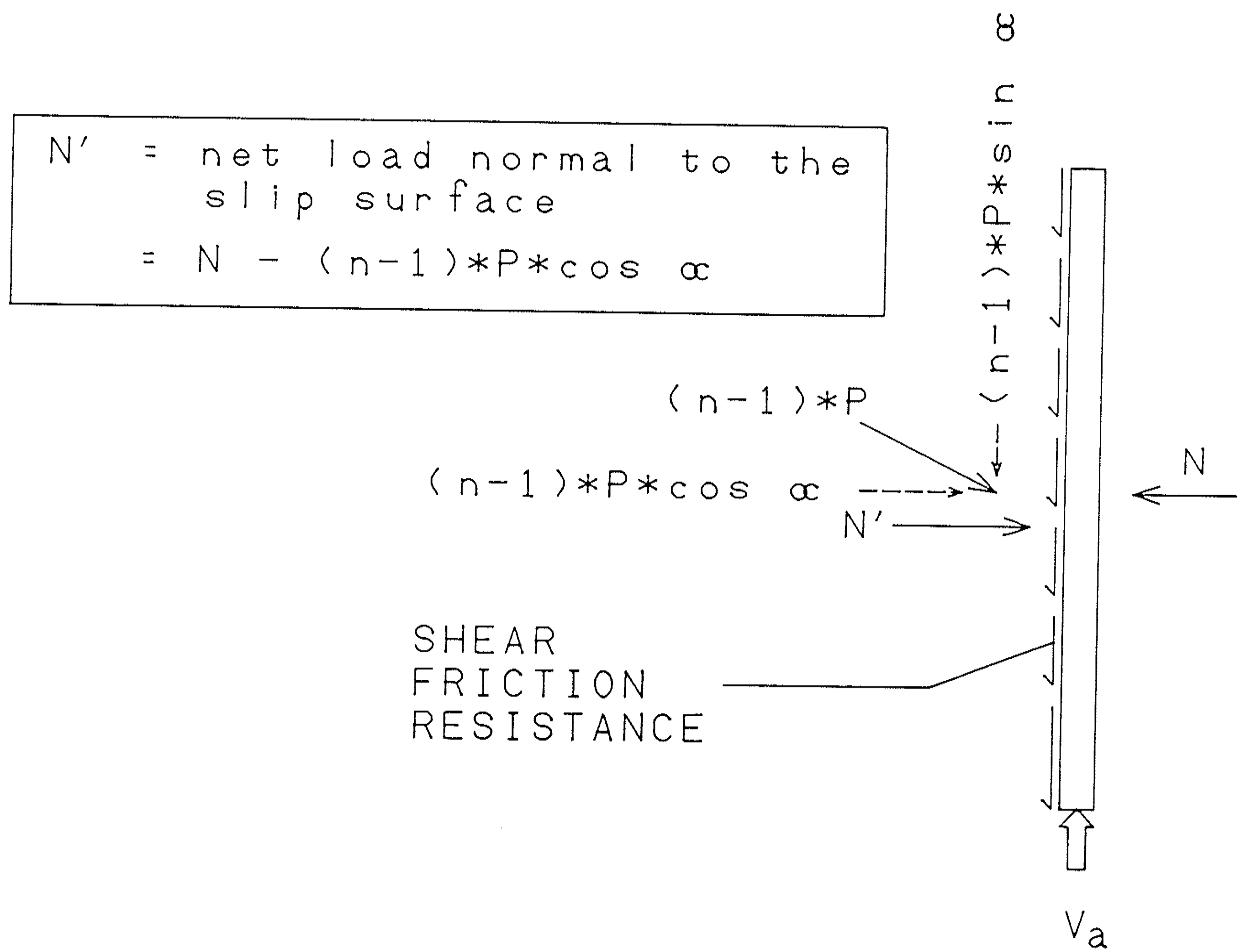

Figure 6.21 Resolution of Forces Acting on the Idealized Panel

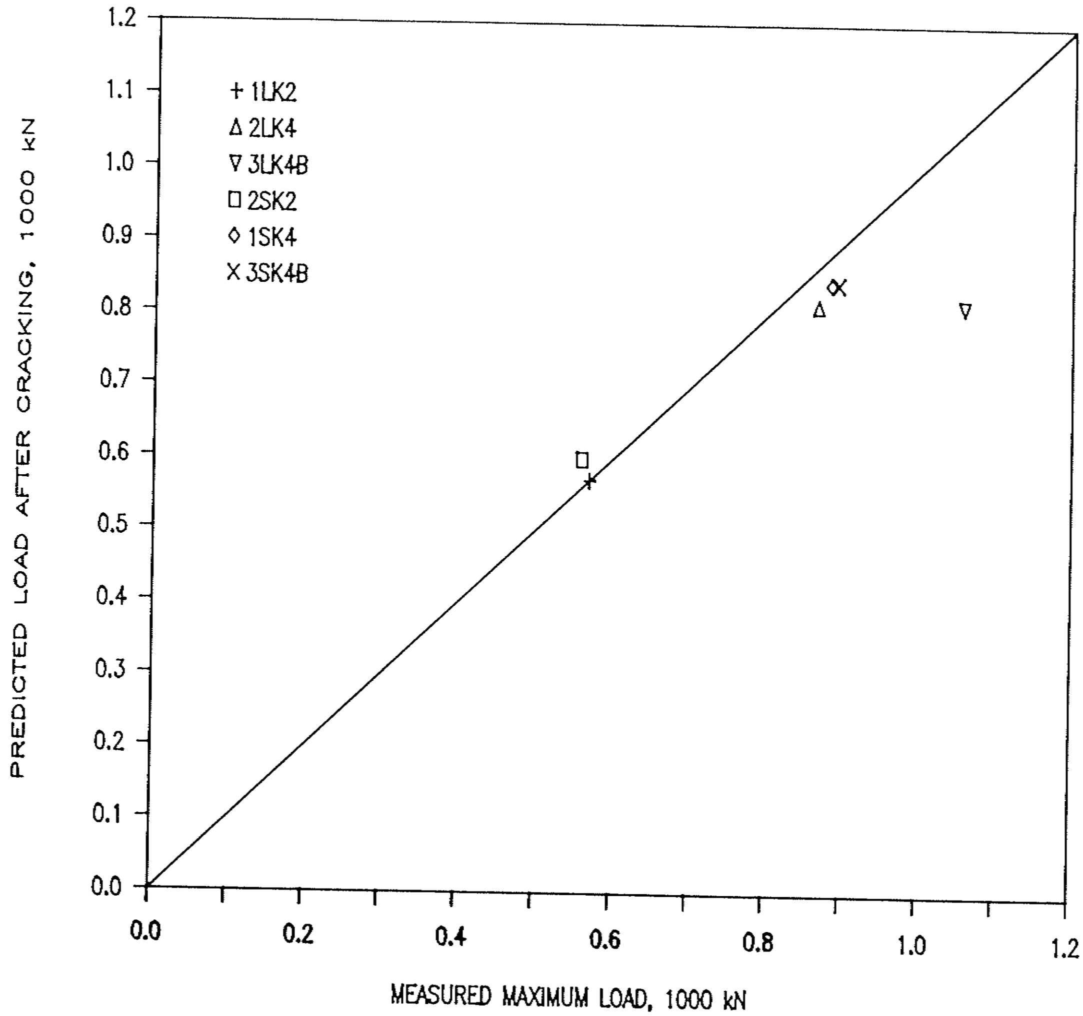

Figure 6.22 Comparison of the Predicted Load After Cracking with the Experimental Results

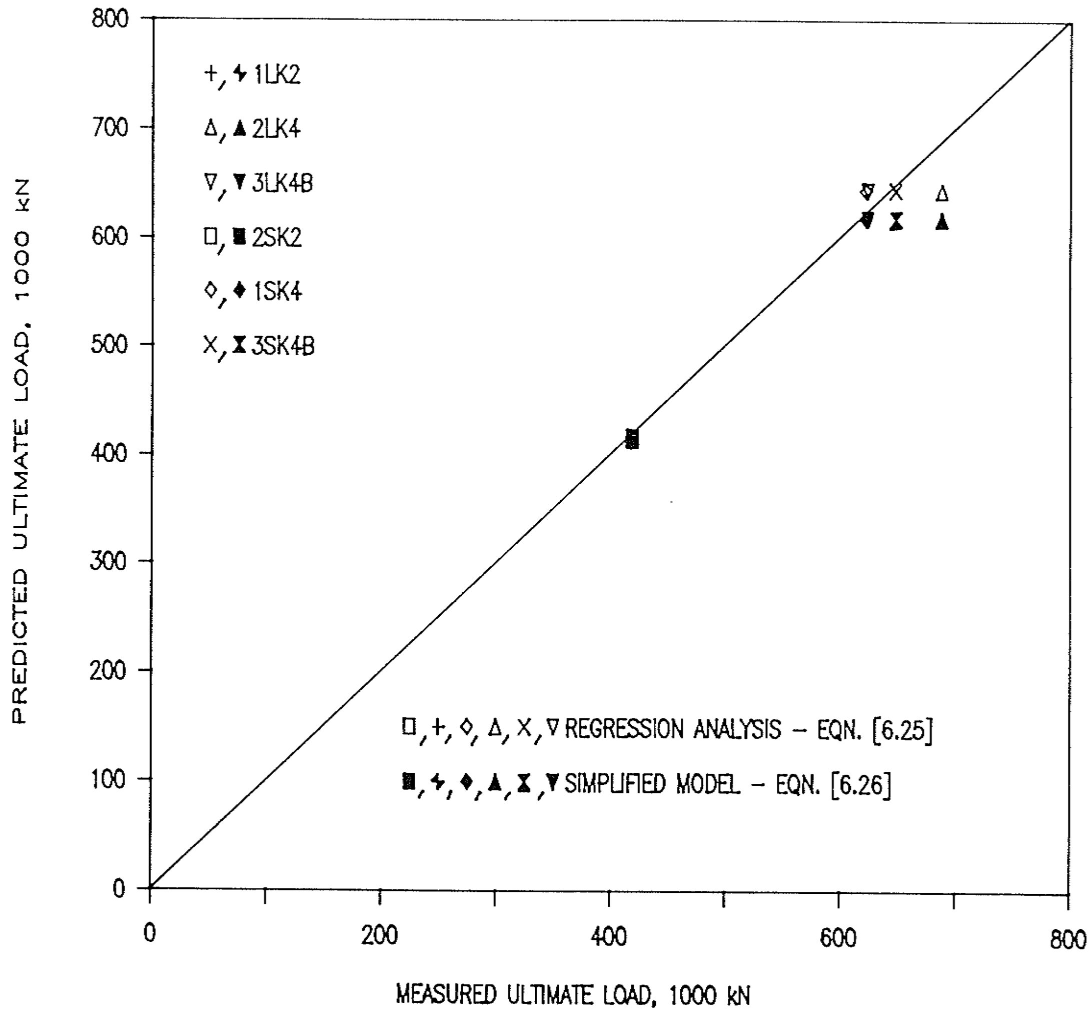

Figure 6.23 Comparison of the Predicted Ultimate Load with the Experimental Results

Appendix A

KEY TO SPECIMEN DESIGNATION

The designation used to identify each specimen has the form iXKjB.

The first letter, i, may take on values between 1 and 3 depending on the order in which the specimen was tested, within its series.

The second and third letters, XK, go together to define the configuration of the connection as follows:

NK : no-key or plain surface connection

SK : small multiple shear key connection (h=50 mm, d=25 mm and θ=7 degrees)

LK : large multiple shear key connection (h=100 mm, d=35 mm and θ=23 degrees)

The fourth letter, j, represents the level of compressive stress normal to the connection. For this study j is defined as follows:

j=2 : 2 MPa prestress normal to the connection

j=4 : 4 MPa prestress normal to the connection

The last letter, B, defines the connections in which bond at the joint interface was artificially eliminated before assembly of the specimen.

Appendix B

SHEAR SLIP AND DILATION

Shear slip and dilation are calculated using the diametrically opposite distance between demec points.

Consider the typical demec point layout at the demec stations on side A of each specimen. Using the numbering system shown in Figure B.1 and noting that d_{ij} defines the distance from point i to point j, the following assumptions, corresponding to the situation before the preload and the shear load are applied can be made:

$$d_{14} = 200 \text{ mm} = d_{36} \tag{B1}$$

$$R1 = 90^{\circ} \tag{B2}$$

$$R2 = 45^{\circ} = R3 \tag{B3}$$

Knowing that,

$$d_{04} = 1/2\ d_{14} \tag{B4}$$

$$d_{06} = 1/2\ d_{36} \tag{B5}$$

and $$d_{46} = d_{04}\cos R2 + d_{06}\cos R3 \tag{B6}$$

then R1, R2 and R3 can be related to d_{04}, d_{06} and d_{46} using cosine rule, as:

$$R2 = \cos^{-1}\left(\frac{(d_{04})^2 + (d_{46})^2 - (d_{06})^2}{2(d_{04})(d_{46})}\right) \tag{B7}$$

$$R3 = \cos^{-1}\left(\frac{(d_{06})^2 + (d_{46})^2 - (d_{04})^2}{2(d_{06})(d_{46})}\right) \tag{B8}$$

and $$R1 = 180 - R2 - R3 \tag{B9}$$

Assuming that d_{46} does not change in length and orientation when the preload and shear load are applied, then R1, R2 and R3 may be recalculated based on the new values of d_{04} (= d''_{04}) and d_{06} (= d''_{06}). The doubled primed quantities represent conditions under which the preload and an applied shear load exist.

Before the preload or shear load is applied, the horizontal component of d_{14}, d_h, is given as:

$$d_h = d_{14} \sin R2 \tag{B10}$$

and the vertical component of d_{14}, d_v, is:

$$d_v = d_{14} \cos R2 \tag{B11}$$

Similarly, as shown in Figure B.3, after the preload and shear load are applied, the new horizontal and vertical components are defined as follows:

$$d''_h = d''_{14} \sin R2'' \tag{B12}$$

$$d''_v = d''_{14} \cos R2'' \tag{B13}$$

In this study, shear slip and dilation are measured after the preload is applied. Therefore, the shear slip, δ_s may be calculated as follows:

$$\begin{aligned} \delta_s &= d'_v - d''_v \\ &= d'_{14} \cos R2' - d'' \ \cos R2'' \end{aligned} \tag{B14}$$

The primed quantities refer to the condition immediately after the preload is applied, as illustrated in Figure B.2. Expanding the terms in Equation B14 gives:

$$\begin{aligned} d'_{14} &= d_{14} \ (1 + L_{c,D2}) \\ &= 200 \ (1 + L_{c,D2}) \end{aligned} \tag{B15}$$

$$\begin{aligned} d''_{14} &= d_{14} \ (1 + L_{c,D2} + \epsilon_{D2}) \\ &= 200 \ (1 + L_{c,D2} + \epsilon_{D2}) \end{aligned} \tag{B16}$$

$$R2' = \cos^{-1}\left[\frac{(d'_{04})^2 + (d_{46})^2 - (d'_{06})^2}{2(d'_{04})(d_{46})}\right] \tag{B16}$$

$$= \cos^{-1}\left[\frac{(d'_{14}/2)^2 + (d_{46})^2 - (d'_{36}/2)^2}{(d'_{14})(d_{46})}\right] \tag{B17}$$

$$R2'' = \cos^{-1}\left[\frac{(d''_{14}/2)^2 + (d_{46})^2 - (d''_{36}/2)^2}{(d''_{14})(d_{46})}\right] \tag{B18}$$

where $L_{c,D2}$ = strain in the D2 direction immediately after the preload is applied

= 8×10^{-6} (demec reading after the preload is applied - demec reading of the 200 mm demec gauge calibration bar)

ϵ_{D2} = increase in strain in the D2 direction after the preload is applied

In a similar manner, the shear dilation, δ_w, may be calculated as:

$$\delta_w = d''_h - d'_h$$

$$= d''_{14} \sin R2'' - d'_{14} \sin R2' \tag{B20}$$

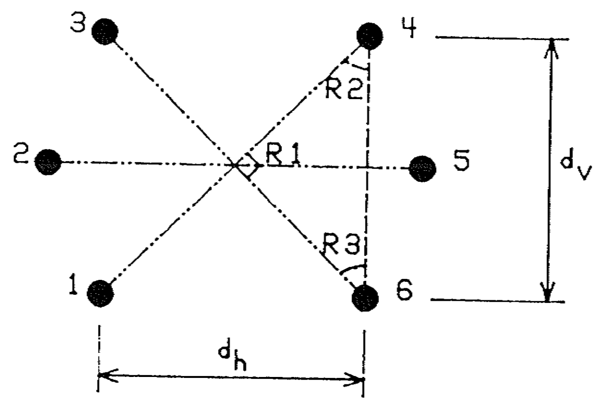

B.1 Demec Point Locations Before the Preload is Applied

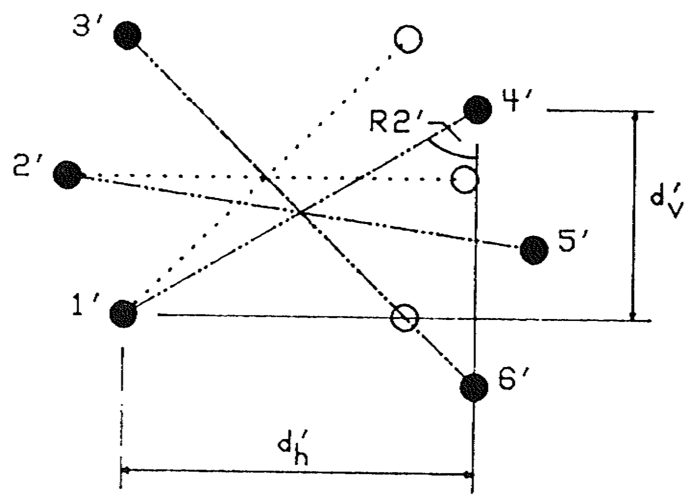

B.2 Demec Point Locations After the Preload is Applied

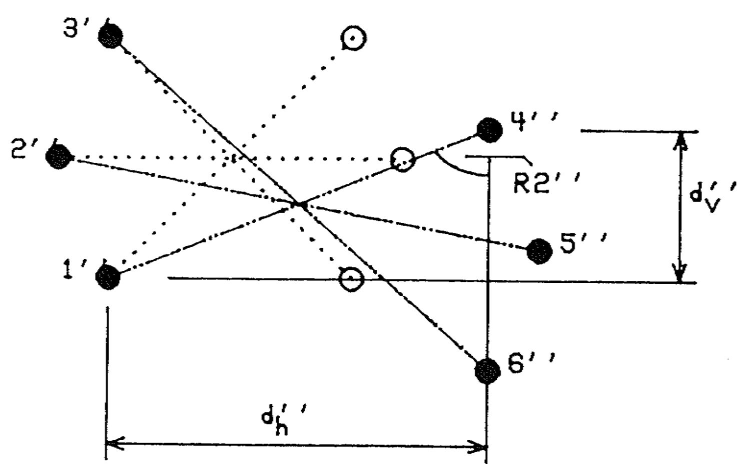

B.3 Demec Point Locations After the Shear Load is Applied

Appendix C

SHEAR STRENGTH PREDICTIONS

Prediction of the shear strength of specimen 2SK2 at the various limit states.

DATA:

Applied stress normal to the connection, σ_n = 2 MPa

Equivalent drypack compressive strength, f'_g = 26.6 MPa

Friction coefficient, μ = 0.6

Number of shear keys, n = 8

Total cross-sectional area of the diagonal cracks,

A_{cr} = 86162 mm^2

Cross-sectional area of the connection, A_c = 204000 mm^2

Inclination of the shear key, θ = 6.8°

Height of the shear key, h = 50 mm

Depth of the shear key, d = 25 mm

Slope of the diagonal crack, α = 68°

Thickness of the connection, t = 200 mm

(a) Cracking Shear Capacity, Equivalent (6.8)

Model I:

$$V_{cr} = \mu\sigma_n(A_c - ndt \times \tan\theta) + \sqrt{f_t(\sigma_n + f_t)}\, A_{cr}$$

The tensile strength, f_t, is estimated as:

$$f_t = 0.6\sqrt{f'_g}$$
$$= 0.6\sqrt{26.6}$$
$$= 3.09 \text{ MPa}$$

therefore, $V_{cr} = [0.6 \times 2 \times (204000 - 8 \times 25 \times 200\tan 6.8)$
$$+ \sqrt{3.09(2 + 3.09)} \times 86162]/1000$$
$$= 580 \text{ kN.}$$

(b) Cracking Shear Capacity, Equation (6.9)

Model II:

$$V_{cr} = \mu\sigma_n(A_c - nht) + \sqrt{f_t(\sigma_n + f_t)}\ A_{cr}$$
$$= [.6 \times 2 \times (204000 - 8 \times 50 \times 200)$$
$$+ \sqrt{3.09 \times (2 + 3.09)}\ 86162]/1000$$
$$= 490 \text{ kN.}$$

(c) Shear Capacity Immediately After Cracking, Equation (6.17)

$$V_a = (n-1)P\sin\alpha + \mu\left(\sigma_n - \frac{(n-1)P\cos\alpha}{A_c}\right)A_c$$

The crushing load, P, for the strut is estimated as

$$P = 0.6f'_g t(w)$$
$$= 0.6f'_g t \times \left[\frac{(b + d)}{2\cos\theta}\right]$$
$$= \left[\frac{0.6}{2} \times 26.6 \times 200 \times \frac{(20 + 25)}{\cos 6.8}\right]/1000$$
$$= 72 \text{ kN.}$$

Therefore, $V_a = (8\text{-}1) \times 72 \times \sin(68)$

$$+ [0.6(2 - \frac{(8\text{-}1) \times 72 \times \cos 68 \times 1000}{204000}) \times 204000]/1000$$

$= 598$ kN.

(d) <u>Ultimate Shear Capacity, Equation (6.25)</u>

Regression Model:

$$V_u = 0.035 f'_g A_c + 0.556 \sigma_n A_c$$

$$= [.035 \times 26.6 \times 204000 + .556 \times 2 \times 204000]/1000$$

$$= 417 \text{ kN.}$$

(e) <u>Ultimate Shear Capacity, Equation (6.26)</u>

Simplified Model:

$$V_u = 0.2\sqrt{f'_g} A_c + \frac{\sigma_n A_c}{2}$$

$$= [0.2\sqrt{26.2} \times 204000 + 2 \times \frac{20400}{2}]/1000$$

$$= 414 \text{ kN.}$$